

# **Polymer-based drug delivery systems**

A study on micro and nanoparticles as carriers for bioactive molecules

Luca Scrivano





# **UNIVERSITY OF CALABRIA**

Department of Pharmacy, Health and Nutritional Sciences

Department of Biology, Ecology and Earth Sciences

**Ph.D. Program in**  
Life Sciences

**CYCLE**  
XXXI

**POLYMER-BASED DRUG DELIVERY SYSTEMS:  
A STUDY ON MICRO AND NANOPARTICLES AS CARRIERS  
FOR BIOACTIVE MOLECULES**

**Scientific-Disciplinary Sector**  
**CHIM/09 Applied Technological Pharmaceutics**

**Coordinator:** Prof. Maria Carmela Cerra

**Supervisor:** Prof. Francesco Puoci

**Ph.D. Candidate:** Luca Scrivano

The research reported in this thesis was performed at the Department of Pharmacy and Health and Nutritional Sciences of the University of Calabria (Italy) and at the Department of Pharmaceutics, Utrecht Institute for Pharmaceutical Sciences UIPS, Utrecht University (the Netherlands).

Cover design and layout by Lorenzo Patera.

Copyright © Luca Scrivano, 2019.

All rights reserved. No parts of this thesis may be reproduced, stored in a retrieval system or transmitted in any form or by any means, without prior written permission of the author and the publisher holding the copyrights of the published articles.



*A mia madre e mio padre*

*True education is a kind of never ending story - a matter of continual beginnings, of habitual fresh starts, of persistent newness.*

J.R.R. Tolkien



# TABLE OF CONTENTS

Preface		1
PART I		
Chapter 1	Molecularly imprinted polymers as drug delivery systems	7
Chapter 2	Molecularly imprinted hydrogels for sustained release of sunitinib in breast cancer therapy	13
Chapter 3	Molecularly imprinted microrods <i>via</i> mesophase polymerization	31
Chapter 4	Smart bandage based on molecularly imprinted polymers (MIPs) for diclofenac controlled release	47
PART II		
Chapter 5	Polymeric nanoparticles for the delivery of poorly water-soluble drugs	77
Chapter 6	Synthesis of sericin-based conjugates by click chemistry: enhancement of sunitinib bioavailability and cell membrane permeation	97
Chapter 7	Biopolymeric self-assembled nanoparticles for enhanced antibacterial activity of Ag-based compounds	123
Chapter 8	Nanobody-conjugated polymeric micelles for targeted delivery of a hydrophobic photosensitizer in photodynamic therapy	149
CONCLUSIONS		
Final remarks		225
APPENDICES		
Abstract in italiano		231
Curriculum vitae		233
List of publications		234
Contributions		237



# PREFACE

The works presented in this book are the result of the research carried out by the candidate, Luca Scrivano, during his 3 years Ph.D. at the Department of Pharmacy, Health and Nutritional Sciences of the University of Calabria (IT). His research was focused on the development of polymeric materials for the preparation of nanosized and micrometric drug delivery systems. Many strategies were explored and four different categories of polymeric particles were investigated: molecularly imprinted polymers, polymer-drug conjugates, polymeric vesicles and polymeric micelles. Both natural and synthetic polymers were employed for the development of these particles. The thesis is divided in two sections:

Part I is focused on molecularly imprinted polymers (MIPs) as drug delivery systems. After a brief introduction about molecular imprinting technology in Chapter 1, the classic approach for the synthesis of MIPs for the delivery and release of an anticancer drug, namely sunitinib, is reported in Chapter 2. In Chapter 3, instead, a novel strategy for the synthesis of molecularly imprinted microrods through mesophase polymerization is presented. Finally, the use of diclofenac imprinted polymers for the production of hybrid smart bandages is described in Chapter 4.

Part II is focused on nanosystems for the delivery of poorly water soluble drugs. Three different systems are presented in this section (and a short introduction is given in Chapter 5): a polymer-drug conjugate, a polymeric vesicle and polymeric micelles. For the polymer-drug conjugate reported in Chapter 6, sericin was used as starting material and sunitinib as drug substance. To achieve the final product, a click chemistry approach was applied, based on free radical grafting in aqueous solution. Oleate functionalization of dextran, described in Chapter 7, was carried out to prepare self-assembled polymeric vesicles, for the delivery a new antibacterial agent, synthesized by the group of medicinal chemistry of the Department of Pharmacy, Health and Nutritional Sciences of University of Calabria. Research on polymeric micelles for the targeted delivery of a photosensitizer for application in photodynamic therapy, reported in Chapter 8, was carried out at the Department of Pharmaceutical Sciences of Utrecht University (NL), under the supervision of Prof. Wim Hennink, Dr. Cornelus F.

## PREFACE

---

van Nostrum and Dr. Sabrina Oliveira, during the last seven months of the Ph.D. course.

In the attempt to explore the wide world of the drug delivery systems, polymeric carriers were chosen exclusively for the investigation carried out by the candidate. Among them, only the systems which may offer great advantages, such as stability, controlled release, high loading capacity and improved solubility of hydrophobic drugs, were selected. But alongside with the advantages are the disadvantages: in the Conclusions is, indeed, reported that all the good qualities can never be found in only one system and that the selection of the polymeric carrier must be done carefully, by taking into account the physical-chemical properties of the drug and the physio-pathological characteristics of the diseased tissue, target site of the bioactive compounds.







# PART I



# **CHAPTER 1**

## **Molecularly imprinted polymers as drug delivery systems**



## GENERAL INTRODUCTION

Molecular imprinting is a technology used to synthesize polymers with specific recognition properties. Molecularly imprinted polymers (MIPs) are highly cross-linked polymers that possess specific binding sites for molecules used as templates during polymerization processes. In this way, polymers can be “programmed” to bind selectively specific templates with high affinity (Chen, Wang et al., 2016).

Compared to conventional polymers, MIPs show many advantages such as high stability in a broad range of temperatures, against mechanical, physical or chemical stresses, they can be stored for long time and they can be regenerated and reused many times without losing affinity for the template (Saylan, Yilmaz et al., 2017).

The pioneers of molecular imprinting were Wulff and Klotz, who synthesized in 1972 the first organic polymers using the now-called “covalent approach” or “pre-organized approach” (Takagishi & Klotz, 1972, Wulff & Sarhan, 1972). In particular, Wulff synthesized polystyrenes capable to separate the enantiomeric forms of several monosaccharides. This method is based on reversible covalent bonds between the functional groups of the polymer and the reactive moieties of the template molecule. The most common bonds used for the covalent approach are esters, imines or ketals. Later, in 1981, Mosbach and Arshady prepared a MIP using only non-covalent bonds between template and polymer, introducing for the first time the “non-covalent approach” or self-assembly approach” (Arshady & Mosbach, 1981). This method is usually based on hydrogen bonds, hydrophobic or van der Waals interactions. In 1995, Whitcombe proposed the “semi-covalent approach”, which is considered an intermediate technique that exploits the advantages of both the previously described methods. However, nowadays the most utilized method for the synthesis of MIPs is the non-covalent approach (Whitcombe, Rodriguez et al., 1995).

Independently from the employed approach, the synthesis of a molecularly imprinted polymer occurs in 4 steps (Figure 1.1):

- assembly, in which functional monomers are linked *via* covalent or non-covalent bonds to the template, to form the so-called “pre-polymerization complex”;

- polymerization: in which fixation of the monomers around the template is achieved by triggering polymerization in presence of a cross-linker;
- extraction: in which the template molecule is removed through washes of the polymeric matrix with proper solvents and reagents;
- rebinding: which represents the goal of the technique and can be obtained by putting into contact a solution of the template with the polymer, that has now complementary cavities for the molecule.

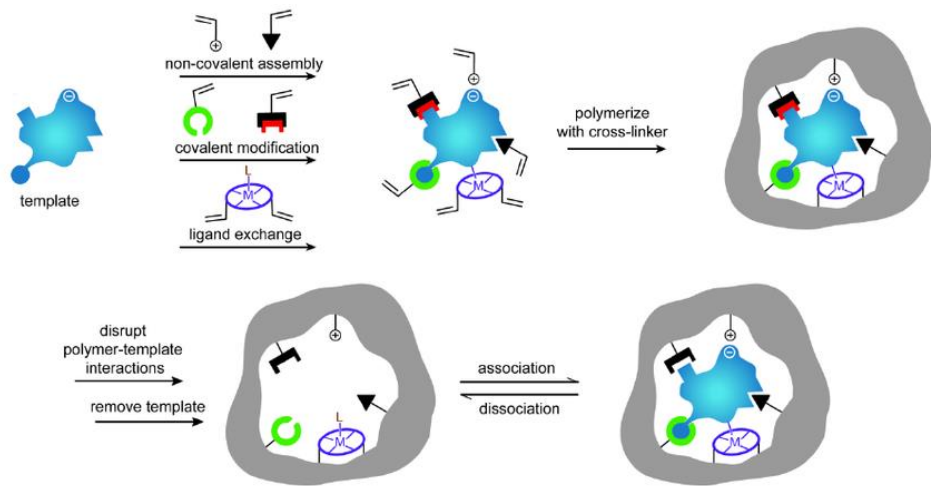


**Figure 1.1** Schematic representation of the molecular imprinting process (Alexander, Andersson et al., 2006).

Rebinding and extraction kinetics depend on the employed technique: the non-covalent approach usually shows faster kinetics but less recognition ability due to the liability of the formed bonds; on the other hand, the covalent approach is characterized by stronger and more stable interactions that can fix the template in the correct position (Alexander et al., 2006).

MIPs found application in many fields: as basic material for extraction of molecules of interest, in chromatography, especially for chiral separations, as artificial antibodies or receptors, as enzymes or catalyst or as detecting component in biosensors (BelBruno, 2018).

An interesting application of MIPs in the biomedical field is the design of smart material for the development of controlled drug delivery systems. The porous and cross-linked structure of MIPs can act as a reservoir for small drugs that accommodate within the matrix with high loading efficiency. Moreover, the drug

release kinetic is influenced by the specific recognition sites, prolonging the residence time of the drug inside the body and reducing, at the same time, the frequency of administration. This characteristic can be advantageously exploited in case of drugs with narrow therapeutic windows, to keep drug concentration below the level at which side effects are predominant (Alvarez-Lorenzo & Concheiro, 2004).

During the design of a molecularly imprinted polymer as drug delivery system, a compromise between stability of the cavities and flexibility is necessary. Indeed, imprinted drug should be able to specifically bind the recognition sites of the polymer and at the same time it should be able to diffuse through the matrix following a precise kinetic. For this reason, non-covalent approach, using acrylic or vinyl monomers, is often preferred. One of the most employed monomers is methacrylic acid (MAA), together with ethylene glycol dimethacrylate (EGDMA) cross-linker. They can form hydrogen bonds with templates through the carboxylic groups and polymerization can be easily triggered using radical initiators. The cross-linked network of poly(MAA-*co*-EGDMA) is highly hydrophilic and capable to absorb large amounts of water and thus it shows all the properties of classic hydrogels (Byrne, Park et al., 2002). Finally, poly(MAA-*co*-EGDMA) has low immunogenicity and high biocompatibility (Hamidi, Azadi et al., 2008) and these characteristics make it the perfect candidate for the development of MIP-based drug delivery systems.

## REFERENCES

Alexander C, Andersson HS, Andersson LI, Ansell RJ, Kirsch N, Nicholls IA, O'Mahony J, Whitcombe MJ (2006) Molecular imprinting science and technology: a survey of the literature for the years up to and including 2003. *Journal of Molecular Recognition: An Interdisciplinary Journal* 19: 106-180.

Alvarez-Lorenzo C, Concheiro A (2004) Molecularly imprinted polymers for drug delivery. *Journal of Chromatography B* 804: 231-245.

Arshady R, Mosbach K (1981) Synthesis of substrate-selective polymers by host-guest polymerization. *Die Makromolekulare Chemie: Macromolecular Chemistry and Physics* 182: 687-692.

BelBruno JJ (2018) Molecularly Imprinted Polymers. *Chemical reviews*.

Byrne ME, Park K, Peppas NA (2002) Molecular imprinting within hydrogels. *Advanced drug delivery reviews* 54: 149-161.

Chen L, Wang X, Lu W, Wu X, Li J (2016) Molecular imprinting: perspectives and applications. *Chemical Society Reviews* 45: 2137-2211.

Hamidi M, Azadi A, Rafiei P (2008) Hydrogel nanoparticles in drug delivery. *Advanced drug delivery reviews* 60: 1638-1649.

Saylan Y, Yilmaz F, Özgür E, Derazshamshir A, Yavuz H, Denizli A (2017) Molecular imprinting of macromolecules for sensor applications. *Sensors* 17: 898.

Takagishi T, Klotz IM (1972) Macromolecule-small molecule interactions; introduction of additional binding sites in polyethyleneimine by disulfide cross-linkages. *Biopolymers: Original Research on Biomolecules* 11: 483-491.

Whitcombe MJ, Rodriguez ME, Villar P, Vulfson EN (1995) A new method for the introduction of recognition site functionality into polymers prepared by molecular imprinting: synthesis and characterization of polymeric receptors for cholesterol. *Journal of the American Chemical Society* 117: 7105-7111.

Wulff G, Sarhan A (1972) Über die Anwendung von enzymanalog gebauten Polymeren zur Racemattrennung. *Angewandte Chemie* 84: 364-364.



## CHAPTER 2

# Molecularly imprinted hydrogels for sustained release of sunitinib in breast cancer therapy

Luca Scrivano<sup>a</sup>, Ortensia Iliaria Parisi<sup>a,b,\*</sup>, Domenico Iacopetta<sup>a</sup>, Mariarosa Ruffo<sup>a,b</sup>, Jessica Ceramella<sup>a</sup>, Maria Stefania Sinicropi<sup>a</sup>, Francesco Puoci<sup>a,b,\*</sup>.

<sup>a</sup> Department of Pharmacy, Health and Nutritional Sciences, University of Calabria, Rende (CS), Italy.

<sup>b</sup> Macrofarm s.r.l., c/o Department of Pharmacy, Health and Nutrition Sciences, University of Calabria, Rende (CS), Italy.

*Polymers for Advanced Technology (2018),*

*DOI: 10.1002/pat.4512*

## ABSTRACT

The present work reports on the synthesis of a molecularly imprinted polymer (MIP) based on methacrylic acid and ethylene glycol dimethacrylate for sunitinib delivery. Sunitinib (SUT) is a tyrosine kinase inhibitor used in many cancer diseases. Like the majority of the anticancer drugs, SUT suffers of a low bioavailability and, at the same time, it is characterized by a narrow therapeutic window. In order to reduce drug systemic toxicity, we synthesized a MIP-based drug delivery system for SUT controlled release.

MIP was obtained by bulk polymerization through the so-called “non-covalent approach”. Rebinding experiments were performed to evaluate the success of the imprinting process and the ability of MIP to bind in a specific and selective fashion the template molecule. Resulting data showed that sunitinib rebinding percentage was 70%, while non-imprinted polymer (NIP) rebinding percentage was 46%. A not significant difference was observed between MIP and NIP in semaxanib binding experiments.

Moreover, the drug release profiles were studied for both MIP and NIP. A sustained release was observed from sunitinib-loaded MIP during 24 h, reaching 58% after 6 h and 76% at the end-point. NIP, on the contrary, released almost 90% of the loaded drug within 6 h.

Furthermore, the drug carrier was tested *in vitro* against MCF-7 cells, in which the cytotoxic effect of sunitinib released from MIP reached the maximum after 72 hours, while NIP completed its effect within 48 hours.

These results demonstrated that molecularly imprinted polymers are suitable systems for SUT sustained release.

## INTRODUCTION

Polymeric hydrogels as drug delivery systems (DDSs) represent highly hydrophilic and biocompatible devices widely employed in the pharmaceutical field. They are characterized by a three-dimensional cross-linked architecture, insoluble in organic solvents and aqueous media, but able to absorb large amounts of water molecules (Tamai, Tanaka et al., 1996). Water absorption causes swelling of the polymeric matrix that, in this way, will resemble more to human tissues. This phenomenon, indeed, contributes to the flexibility and softness of the material and reduces irritation of cells exposed to it (Xinming, Yingde et al., 2008). The swelling ability is also an important characteristic that must be taken into account during the design of these systems, since it greatly influences drug loading and release. Polymeric hydrogels can be engineered in order to control swelling degree in biological fluids. The swelling degree, indeed, allows to modulate drug release kinetics when the release process is based on a diffusive mechanism across the polymeric matrix. The modulation of the swelling capability can be usefully exploited to reduce dose-dependent adverse side effects and to maintain the desired drug concentration within the therapeutic window, avoiding administration of high doses of drug. This characteristic is important when hydrogels are applied as DDSs, especially for cytotoxic drugs, such as anticancer agents.

In this scenario, molecularly imprinted polymers (MIPs) are smart materials that can be applied as drug delivery hydrogel systems, endowed of the ability to selectively recognize a specific molecule (Cormack & Elorza, 2004). Recognition is based on the interactions between functional chemical groups exposed on the internal surface of the polymer cavities and the drug substance. The creation of complementary cavities is possible thanks to the presence of the drug molecule that acts as template during polymerization process (Cormack & Elorza, 2004). In order to synthesize MIPs, generally the template molecule is added to a mixture containing one or more functional monomers, forming the so-called pre-polymerization complex. Subsequently, a suitable cross-linker is added to achieve the reticulated network, which is the basic structure of the hydrogel. The formation of the complex can be obtained by different interactions, such as covalent, non-covalent, metal ions mediated and non-polar bonds (Mayes & Whitcombe, 2005).

In MIP-based delivery systems, drug release rate is usually decreased, if compared to conventional hydrogels, due to the specific interactions between monomer functional groups and template chemical moieties. The affinity of the drug for the polymer binding sites and, eventually, the release rate, can be finely tuned by controlling the amount, number and type of co-monomers and cross-linkers used during polymerization process. Hydrogels are usually synthesized starting from polar monomers that can be also exploited to form polar interactions with templates in molecularly imprinting polymerizations. At the same time, pH-sensitive or thermo-sensitive monomers can be inserted in the polymeric matrix in order to achieve stimuli-responsive systems (Curcio, Puoci et al., 2010, Gemeinhart, Chen et al., 2000).

In the present work, methacrylic acid (MAA) and ethylene glycol dimethacrylate (EGDMA) have been employed as functional monomer and cross-linker, respectively, to prepare a sunitinib imprinted polymer. MAA and EGDMA are monomeric compounds largely used as building blocks for hydrogels synthesis (Ahmed, 2015, Xinming et al., 2008). The polymeric form of MAA, namely poly(methacrylic acid) (PMAA) has been demonstrated to be a good biomaterial for medical and pharmaceutical applications in several papers (Cosmetic Ingredient Review Expert, 2005, Lally, Mackenzie et al., 2007). Poly(methacrylic acid) is a versatile and cheap polymer: it can be easily produced *via* free radical polymerization or anionic polymerization, with a strict control of the molecular weight (Leon, Vincent et al., 1994). Due to the presence of carboxylic moieties in the backbone, PMAA is a good hydrogen bonds acceptor and donor macromolecule. Moreover, the 3D cross-linked MAA-EGDMA copolymer is a suitable material, widely employed for bulk synthesis of MIPs applied as DDSs (Parisi, Morelli et al., 2014, Puoci, Cirillo et al., 2008). In MAA-based MIPs the amount of monomer can be set to obtain more specific or more non-specific bonds with the template. On the other hand, the amount of EGDMA is responsible for the rigidity of the network and contributes to the swelling property (the lower the EGDMA quantity, the higher the flexibility of the matrix and the higher the swelling degree) (Wolfe & Scopazzi, 1989). For this reason, the MAA/EGDMA ratio should be carefully chosen in order to obtain the aimed characteristics.

Several research works report on MIPs as DDSs for different kind of drugs such as FANS (Mahkam & Poorgholy, 2011), antibiotics (Alvarez-Lorenzo, Yanez et al., 2006), anti-asthmatic (Norell, Andersson et al., 1998), corticosteroids (Wang,

Javadi et al., 2010) and anticancer drugs (Puoci, Iemma et al., 2007). However, the main commercialized application of MIPs concerns the field of chromatography and solid phase extraction (SPE). A number of companies, indeed, have introduced on the market MIP-based products for a range of applications including SPE, HPLC and drug screening (Lok & Son, 2009, van Nostrum, 2005). On the contrary, molecularly imprinted polymers have yet not found any commercial applications as drug carriers, but several research studies are in progress in the aim to develop MIP-based DDSs to be marketed.

In this article, it is shown the successful imprinting of sunitinib (SUT), a third-generation multi-targeted tyrosine kinase inhibitor, administered *per os* for the treatment of gastrointestinal stromal tumors, advanced renal cell carcinoma and progressive, well-differentiated pancreatic neuroendocrine tumors (Blumenthal, Cortazar et al., 2012, Rock, Goodman et al., 2007). Moreover, SUT release profile and activity on MCF-7 human breast cancer cell line have been studied. It is, indeed, known that SUT has a potential cytotoxic activity on breast cancer cells, as published in previous papers (Parisi, Morelli et al., 2015, Scrivano, Iacopetta et al., 2017).

## EXPERIMENTAL SECTION

### Materials

Methacrylic acid (MAA), ethylene glycol dimethacrylate (EGDMA), 2,2'-azobisisobutyronitrile (AIBN), sunitinib malate (SUT), semaxanib (SEM), bovine serum albumin (BSA), disodium hydrogen phosphate ( $\text{Na}_2\text{HPO}_4$ ), sodium dihydrogen phosphate ( $\text{NaH}_2\text{PO}_4$ ), hydrochloric acid (HCl), acetic acid ( $\text{CH}_3\text{COOH}$ ) and HPLC-grade solvents were purchased by Sigma-Aldrich s.r.l.

AIBN was recrystallized in methanol and MAA was purified on alumina column before use.

Absorption spectra were recorded with a Jasco V-530 UV/Vis spectrometer.

### Synthesis of sunitinib molecularly imprinted polymer

Sunitinib imprinted polymer was synthesized *via* free radical bulk polymerization (Puoci et al., 2008).

In brief, 0.5 mmol of SUT and 16 mmol of MAA were dissolved in 5 mL of chloroform in a glass vial. The vial was put in a sonicating water bath for 10 min at room temperature to allow the complete dissolution of the template molecule and the formation of the pre-polymerization complex. Afterwards, 25 mmol and 100 mg of EGDMA and AIBN, respectively, were added to the solution and sonicated again in a water bath at 4°C for 5 min. The mixture was then purged with nitrogen in order to remove oxygen and the vial was sealed and put in an oil bath at 60°C, to initiate the radical polymerization. Reaction was left stirring overnight.

After 24 h, the bulk was recovered and grinded using a mill machine and the powder was passed through a 63 µm steel sieve. Particles below 63 µm were suspended in acetone for 30 min and the supernatant was discarded. Pelleted MIP particles were washed three times with DMSO and then with a Soxhlet system with acetonitrile/acetic acid mixture (9:1) for 6 h and with acetonitrile for further 6 h, in order to remove SUT template. Finally, SUT-imprinted polymer was washed with acetone and diethyl ether 3 times each and dried under vacuum overnight. No remaining template was detected using UV/Vis spectrophotometry.

A control non-imprinted polymer (NIP) was synthesized and purified following exactly the same procedure, but in the absence of SUT.

### **Binding experiments**

In order to evaluate SUT binding affinity towards MIP, rebinding studies were carried out dispersing 100 mg of MIP or NIP in 1 mL of SUT standard solution 0.30 mM in acetonitrile. The suspensions were kept under agitation at room temperature for 6 h, and then they were centrifuged at 9000 rpm for 10 min. Supernatants were finally read using UV/Vis spectrophotometer at SUT  $\lambda_{\text{max}}=430$  nm. Concentrations were calculated using the equation of the calibration curve of SUT in acetonitrile, recorded in the range of 400-500 nm.

MIP selectivity was investigated applying the same protocol but using a SEM standard solution 0.30 mM in acetonitrile. As previously mentioned, blank polymer NIP was also used as control for selectivity studies.

All the experiments were repeated three times.

### Water content and swelling ability

In order to estimate the swelling ability of the polymers, the water content after immersing them in phosphate buffered saline (PBS) solution was measured.

Briefly, dry aliquots of ~50 mg of MIP or NIP particles were placed in two different 5 mL sintered glass filters ( $\varnothing$  10 mm – 4 porosity), weighed, immersed in PBS solution at pH 7.4 and left to swell until they reached the maximum water content. Tares were obtained by weighing wet filters after centrifugation at 2500 rpm for 5 min. At 0, 2, 4, 6, 8, 24, 48, 72, 168 h time points the excess of water was removed from the samples by percolation at atmospheric pressure and then by centrifugation of the filters at 2500 rpm for 5 min. Finally, filters were weighed and the water content percentage was calculated through the following equation (2.1):

$$WR \% = \frac{W_s - W_d}{W_d} \times 100 \quad (2.1)$$

where  $W_s$  and  $W_d$  represent weights of swollen and dry polymer particles, respectively.

Each experiment was carried out in triplicate.

### Bovine serum albumin adsorption

Two sets, for both MIP and NIP, of three samples were prepared by packing 300 mg of polymer particles into a 6.0 mL polypropylene SPE column. The columns were attached through stopcocks to reservoirs at the bottom end.

Preconditioning of the columns was carried out prior to use by several washing steps with water, HCl (0.07 M), water, methanol/water mixture 1:1, water, and 25 mM PBS solution. Afterwards, the columns were loaded with 2.0 mL of a BSA standard solution 1.2 mg/mL in PBS. The eluted solution was analyzed with a UV/Vis spectrophotometer at BSA  $\lambda_{\max}$ =280 nm and the amount of adsorbed BSA was calculated using the equation obtained from the BSA calibration curve recorded at 280 nm.

### Drug loading and release studies

20 mg of SUT was put in a 10 mL round bottom flask, dissolved with 2 mL of acetonitrile and sonicated for 2 min at room temperature. Later, 180 mg of MIP

was added to the solution and soaked under agitation at room temperature in the dark. Samples were kept away from light for 3 days and then dried under vacuum to remove the organic solvent. The same protocol was followed to load the NIP particles with the drug.

Following the drug loading, in a 15 mL tube 10 mg of SUT-loaded MIP was put together with 5 mL of HCl solution 0.1 N (pH 1.0) and incubated under shaking for 2 h at 37°C. After 2 h, 1.25 mL of a solution Na<sub>2</sub>HPO<sub>4</sub> 0.4 M was added to increase pH value to 6.8. Withdrawals of 1 mL were made at predetermined intervals of time (1, 2, 3, 4, 5, 6 and 24 h), and at each time the final volume was restored adding 1 mL of medium.

Withdrawn volumes were read with a UV-Vis spectrophotometer and the amounts of released SUT were calculated from the equation of the calibration curve of SUT.

Experiments were conducted in triplicate.

### **Cell viability**

*Cell culture.* The cell lines used in this work have been purchased from American Type Culture Collection (ATCC, Manassas, VA, USA). Media and additives have been purchased from Thermo Fisher (Milan, Italy) unless otherwise stated.

Human estrogen receptor (ER)-positive MCF-7 breast cancer cells were cultured in DMEM-F12 medium containing 10% Fetal Bovine Serum (FBS), supplemented with 2 mmol/L L-glutamine and 1 mg/mL penicillin-streptomycin.

MCF-10a human mammary epithelial cells were cultured in DMEM/F12 medium, supplemented with 5% Horse Serum (HS), 100 U/mL penicillin/streptomycin, 0.5 mg/mL hydrocortisone, 20 ng/mL human epidermal growth factor (hEGF), 10 µg/mL insulin and 0.1 mg/mL cholera enterotoxin (Sigma-Aldrich, Milan, Italy).

*MTT assays.* Cell viability was determined by using the 3-(4,5-dimethylthiazol-2-yl)-2,5-diphenyltetrazolium (MTT, Sigma, Milan, Italy) assay, as previously described (Rizza, Pellegrino et al., 2016).

Briefly, cells were plated in quadruplicate on 48-well plates (full media), then serum starved for 24 hours and treated with vehicle (DMSO, Sigma, Milan, Italy) or MIP, SUT and MIP and NIP particles loaded with the drug (MIP-SUT and



NIP-SUT, respectively) at the concentration of 76  $\mu\text{M}$  in 1% FBS (MCF-7) or HS (MCF-10a). At the end of the experiment, 100  $\mu\text{L}$  of MTT stock solution (2 mg/mL) in phosphate buffered saline (PBS, Thermo Fisher, Milan, Italy) was added into each well and incubated for 2 hours at 37°C, followed by removal of media and addition of 500  $\mu\text{L}$  of DMSO. Plates were shaken for 15 minutes, and the absorbance was measured at 570 nm in each well, including the blanks. Standard deviations are shown as error bars.

## RESULTS AND DISCUSSION

### Synthesis of the polymers

Sunitinib imprinted polymers were synthesized by bulk polymerization with a non-covalent approach and using SUT, MAA, EGDMA, chloroform and AIBN as template, functional monomer, cross-linker co-monomer, porogenic organic solvent and initiator, respectively. The non-covalent approach is based on hydrogen bonds, Van der Waals or hydrophobic interactions between template and monomers. This approach is widely used for molecular imprinting technique since it provides faster kinetic of pre-polymerization complex formation and template removal. MAA in particular is a good acceptor and donor of hydrogen bonds and most likely it can establish them with the amide groups of SUT molecule (Figure 2.1).

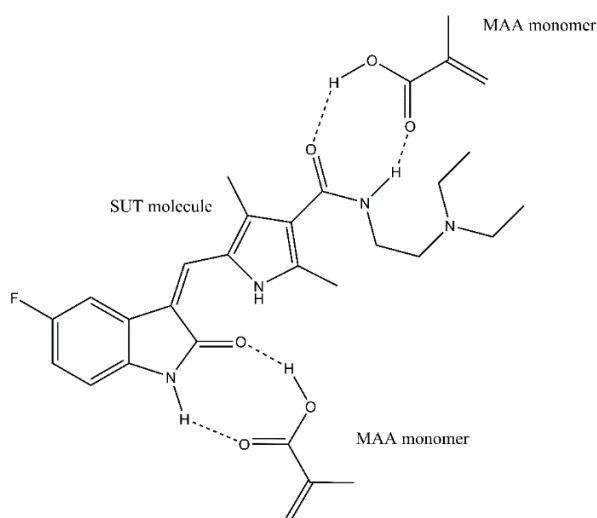


**Figure 2.1** SUT-MAA pre-polymerization complex.

The chosen cross-linker, EGDMA, affects MIPs binding capacity and selectivity. The cross-linking agent, indeed, is able to stabilize the position of monomer functional groups around the analyte. This leads to the formation of a highly cross-linked polymer characterized by a three-dimensional macroporous structure, which contains binding cavities complementary to the template. At the same time, chloroform contributes to the formation of the cavities thanks to its porogenic activity. The solvent is also employed to obtain a homogeneous mixture of all the components and to maximize the interaction between template and monomers. For this reason, a low polar organic solvent, such as chloroform, was used for the purpose (Haginaka, Tabo et al., 2008, Meier, Schott et al., 2012).

According to our experience and to the obtained results, the optimal SUT/MAA/EGDMA molar ratio for sunitinib imprinted polymer is 0.5:16:25.

The synthesized polymer monolith was grinded, sieved and suspended in acetone in order to collect particles with irregular shape in the range of 20-63  $\mu\text{m}$ .

### Imprinting and binding studies

After complete removal of the template from MIP, SUT rebinding experiments were carried out in order to evaluate the success of the imprinting process and the ability to specifically and selectively bind the template molecule. For this purpose, binding comparison between SUT and its analogue semaxanib (SEM) was performed. As shown in Figure 2.2, both molecules share the pyrrol-indolinone core, which represents the basic structure of this kind of drugs, i.e. tyrosine kinase inhibitors.

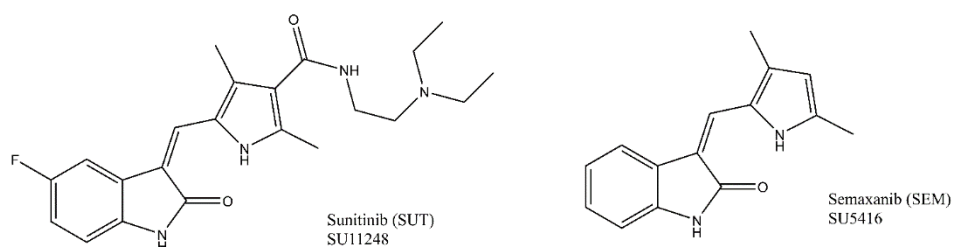


**Figure 2.2.** Chemical structures of sunitinib (SUT) and semaxanib (SEM).

In Table 2.1 rebinding results are reported. Data showed that sunitinib rebinding percentage was 70%, while non-imprinted polymer (NIP) rebinding percentage was 46%. In this case, the molecular imprinting efficiency ( $\alpha$ ), expressed as the ratio of MIP rebinding percentage to NIP rebinding percentage ( $\alpha = \text{MIP}$

rebinding %: NIP rebinding %), is 1.52 that is an acceptable value in the field of molecularly imprinted polymers (Muhammad, Tu et al., 2017).

On the other hand, a not significant difference was observed between MIP and NIP in semaxanib binding experiments and the selectivity coefficient ( $\epsilon$ ), expressed as the ratio SUT binding percentage to SEM binding percentage for MIP, is 1.38. Therefore, the imprinted polymer is 1.38 times more selective for the therapeutic agent than the non-imprinted material.

**Table 2.1** Binding percentage of both MIP and NIP when put in contact with SUT and its structural analogue SEM. Data are shown as means  $\pm$  standard deviations (SD).

Polymer	SUT binding (%)	SEM binding (%)
MIP	70.0 $\pm$ 0.7	50.9 $\pm$ 1.0
NIP	46.0 $\pm$ 0.6	48.3 $\pm$ 0.7

### Swelling and hydrophilic properties: water and BSA adsorptions

Although molecularly imprinted polymers are usually highly cross-linked networks, MIPs still preserve swelling ability in aqueous environments, such as interstitial, gastrointestinal and lymphatic fluids, blood and so on. There are no statistically significant differences between MIP and NIP. Both maintain the same swelling degree over time, meaning that the imprinting process does not affect the swelling behaviour. However, the maximum water absorption capacity in PBS is readily reached after 2 h and it is kept constant (Figure 2.3 *left*).

Moreover, protein adsorption was evaluated using albumin as model protein; BSA represents indeed a good model, being a small water soluble protein, characterized by several hydrophobic  $\alpha$ -helix domains (Militello, Vetri et al., 2003). For this purpose, a solid-phase extraction apparatus was employed. From the eluted fractions, the percentages of adsorbed BSA were calculated: 73.6%  $\pm$  0.7 and 75.5%  $\pm$  0.9 for MIP and NIP, respectively.

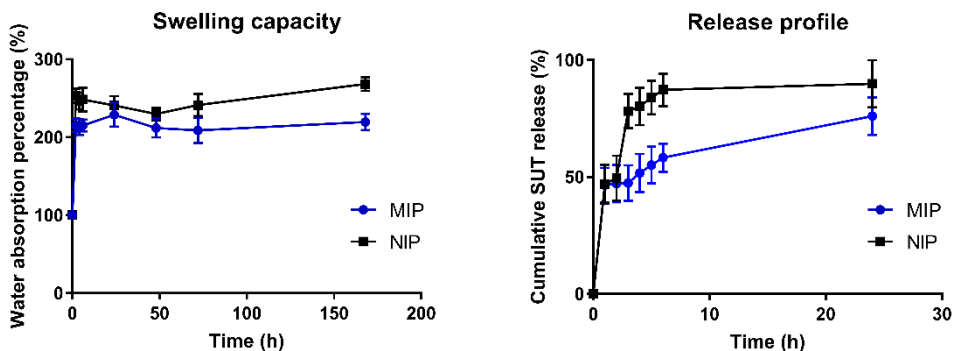


**Figure 2.3** MIP (●) and NIP (■) swelling kinetics over time (1 week) (*left*); *in vitro* sunitinib release profile (*right*).

### Drug release profile

MIP and NIP microparticles were loaded with SUT in 1:9 SUT/polymer mass ratio and the drug release profiles were studied for both the polymeric materials.

A sustained release was observed from sunitinib-loaded MIP during 24 h, reaching 58% after 6 h and 76% at the end point. NIP, on the contrary, released almost 90% of the loaded drug within the first 6 h (Figure 2.3 *right*). The drug impregnation method is responsible for the burst release. The first point represents, in fact, the amount of SUT adsorbed on polymers surface, namely non-specifically bound. This phenomenon might be exploited to rapidly reach the therapeutic concentration, which is then kept within the therapeutic window thanks to the controlled release of SUT.

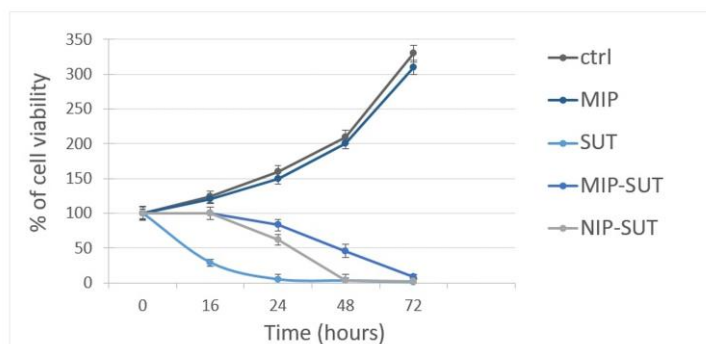
### *In vitro* cytotoxicity

In order to evaluate the effectiveness of MIP-SUT and NIP-SUT on the viability of MCF-7 cells, we performed MTT assays using a concentration of SUT able to kill breast cancer cells after 24 h of treatment. This concentration, equal to 76  $\mu\text{M}$ , was extrapolated from SUT  $\text{IC}_{50}$  value calculation obtained from our previous study (data not shown) using our MCF-7 cell cultures. Effectively, the viability of SUT-treated MCF-7 cells after 16 h was of about 30% compared to the vehicle-treated cells and, as attended, kills all the cells after 24 h. Conversely, MIP-SUT and NIP-SUT did not exert any measurable effect after 16 h, but after 24 h a reduction in cell viability of about  $38 \pm 0.8\%$  and  $27 \pm 0.6\%$  for MIP-SUT and NIP-SUT, respectively, was observed. Moreover, after 48 h NIP-SUT treated

cells viability was drastically reduced indicating the death of almost all cancer cells in the wells, whereas a residual viability of about the  $45 \pm 1.0\%$  was observed in MIP-SUT treated cells. Finally, after 72 h MIP-SUT effects on cell viability were total. These results clearly highlight how NIP and MIP formulations of SUT were able to release the drug in a time dependent manner, inducing slight effects after 24 h and reaching the higher antitumor activity after 48 and 72 h for NIP and MIP, respectively. We also evaluate the possible cytotoxic effects of MIP by itself during the time of the experiment, but, as noticeable from Figure 2.4, viability of MIP-treated cells did not differ from that of vehicle treated cells (ctrl) at each time point, suggesting that MIP alone did not affect cell growth.

Moreover, the treatment of SUT, MIP-SUT and NIP-SUT did not affect the viability of MCF-10a cells used as non-tumor counterpart, in order to verify the absence of possible cytotoxic effects of our materials.

Panel A: MCF-7



Panel B: MCF-10a

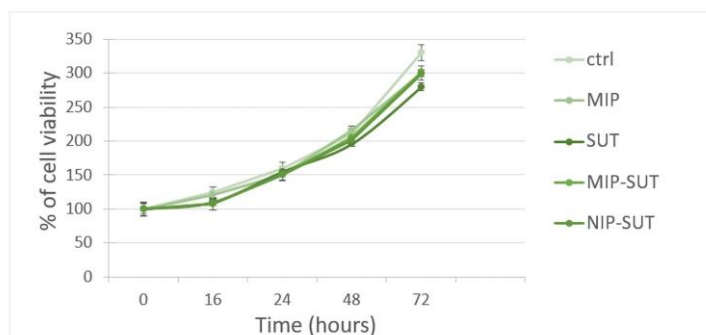


**Figure 2.4** Viability evaluation of MCF-7 (Panel A) or MCF-10a (Panel B) cells treated with SUT alone or encapsulated in MIP and NIP polymers. Figure shows also the vehicle treated cells and the polymer by itself activity on cell proliferation.

## CONCLUSIONS

In the present article, the successful synthesis of sunitinib imprinted polymers has been demonstrated. Selectivity and specificity of MIP has been proven by rebinding studies with good results (see  $\alpha$  and  $\epsilon$  values). The swelling behaviour and the application of the polymer as drug delivery hydrogel has been also tested, demonstrating that this system possesses a controlled drug release and, at the same time, the ability to absorb large amounts of water. Moreover, the imprinting effect and controlled release has been successfully exploited in *in vitro* cell viability test.

These results demonstrated once again that molecularly imprinted polymers are suitable systems for anticancer drug release and, in particular, MAA-co-EGDMA-based polymers, imprinted using SUT as template, are suitable carriers for breast cancer treatment.

## REFERENCES

- Ahmed EM (2015) Hydrogel: Preparation, characterization, and applications: A review. *Journal of advanced research* 6: 105-121.
- Alvarez-Lorenzo C, Yanez F, Barreiro-Iglesias R, Concheiro A (2006) Imprinted soft contact lenses as norfloxacin delivery systems. *Journal of Controlled Release* 113: 236-244.
- Blumenthal GM, Cortazar P, Zhang JJ, Tang S, Sridhara R, Murgo A, Justice R, Pazdur R (2012) FDA approval summary: sunitinib for the treatment of progressive well-differentiated locally advanced or metastatic pancreatic neuroendocrine tumors. *The oncologist: theoncologist-2012*.
- Cormack PAG, Elorza AZ (2004) Molecularly imprinted polymers: synthesis and characterisation. *Journal of chromatography B* 804: 173-182.
- Cosmetic Ingredient Review Expert P (2005) Final report of the safety assessment of methacrylic acid. *International journal of toxicology* 24: 33.
- Curcio M, Puoci F, Spizzirri UG, Iemma F, Cirillo G, Parisi OI, Picci N (2010) Negative thermo-responsive microspheres based on hydrolyzed gelatin as drug delivery device. *Aaps Pharmscitech* 11: 652-662.
- Gemeinhart RA, Chen J, Park H, Park K (2000) pH-sensitivity of fast responsive superporous hydrogels. *Journal of Biomaterials Science, Polymer Edition* 11: 1371-1380.
- Haginaka J, Tabo H, Kagawa C (2008) Uniformly sized molecularly imprinted polymers for d-chlorpheniramine: Influence of a porogen on their morphology and enantioselectivity. *Journal of pharmaceutical and biomedical analysis* 46: 877-881.
- Lally S, Mackenzie P, LeMaitre CL, Freemont TJ, Saunders BR (2007) Microgel particles containing methacrylic acid: pH-triggered swelling behaviour and potential for biomaterial application. *Journal of colloid and interface science* 316: 367-375.
- Leon A, Vincent B, Cawdery N (1994) The synthesis and characterization of monodisperse poly (acrylic acid) and poly (methacrylic acid). *Colloid and Polymer Science* 272: 427-432.

Lok CM, Son R (2009) Application of molecularly imprinted polymers in food sample analysis—a perspective. *International Food Research Journal* 16: 127-140.

Mahkam M, Poorgholy N (2011) Imprinted polymers as drug delivery vehicles for anti-inflammatory drugs. *Nat Sci* 9: 163-168.

Mayes AG, Whitcombe MJ (2005) Synthetic strategies for the generation of molecularly imprinted organic polymers. *Advanced drug delivery reviews* 57: 1742-1778.

Meier F, Schott B, Riedel D, Mizaikoff B (2012) Computational and experimental study on the influence of the porogen on the selectivity of 4-nitrophenol molecularly imprinted polymers. *Analytica chimica acta* 744: 68-74.

Militello V, Vetri V, Leone M (2003) Conformational changes involved in thermal aggregation processes of bovine serum albumin. *Biophysical chemistry* 105: 133-141.

Muhammad P, Tu X, Liu J, Wang Y, Liu Z (2017) Molecularly imprinted plasmonic substrates for specific and ultrasensitive immunoassay of trace glycoproteins in biological samples. *ACS applied materials & interfaces* 9: 12082-12091.

Norell MC, Andersson HS, Nicholls IA (1998) Theophylline molecularly imprinted polymer dissociation kinetics: a novel sustained release drug dosage mechanism. *Journal of Molecular Recognition: An Interdisciplinary Journal* 11: 98-102.

Parisi OI, Morelli C, Puoci F, Saturnino C, Caruso A, Sisci D, Trombino GE, Picci N, Sinicropi MS (2014) Magnetic molecularly imprinted polymers (MMIPs) for carbazole derivative release in targeted cancer therapy. *Journal of Materials Chemistry B* 2: 6619-6625.

Parisi OI, Morelli C, Scrivano L, Sinicropi MS, Cesario MG, Candamano S, Puoci F, Sisci D (2015) Controlled release of sunitinib in targeted cancer therapy: smart magnetically responsive hydrogels as restricted access materials. *RSC Advances* 5: 65308-65315.

Puoci F, Cirillo G, Curcio M, Iemma F, Parisi OI, Castiglione M, Picci N (2008) Molecularly imprinted polymers for  $\alpha$ -tocopherol delivery. *Drug delivery* 15: 253-258.



Puoci F, Iemma F, Cirillo G, Picci N, Matricardi P, Alhaique F (2007) Molecularly imprinted polymers for 5-fluorouracil release in biological fluids. *Molecules* 12: 805-814.

Rizza P, Pellegrino M, Caruso A, Iacopetta D, Sinicropi MS, Rault S, Lancelot JC, El-Kashef H, Lesnard A, Rochais C (2016) 3-(Dipropylamino)-5-hydroxybenzofuro [2, 3-f] quinazolin-1 (2H)-one (DPA-HBFQ-1) plays an inhibitory role on breast cancer cell growth and progression. *European journal of medicinal chemistry* 107: 275-287.

Rock EP, Goodman V, Jiang JX, Mahjoob K, Verbois SL, Morse D, Dagher R, Justice R, Pazdur R (2007) Food and Drug Administration drug approval summary: Sunitinib malate for the treatment of gastrointestinal stromal tumor and advanced renal cell carcinoma. *The oncologist* 12: 107-113.

Scrivano L, Iacopetta D, Sinicropi MS, Saturnino C, Longo P, Parisi OI, Puoci F (2017) Synthesis of sericin-based conjugates by click chemistry: enhancement of sunitinib bioavailability and cell membrane permeation. *Drug delivery* 24: 482-490.

Tamai Y, Tanaka H, Nakanishi K (1996) Molecular dynamics study of polymer-water interaction in hydrogels. 1. Hydrogen-bond structure. *Macromolecules* 29: 6750-6760.

van Nostrum CF (2005) Molecular imprinting: A new tool for drug innovation. *Drug discovery today: technologies* 2: 119-124.

Wang C, Javadi A, Ghaffari M, Gong S (2010) A pH-sensitive molecularly imprinted nanospheres/hydrogel composite as a coating for implantable biosensors. *Biomaterials* 31: 4944-4951.

Wolfe MS, Scopazzi C (1989) Rheology of swellable microgel dispersions: Influence of crosslink density. *Journal of colloid and interface science* 133: 265-277.

Xinming L, Yingde C, Lloyd AW, Mikhalovsky SV, Sandeman SR, Howel CA, Liewen L (2008) Polymeric hydrogels for novel contact lens-based ophthalmic drug delivery systems: A review. *Contact Lens and Anterior Eye* 31: 57-64.



## CHAPTER 3

# Molecularly imprinted microrods *via* mesophase polymerization

Ortensia Ilaria Parisi<sup>a,b</sup>, Luca Scrivano<sup>a</sup>, Sebastiano Candamano<sup>c</sup>, Mariarosalia Ruffo<sup>b</sup>, Anna Francesca Vattimo<sup>b</sup>, Maria Vittoria Spanedda<sup>d</sup> and Francesco Puoci<sup>a,b,\*</sup>.

<sup>a</sup> Department of Pharmacy, Health and Nutritional Sciences, University of Calabria, Rende (CS), Italy.

<sup>b</sup> Macrofarm s.r.l., c/o Department of Pharmacy, Health and Nutrition Sciences, University of Calabria, Rende (CS), Italy.

<sup>c</sup> Department of Environmental and Chemical Engineering, University of Calabria, Rende (CS), Italy.

<sup>d</sup> Faculty of Pharmacy, CNRS-University of Strasbourg, Illkirch, France.

*Molecules* (2018), 23, 63.

DOI: 10.3390/molecules23010063

## ABSTRACT

The aim of the present research work was the synthesis of molecularly imprinted polymers (MIPs) with a rod-like geometry *via* “mesophase polymerization”. The ternary lyotropic system consisting of sodium dodecyl sulfate (SDS), water and decanol was chosen to prepare a hexagonal mesophase to direct the morphology of the synthesized imprinted polymers using theophylline, methacrylic acid and ethylene glycol dimethacrylate as a drug model template, a functional monomer, and a cross-linker, respectively. The obtained molecularly imprinted microrods (MIMs) were assessed by performing binding experiments and *in vitro* release studies, and the obtained results highlighted good selective recognition abilities and sustained release properties. In conclusion, the adopted synthetic strategy involving a lyotropic mesophase system allows for the preparation of effective MIPs characterized by a rod-like morphology.

## INTRODUCTION

Nowadays, particles characterized by an anisotropic shape are attracting significant interest due to their use for the production of materials with advanced microstructure, special symmetries, and unique structural, mechanical, optical, and electrical properties. Among them, rod-like polymeric particles on a micrometer scale enjoy a variety of applications as, for example, fibrillar matrices for cell attachment and growth and as delivery systems for the local release of drugs, growth factors, and bioactive molecules in tissue repair and regeneration (Doroudian, Pinney et al., 2014).

Molecularly imprinted polymers (MIPs) have been widely used for the development of drug delivery systems (DDSs) able to release therapeutic agents in a sustainable way (Fareghi, Moghadam et al., 2017, Luliński, 2017, Parisi, Morelli et al., 2014, Puoci, Cirillo et al., 2008). These polymeric materials are characterized by the presence of recognition cavities complementary in shape, size, and functional groups to a target molecule, which acts as a template during the polymerization process. Molecular imprinting, indeed, represents an advanced and effective technique for the preparation of polymeric matrices with selective recognition capabilities for a desired template molecule in preference to other closely related compounds and involves three main steps for the synthesis of MIPs (Gui, Jin et al., 2018). The first one consists of the formation of a pre-polymerization complex between the template molecule and suitable functional monomers. For this purpose, the chosen monomers have to exhibit chemical structures able to interact with the functional groups of the template in a covalent or non-covalent way. The second phase involves the polymerization around the target molecule, in the presence of a porogenic solvent and a cross-linking agent, resulting in a highly cross-linked three-dimensional matrix. Finally, the template removal allows for obtaining a porous polymeric material with specific binding sites able to recognize and rebind the target molecule in a selective way.

Few examples of imprinted polymeric microrods have been reported in the literature describing the electrochemical synthesis of surface-imprinted polymers selective for protein recognition and characterized by the presence of protein-binding sites located on their surface (Ceolin, Orbán et al., 2013, Menaker, Syritski et al., 2009). The synthetic approach involves the use of sacrificial cylindrical microreactors such as track-etched polycarbonate membrane (PCM) filters. For instance, nanostructured molecularly imprinted polymeric films

prepared in a liquid crystalline medium (triton X-100/water) and exhibiting discernible 40 nm thick nanofiber structures were reported by Suriyanarayanan et al. (Suriyanarayanan, Nawaz et al., 2014). Despite the relevant progress made in the field of nanorod, nanowire, and nanotube preparation (Biazar, 2017, Oladipo, Oluwafemi et al., 2017, Sharma, Jain et al., 2013, Zhou, Ma et al., 2013), few synthetic strategies have been established for the development of rod-like particles on a micrometer scale.

In this context, the aim of the present research study was to synthesize imprinted polymeric microrods selective for a model drug template, such as theophylline (THEO), *via* “mesophase polymerization”.

For this purpose, methacrylic acid (MAA) and ethylene glycol dimethacrylate (EGDMA) were used as a functional monomer and a cross-linking agent, respectively. This choice was motivated by their biocompatibility in polymerized form. Several works, indeed, report on the extensive use of MAA and EGDMA for the preparation of polymeric materials to be used in biomedical and pharmaceutical fields as drug delivery systems or for tissue engineering applications (Girones Molera, Mendez et al., 2012, Priya James, John et al., 2014, Traitel, Goldbart et al., 2008, Xinming, Yingde et al., 2008).

Polymerization within a lyotropic liquid crystalline media represents one of the most promising approaches for the synthesis of functional polymeric materials with controlled geometries and unique properties that cannot be reached using conventional bulk or precipitation polymerization.

The adoption of this kind of strategy based on mesophase polymerization for the synthesis of molecularly imprinted microrods (MIMs) represents a challenge in the world of molecular imprinting. This system could indeed interfere with the formation of specific interactions between the target molecule and the functional monomers during the pre-polymerization step, which is crucial to confer selective recognition abilities to the polymers. The strength and the stability of the initial interactions, indeed, strongly affect the selective adsorption capacities of MIPs. In the present study, the synthesis of molecularly imprinted microrods *via* mesophase polymerization was successfully reported for the first time.

## RESULTS AND DISCUSSION

### **Synthesis of molecularly imprinted microrods (MIMs) *via* mesophase polymerization**

The use of a lyotropic system as a “template” allows for the preparation of polymeric materials characterized by a highly anisotropic structure, which can be useful for a wide range of applications including ultrafiltration, biological membranes, and tissue scaffolds.

The formation of lyotropic liquid crystalline mesophases (LLCs) is due to the self-assembling of amphiphilic molecules in the presence of solvent and a number of different LLC morphologies can be achieved varying the nature of the surfactant, its concentration and temperature (DePierro & Guymon, 2014). In particular, micelles are obtained at low concentrations of surfactant in polar solvent, while hexagonal and lamellar phases are observed at higher concentrations.

Three main strategies can be employed: the polymerization of conventional monomers in a non-polymerizable mesophase, the polymerization of polymerizable surfactant mesophases, and, finally, the copolymerization of traditional monomers with polymerizable surfactant mesophases (Yan & Texter, 2006).

In the present research work, the ternary lyotropic system consisting of sodium dodecyl sulfate (SDS), water and decanol was chosen to prepare a hexagonal mesophase, in which monomers were segregated into an ordered geometry, to direct the morphology of the synthesized theophylline imprinted polymers.

For this purpose, the three components of the lyotropic system were mixed according to a definite weight ratio, such as 29.0:66.5:4.5 (SDS/water/decanol wt. %), to obtain a hexagonal mesophase characterized by rod-like micellar aggregates. Then, the previously prepared mesophase was doped with a polymerization reaction mixture, consisting of theophylline (THEO), methacrylic acid (MAA), ethylene glycol dimethacrylate (EGDMA), and ammonium persulfate, and placed at 40°C to start the reaction, which involves a conventional radical polymerization.

It is reasonable to hypothesize that functional monomers and cross-linking molecules are segregated mainly in the hydrophilic regions and at the interface

of the mesophase, respectively, adopting a geometry that directly resembles rod-like morphology. The template molecule, introduced into the system in order to synthesize the imprinted materials, interacts with the functional monomers allowing for the formation of the pre-polymerization complex, which represents the key step of the imprinting process. Moreover, the occurred template-monomer interactions work to improve theophylline solubility within the lyotropic system without affecting the doped mesophase and leading to imprinted polymeric particles characterized by a similar rod-like morphology.

In order to synthesize THEO-imprinted microrods, the non-covalent approach was adopted.

This methodology is based on the formation of relatively weak non-covalent interactions, such as hydrogen bonding, in both the pre-polymerization step and the rebinding phase and represents the predominant used strategy due to its flexibility, the wide range of available functional monomers and the fast kinetics of binding.

Non-molecularly imprinted microrods (NIMs) were also prepared using the same experimental procedure, but in the absence of THEO during the polymerization process, with the aim of having a control material to be used as a reference for the evaluation of imprinting efficiency and selectivity. The adopted synthetic conditions were the same for both the imprinted and non-imprinted materials, except for the presence of the template molecule during polymerization, which not only induces the formation of selective binding sites, but also affects the physical properties of such polymers. After polymerization, indeed, the template is removed obtaining a porous material that contains specific cavities able to recognize and rebind the analyte. Surface area of MIPs, therefore, tends to be greater than surface area of NIPs due to the presence of these cavities (Sikiti, Msagati et al., 2014, Yu, Yun et al., 2011). The NIP approach, indeed, presents one limit consisting of the different porosity of the non-imprinted material, which is usually reduced due to the absence of the template molecule during the polymerization process (Cywinski, 2013).

This reduced porosity avoids the free analyte diffusion through the NIP. On the other hand, the template removal leaves a pore channel structure within the MIP matrix, which promotes the adsorption performance of the material.



The rod-like geometry of the obtained polymers templated from the hexagonal mesophase was confirmed by SEM analysis, and no significant morphological differences between the imprinted (Figure 3.1, panel a) and non-imprinted (Figure 3.1, panel b) materials were observed.

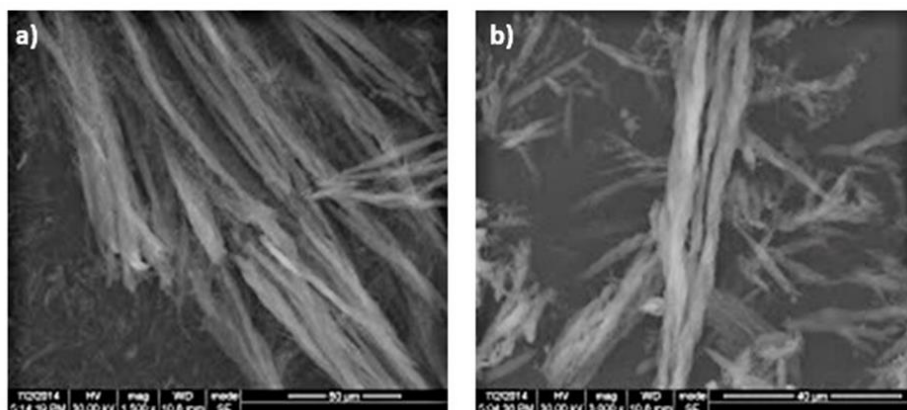


**Figure 3.1** Scanning electron micrographs of the synthesized molecularly imprinted microrods (MIMs) (a) and non-molecularly imprinted microrods (NIMs) (b).

### Imprinting effect and selectivity assessment

Binding studies were carried out with the aim of investigating the imprinting effect of the prepared MIMs.

For this purpose, amounts of the imprinted and non-imprinted microrods were incubated for 3, 6, and 24 h with THEO standard solutions prepared in  $\text{CH}_3\text{CN}$  at different concentrations, and the obtained results are reported in Table 3.1.

**Table 3.1** Percentages of bound theophylline (THEO) by imprinted (MIMs) and non-imprinted (NIMs) microrods. Data are shown as means  $\pm$  S.D.

Incubation Time (h)	Bound THEO (%) 0.6 mM		Bound THEO (%) 0.06 mM	
	MIMs	NIMs	MIMs	NIMs
3	45.8 $\pm$ 1.1	58.4 $\pm$ 0.8	23.4 $\pm$ 1.0	33.2 $\pm$ 1.1
6	50.6 $\pm$ 0.9	42.5 $\pm$ 0.7	42.7 $\pm$ 0.6	31.5 $\pm$ 0.7
24	60.7 $\pm$ 0.8	46.6 $\pm$ 0.7	49.2 $\pm$ 0.7	39.1 $\pm$ 1.2

As can be seen, the best results with a difference of about 14% between imprinted and non-imprinted microrods were obtained after 24 h of incubation and using a THEO concentration equal to 0.6 mM. The higher adsorption properties of MIMs

are due to the presence of binding cavities specific for the template molecule, which were formed during the polymerization process.

The selectivity of the synthesized imprinted polymers was investigated by performing the rebinding experiments using a 0.6 mM standard solution of caffeine (CAFF), which is a structural analogue of THEO. After 24 h of incubation, the amount of CAFF bound by MIMs and NIMs was practically the same and equal to  $39.1 \pm 0.7\%$  and  $38.3 \pm 1.1\%$ , respectively, confirming the non-specific nature of these interactions.

Molecular recognition properties and selectivity of the prepared imprinted microrods can also be expressed using two coefficients such as  $\alpha$  and  $\epsilon$ . The imprinting efficiency  $\alpha$  is determined as the ratio of adsorption percentages between MIMs and NIMs for each analyte such as THEO and CAFF, while the selectivity coefficient  $\epsilon$  is the ratio between the amount of template and analogue bound by MIMs. The  $\alpha$  and  $\epsilon$  values were calculated considering the binding percentages obtained after 24 h of incubation using 0.6 mM standard solutions of THEO and CAFF and reported in Table 3.2.

**Table 3.2** Imprinting efficiency ( $\alpha$ ) and selectivity coefficient ( $\epsilon$ ).

Imprinting Efficiency ( $\alpha$ )		Selectivity Coefficient ( $\epsilon$ )
$\alpha$ THEO	$\alpha$ CAFF	
1.3	1.0	1.5

The obtained  $\alpha$  and  $\epsilon$  values highlighted the higher binding ability and inherent selectivity for theophylline of the imprinted microrods than the corresponding NIMs ascribable to the presence of recognizing cavities into the polymeric matrix, which are formed during the polymerization process due to the addition of template molecules. These binding cavities are characterized by a shape and an orientation of the functional groups that match the template molecules leading to specific interactions. On the contrary, the intensity of the formed interactions is very weak in the absence of recognizing sites.

### ***In vitro* drug release studies**

The ability of MIMs and NIMs to act as controlled drug delivery systems was assessed in phosphate buffered saline (PBS) at pH 7.4 by the dialysis bag diffusion technique.

After the impregnation step, the drug loading content (DLC) and the drug loading efficiency (DLE) were calculated based on equations (3.1) and (3.2), respectively:

$$DLC(\%) = \frac{W_{ld}}{W_{ld} + W_{mr}} \times 100 \quad (3.1)$$

$$DLE(\%) = \frac{W_{ld}}{W_d} \times 100 \quad (3.2)$$

in which  $W_{ld}$ ,  $W_d$ , and  $W_{mr}$  are the weight of the loaded drug within the microrods, the weight of the total drug used for the impregnation procedure, and the weight of the dried microrods, respectively. The obtained DLC and DLE values are reported in Table 3.3.

**Table 3.3** Drug loading content (DLC) and drug loading efficiency (DLE).

DLC (%)		DLE (%)	
MIMs	NIMs	MIMs	NIMs
$8.9 \pm 0.6$	$7.7 \pm 0.8$	$89.0 \pm 0.7$	$76.5 \pm 0.8$

The imprinted microrods loaded a higher amount of THEO during the impregnation procedure than the corresponding non-imprinted rod-like particles due to their greater affinity for the drug molecule.

During the polymerization process, indeed, the presence of the template molecule allows for the formation of recognition sites inside the polymeric matrix, which are responsible for the higher tendency of the imprinted material to adsorb theophylline.

Furthermore, the presence of binding cavities results in a controlled THEO release by MIMs, which is more evident during the first stages (Figure 3.2).

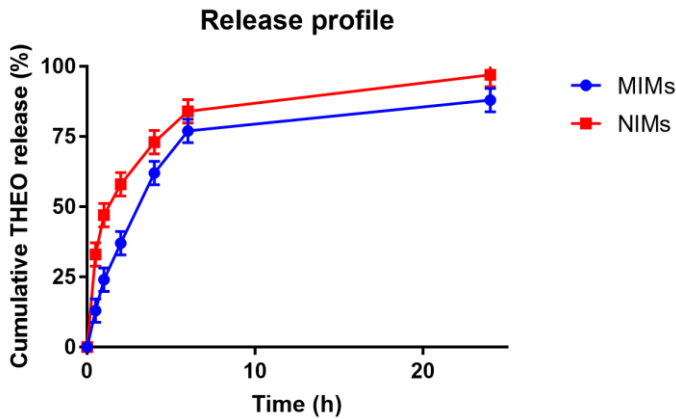


Figure 3.2 THEO release profiles from the microrods.

## MATERIALS AND METHODS

### Materials

Sodium dodecyl sulfate (SDS), theophylline (THEO), caffeine (CAFF), methacrylic acid (MAA), ethylene glycol dimethacrylate (EGDMA), ammonium persulfate, disodium hydrogen phosphate, sodium dihydrogen phosphate were purchased from Sigma-Aldrich (Milan, Italy).

In the aim to remove stabilizer and impurities, methacrylic acid was purified before use by a single-step passage through an alumina column.

All solvents were reagent or HPLC grade and supplied by VWR (Milan, Italy).

Dialysis membranes of 6-27/32” Medicell International LTD (MWCO: 12-14000 Da) were employed for the *in vitro* release studies.

### Instrumentation

The HPLC analyses were carried out using a Jasco PU-2080 liquid chromatograph (Tokyo, Japan) equipped with a Rheodyne 7725i injector (fitted with a 20  $\mu$ L loop), a Jasco UV-2075 HPLC detector and a Jasco-Borwin integrator (Jasco Europe s.r.l., Cremella (LC), Italy). The adopted HPLC conditions for theophylline and caffeine analysis were previously reported in literature (Parisi, Cirillo et al., 2010).

The scanning electron microscopy (SEM) micrographs were obtained with a Jeol JSMT 300 A (JEOL (ITALIA) S.p.A., Milan, Italy); the samples were made conductive by gold layer deposition on sample surfaces in a vacuum chamber. The particle size distribution range was calculated employing an image processing and analysis system, a Leica DMRB endowed with a LEICA Wild 3D.

### **Synthesis of molecularly imprinted microrods (MIMs) *via* mesophase polymerization**

The developed synthetic procedure involves two main consecutive steps: the preparation of the hexagonal mesophase and the radical polymerization.

The hexagonal mesophase based on the ternary lyotropic system consisting of SDS/water/decanol (29.0:66.5:4.5 wt. %) was prepared as reported in the literature with suitable modifications (Yıldız & Kazancı, 2008).

In a sealed flask, 2.9 g of SDS was dissolved in 6.65 mL of water and decanol was then added to the solution. The obtained mixture was homogenized by vortex mixing and mechanical stirring, and the flask was then kept at 35°C under magnetic stirring. After 24 h, the obtained mesophase was doped with template, functional monomer, cross-linker, and initiator for the polymerization step using a THEO/MAA/EGDMA molar ratio equal to 1:8:20. For this purpose, 180 mg of theophylline and 0.68 mL of MAA were dissolved in 3 mL of  $\text{CHCl}_3$  and the obtained mixture was sonicated for 10 min in order to promote the formation of the pre-polymerization complex. Finally, 3.77 mL of EGDMA and 100 mg of ammonium persulfate were added to the reaction mixture, which was purged with nitrogen and sonicated for another 10 min. The polymerization mixture was added to the previously prepared mesophase, homogenized by mechanical stirring and, finally, polymerized by keeping the system at 40°C for three days. The obtained polymeric materials were washed with water in order to remove the surfactant, ethanol, acetone and diethyl ether by centrifugation at 10000 rpm for 10 min. A further washing step for template removal was carried out by Soxhlet extraction using 200 mL of an acetic acid/methanol (1:9, v/v) mixture for at least 4 h, followed by 200 mL of methanol for another 4 h. Finally, the polymeric particles were dried under vacuum overnight at 40°C.

MIMs were checked to be free of THEO and any other compound by HPLC analysis.

Non-molecularly imprinted microrods (NIMs) were also synthesized using the same experimental procedure, but in the absence of THEO during the polymerization process, and treated in the same conditions.

### **Binding studies: imprinting effect and selectivity assessment**

With the aim of investigating the selective recognition properties of the synthesized microrods, binding studies were carried out as described below.

Fifty milligrams of polymeric imprinted and non-imprinted microrods were mixed with 0.5 mL of CH<sub>3</sub>CN and 0.5 mL of a THEO standard solution in CH<sub>3</sub>CN. Samples were shaken in a water bath at 37 ± 0.5 °C for 3, 6 and 24 h and centrifuged at 12000 rpm for 20 min, and the concentration of free THEO in the supernatant was finally measured by HPLC analysis.

The binding experiments were carried out using different THEO standard solutions in order to study the effect of theophylline concentration.

MIM selectivity was evaluated by performing binding studies under the same experimental conditions but using a standard solution of caffeine, which is a THEO analogue.

All experiments were repeated three times.

### **Drug loading by soaking procedure and *in vitro* release studies**

Theophylline loading was achieved by immersing 180 mg of imprinted and non-imprinted microrods in 3 mL of a THEO solution in CH<sub>3</sub>OH (37 mM). The obtained suspensions were soaked in dark conditions and, after 24 h, were placed in a sintered glass filter in order to remove the excess of solvent by percolation at atmospheric pressure. Then, the resultant polymeric microrods were dried under vacuum overnight, and the amount of non-loaded THEO in the excess of solvent was measured by HPLC analyses. Finally, the quantity of loaded drug by imprinted and non-imprinted matrices was calculated by difference from the total amount.

The dialysis bag diffusion technique was employed in the *in vitro* release studies. For this purpose, 10 mg of loaded MIMs and NIMs were introduced into dialysis membrane bags, which were immersed in 10 mL of PBS (0.01 M) at pH 7.4 and maintained at 37 ± 0.5 °C in a water bath with horizontal shaking. After pre-determined time intervals (0.5, 1, 2, 4, 6 and 24 h), 3 mL of the dissolution

medium was withdrawn and replaced with the same volume of PBS. The amount of released theophylline was quantified by HPLC analysis, and the percentage of released drug was calculated considering 100% of the THEO content in polymeric microrods after the drying procedure. The cumulative amount was plotted as a function of time.

Experiments were repeated in triplicate.

## CONCLUSIONS

In the present research study, the synthesis of MIMs selective for theophylline *via* mesophase polymerization was successfully reported for the first time using methacrylic acid and ethylene glycol dimethacrylate as functional monomer and cross-linker, respectively. The choice of this polymer composition is due to the confirmed biocompatibility of polymeric materials based on MAA and EGDMA and widely employed in biomedical and pharmaceutical fields.

For this purpose, the ternary lyotropic system consisting of SDS, water and decanol was chosen to prepare a hexagonal mesophase, which acts as a “template” in order to impart a rod-like morphology to the synthesized polymeric particles. The obtained MIMs have been shown to have good selective recognition abilities and controlled release properties. Furthermore, during the impregnation process, the imprinted microrods were able to load a higher amount of THEO compared to the corresponding non-imprinted materials.

The observed properties depend on the affinity of the imprinted matrices for the target molecule due to the presence of specific recognition cavities, which are formed during the polymerization. Therefore, based on the obtained results, it is possible to state that the adopted synthetic strategy involving a lyotropic mesophase system does not negatively interfere with the formation of the pre-polymerization complex or thus with the imprinting properties of the prepared polymers.

Future studies will involve the use of bioactive molecules as a template for the preparation of MIMs *via* mesophase polymerization, which has potential for use as active tissue scaffolds able to release templates in a controlled manner during tissue repair and regeneration processes.

## REFERENCES

Physics of Self-Assembly of Lyotropic Liquid Crystals. In *Self-Assembled Supramolecular Architectures*.

Biazar E (2017) Application of polymeric nanofibers in medical designs, part III: Musculoskeletal and urological tissues. *International Journal of Polymeric Materials and Polymeric Biomaterials* 66: 28-37.

Ceolin G, Orbán Á, Kocsis V, Gyurcsányi RE, Kézsmárki I, Horváth V (2013) Electrochemical template synthesis of protein-imprinted magnetic polymer microrods. *Journal of Materials Science* 48: 5209-5218.

Cywinski P (2013) Fluorescent Molecularly Imprinted Polymers in Sensing of cAMP and cGMP. *J Phys Chem Biophys* 3: 1-2.

DePierro MA, Guymon CA (2014) Polymer Structure Development in Lyotropic Liquid Crystalline Solutions. *Macromolecules* 47: 5728-5738.

Doroudian G, Pinney J, Ayala P, Los T, Desai TA, Russell B (2014) Sustained delivery of MGF peptide from microrods attracts stem cells and reduces apoptosis of myocytes. *Biomedical microdevices* 16: 705-15.

Fareghi AR, Moghadam PN, Khalafy J, Bahram M, Moghtader M (2017) Preparation of a new molecularly imprinted polymer based on self-crosslinkable cellulose acrylate in aqueous solution: A drug delivery system for furosemide. *Journal of Applied Polymer Science* 134: 45581.

Girones Molera J, Mendez JA, San Roman J (2012) Bioresorbable and nonresorbable polymers for bone tissue engineering. *Current pharmaceutical design* 18: 2536-57.

Gui R, Jin H, Guo H, Wang Z (2018) Recent advances and future prospects in molecularly imprinted polymers-based electrochemical biosensors. *Biosensors and Bioelectronics* 100: 56-70.

Luliński P (2017) Molecularly imprinted polymers based drug delivery devices: a way to application in modern pharmacotherapy. A review. *Materials Science and Engineering: C* 76: 1344-1353.

Menaker A, Syritski V, Reut J, Öpik A, Horváth V, Gyurcsányi RE (2009) Electrosynthesized Surface-Imprinted Conducting Polymer Microrods for Selective Protein Recognition. *Advanced Materials* 21: 2271-2275.



- Oladipo AO, Oluwafemi OS, Songca SP, Sukhbaatar A, Mori S, Okajima J, Komiya A, Maruyama S, Kodama T (2017) A novel treatment for metastatic lymph nodes using lymphatic delivery and photothermal therapy. *Scientific Reports* 7: 45459.
- Parisi OI, Cirillo G, Curcio M, Puoci F, Iemma F, Spizzirri UG, Picci N (2010) Surface modifications of molecularly imprinted polymers for improved template recognition in water media. *Journal of Polymer Research* 17: 355-362.
- Parisi OI, Morelli C, Puoci F, Saturnino C, Caruso A, Sisci D, Trombino GE, Picci N, Sinicropi MS (2014) Magnetic molecularly imprinted polymers (MMIPs) for carbazole derivative release in targeted cancer therapy. *Journal of Materials Chemistry B* 2: 6619-6625.
- Priya James H, John R, Alex A, Anoop KR (2014) Smart polymers for the controlled delivery of drugs - a concise overview. *Acta pharmaceutica Sinica B* 4: 120-7.
- Puoci F, Cirillo G, Curcio M, Iemma F, Parisi OI, Castiglione M, Picci N (2008) Molecularly Imprinted Polymers for  $\alpha$ -Tocopherol Delivery. *Drug Delivery* 15: 253-258.
- Sharma A, Jain N, Sareen R (2013) Nanocarriers for diagnosis and targeting of breast cancer. *BioMed research international* 2013: 960821.
- Sikiti P, Msagati TA, Mamba BB, Mishra AK (2014) Synthesis and characterization of molecularly imprinted polymers for the remediation of PCBs and dioxins in aqueous environments. *Journal of environmental health science & engineering* 12: 82-82.
- Suriyanarayanan S, Nawaz H, Ndizeye N, Nicholls AI (2014) Hierarchical Thin Film Architectures for Enhanced Sensor Performance: Liquid Crystal-Mediated Electrochemical Synthesis of Nanostructured Imprinted Polymer Films for the Selective Recognition of Bupivacaine. *Biosensors* 4.
- Traitel T, Goldbart R, Kost J (2008) Smart polymers for responsive drug-delivery systems. *Journal of biomaterials science Polymer edition* 19: 755-67.
- Xinming L, Yingde C, Lloyd AW, Mikhalovsky SV, Sandeman SR, Howel CA, Liewen L (2008) Polymeric hydrogels for novel contact lens-based ophthalmic drug delivery systems: a review. *Contact lens & anterior eye : the journal of the British Contact Lens Association* 31: 57-64.

Yan F, Texter J (2006) Polymerization of and in mesophases. *Advances in Colloid and Interface Science* 128-130: 27-35.

Yıldız T, Kazancı N (2008) Investigation of temperature dependence of mesomorphism and refracting index of sodium dodecylsulphate+water+decanol lyotropic system. *Journal of Molecular Structure* 886: 158-165.

Yu L, Yun Y, Zhang W, Wang L (2011) Preparation, recognition characteristics and properties for quercetin molecularly imprinted polymers. *Desalination and Water Treatment* 34: 309-314.

Zhou Z, Ma X, Jin E, Tang J, Sui M, Shen Y, Van Kirk EA, Murdoch WJ, Radosz M (2013) Linear-dendritic drug conjugates forming long-circulating nanorods for cancer-drug delivery. *Biomaterials* 34: 5722-5735.

## CHAPTER 4

# Smart bandage based on molecularly imprinted polymers (MIPs) for diclofenac controlled release

Ortensia Iliaria Parisi<sup>a,b</sup>, Mariarosa Ruffo<sup>a,b</sup>, Luca Scrivano<sup>a</sup>, Rocco Malivindi<sup>a,b</sup>, Antonio Vassallo<sup>c</sup> and Francesco Puoci<sup>a,b,\*</sup>.

<sup>a</sup> Department of Pharmacy, Health and Nutritional Sciences, University of Calabria, Rende (CS), Italy.

<sup>b</sup> Macrofarm s.r.l., c/o Department of Pharmacy, Health and Nutrition Sciences, University of Calabria, Rende (CS), Italy.

<sup>c</sup> Department of Science, University of Basilicata, Potenza, Italy.

*Pharmaceuticals* (2018), 11, 92.

DOI:10.3390/ph11040092

**ABSTRACT**

The aim of the present study was the development of a smart bandage for the topical administration of diclofenac, in the treatment of localized painful and inflammatory conditions, incorporating molecularly imprinted polymers (MIPs) for the controlled release of this anti-inflammatory drug. For this purpose, MIP spherical particles were synthesized by precipitation polymerization, loaded with the therapeutic agent and incorporated into the bandage surface. Batch adsorption binding studies were performed to investigate the adsorption isotherms and kinetics and the selective recognition abilities of the synthesized MIP. *In vitro* diffusion studies were also carried out using Franz cells and the obtained results were reported as percentage of the diffused dose, cumulative amount of diffused drug, steady-state drug flux and permeability coefficient. Moreover, the biocompatibility of the developed device was evaluated using the EPISKIN™ model. The Scatchard analysis indicated that the prepared MIP is characterized by the presence of specific binding sites for diclofenac, which are not present in the corresponding non-imprinted polymer, and the obtained results confirmed both the ability of the prepared bandage to prolong the drug release and the absence of skin irritation reactions. Therefore, these results support the potential application of the developed smart bandage as topical device for diclofenac sustained release.

## INTRODUCTION

Diclofenac (DC) is a phenylacetic acid derivative belonging to non-steroidal anti-inflammatory drugs (NSAIDs) and characterized by anti-inflammatory, analgesic and antipyretic activities (Premarathne, Karunaratne et al., 2016, Scavone, Bonagura et al., 2016, Vieira, Glassmann et al., 2016). This therapeutic agent is a non-selective inhibitor of the cyclooxygenase activity of prostaglandin H synthase (Barnett, Chow et al., 1994) and it finds application in the treatment of inflammation and pain states related to several clinical conditions including arthritis, osteoarthritis, rheumatoid arthritis and acute gout, but also muscle injuries.

The topical administration of diclofenac for the treatment of localized painful and inflammatory conditions has several advantages including avoiding first-pass hepatic metabolism and enzymatic degradation by the gastrointestinal tract and gastrointestinal irritation, but also the reduction of side effects and toxicity to other organs. Moreover, DC topical application using a bandage represents a less invasive option for the self-administration of this therapeutic agent.

In this context, the development of a smart bandage for DC topical administration able to release the drug in a controlled way can be a further advance allowing the reduction in dosing frequency and, thus, dose related adverse effects. All these factors contribute to a better patient compliance. Therefore, the present research study has exploited molecular imprinting technology for the preparation of diclofenac imprinted polymers to be used as drug delivery system incorporated into the bandage.

Molecularly imprinted polymers (MIPs) are synthetic polymers characterized by high selective recognition properties for a chosen target compound also in the presence of structurally similar molecules (Cirillo, Parisi et al., 2010, Parisi, Morelli et al., 2014, Parisi & Puoci, 2015). These systems are synthesized by polymerization of suitable functional monomers around the template molecule in the presence of a cross-linker in order to obtain a polymeric matrix characterized by specific binding cavities, which are complementary to the template in terms of size, shape and functionalities. The presence of these selective binding sites is due to the formation of a pre-polymerization complex between the template and the chosen functional monomers able to interact with the analyte *via* covalent or non-covalent way. Once the pre-polymerization complex is formed, the reaction

occurs in the presence of the cross-linking agent leading to a polymeric material, which is later subjected to an extraction process in order to remove the template molecule.

This kind of polymeric materials finds application in a wide range of fields as stationary phases in chromatography, adsorbents in solid-phase extraction (SPE) procedures, synthetic receptors, antibodies and enzymes and drug delivery systems (DDS). MIPs, indeed, can be used as drug carriers due to their ability to control the release of the therapeutic agent used as template during the polymerization process. This capability allows to overcome the drawbacks associated to a narrow therapeutic index reducing the side effects and improving the patient compliance.

Based on these considerations, diclofenac imprinted polymers for the sustained release of this anti-inflammatory agent were synthesized and incorporated into a bandage in order to prepare a novel smart dressing for the topical administration of DC by covering the textile with the drug loaded polymeric particles.

## **RESULTS**

### **Adsorption properties and adsorption kinetics**

In the aim to investigate the imprinting efficacy of the prepared polymeric materials, binding experiments were performed incubating amounts of imprinted and non-imprinted particles in diclofenac standard solutions prepared in PBS at pH 7.4.

The *binding capacity* of the synthesized MIP and the corresponding control material, non-imprinted polymer (NIP), was evaluated taking into account the amount of DC bound to the polymers at equilibrium ( $Q_e$ , mol/g), which was calculated according to the following equation (4.1) (Fayazi, Taher et al., 2015):

$$Q_e = \frac{(C_i - C_e) \times V}{m} \quad (4.1)$$

where  $C_i$  and  $C_e$  (mol/L) are the initial and equilibrium concentrations of DC in solution, respectively,  $V$  (L) is the volume of the solution and  $m$  (g) is the weight of the polymers.

By plotting  $Q_e$  versus  $C_i$ , the adsorption isotherms of diclofenac on MIP and NIP were obtained and reported in Figure 4.1, panel A.

The same batch binding studies were performed using standard solutions of phenylacetic acid (PAA), which is a structural analogue of diclofenac, in order to evaluate also the selectivity properties of the imprinted polymer. The obtained isotherms curves were reported in Figure 4.1, panel B, while Table 4.1 shows the observed percentages of bound diclofenac and phenylacetic acid by imprinted and non-imprinted polymers confirming both the imprinting effect and the selectivity of the prepared imprinted particles.

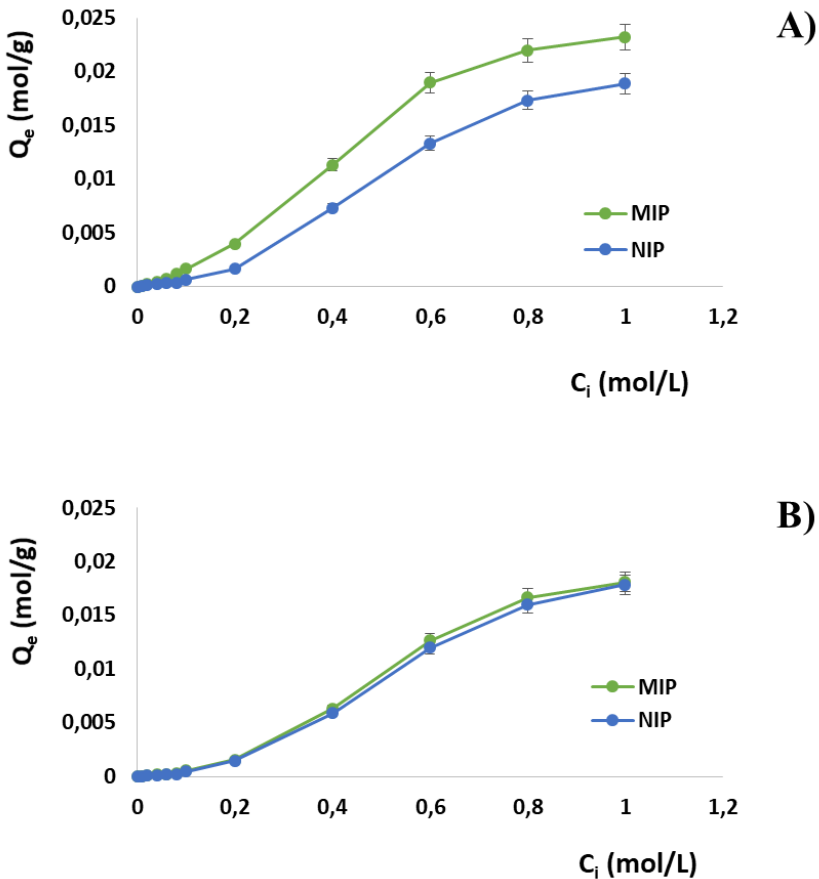


Figure 4.1 Adsorption isotherms of A) DC and B) PAA on MIP and NIP.

The imprinting factor ( $\alpha$ ) and the selectivity coefficient ( $\epsilon$ ) were also reported in Table 4.1. The first one is the ratio between the adsorption percentages of MIP and NIP for each analyte, such as the template ( $\alpha$  DC) and its structural analogue ( $\alpha$  PAA); the second coefficient represents the ratio between the adsorption percentages of DC and PAA observed for the imprinted polymer.

The *Scatchard model* is often used to characterize MIP adsorption properties and collect information about the affinity distribution of the binding sites discerning whether these sites are homogeneous or heterogeneous. Scatchard analysis was provided by the following equation (4.2):

$$\frac{Q_e}{C_e} = (B_{max} - Q_e)K_a \quad (4.2)$$

where  $Q_e$  is the amount of DC bound per gram of polymer at the equilibrium (mol/g),  $C_e$  is the analyte equilibrium concentration (mol/L),  $B_{max}$  (mM/g) is the apparent maximum binding capacity and  $K_a$  ( $M^{-1}$ ) is the association constant. By plotting  $Q_e/C_e$  versus  $Q_e$ ,  $K_a$  and  $B_{max}$  of the polymer were determined from the slope and the intercept, respectively (Figure 4.2, panel A).

**Table 4.1** Percentages of bound diclofenac (DC) and phenylacetic acid (PAA) by imprinted (MIP) and non-imprinted (NIP) polymers and  $\alpha$  and  $\epsilon$  values for different  $C_i$ . Data are shown as means  $\pm$  S.D.

$C_i$ (M)	Bound DC (%)		Bound PAA (%)		$\alpha$ DC	$\alpha$ PAA	$\epsilon$
	MIP	NIP	MIP	NIP			
<b>0.01</b>	20.0 $\pm$ 0.8	10.0 $\pm$ 0.5	7.0 $\pm$ 0.4	5.6 $\pm$ 0.9	2.00	1.25	2.86
<b>0.02</b>	35.0 $\pm$ 0.6	20.0 $\pm$ 0.6	16.5 $\pm$ 0.7	12.9 $\pm$ 0.7	1.75	1.28	2.12
<b>0.04</b>	35.0 $\pm$ 0.3	17.5 $\pm$ 0.9	12.5 $\pm$ 0.7	9.5 $\pm$ 0.4	2.00	1.32	2.80
<b>0.06</b>	35.0 $\pm$ 0.7	15.0 $\pm$ 0.4	11.7 $\pm$ 0.8	9.3 $\pm$ 0.6	2.33	1.25	3.00
<b>0.08</b>	43.8 $\pm$ 0.4	12.5 $\pm$ 0.5	10.0 $\pm$ 0.4	6.9 $\pm$ 0.7	3.50	1.45	4.38
<b>0.1</b>	50.0 $\pm$ 0.6	20.0 $\pm$ 0.3	17.0 $\pm$ 0.7	14.0 $\pm$ 0.6	2.50	1.21	2.94
<b>0.2</b>	60.0 $\pm$ 0.6	25.0 $\pm$ 0.7	23.5 $\pm$ 0.5	22.0 $\pm$ 0.5	2.40	1.07	2.55
<b>0.4</b>	85.0 $\pm$ 0.5	55.0 $\pm$ 0.5	47.5 $\pm$ 0.6	44.3 $\pm$ 0.8	1.55	1.07	1.79
<b>0.6</b>	95.0 $\pm$ 0.8	66.7 $\pm$ 0.6	63.3 $\pm$ 0.4	60.0 $\pm$ 0.5	1.43	1.06	1.50
<b>0.8</b>	82.5 $\pm$ 0.4	65.0 $\pm$ 0.5	62.5 $\pm$ 0.8	60.0 $\pm$ 0.7	1.27	1.04	1.32
<b>1.0</b>	69.6 $\pm$ 0.7	56.7 $\pm$ 0.5	54.3 $\pm$ 0.6	53.5 $\pm$ 0.4	1.23	1.01	1.28



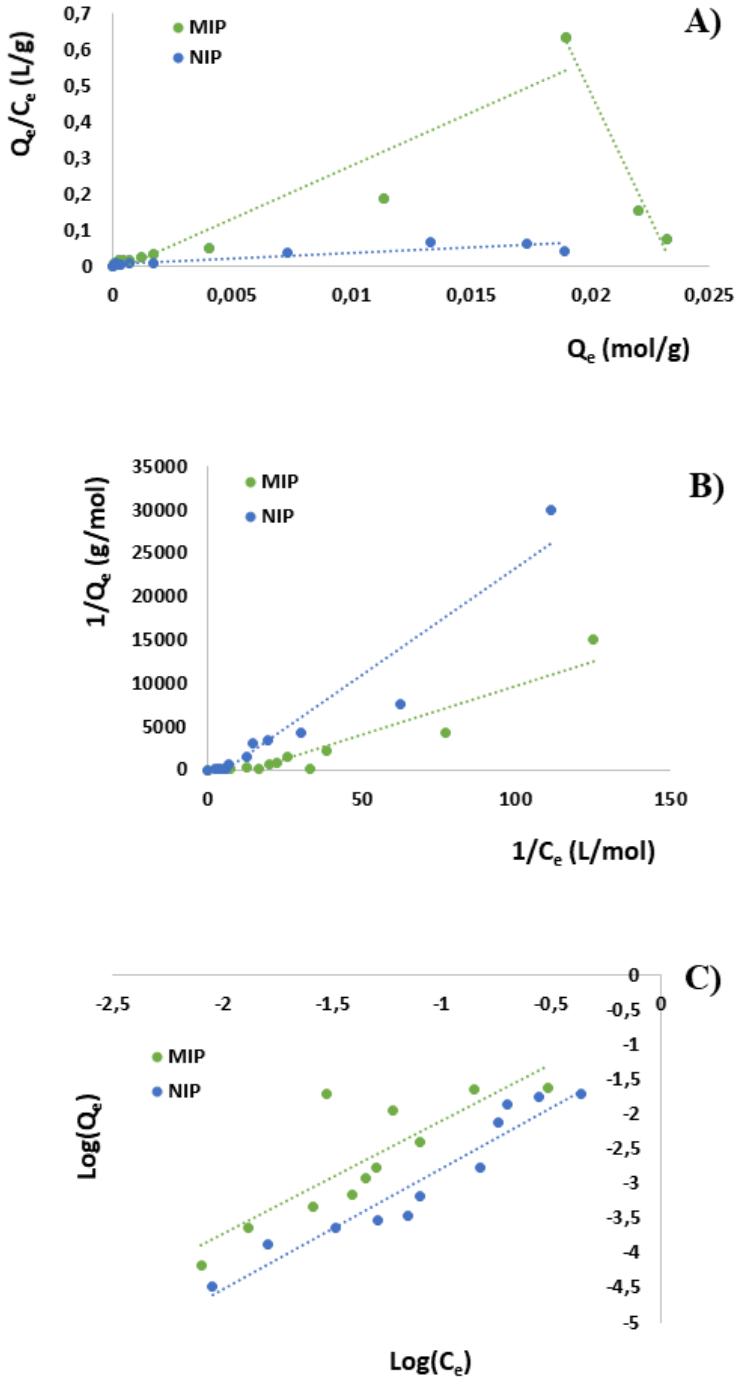


**Figure 4.2** A) Scatchard analysis; B) Langmuir adsorption isotherms and C) Freundlich adsorption isotherms.

As reported in Table 4.2, the high-affinity and low-affinity binding sites of MIP showed association constants ( $K_a$ ) equal to 137.64 and 29.48  $M^{-1}$ , respectively, while the apparent maximum binding capacity ( $Q_{max}$ ) of high-affinity and low-affinity binding sites were 23.50 and 0.49  $mM/g$ .

**Table 4.2**  $K_a$ ,  $B_{max}$  and  $R^2$  values obtained by Scatchard analysis.

Polymer	High Affinity Sites			Low Affinity Sites		
	$K_a$ ( $M^{-1}$ )	$B_{max}$ ( $mM/g$ )	$R^2$	$K_a$ ( $M^{-1}$ )	$B_{max}$ ( $mM/g$ )	$R^2$
<b>MIP</b>	137.64	23.50	0.98	29.48	0.49	0.91
<b>NIP</b>	-	-	-	3.05	2.13	0.84

In the aim to further study the adsorption properties of the synthesized polymeric particles, the obtained experimental data were fitted using the Langmuir and Freundlich models.

The *Langmuir model*, which represents the simplest model used in adsorption studies, involves a monolayer adsorption on a uniform surface containing a limited number of homogeneous binding sites able to accommodate one template molecule, meaning that no further adsorption can take place at that site (Corton, García-Calzón et al., 2007). This model assumes that the ability of the target molecule to bind at a given site is not affected by the occupation of nearby sites. Therefore, Langmuir isotherms are used to evaluate the maximum adsorption capacity, which is reached when surface achieves saturation, according to the following equation (4.3):

$$\frac{1}{Q_e} = \frac{1}{Q_{max} C_e K_L} + \frac{1}{Q_{max}} \quad (4.3)$$

where  $Q_e$  is the amount of DC bound per gram of polymer at the equilibrium ( $mol/g$ ),  $C_e$  is the analyte equilibrium concentration ( $mol/L$ ),  $Q_{max}$  is the maximum adsorption capacity corresponding to complete monolayer coverage on the surface ( $mol/g$ ) and  $K_L$  is the Langmuir constant related to the energy or net enthalpy of sorption ( $L/mol$ ). By plotting  $1/Q_e$  versus  $1/C_e$  (Figure 4.2, panel B),  $K_L$  and  $Q_{max}$  of the polymer were determined (Table 4.3).

**Table 4.3**  $K_L$ ,  $Q_{max}$  and  $R^2$  and  $K_F$ ,  $m$  and  $R^2$  values obtained by Langmuir and Freundlich models, respectively.

Polymer	Langmuir Model			Freundlich Model		
	$K_L$ (L/mol)	$Q_{max}$ (mmol/g)	$R^2$	$K_F$	$M$	$R^2$
<b>MIP</b>	13.29	0.67	0.88	0.33	1.63	0.69
<b>NIP</b>	5.72	0.71	0.92	0.09	1.74	0.92

*Freundlich isotherm* allows to better fit the experimental data describing the surface heterogeneity of polymeric materials (Rushton, Karns et al., 2005, Umpleby II, Baxter et al., 2004, Viveiros, Lopes et al., 2017) and it is expressed as follows (4.4):

$$Q_e = K_F C_e^m \quad (4.4)$$

where  $K_F$  is the Freundlich constant related to the binding affinity ((mol/g)(mol/L)<sup>m</sup>) and  $m$  is the heterogeneity index (dimensionless), which ranges from 0 (for a heterogeneous system) to 1 (for a homogeneous system).

Equation (4.4) in its linear form is expressed as follows (4.5):

$$\log Q_e = \log K_F + m \log C_e \quad (4.5)$$

By plotting  $\log Q_e$  versus  $\log C_e$ ,  $K_F$  and  $m$  values can be determined (Figure 4.2, panel C and Table 4.3). Freundlich isotherms are based on the adsorption on heterogeneous surface assuming that as the template concentration increases, the concentration of template on the adsorbent surface will increase.

The *kinetics of adsorption* that describe DC uptake rate were investigated immersing 30 mg of polymeric particles in a 0.6 M solution of the drug and monitoring the therapeutic agent concentration at different time intervals. The amount of DC bound at time  $t$  ( $Q_t$ , mol/g) was calculated by the difference between the initial drug concentration at  $t = 0$  ( $C_i$ , mol/L) and the residual concentration at the adsorption time  $t$  ( $C_t$ , mol/L) according to equation (4.6):

$$Q_t = \frac{(C_i - C_t) \times V}{m} \quad (4.6)$$

where  $V$  is the volume of the incubation solution (L) and  $m$  is the amount of polymeric material (g).

In the aim to study the kinetic of DC adsorption on the imprinted polymer, two different models can be used such as the pseudo-first order and pseudo-second order models.

The first one is based on the assumption that one molecule adsorbs within the active site of the polymer (Naowanat, Touchprasitchai et al., 2016) and it is given by the following equation (4.7):

$$\log(Q_e - Q_t) = \log Q_e - \frac{K_1}{2.303} t \quad (4.7)$$

where  $Q_e$  is the amount of adsorbed drug at the equilibrium time,  $K_1$  is the first-order adsorption rate constant and  $t$  is the adsorption time.

The pseudo-second order model is based on the assumption that one adsorbed molecule interacts with two active sites (Naowanat et al., 2016) and it is described by equation (4.8):

$$\frac{t}{Q_t} = \frac{1}{K_2 Q_e^2} + \frac{1}{Q_e} t \quad (4.8)$$

where  $K_2$  is the pseudo-second order adsorption rate constant.

The adsorption kinetic curves for MIP and NIP were reported in Figure 4.3, panel A by plotting  $Q_t$  versus  $t$ .

The imprinted particles showed a fast template adsorption within the first 8 h followed by a plateau phase. After the first hour, indeed, 20% of DC was adsorbed by MIP reaching 68%, 83% and 90% at the time point of 4, 6 and 8 h, respectively. A plateau phase was observed between 8 and 24 h (95%). On the contrary, the amount of bound DC within the first h was equal to 7% for the corresponding non-imprinted material getting 33%, 38% 47% and 67% at the time point of 4, 6, 8 and 24 h, respectively.

In order to investigate the adsorption mechanism, pseudo-first order and pseudo-second order kinetic models were adopted according to equations (4.7) and (4.8), which were plotted in Figure 4.3, panels B and C and the correlation coefficients and  $Q_e$  values were reported in Table 4.4.

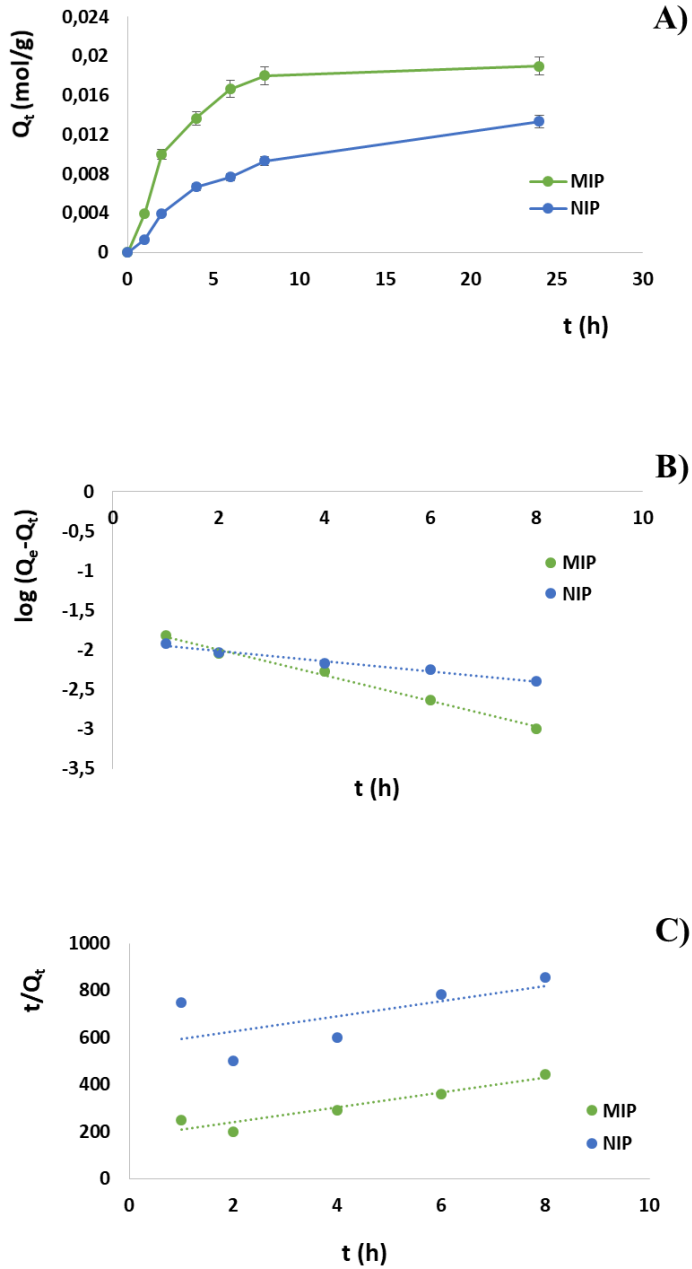


**Figure 4.3** A) DC adsorption kinetic curves for MIP and NIP; B) DC adsorption kinetics according to pseudo-first order model and C) pseudo-second order model.

**Table 4.4** Kinetic fitting data for MIP and NIP.

Polymer	Pseudo-first order			Pseudo-second order		
	K <sub>1</sub>	Q <sub>e</sub>	R <sup>2</sup>	K <sub>2</sub>	Q <sub>e</sub>	R <sup>2</sup>
<b>MIP</b>	0.38	0.02	0.99	6.30	0.03	0.90
<b>NIP</b>	0.15	0.01	0.98	1.97	0.03	0.40

### Drug loading content and drug loading efficiency

The Drug Loading Content (DLC) and the Drug Loading Efficiency (DLE) were calculated according to equations (4.9) and (4.10), respectively (Parisi, Morelli et al., 2015):

$$DLC (\%) = \frac{\text{weight of loaded DC}}{\text{weight of loaded DC} + \text{weight of microspheres}} \times 100 \quad (4.9)$$

$$DLE (\%) = \frac{\text{weight of loaded DC}}{\text{weight of DC used in loading procedure}} \times 100 \quad (4.10)$$

DLC values were  $7.1 \pm 0.2\%$  and  $5.7 \pm 0.5\%$ , while DLE were  $68.0 \pm 0.4\%$  and  $54.0 \pm 0.3\%$  for MIP and NIP, respectively.

### *In vitro* diffusion studies

*In vitro* diffusion studies were carried out using Franz diffusion cells and a synthetic membrane-based model with diffusion characteristics correlated to human skin. The adopted experimental model was employed as a screening tool, without replacing human skin, in order to perform a pilot study of diffusion tests and collect preliminary data.

The experiments were performed using two different bandages, which were prepared employing DC loaded MIP and NIP particles, respectively, and the obtained results were reported as percentage of the diffused dose, cumulative amount (Q<sub>t</sub>) of drug diffused through the membrane, steady-state drug flux (J) and permeability coefficient (K<sub>p</sub>) using receptor fluid data.

The percentage of the diffused dose and the cumulative amount of diffused drug Q<sub>t</sub>, expressed as  $\mu\text{g}/\text{cm}^2$ , for each tested item were reported in Figure 4.4 and Figure 4.5, respectively.

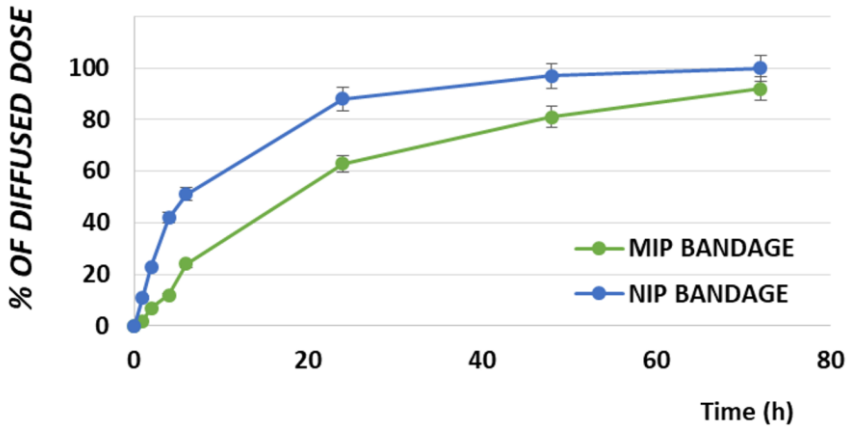


Figure 4.4 Percentage of DC diffused dose for MIP and NIP bandages.

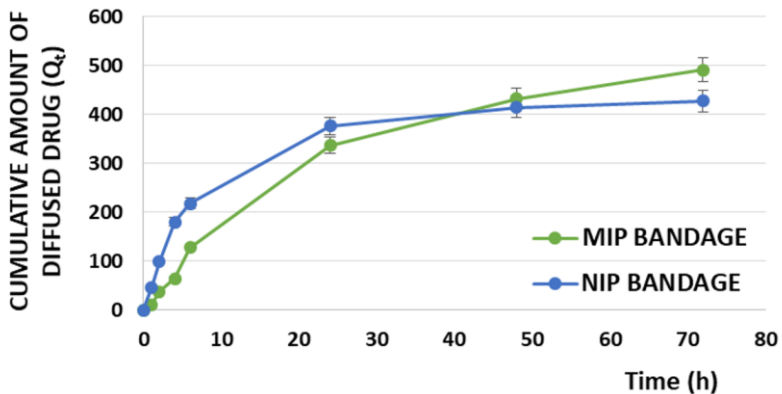


Figure 4.5 *In vitro* profiles of cumulative diffused amount  $Q_t$  per unit area ( $\mu\text{g}/\text{cm}^2$ ) in time of diclofenac for MIP and NIP bandages.

Other two significant parameters are represented by the steady-state flux ( $J$ ) and the permeability coefficient ( $K_p$ ), which were reported in Table 4.5. for MIP and NIP based bandages.

Steady-state flux represents the amount of drug crossing the membrane at a constant rate, while the permeability coefficient is obtained from the relation between the flux and the initial concentration ( $C_d$ ) of diclofenac added to the donor compartment as reported in equation (4.11):

$$K_p = \frac{J}{C_d} \quad (4.11)$$

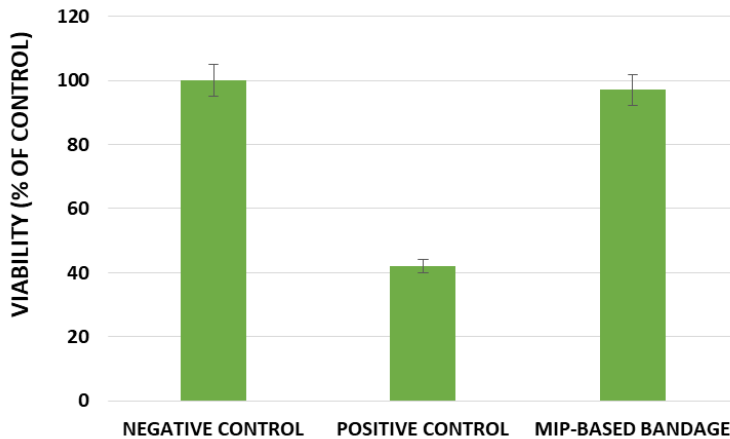
**Table 4.5** Permeation parameters of diclofenac for MIP and NIP bandages: steady-state flux (J) and permeability coefficient ( $K_p$ ).

MIP Bandage		NIP Bandage	
J ( $\mu\text{g}/\text{cm}^2 \text{ h}$ )	$K_p \times 10^{-3}$ (cm/h)	J ( $\mu\text{g}/\text{cm}^2 \text{ h}$ )	$K_p \times 10^{-3}$ (cm/h)
$8.0 \pm 0.3$	$16.3 \pm 0.6$	$7.6 \pm 0.5$	$19.3 \pm 0.4$

### ***In vitro* skin irritation by EPISKIN™ model**

In the present study, the EPISKIN prediction model was employed according to OECD TG439 version 2015 in the aim to investigate the skin irritation potential of the developed smart bandage prepared using diclofenac imprinted particles.

For this purpose, the *in vitro* reconstructed human epidermis was treated with  $16 \text{ mg} \pm 2 \text{ mg}$  (i.e.  $32 \text{ mg}/\text{cm}^2$ ) of bandage according to the “42 bis” procedure, which involves a 42 min exposure followed by a rinsing step and a 42 h post-incubation. Then, cell viability was evaluated by the MTT assay and the obtained results were reported in Figure 4.6.

**Figure 4.6** Effect of the developed smart bandage in EPISKIN™ RHE/L/13.

## **DISCUSSION**

### **Diclofenac imprinted polymers and their adsorption properties**

As already reported in a previous work (Puoci, Hampel et al., 2013), the non-covalent approach for the synthesis of MIPs was chosen as the more appropriate



to address our research purpose due to its advantages compared to the other ones. This synthetic methodology, indeed, involves relatively weak non-covalent interactions, such as hydrogen bonds, dipole-dipole interactions, van der Waals forces and ionic interactions, which are formed between the selected template molecule and functional monomers both during the pre-polymerization and the rebinding steps. Therefore, an easy experimental procedure is required for both the imprinted polymers preparation and the subsequent removal of the template molecules, which leads to a polymeric matrix characterized by the presence of specific and highly selective recognition cavities. Moreover, an extensive range of monomers able to form pre-polymerization complexes with several template functionalities, including hydroxyl, carboxyl, amino and keto groups, is available. This makes possible to imprint a great variety of different analytes involving fast kinetics of recognition and binding.

Methacrylic acid and ethylene glycol dimethacrylate were selected as functional monomer and cross-linker, respectively. The first one, indeed, is able to interact with diclofenac molecules by hydrogen bonds, while EGDMA stabilizes the polymer structure around the template. The employed DC/MAA/EGDMA molar ratio was the same identified in the previous study to obtain the best imprinting effect. Precipitation polymerization was adopted as simple method to obtain polymeric particles characterized by a spherical geometry. This technique consists of a single-step reaction carried out in a higher amount of porogenic solvent compared to bulk polymerization and allows to exert a good control of particle size. As reported in a previous work (Puoci et al., 2013), the dimensional analyses of MIP highlighted a diameter of about 900 nm; on the other hand, the binding cavities are complementary in size to the template and, thus, characterized by a smaller dimension.

Binding experiments were carried out in order to explore the imprinting efficacy and selectivity of the prepared polymeric materials. In particular, isotherms studies are useful to provide information about the nature of the template-polymer interaction and the obtained binding isotherms (Figure 4.1) showed that the adsorption abilities of the two compared polymers improved with the increasing diclofenac initial concentration  $C_i$  until a saturation point. As it is possible to observe, the imprinted material is able to bind a higher amount of DC compared to the corresponding non-imprinted polymer. Moreover, the obtained  $\alpha$  and  $\varepsilon$  values confirmed the selective binding properties for diclofenac of the imprinted

particles compared to the corresponding non-imprinted material. The imprinting efficiency  $\alpha$ , indeed, takes values greater than 1 for each adopted  $C_i$ , which means that MIP is characterized by a higher capability to bind the drug compared to the corresponding NIP (Table 4.1). In addition, the obtained selectivity coefficient values indicate that MIP is from 1.28 to 4.38 times more selective for the drug than the corresponding control polymer in the adopted experimental conditions.

The observed selective recognition ability of diclofenac imprinted polymers is due to the presence of specific binding sites into the polymeric matrix. These selective cavities are formed during the polymerization process carried out in the presence of the drug molecule and are complementary in terms of size, shape and electronic entourage with that of the template. On the contrary, non-specific interactions are responsible for the bound amount of PAA, which is equal for MIP and NIP particles.

The Scatchard model was used to characterize MIP adsorption properties and, as it is possible to observe in Figure 4.2, panel A, the obtained MIP plot is not linear, but composed of two different straight lines; on the contrary, NIP plot consists of one line. The Scatchard analysis indicated that the recognition cavities of the imprinted polymer are not uniform in nature; therefore, MIP possesses heterogeneous binding sites consisting of two different types such as high-affinity and low-affinity ones. On the other hand, NIP showed a linear slope revealing homogeneous binding sites.

The obtained experimental data were also fitted using the Langmuir and Freundlich models (Figure 4.2, panels B and C). As it is possible to observe from the Langmuir model, NIP presents a higher  $Q_{\max}$  value than MIP (Table 4.3). This result is acceptable because this kind of model assumes that all the binding sites are homogeneous. However, this assumption is far from being true for all cases of molecularly imprinted polymers that cannot fit so well to a homogeneous model. On the contrary, the Freundlich model proposes a non-ideal adsorption on heterogeneous surfaces, which is not restricted to the formation of a monolayer.

Generally, MIPs present a higher degree of heterogeneity and, thus, a lower heterogeneity index ( $m$ ) than the corresponding NIPs (Tang, Zhao et al., 2015). In the present study, Freundlich isotherm did not show a good linearity for DC adsorption on MIP ( $R^2$  equal to 0.69) and both imprinted and non-imprinted polymers showed  $m$  values above 1, which indicate a cooperative adsorption

process, which occurs when the binding of one molecule affects the binding of others (Viveiros et al., 2017).

Based on the values reported in Table 4.3, the obtained experimental data and, therefore, diclofenac adsorption on MIP better fit the Langmuir isotherm model with a higher  $R^2$  (0.88) indicating that the adsorption took place at specific homogeneous sites leading to a monolayer coverage of DC at the polymer surface.

The kinetics of DC adsorption were also investigated and, according to the correlation coefficients reported in Table 4.4, the experimental data fitted very well the pseudo-first order kinetic equations, which are characterized by correlation coefficients  $R^2$  of 0.99 and 0.98 and apparent adsorption rate constant  $K_1$  values of 0.38 and 0.15 for MIP and NIP, respectively. Moreover, the theoretical  $Q_e$  values estimated from pseudo-first order kinetic model were equal to 0.02 and 0.01 mol/g for MIP and NIP respectively and, therefore, very close to the experimental ones. On the contrary, the pseudo-second order kinetic equations were not suitable to describe the adsorption kinetic due to correlation coefficients of only 0.90 and 0.40 for MIP and NIP, respectively.

The obtained kinetic results indicated that the pseudo-first order adsorption mechanism was predominant in the adsorption process of diclofenac on the synthesized imprinted polymer and the higher MIP  $K_1$  value suggested that the adsorption rate of the imprinted material was apparently greater than that of the corresponding NIP.

### **Drug loading and smart bandage preparation**

The diclofenac loading process into the imprinted and non-imprinted materials is based on the physical diffusion of the drug molecules into the two synthesized polymeric matrices. This loading mechanism involves the formation of interactions between the drug molecules and the polymeric particles, which consist of hydrogen bonds and electrostatic and non-covalent interactions and depend on the functionalities exposed on template and polymers.

The Drug Loading Content (DLC) and the Drug Loading Efficiency (DLE) were calculated according to equations (4.9) and (4.10) and the achieved values further confirmed the ability of the prepared imprinted particles to selectively interact with diclofenac due to the presence of specific binding sites.

In the present research study, diclofenac imprinted particles were synthesized and used for the preparation of a smart bandage for the topical treatment of inflammatory states involving joints, muscles, tendons or ligaments. For this purpose, a solution of polyvinyl alcohol (PVA) and polyvinyl pyrrolidone (PVP) K30, which are widely employed also in the textile industry, was used to allow the adhesion of DC loaded particles to the elastic bandage.

PVA was chosen for its water solubility and film forming properties (Hong, 2016, Lee, Mensire et al., 2011), while PVP was selected due to its thickening and adhesive properties and the ability to form a flexible film (Foltmann & Quadir, 2008, Teodorescu & Bercea, 2015). The adopted PVA and PVP amounts were optimized in order to obtain an elastic bandage easily applicable around the affected area and, at the same time, to allow the effective adhesion of the drug loaded particles to the tissue avoiding the loss of polymeric material and, therefore, of the therapeutic potential of the final product. Lower amounts of PVA and PVP, indeed, exposed to the risk of loss of polymeric material; on the contrary, higher amounts made the tissue too rigid.

### ***In vitro* diffusion studies**

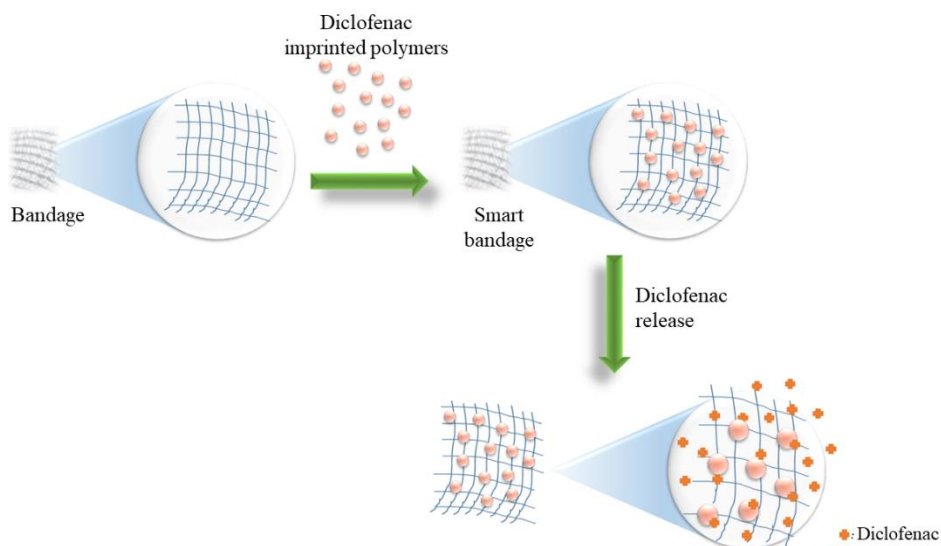
The developed diclofenac delivery system has been designed for the treatment of localized pain, through topical application, which could be related to several inflammatory and clinical conditions including soft tissue musculoskeletal disorders, muscle injuries, arthritis, osteoarthritis, rheumatoid arthritis and acute gout. Therefore, the present study aims to increase the efficacy of the drug at the site of action. When the device is positioned in contact with the skin, the therapeutic agent migrates from the device, it is partitioned across the device/skin interface and, finally, migrates into the skin to reach the site of action.

The *in vitro* diffusion experiments were performed using two different bandages, which were prepared using DC loaded MIP and NIP particles respectively, and a synthetic membrane was employed instead of human skin. The correlation to human skin and the use of Strat-M<sup>®</sup> was widely reported in literature suggesting that this kind of experimental model could be employed as screening tool in order to perform a pilot study of diffusion tests collecting preliminary data (Haq, Dorrani et al., 2018, Haq, Goodyear et al., 2018).

As it is possible to observe in Figure 4.4, the drug diffusion process is characterized by three different steps such as burst, time delay and stable

diffusion. The bandage prepared using DC loaded NIP particles showed a percentage of the diffused dose equal to 51% within the first 6 h reaching the 88%, 97% and 100% in 24, 48 and 72 h, respectively. On the other hand, the bandage incorporating DC loaded MIP particles exhibited a value of 24% after the first 6 h achieving the 63%, 81% and 92% at the time points of 24, 48 and 72 h.

The obtained profiles confirmed the drug prolonged diffusion through the membrane and, therefore, the prolonged drug release from the smart bandage prepared using DC imprinted polymer due to the presence of specific binding sites able to interact strongly with the drug molecules (Scheme 4.1).



**Scheme 4.1** Schematic illustration of MIP-based bandage preparation and diclofenac release.

In Figure 4.5 the cumulative amount ( $Q_t$ ) of diffused diclofenac was reported. The obtained *in vitro* profiles are due to the different polymeric matrices employed in the preparation of the two tested textiles. The imprinted polymer, indeed, is able to load a higher amount of drug compared to the non-imprinted one in the same experimental conditions. This explains the observed  $J$  and  $K_p$  values (Table 4.5) and why the cumulative amount of diffused DC at 72 h is higher for the MIP-based bandage despite the percentages of diffused dose at the same time were 92% and 100% for MIP and NIP textiles, respectively.

### ***In vitro* skin irritation by EPISKIN™ model**

The EPISKIN prediction model was used in order to evaluate the skin irritation potential of the developed smart bandage prepared using the DC imprinted particles. The obtained results in the terms of cell viability were reported in Figure 4.6 and confirmed the absence of irritation effects for the smart bandage.

## **MATERIALS AND METHODS**

### **Materials**

Diclofenac sodium salt (DC), methacrylic acid (MAA), ethylene glycol dimethacrylate (EGDMA), 2,2'-azoisobutyronitrile (AIBN), phenylacetic acid (PAA), poly(vinyl alcohol) (PVA), polyvinylpyrrolidone K30 (PVP), disodium hydrogen phosphate, sodium dihydrogen phosphate, ammonium acetate, acetic acid, 3-[4,5-di-methyl-thiazol-2-yl]-2,5-diphenyl tetrazolium bromide (MTT) were purchased from Sigma-Aldrich (Milan, Italy).

The functional monomer and the radical initiator were purified before use by a single-step passage through an alumina column and recrystallization in methanol, respectively.

All solvents were reagent or HPLC grade and purchased from VWR (Milan, Italy).

Strat-M® membranes (25 mm discs, Cat. No. SKBM02560) were purchased by Merck Millipore.

*Flexa Elast* universal elastic bandage 5 cm × 4.5 m was purchased by Pic®.

The EPISKIN™ RHE/L/13 human skin equivalent kit was obtained from SkinEthic Laboratories (Lyon, France).

### **Instrumentation**

The HPLC analyses were carried out using a Jasco PU-2080 liquid chromatograph (Tokyo, Japan) equipped with a Rheodyne 7725i injector (fitted with a 20 µL loop), a Jasco UV-2075 HPLC detector and a Jasco-Borwin integrator (Massachusetts, USA). The adopted HPLC conditions for diclofenac analysis were previously reported in literature (Puoci et al., 2013).

*In vitro* diffusion studies were carried out using Franz diffusion cells (Disa, Milan, Italy; permeation area 0.4614 cm<sup>2</sup>).

### **Synthesis of molecularly imprinted polymers (MIPs)**

Diclofenac molecularly imprinted polymers were synthesized *via* precipitation polymerization method using methacrylic acid, ethylene glycol dimethacrylate and 2,2'-azoisobutyronitrile as functional monomer, cross-linking agent and radical initiator, respectively. The adopted reaction conditions were reported in a previous work (Puoci et al., 2013).

In order to remove DC template molecules, the extraction procedure was carried out using a Soxhlet apparatus and an acetic acid solution in methanol (10% v/v) for the first 24 h followed by methanol for other 24 h as extraction solvents. Finally, the polymeric particles were dried overnight at 40°C.

The corresponding NIPs were also prepared following the same experimental procedure but in the absence of the template molecule.

### **Batch adsorption binding studies**

The binding studies were designed in order to verify both the imprinting efficiency and the selectivity of the synthesized polymeric particles.

The experiments were carried out in phosphate buffer solution at pH 7.4 (10<sup>-3</sup> M) and using 30 mg of dried polymeric particles, which was mixed with 1 mL of DC standard solution (0.01-1.0 M). After 24 h, the samples were centrifuged at 10000 rpm for 20 min and the drug concentration was quantified by HPLC analysis.

Similar binding experiments were carried out with phenylacetic acid (PAA) in the aim to evaluate the selectivity of the prepared imprinted polymer.

The binding protocol was repeated three times.

### **Kinetic adsorption binding studies**

The adsorption kinetics were investigated by batch adsorption experiments in which 30 mg of polymeric particles was mixed with 1 mL of a DC standard solution (0.6 M) prepared in phosphate buffer at pH 7.4 (10<sup>-3</sup> M). DC concentration was monitored by HPLC analysis at different incubation times (1-24 h), after which each sample was centrifuged at 10000 rpm for 20 min.

The experiments were repeated in triplicate.

### **Drug loading procedure**

In a 10 mL round-bottom flask, 180 mg of the synthesized polymeric imprinted and non-imprinted particles were immersed in 2 mL of a 31.4 mM diclofenac solution previously prepared using an acetonitrile/methanol mixture (1:1 v/v). The samples were soaked under continuous stirring in dark conditions and at room temperature; after three days, the polymeric particles were transferred into sintered glass filters in order to remove the solvent by percolation and, finally, dried under vacuum at 40°C overnight.

The leachate was analyzed for the quantification of unloaded DC by HPLC and Drug Loading Content (DLC) and Drug Loading Efficiency (DLE) were calculated according to equations (4.9) and (4.10), respectively.

### **Smart bandage preparation**

For the preparation of the smart bandage, 30 mg of the drug loaded particles was dispersed in 0.5 mL of a PVA aqueous solution (4% w/v) containing 12.5 mg of PVP. The obtained dispersion was used to coat in a uniform way the surface of a 2 cm × 2 cm portion of the elastic bandage, which was then dried in an oven at 55°C for one hour.

Two different smart bandages were prepared using loaded MIP and NIP particles, respectively.

### ***In vitro* diffusion studies**

The efficacy of the developed smart bandage was investigated by performing *in vitro* diffusion studies. All the experiments were conducted at  $37 \pm 0.5^\circ\text{C}$  and using Strat-M<sup>®</sup> membranes, which were placed between the donor and the receptor compartments of the Franz diffusion cells (Parisi, Malivindi et al., 2017).

The smart bandage was positioned on the Strat-M<sup>®</sup> membrane with the particles layer facing towards the acceptor compartment; then, the two chambers were fixed together. The donor and receptor compartments were filled with 0.5 mL and 5.5 mL of phosphate buffer at pH 7.4 ( $10^{-3}$  M), respectively. The content of the receptor chamber was removed at several time intervals (1, 2, 4, 6, 24, 48 and 72 h) for HPLC analysis and replaced with fresh phosphate buffer.



The experiments were performed in triplicate using two different bandages, which were prepared employing DC loaded MIP and NIP particles, respectively.

The obtained results were reported as percentage of the diffused dose, cumulative amount ( $Q_t$ ) of drug diffused through the membrane, steady-state drug flux ( $J$ ) and permeability coefficient ( $K_p$ ) using receptor fluid data.

### ***In vitro* skin irritation by EPISKIN™ model**

In the aim to investigate the skin irritation potential of the developed bandage incorporating diclofenac imprinted polymers, the EPISKIN™ RHE/L/13 human skin was treated with  $16 \text{ mg} \pm 2 \text{ mg}$  (i.e.  $32 \text{ mg/cm}^2$ ) of bandage, phosphate buffer as negative control and SDS (5% w/v) as positive control following the OECD TG439 version 2015 according to the “42 bis” procedure (Parisi et al., 2017).

The experiments were carried out in triplicate.

## **CONCLUSIONS**

The present study was focused on the development of a bandage incorporating molecularly imprinted polymers for the topical administration of an anti-inflammatory drug such as diclofenac.

Batch binding studies were carried out to explore the adsorption isotherms and kinetics and confirmed the selective recognition abilities of the prepared DC imprinted particles. The Scatchard analysis indicated that the synthesized MIP is characterized by the presence of specific binding sites for the therapeutic agent, which are not present in the corresponding non-imprinted polymer. The kinetic data were also analyzed showing that diclofenac adsorption on MIP better fit the Langmuir isotherm model.

The performed *in vitro* diffusion studies demonstrated the ability of the prepared dressing to release the therapeutic agent in a controlled manner due to the presence of diclofenac imprinted particles. The observed drug diffusion, indeed, appears to be prolonged over time reaching an amount of released DC equal to 92% within 72 h. The achieved DLC and DLE values confirmed the good loading ability of MIP particles due to the presence of specific binding cavities, which make this polymeric material a suitable carrier.

Moreover, the employed EPISKIN model confirmed the absence of skin irritation potential and, therefore, the bioavailability of the developed MIP-based bandage. Therefore, these results support the potential application of the developed smart bandage as topical device for diclofenac sustained release.

## REFERENCES

- Barnett J, Chow J, Ives D, Chiou M, Mackenzie R, Osen E, Nguyen B, Tsing S, Bach C, Freire J (1994) Purification, characterization and selective inhibition of human prostaglandin G/H synthase 1 and 2 expressed in the baculovirus system. *Biochimica et Biophysica Acta (BBA)-Protein Structure and Molecular Enzymology* 1209: 130-139.
- Cirillo G, Parisi OI, Curcio M, Puoci F, Iemma F, Spizzirri UG, Picci N (2010) Molecularly imprinted polymers as drug delivery systems for the sustained release of glycyrrhizic acid. *Journal of Pharmacy and Pharmacology* 62: 577-582.
- Corton E, García-Calzón J, Díaz-García M (2007) Kinetics and binding properties of cloramphenicol imprinted polymers. *Journal of Non-Crystalline Solids* 353: 974-980.
- Fayazi M, Taher MA, Afzali D, Mostafavi A (2015) Preparation of molecularly imprinted polymer coated magnetic multi-walled carbon nanotubes for selective removal of dibenzothiophene. *Materials Science in Semiconductor Processing* 40: 501-507.
- Foltmann H, Quadir A (2008) Polyvinylpyrrolidone (PVP)—one of the most widely used excipients in pharmaceuticals: an overview. *Drug Deliv Technol* 8: 22-27.
- Haq A, Dorrani M, Goodyear B, Joshi V, Michniak-Kohn B (2018) Membrane properties for permeability testing: Skin versus synthetic membranes. *International journal of pharmaceutics* 539: 58-64.
- Haq A, Goodyear B, Ameen D, Joshi V, Michniak-Kohn B (2018) Strat-M® synthetic membrane: Permeability comparison to human cadaver skin. *International journal of pharmaceutics* 547: 432-437.
- Hong KH (2016) Preparation and properties of polyvinyl alcohol/tannic acid composite film for topical treatment application. *Fibers and Polymers* 17: 1963-1968.
- Lee H, Mensire R, Cohen RE, Rubner MF (2011) Strategies for hydrogen bonding based layer-by-layer assembly of poly (vinyl alcohol) with weak polyacids. *Macromolecules* 45: 347-355.

Naowanat N, Thouchprasitchai N, Pongstabodee S (2016) Adsorption of emulsified oil from metalworking fluid on activated bleaching earth-chitosan-SDS composites: Optimization, kinetics, isotherms. *Journal of environmental management* 169: 103-115.

Parisi OI, Malivindi R, Amone F, Ruffo M, Malanchin R, Carlomagno F, Piangiolino C, Nobile V, Pezzi V, Scrivano L (2017) Safety and Efficacy of Dextran-Rosmarinic Acid Conjugates as Innovative Polymeric Antioxidants in Skin Whitening: What Is the Evidence? *Cosmetics* 4: 28.

Parisi OI, Morelli C, Puoci F, Saturnino C, Caruso A, Sisci D, Trombino GE, Picci N, Sinicropi MS (2014) Magnetic molecularly imprinted polymers (MMIPs) for carbazole derivative release in targeted cancer therapy. *Journal of Materials Chemistry B* 2: 6619-6625.

Parisi OI, Morelli C, Scrivano L, Sinicropi MS, Cesario MG, Candamano S, Puoci F, Sisci D (2015) Controlled release of sunitinib in targeted cancer therapy: smart magnetically responsive hydrogels as restricted access materials. *RSC Advances* 5: 65308-65315.

Parisi OI, Puoci F (2015) Stimuli-responsive Molecularly Imprinted Polymers. In *Chemoresponsive Materials*, pp 364-383.

Premarathne E, Karunaratne D, Perera AC (2016) Controlled release of diclofenac sodium in glycolipid incorporated micro emulsions. *International journal of pharmaceutics* 511: 890-898.

Puoci F, Hampel S, Parisi OI, Hassan A, Cirillo G, Picci N (2013) Imprinted microspheres doped with carbon nanotubes as novel electroresponsive drug-delivery systems. *Journal of Applied Polymer Science* 130: 829-834.

Rushton GT, Karns CL, Shimizu KD (2005) A critical examination of the use of the Freundlich isotherm in characterizing molecularly imprinted polymers (MIPs). *Analytica chimica acta* 528: 107-113.

Scavone C, Bonagura AC, Fiorentino S, Cimmaruta D, Cenami R, Torella M, Fossati T, Rossi F (2016) Efficacy and safety profile of diclofenac/cyclodextrin and progesterone/cyclodextrin formulations: a review of the literature data. *Drugs in R&D* 16: 129-140.

Tang L, Zhao C-Y, Wang X-H, Li R-S, Yang J-R, Huang Y-P, Liu Z-S (2015) Macromolecular crowding of molecular imprinting: A facile pathway to produce

drug delivery devices for zero-order sustained release. *International journal of pharmaceutics* 496: 822-833.

Teodorescu M, Bercea M (2015) Poly (vinylpyrrolidone)—a versatile polymer for biomedical and beyond medical applications. *Polymer-Plastics Technology and Engineering* 54: 923-943.

Umpleby II RJ, Baxter SC, Rampey AM, Rushton GT, Chen Y, Shimizu KD (2004) Characterization of the heterogeneous binding site affinity distributions in molecularly imprinted polymers. *Journal of Chromatography B* 804: 141-149.

Vieira V, Glassmann D, Marafon P, Pereira P, Gomez R, Coitinho AS (2016) Effect of diclofenac sodium on seizures and inflammatory profile induced by kindling seizure model. *Epilepsy research* 127: 107-113.

Viveiros R, Lopes MI, Heggie W, Casimiro T (2017) Green approach on the development of lock-and-key polymers for API purification. *Chemical Engineering Journal* 308: 229-239.



# PART II





# CHAPTER 5

## **Polymeric nanoparticles for the delivery of poorly water-soluble drugs**

*Adapted from*

**Polymer-based nanodevices for effective antimicrobial therapy: synthetic strategies and applications**

Luca Scrivano<sup>a</sup>, Ortensia I. Parisi<sup>a,\*</sup> and Francesco Puoci<sup>a</sup>.

<sup>a</sup> Department of Pharmacy, Health and Nutritional Sciences, University of Calabria, Rende (CS), Italy.

*Current Applied Polymer Science* (2017) 1, 3-18.

DOI: 10.2174/2452271601666170221123833



## INTRODUCTION

Over the last few decades, there has been a significant increase in the percentage of poorly soluble drugs used in the pharmaceutical industry. Insufficient water solubility is usually accompanied by undesired pharmacokinetics properties including poor oral bioavailability, uncontrollable precipitation after dosing and lack of dose proportionality. There are several ways to enhance the solubility of drugs without compromising their pharmaceutical ability. One of which is represented by the employment of polymeric nanocarriers such as polymer-drug conjugates, polymeric micelles and polymeric vesicles.

## POLYMER-DRUG CONJUGATES

Polymer-drug conjugates, also known by the name of polymer therapeutics, are a special kind of drug delivery system (DDS), in which the bioactive molecule (small drugs, hormones or peptides) is covalently linked to the polymer backbone, directly or through a cleavable linkage (Ringsdorf, 1978). The concept of a polymer-drug conjugates was firstly proposed by Helmut Ringsdorf in 1975, who defined them as “synthetic polymeric drugs” or “pharmacologically active polymers” (Ringsdorf). The model proposed by Ringsdorf was based on three elements: a drug, a hydrophilic biostable and biodegradable polymer and a transporting unit (Figure 5.1).

Ideal candidates for this type of system are hydrophobic drugs that suffer from poor solubility in aqueous media and, for this reason, conjugation with hydrophilic polymers could be of great advantage. Selection of the drug must be carefully made because only molecules that are stable enough in conjugation condition can be employed. Indeed, conjugation should not affect substance’s biological activity, as well as the spacer should be cleavable and should not modify the chemical structure of the drug.

In addition to the improvement of drug water solubility, the hydrophilic polymer can contribute to lower the toxicity of the drug and prolong drug circulation time. It is, indeed, fundamental that the polymer is non-toxic and non-immunogenic, clearable from the body without any accumulations in tissues or organs, characterized by a controlled average molecular weight (mw) and molecular weight distribution avoiding undesirable responses of low or high mw polymer-

drug conjugates, highly pure and possible to be sterilized. Polymer properties can be controlled by specific structural characteristics. For instance, water solubility can be improved by introducing N-vinyl pyrrolidone or acrylamides co-monomers, whilst partial lipid solubility can be given by introducing hydrophobic co-monomers, such as molecules bearing alkyl groups.

The third element of the Ringsdorf's model is the transporting unit which represents the targeting agent, responsible for the delivery of the system to the diseased site. The most common agents are receptor-ligands, immunoglobulins, enzymes, hormones or special drugs. However, to the transporting unit's category, also skin penetration enhancers can be included for system designed for transdermal administration, as well as other absorption enhancers depending on the route of administration (Elvira, Gallardo et al., 2005).

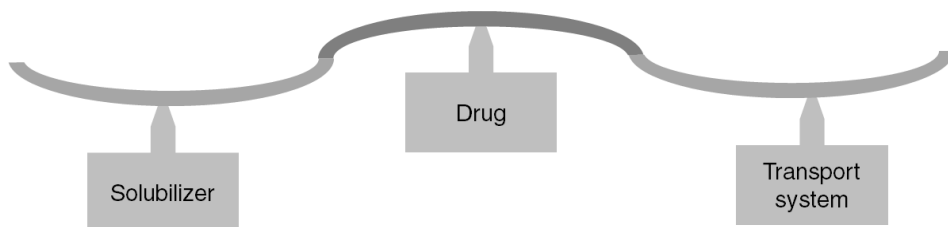


**Figure 5.1** Ringsdorf model of a polymer-drug conjugate.

Polymer-drug conjugates are greatly attractive systems because they are designed on the molecular basis. However, in spite of the high versatility and possibility of engineering, it is difficult to find marketed products mainly because they are considered as new drug molecules or pro-drugs.

### **Preparation of polymer-drug conjugates**

Until today, two main methods have been used for polymer-drug conjugates production: functionalization of the polymer *via* reactive end groups or on the side chain (*via* reactive pendant groups).

The most widely used polymer for end groups modification is poly(ethylene glycol) (PEG). PEG found its major application in proteins modification and this approach goes by the name of PEGylation (Abuchowski, McCoy et al., 1977). Functionalization of proteic drugs through PEGylation can be advantageous for many reasons: PEG is essentially non-toxic and approved for human use; it is easily activated for conjugation and it is not expensive; conjugates have improved

solubility and stability in plasma; it can confer resistance to surface adsorption and prolong circulation time of the system in the bloodstream; it has reduced immunogenicity and antigenicity (Greenwald, Choe et al., 2003). On the other hand, PEGylation of proteins may occur on the pharmacologically active region and thus interfere with its biological activity. In spite of this, many are the examples of protein PEGylation reported in literature that do not affect or improve the therapeutic activity of the protein (Greenwald, 2001).

End groups modification of PEG with small drug has the crucial limit of low drug to polymer ratio, especially for high molecular weight PEG. This drawback may be circumvented by using branched or PEG dendrons that possess multiple end groups (Pasut & Veronese, 2009).

In the pendant groups modification approach, the same or different biomolecules can be conjugated to a given polymer chain by controlling the number of the reactive pendant groups and the bioactive molecule. A variety of different polymers with potentially infinite range of composition can be used for the design of this type of polymer-drug conjugates. Furthermore, the frequency of reactive functional groups can be controlled by the preparation of alternating copolymers regularly repeating the reactive groups along the copolymer chain. In this latter case, many different types of bioactive molecules can be linked to the same polymer chain, exploiting different reactivity of the functional side groups.

## **POLYMERIC MICELLES**

Polymeric micelles are nanosized particles characterized by a core-shell structure fabricated through the self-assembly of amphiphilic copolymers, of the kind A-B, in which represent the shell-forming hydrophilic block and the core-forming hydrophobic block, respectively. The core acts as a reservoir for drug loading, whereas the shell is responsible for micelle stabilization in aqueous environment and interaction with cell membranes, avoiding opsonization and degradation of the system. Also multiblock copolymers can self-organize in micelles and be used as drug carriers (Jones & Leroux, 1999).

Many biodegradable materials could be used in order to construct the hydrophobic core, such as poly( $\beta$ -benzyl-L-aspartate) (PBLA), poly(lactic acid) (PLA) or poly( $\epsilon$ -caprolactone) (PCL), or alternatively a hydrophilic and water

soluble polymer, like poly(aspartic acid), could be used after chemical modification or hydrophobic molecule conjugation (Yokoyama, Kwon et al., 1992, Yokoyama, Miyauchi et al., 1990, Yokoyama, Okano et al., 1996). The main function of the core is to act as a container for hydrophobic drugs, that are protected from the aqueous environment. The use of less biodegradable polymers such as poly(styrene) (Zhang & Eisenberg, 1995, Zhao, Winnik et al., 1990) or poly(methyl methacrylate) (PMMA) (Inoue, Chen et al., 1998) for the assembly of the inner core offers the possibility of a glassy state of the polymer that would strongly contribute to the stability of the micelle core. However, in order to be considered clinically relevant drug carrier materials, non-biodegradable polymers must be biocompatible and have a molecular weight as low to guarantee its excretion *via* the renal route (Seymour, Duncan et al., 1987). The hydrophobic block can be either attached to the head or tail of the hydrophilic polymer (Winnik, Adronov et al., 1995) or randomly grafted onto the backbone (Ringsdorf, Simon et al., 1992, Schild & Tirrell, 1991).

The shell represents the outmost layer, which is exposed to the external environment and interacts with plasmatic proteins and cell membranes in the physiological fluids. The main function exerted by the shell is the micellar structure stabilization over time. It is usually made of non-biodegradable, hydrophilic and biocompatible polymers, like PEG. Biodistribution of the nanoparticles is mainly affected by the hydrophilicity of the shell (Yokoyama, 1998). Other polymers such as poly(N-isopropylacrylamide) (PNIPA) (Cammis, Suzuki et al., 1997, Chung, Yokoyama et al., 1998, Chung, Yokoyama et al., 1997) and poly(alkylacrylic acid) (Chen, Alexandridis et al., 1995) can confer temperature or pH-responsiveness, and could be used to impart bioadhesive characteristics (Inoue et al., 1998). Targeting molecule conjugation onto micelles that present functional groups on the surface has been also reported (Astafieva, Zhong et al., 1993, Cammas & Kataoka, 1995, Kabanov, Batrakova et al., 1992, Nagasaki, Okada et al., 1998).

The advantages of these nanocarriers reside in the ease of preparation, the submicrometric dimension for deeper penetration in infected tissues, the high payload amount to particle volume ratio, the tunable release kinetic and drug targeting ability through surface decoration with specific targeting ligands (Jones & Leroux, 1999).

## Preparation of polymeric micelles

Polymeric micelles are self-assembled particles (size < 200 nm) made of amphiphilic random graft copolymers or di-block copolymers. Micelles assembly is the result of two opposite forces: an attractive one that drives towards the association of the macromolecules, and a repulsive force that prevents micelles uncontrolled growth (Price, 1983). Amphiphilic copolymers possess the ability to self-assemble when dissolved in a good solvent for either hydrophilic or hydrophobic block. Auto-association of amphiphilic copolymers is described as follows: at very low polymer concentrations, macromolecules are dissolved in the solution and only free chains are present; as the concentration increases and reaches the so-called critical micelle concentration (CMC), di-block polymers start to interact with each other to form micelles. For instance, the rearrangement of the hydrophobic part of the copolymer avoids contact of the core with the water solution in which the polymer is diluted. At the CMC, a relevant amount of solvent is still inside the micellar core and the particle can be found as loose aggregates. At this concentrations, the equilibrium will favour micelle formation, adopting a configuration characterized by a low energy state. In this phase micelles have a larger size than micelles formed at higher concentrations (Gao & Eisenberg, 1993). In a second phase, the remaining molecules of solvent will be gradually expelled from the core leading to a decrease in micellar size. Compared to low molecular weight surfactants, amphiphilic copolymers usually have a much lower CMC.

Two different types of micelles can be obtained by micellization of amphiphilic copolymers, depending on whether the hydrophobic chain is randomly bound to the hydrophilic polymer or grafted to one end of the hydrophilic chain (Figure 5.2).

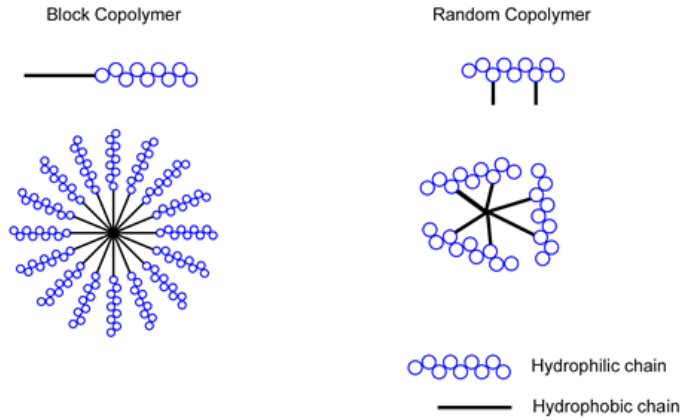


**Figure 5.2** Schematic representation of (*left*) block and (*right*) random copolymer micelles.

The hydrophobic forces, that drive the assembling of the core, and the steric repulsions are responsible for micellar mean diameter determination, (Ringsdorf et al., 1992); a shift in the equilibrium established between these two forces influences micellar size in both random and di-block copolymers. Micelles from randomly grafted polymers are usually smaller than end-modified polymers (Winnik, Davidson et al., 1992).

It is worth mentioning that when head-tail hydrophilic-hydrophobic block polymers self-assemble to form micelles, the water molecules that are blocked nearby the hydrophobic part of the polymer, are subsequently expelled from the core during its formation. At this point, no direct interaction can be established between the core and the hydrophilic shell (that remains constituted by mobile linear chains), as well as no water molecules have now access to the core (Chung et al., 1998, Winnik et al., 1992). On the contrary, random block copolymers associate in such a way that hydrophobic and hydrophilic parts of the polymer assume a conformation that still permit the contact between the core and the aqueous media. In this case, the hydrophilic chains forming the shell are less mobile. This is an important issue since exposed hydrophobic cores may result in secondary aggregation of polymeric micelles (Gao & Eisenberg, 1993, La, Okano et al., 1996, Yokoyama, Okano et al., 1994).



## **POLYMERSOMES**

Polymersomes are nanoscale polymeric vesicles obtained by self-assembly of amphiphilic block copolymers. The major difference that distinguishes polymeric micelles from polymersomes is the organization of the latter in bi-layers, in which the central part of the membrane consists of hydrophobic polymeric blocks, while the inner and outer surfaces consist of hydrophilic polymeric blocks. The so-obtained membrane separates the central aqueous core from the external environment (Levine, Ghoroghchian et al., 2008). This kind of structure possesses the great advantage of being able to encapsulate water-soluble drugs within the aqueous core and liposoluble or amphiphilic compounds in the thickness of the bi-layer. Polymersomes assembly occurs in water solutions and the yield depends on the hydrophilic/hydrophobic block volume ratio: if the contribution of the hydrophilic block is over 45% polymeric micelles are expected, while a contribution lower than 35 - 45% will produce polymersomes (Discher & Ahmed, 2006).

Polymersomes are generally considered as an independent category of drug delivery nanosystems, but they belong to the wider class of nanocapsules, since they are drug nanocarrier characterized by a reservoir structure. Polymersomes properties, such as responsiveness to environmental stimuli, either endogenous (i.e. pH, enzymes, oxidative stress, etc.) or exogenous (i.e. temperature, magnetic field, light, ultrasound) can be designed by careful selection of the building blocks (Ahmed, Pakunlu et al., 2006a, Ahmed, Pakunlu et al., 2006b, Discher & Ahmed, 2006, Onaca, Enea et al., 2009). Similarly to other systems, polymeric vesicles can be engineered for the targeted delivery of therapeutic agents through linkage of targeting ligands to the particle surface (Meng, Zhong et al., 2009).

### **Polymersomes preparation**

For self-assembled polymersomes preparation, block copolymers with a wide range of properties can be used. Block copolymers with different molecular weights, functional groups, monomeric compositions and molecular architectures can be applied in order to produce polymersomes with a variety of potential applications. Block copolymers intended for vesicles formation generally consists of two or more homopolymeric chains. In the case of heteropolymeric blocks the monomeric composition will confer unique physical- chemical properties together with the hydrophobic or hydrophilic character. It is possible

to prepare di-block, tri-block or multi-block copolymers and these structural elements are used for the design of polymersome membranes, assuming different types of conformation and substructures.

The hydrophobic portion of the copolymer can be made either by non-biodegradable polymers, such as poly(ethyl ethylene) (PEE), poly(butadiene) (PBD), poly(dimethylsiloxane) (PDMS), and poly(styrene) (PS) or by biodegradable poly(lactide) (PLA), poly( $\epsilon$ -caprolactone) (PCL) and poly(trimethylene carbonate) (PTMC) (Lee & Feijen, 2012). Biodegradability is dictated by the presence of cleavable bonds in the polymer backbone, like ester and carbonate bonds. The hydrolysis of these bonds depends on the characteristics of the block and its molecular weight, and sometimes requires a certain environmental pH value and/or enzyme (Armentano, Dottori et al., 2010, Leja & Lewandowicz, 2010). On the other hand, poly(acrylic acid) (PAA), poly(L-glutamic acid) (PGA) and PEG have been applied as hydrophilic blocks (Lee & Feijen, 2012). PEG, in particular, has been chosen most frequently thanks to the lower blood proteins adsorption while present on the surface of the vesicle (Gref, Lück et al., 2000, Kim, Kim et al., 2005).

Different possibilities exist for bi-layer assembly in water for AB di-block, and ABA, BAB and ABC tri-block copolymers, in which A and C represent two different hydrophilic blocks and B is the hydrophobic block (Figure 5.3 and Figure 5.4). The hydrophobic interactions between blocks and the hydrophilic interactions between the blocks of the polymer and the aqueous environment define the position and the geometric shape that the amphiphiles will assume in the water suspended vesicles (LoPresti, Lomas et al., 2009, Massignani, Lomas et al., 2010). For AB di-block polymer only the cylindrical conformation is permitted, while BAB tri-block polymers should be arranged in a curved shape in order to compose a stable bi-layer (Figure 5.3). In this way, the hydrophobic chains will be inserted in the central layer of the membrane to minimize the surface tension with water by positioning the hydrophilic blocks on the outer sides of the membrane. Otherwise, ABA copolymers can exist in two permitted conformations at the same time. The hydrophobic block can be curved, so as to expose both hydrophilic portions outside or inside the vesicle, while the loop constitutes the hydrophobic layer of the membrane, or the entire copolymer can be stretched in a cylindrical shape, with the two hydrophilic blocks on the opposite edges, crossing from side to side the thickness of the membrane.

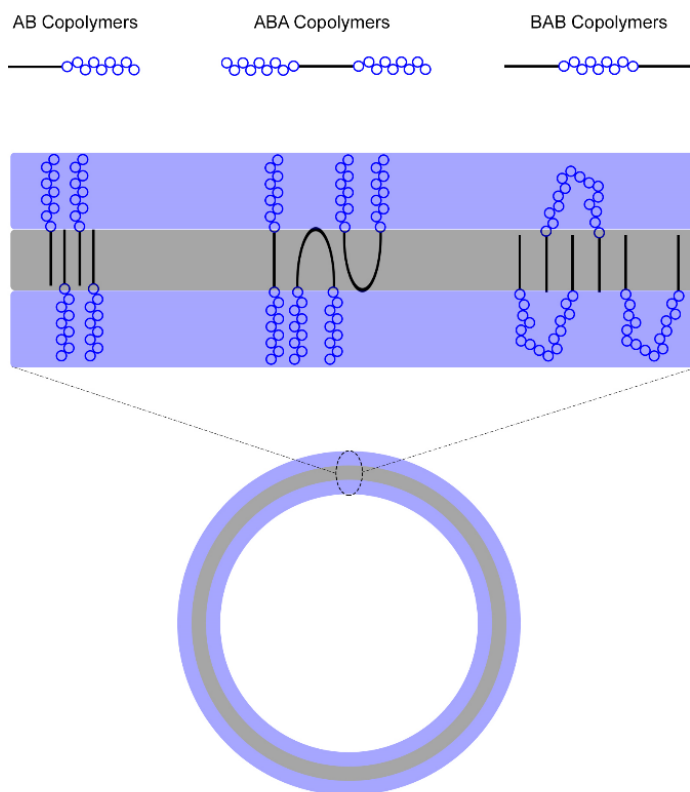


**Figure 5.3** Membrane conformation of polymersomes formed by di-block (AB) and tri-block (ABA) copolymers with permission.

Differently from the previous cases, in ABC copolymers, A and C represent two chemically different hydrophilic blocks. The orientation of the copolymer is driven by the molecular weights, the charge and the solubility of these blocks. In this way, the self-assembled polymersomes will show an asymmetric membrane with different internal and external surfaces (Figure 5.4). Larger hydrophilic fractions preferentially occupy the outer layer of the membrane (Battaglia & Ryan, 2005, Blanazs, Armes et al., 2009). pH, temperature, ionic strength or other environmental parameters can also influence the polymer position, leading to a potential spontaneous inversion or rearrangement of the membrane polarity.

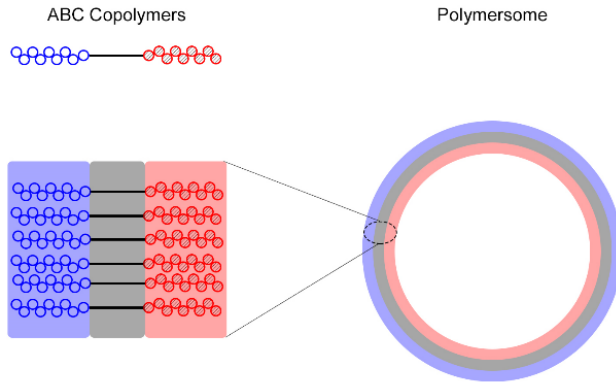


**Figure 5.4** Membrane conformation of polymersomes formed by triblock (ABC) copolymers with permission.

Many techniques have been developed since first polymersomes were prepared. They are all based on the self-assembly of amphiphilic macromolecules. The most applied methods can be regrouped into two classes: solvent-switching method and polymer rehydration method (Du & O'Reilly, 2009, Kita-Tokarczyk, Grumelard et al., 2005, LoPresti et al., 2009, Malinova, Belegriinou et al., 2009, Massignani et al., 2010).

In the solvent-switch technique, copolymers are dissolved in an organic solvent that is a good dissolution medium for both hydrophilic and hydrophobic blocks. The following step is the hydration of the mixture. Hydration can be achieved through a gentle addition of water to the organic solution or, inversely, by injecting the organic copolymer solution into an aqueous medium. The large excess of water increases the interfacial tension, due to the presence of the hydrophobic block that is insoluble in water. When the interfacial tension reaches a critical value, the vesicles self-assembly is triggered (Luo & Eisenberg, 2001, Zhang & Eisenberg, 1995). According to the procedure described, this technique is also called 'phase inversion method'. Vesicles size and polydispersity can be regulated by choosing a proper organic solvent (Meng, Hiemstra et al., 2003).

In the polymer rehydration method, the polymersome self-assembly is obtained by amphiphilic copolymer film hydration. A polymeric thin film is prepared by solvent evaporation of the organic medium in which the copolymer is dissolved. Secondly, the hydration of the film through water addition leads to vesicles formation. This step involves the penetration of water molecules under the

polymeric layer, with formation of water inflated bubbles, that will eventually leave the film in form of vesicles (Kita-Tokarczyk et al., 2005, Malinova et al., 2009). Also in this method, the assembly driving force is the increase in interfacial tension. Polymersomes obtained in this way usually show high polydispersity index. In order to improve the quality of the sample, extrusion under pressure through filters with different cut-offs is often needed (LoPresti et al., 2009). Also the application of an electrical field produces narrower size distribution (Battaglia & Ryan, 2005, Lomas, Massignani et al., 2008). The water flow and the hydration rate of the polymeric film can be controlled by tuning the alternating current applied to the system (Angelova & Dimitrov, 1986). Generally, many shapes can be achieved from amphiphilic block copolymers self-assembling, such as spherical, ellipsoidal or cylindrical micelles or vesicles (Antonietti & Förster, 2003, Blanz et al., 2009, Du & O'Reilly, 2009).

## REFERENCES

- Abuchowski A, McCoy JR, Palczuk NC, van Es T, Davis FF (1977) Effect of covalent attachment of polyethylene glycol on immunogenicity and circulating life of bovine liver catalase. *Journal of Biological Chemistry* 252: 3582-3586.
- Ahmed F, Pakunlu RI, Brannan A, Bates F, Minko T, Discher DE (2006a) Biodegradable polymersomes loaded with both paclitaxel and doxorubicin permeate and shrink tumors, inducing apoptosis in proportion to accumulated drug. *Journal of Controlled Release* 116: 150-158.
- Ahmed F, Pakunlu RI, Srinivas G, Brannan A, Bates F, Klein ML, Minko T, Discher DE (2006b) Shrinkage of a rapidly growing tumor by drug-loaded polymersomes: pH-triggered release through copolymer degradation. *Molecular pharmaceutics* 3: 340-350.
- Angelova MI, Dimitrov DS (1986) Liposome electroformation. *Faraday discussions of the Chemical Society* 81: 303-311.
- Antonietti M, Förster S (2003) Vesicles and liposomes: a self-assembly principle beyond lipids. *Advanced Materials* 15: 1323-1333.
- Armentano I, Dottori M, Fortunati E, Mattioli S, Kenny J (2010) Biodegradable polymer matrix nanocomposites for tissue engineering: a review. *Polymer degradation and stability* 95: 2126-2146.
- Astafieva I, Zhong XF, Eisenberg A (1993) Critical micellization phenomena in block polyelectrolyte solutions. *Macromolecules* 26: 7339-7352.
- Battaglia G, Ryan AJ (2005) Bilayers and interdigitation in block copolymer vesicles. *Journal of the American Chemical Society* 127: 8757-8764.
- Blanazs A, Armes SP, Ryan AJ (2009) Self-assembled block copolymer aggregates: from micelles to vesicles and their biological applications. *Macromolecular rapid communications* 30: 267-277.
- Cammas S, Kataoka K (1995) Functional poly [(ethylene oxide)-co-( $\beta$ -benzyl-L-aspartate)] polymeric micelles: block copolymer synthesis and micelles formation. *Macromolecular Chemistry and Physics* 196: 1899-1905.
- Cammas S, Suzuki K, Sone C, Sakurai Y, Kataoka K, Okano T (1997) Thermo-responsive polymer nanoparticles with a core-shell micelle structure as site-specific drug carriers. *Journal of controlled release* 48: 157-164.

Chen W-Y, Alexandridis P, Su C-K, Patrickios CS, Hertler WR, Hatton TA (1995) Effect of block size and sequence on the micellization of ABC triblock methacrylic polyampholytes. *Macromolecules* 28: 8604-8611.

Chung J, Yokoyama M, Aoyagi T, Sakurai Y, Okano T (1998) Effect of molecular architecture of hydrophobically modified poly (N-isopropylacrylamide) on the formation of thermoresponsive core-shell micellar drug carriers. *Journal of Controlled Release* 53: 119-130.

Chung J, Yokoyama M, Suzuki K, Aoyagi T, Sakurai Y, Okano T (1997) Reversibly thermo-responsive alkyl-terminated poly (N-isopropylacrylamide) core-shell micellar structures. *Colloids and Surfaces B: Biointerfaces* 9: 37-48.

Discher DE, Ahmed F (2006) Polymersomes. *Annu Rev Biomed Eng* 8: 323-341.

Du J, O'Reilly RK (2009) Advances and challenges in smart and functional polymer vesicles. *Soft Matter* 5: 3544-3561.

Elvira C, Gallardo A, Roman JS, Cifuentes A (2005) Covalent polymer-drug conjugates. *Molecules (Basel, Switzerland)* 10: 114-25.

Gao Z, Eisenberg A (1993) A model of micellization for block copolymers in solutions. *Macromolecules* 26: 7353-7360.

Greenwald RB (2001) PEG drugs: an overview. *Journal of Controlled Release* 74: 159-171.

Greenwald RB, Choe YH, McGuire J, Conover CD (2003) Effective drug delivery by PEGylated drug conjugates. *Advanced drug delivery reviews* 55: 217-250.

Gref R, Lück M, Quellec P, Marchand M, Dellacherie E, Harnisch S, Blunk T, Müller R (2000) 'Stealth'corona-core nanoparticles surface modified by polyethylene glycol (PEG): influences of the corona (PEG chain length and surface density) and of the core composition on phagocytic uptake and plasma protein adsorption. *Colloids and Surfaces B: Biointerfaces* 18: 301-313.

Inoue T, Chen G, Nakamae K, Hoffmana AS (1998) An AB block copolymer of oligo (methyl methacrylate) and poly (acrylic acid) for micellar delivery of hydrophobic drugs. *Journal of Controlled Release* 51: 221-229.

Jones M-C, Leroux J-C (1999) Polymeric micelles—a new generation of colloidal drug carriers. *European journal of pharmaceutics and biopharmaceutics* 48: 101-111.

Kabanov AV, Batrakova EV, Melik-Nubarov NS, Fedoseev NA, Dorodnich TY, Alakhov VY, Chekhonin VP, Nazarova IR, Kabanov VA (1992) A new class of drug carriers: micelles of poly (oxyethylene)-poly (oxypropylene) block copolymers as microcontainers for drug targeting from blood in brain. *Journal of Controlled Release* 22: 141-157.

Kim P, Kim DH, Kim B, Choi SK, Lee SH, Khademhosseini A, Langer R, Suh KY (2005) Fabrication of nanostructures of polyethylene glycol for applications to protein adsorption and cell adhesion. *Nanotechnology* 16: 2420.

Kita-Tokarczyk K, Grumelard J, Haefele T, Meier W (2005) Block copolymer vesicles—using concepts from polymer chemistry to mimic biomembranes. *Polymer* 46: 3540-3563.

La SB, Okano T, Kataoka K (1996) Preparation and characterization of the micelle-forming polymeric drug indomethacin-incorporated poly (ethylene oxide)-poly ( $\beta$ -benzyl L-aspartate) block copolymer micelles. *Journal of pharmaceutical sciences* 85: 85-90.

Lee JS, Feijen J (2012) Polymersomes for drug delivery: design, formation and characterization. *Journal of controlled release* 161: 473-483.

Leja K, Lewandowicz G (2010) Polymer biodegradation and biodegradable polymers—a review. *Polish Journal of Environmental Studies* 19: 255-266.

Levine DH, Ghoroghchian PP, Freudenberg J, Zhang G, Therien MJ, Greene MI, Hammer DA, Murali R (2008) Polymersomes: a new multi-functional tool for cancer diagnosis and therapy. *Methods* 46: 25-32.

Lomas H, Massignani M, Abdullah KA, Canton I, Presti CL, MacNeil S, Du J, Blanz A, Madsen J, Armes SP (2008) Non-cytotoxic polymer vesicles for rapid and efficient intracellular delivery. *Faraday discussions* 139: 143-159.

LoPresti C, Lomas H, Massignani M, Smart T, Battaglia G (2009) Polymersomes: nature inspired nanometer sized compartments. *Journal of Materials Chemistry* 19: 3576-3590.



- Luo L, Eisenberg A (2001) Thermodynamic stabilization mechanism of block copolymer vesicles. *Journal of the American Chemical Society* 123: 1012-1013.
- Malinova V, Belegriou S, de Bruyn Ouboter D, Meier WP (2009) Biomimetic block copolymer membranes. In *Organic Electronics*, pp 213-258. Springer.
- Massignani M, Lomas H, Battaglia G (2010) Polymersomes: a synthetic biological approach to encapsulation and delivery. In *Modern Techniques for Nano-and Microreactors/-reactions*, pp 115-154. Springer.
- Meng F, Hiemstra C, Engbers GH, Feijen J (2003) Biodegradable polymersomes. *Macromolecules* 36: 3004-3006.
- Meng F, Zhong Z, Feijen J (2009) Stimuli-responsive polymersomes for programmed drug delivery. *Biomacromolecules* 10: 197-209.
- Nagasaki Y, Okada T, Scholz C, Iijima M, Kato M, Kataoka K (1998) The reactive polymeric micelle based on an aldehyde-ended poly (ethylene glycol)/poly (lactide) block copolymer. *Macromolecules* 31: 1473-1479.
- Onaca O, Enea R, Hughes DW, Meier W (2009) Stimuli-Responsive Polymersomes as Nanocarriers for Drug and Gene Delivery. *Macromolecular bioscience* 9: 129-139.
- Pasut G, Veronese FM (2009) PEG conjugates in clinical development or use as anticancer agents: an overview. *Advanced drug delivery reviews* 61: 1177-1188.
- Price C (1983) Micelle formation by block copolymers in organic solvents. *Pure and Applied Chemistry* 55: 1563-1572.
- Ringsdorf H Structure and properties of pharmacologically active polymers. In pp 135-153. Wiley Online Library.
- Ringsdorf, H (1978). Synthetic Polymeric Drugs, In *Polymeric Delivery Systems*; Kostelnik, R.J., Ed.; Gordon and Breach Science Publishers, Inc.: New York; pp. 197-225.
- Ringsdorf H, Simon J, Winnik F (1992) Hydrophobically-modified poly (N-isopropylacrylamides) in water: probing of the microdomain composition by nonradiative energy transfer. *Macromolecules* 25: 5353-5361.

Schild HG, Tirrell DA (1991) Microheterogeneous solutions of amphiphilic copolymers of N-isopropylacrylamide. An investigation via fluorescence methods. *Langmuir* 7: 1319-1324.

Seymour L, Duncan R, Strohalm J, Kopeček J (1987) Effect of molecular weight (Mw) of N-(2-hydroxypropyl) methacrylamide copolymers on body distribution and rate of excretion after subcutaneous, intraperitoneal, and intravenous administration to rats. *Journal of biomedical materials research* 21: 1341-1358.

Winnik FM, Adronov A, Kitano H (1995) Pyrene-labeled amphiphilic poly-(N-isopropylacrylamides) prepared by using a lipophilic radical initiator: synthesis, solution properties in water, and interactions with liposomes. *Canadian journal of chemistry* 73: 2030-2040.

Winnik FM, Davidson AR, Hamer GK, Kitano H (1992) Amphiphilic poly (N-isopropylacrylamides) prepared by using a lipophilic radical initiator: synthesis and solution properties in water. *Macromolecules* 25: 1876-1880.

Yokoyama M (1998) Novel passive targetable drug delivery with polymeric micelles. *Biorelated polymers and gels*: 193-229.

Yokoyama M, Kwon GS, Okano T, Sakurai Y, Seto T, Kataoka K (1992) Preparation of micelle-forming polymer-drug conjugates. *Bioconjugate chemistry* 3: 295-301.

Yokoyama M, Miyauchi M, Yamada N, Okano T, Sakurai Y, Kataoka K, Inoue S (1990) Characterization and anticancer activity of the micelle-forming polymeric anticancer drug adriamycin-conjugated poly (ethylene glycol)-poly (aspartic acid) block copolymer. *Cancer Research* 50: 1693-1700.

Yokoyama M, Okano T, Sakurai Y, Kataoka K (1994) Improved synthesis of adriamycin-conjugated poly (ethylene oxide)-poly (aspartic acid) block copolymer and formation of unimodal micellar structure with controlled amount of physically entrapped adriamycin. *Journal of controlled release* 32: 269-277.

Yokoyama M, Okano T, Sakurai Y, Suwa S, Kataoka K (1996) Introduction of cisplatin into polymeric micelle. *Journal of controlled release* 39: 351-356.

Zhang L, Eisenberg A (1995) Multiple morphologies of "crew-cut" aggregates of polystyrene-b-poly (acrylic acid) block copolymers. *Science* 268: 1728-1731.

Zhao CL, Winnik MA, Riess G, Croucher MD (1990) Fluorescence probe techniques used to study micelle formation in water-soluble block copolymers. *Langmuir* 6: 514-516.



## CHAPTER 6

# Synthesis of sericin-based conjugates by click chemistry: enhancement of sunitinib bioavailability and cell membrane permeation

Luca Scrivano<sup>1,a</sup>, Domenico Iacopetta<sup>1,a</sup>, Maria Stefania Sinicropi<sup>a</sup>, Carmela Saturnino<sup>b</sup>, Pasquale Longo<sup>c</sup>, Ortensia Ilaria Parisi<sup>a,\*</sup>, and Francesco Puoci<sup>a</sup>.

<sup>1</sup> These authors contributed equally to this work.

<sup>a</sup> Department of Pharmacy, Health and Nutritional Sciences, University of Calabria, Rende, CS, Italy.

<sup>b</sup> Department of Sciences, University of Basilicata, Potenza, Italy.

<sup>c</sup> Department of Chemistry and Biology, University of Salerno, Fisciano, SA, Italy.

*Drug Delivery* (2017) 24(1), 482-490.

DOI: 10.1080/10717544.2016.1267822

## ABSTRACT

Sericin is a natural protein that has been used in biomedical and pharmaceutical fields as raw material for polypeptide-based drug delivery systems. In this paper it has been employed as pharmaceutical biopolymer for the production of sunitinib-polypeptide conjugate. The synthesis has been carried out by simple click reaction in water, using the redox couple L-ascorbic acid/hydrogen peroxide as free radical grafting initiator. The bioconjugate molecular weight ( $50 \text{ kDa} < M_w < 75 \text{ kDa}$ ) was obtained by SDS-PAGE, while the spectroscopic characteristics have been studied in order to reveal the presence of grafted sunitinib. In both FT-IR and UV/Vis spectra, signals corresponding to sunitinib functional groups have been identified.

Since sunitinib is an anticancer drug characterized by low bioavailability and low permeability, the bioconjugation aimed at their enhancement. *In vitro* studies demonstrated that bioavailability has been increased to almost 74%, compared to commercial formulation. Also cell membrane permeability has been augmented in *in vitro* tests, in which membrane models have been used to determine the lipid membrane/physiological fluid partition coefficient ( $K_p$ ). The  $\log(K_p)$  value of the bioconjugate was increased to over 4. This effect resulted in a three-fold decrease of  $IC_{50}$  value against MCF-7 breast cancer cells.

## INTRODUCTION

Biopolymer-drug conjugates have recently attracted much attention as drug delivery systems (DDSs). Bioconjugates generally aim at the exploitation of the properties of the biopolymeric material at which the drug is attached (Kok, Grijpstra et al., 1999). The scientific literature is rich of examples of drug-polymer conjugates: some of them are represented by chitosan-drug conjugates, in which the highly biocompatible and biodegradable natural occurring polysaccharide bears therapeutic molecules, like methotrexate, through covalent linkage (Fattahi, Asgarshamsi et al., 2015), or by dextran-catechin grafted conjugates (Vittorio, Cirillo et al., 2012). Several studies demonstrated that conjugation of both natural or synthetic polymers (Etrych, Šubr et al., 2012, Puoci, Morelli et al., 2012) with small anticancer molecules could be carried out for the achievement of a more stable, but still endowed of intrinsic activity, drug-conjugate. Conjugation, usually, results in the production of stable drug delivery systems characterized by long term activity.

Besides, protein-drug conjugates, such as antibody-anticancer drug conjugates, optimize specificity and target the delivery of cytotoxic agents to the tumor. Thereby, targeting will affect the biodistribution of the drugs, sparing normal tissue exposure to the cytotoxic agent and allowing the use of potent agents that would cause high toxicity for systemic use (Akash, Rehman et al., 2016, Alley, Okeley et al., 2010).

For information about drug-polymer conjugates, a more detailed review of the literature can be found elsewhere (Coburn & Kaplan, 2015, Pang, Du et al., 2013, Vicent, 2007).

In the present work a bioconjugate was obtained *via* grafting of a model drug onto silk-derived protein sericin (SER), a by-product of textile industry. Silk filaments, produced by the silkworm *Bombyx Mori*, are made of a double strand of fibroin, held together by a gummy coating mainly constituted by SER. During silk processing, the silk filaments are treated with boiling water. In this way, SER is removed and discarded (degumming).

Sericin's molecular weight, ranging from about 10 to over 400 kDa, strongly depends on the extraction and isolation methods used. Molecular weight also influences the solubility in aqueous solutions: smaller polypeptides having a molecular weight less than 60 kDa are more soluble in cold water; on the other

hand, SER fractions having molecular weight over 60 kDa are poorly soluble in water at room temperature, but still soluble in hot water (Zhang, Tao et al., 2006b).

The highly water-soluble SER is a biocompatible and biodegradable protein, easily hydrolyzed by proteolytic enzymes (Deng, Zhang et al., 2014, Liu, Song et al., 2015), which makes it a bioresorbable material useful for medical and pharmaceutical applications (Lamboni, Gauthier et al., 2015, Padamwar & Pawar, 2004, Parisi, Fiorillo et al., 2015). When used in combination with a drug, sericin is able to establish weak interactions that only slightly affect its secondary structure (Napavichayanun, Amornsudthiwat et al., 2015).

Currently, only a few examples of SER-based conjugates have been developed as DDSs. In 2006, Zhang et al. have prepared two SER bioconjugates. In a first report, a sericin-L-asparaginase conjugate for L-asparaginase modification and delivery was produced. The enzyme is, in fact, used as chemotherapeutic agent in the management of acute lymphoblastic leukemia. The conjugation resulted in a greatly improved affinity between L-asparaginase and its substrate, L-asparagine (Zhang et al., 2006b). In the same year, a SER-insulin bioconjugate with improved biological stability was reported. SER-insulin conjugates were found to have a prolonged half-life compared to bovine serum albumin-insulin conjugates and native insulin (Zhang, Ma et al., 2006a). Immunogenicity and antigenicity were not observed for both conjugates in *in vivo* experiments. Thus, these authors demonstrated that SER bioconjugates can be efficiently applied as delivery systems.

In this paper, we report for the first time the conjugation of a synthetic drug to sericin. In this work, a small molecular tyrosine kinase inhibitor (Sunitinib, SUT) has been chosen as model drug.

Small molecular tyrosine kinase inhibitors (smTKIs) are powerful anticancer drugs that are experiencing rapid growth. SmTKIs include imatinib, gefitinib, erlotinib, afatinib, dasatinib, bosutinib, ponatinib, etc., divided in first-, second- and third-generation TKIs (Jabbour, Kantarjian et al., 2015).

Among smTKIs, SUT, a second-generation drug, is a multi-targeted receptor TKI orally administered for the treatment of gastrointestinal stromal tumors, advanced renal cell carcinomas and progressive, well-differentiated pancreatic neuroendocrine tumors (Parisi, Morelli et al., 2015, Wu, Zhang et al., 2014). SUT



possesses anti-cancer and anti-angiogenic activities, due to the potent inhibition of vascular endothelial growth factor receptors (types 1-3), platelet derived growth factor receptor ( $\alpha$  and  $\beta$ ), as well as fms-like tyrosine kinase 3, stem-cell factor receptor, colony-stimulating factor receptor (type 1) and glial cell-line derived neurotrophic factor receptor (Izzedine, Buhaescu et al., 2007, Papaetis & Syrigos, 2009).

From a pharmacokinetic point of view, sunitinib is classified by the biopharmaceutics classification system (BCS) as a class IV drug (Herbrink, Nuijen et al., 2015). BCS establishes possible absorption-related issues for drugs, like SUT, characterized by low bioavailability. Drug solubility and cell permeability are, indeed, critical parameters that influence the absorption process, hence the bioavailability. BCS classifies drugs as: Case I: high solubility and high permeability; Case II: low solubility and high permeability; Case III: high solubility and low permeability; Case IV: low solubility and low permeability (Amidon, Lennernäs et al., 1995). SUT indeed is very poorly soluble in water and ethanol, but highly soluble in DMSO (Kassem, Motiur Rahman et al., 2012), thus the therapeutic effect of SUT might be limited in physiological aqueous media. In order to improve the solubility of SUT in aqueous solutions, conjugation with water soluble biopolymeric macromolecules is a valuable method.

With the purpose of improving its solubility and cell permeability, a sericin-sunitinib (SER-SUT) bioconjugate was obtained *via* free radical grafting of sunitinib onto sericin. An easy click reaction has been employed to carry out the synthesis. The product SER-SUT conjugate, has been studied by FT-IR and UV/Vis spectroscopy and SDS-PAGE. Bioavailability, membrane permeability and cytotoxic activity have been evaluated through *in vitro* models.

Conjugation with SER could be applied to a variety of drugs that are similar to SUT, such as bosutinib, crizotinib, nilotinib, vemurafenib among smTKIs, but also amphotericin B, chlorothiazide, colistin, ciprofloxacin, mebendazole, methotrexate, neomycin, furosemide, hydrochlorothiazide. They are all classified as Class IV drugs by BCS and possess similar properties to SUT (Herbrink et al., 2015, Wu et al., 2014).

## METHODS

### Materials and instrumentations

Sunitinib malate, hydrogen peroxide (H<sub>2</sub>O<sub>2</sub>), L-ascorbic acid (AA), hydrochloric acid (37% w/w), disodium hydrogen phosphate, sodium dihydrogen phosphate, sodium hydrogen carbonate, pepsin from porcine gastric mucosa, esterase from porcine liver,  $\alpha$ -amylase from porcine pancreas, pancreatin from porcine pancreas, sodium cholate, bile extract porcine and L- $\alpha$ -Phosphatidylcholine from egg yolk were purchased by Sigma-Aldrich (Sigma Chemical Co., St. Louis, MO, USA).

All solvents were reagent-grade or HPLC-grade and provided by Carlo Erba Reagents (Milan, Italy).

Dialysis tubes MWCO: 3500 Da and 12000-14000 Da were provided by Spectrum Laboratories Inc., U.S.A.

IR spectra were recorded as films or KBr pellets on a Jasco FT-IR 4200. Absorption spectra were recorded with a Jasco V-530 UV/Vis spectrometer.

### Sericin extraction

The water in which the silkworm cocoons are boiled during silk production has been provided by a local silk manufacturer. The water soluble fraction (sericin) dissolved in the solution was collected after centrifugation at 7000 rpm for 20 min. The light colored supernatant was then dialyzed for 72 h against distilled water using 3.5 kDa MWCO dialysis membrane. After 24 h of lyophilization, the sericin powder was obtained and used for further experimentations.

### Sericin-sunitinib conjugate synthesis

Single-step grafting of sunitinib onto sericin, by employing hydrogen peroxide/L-ascorbic acid as redox pair, was carried out as follows: in a suitable beaker 40 mL of water and 15 mL of ethanol were poured. 200 mg of sericin and 40 mg of sunitinib malate were dissolved in the reaction mixture. After complete dissolution, 2.5 mL of H<sub>2</sub>O<sub>2</sub> (30% v/v) containing 83.5 mg of L-ascorbic acid was added. The mixture was maintained under magnetic stirring at 25°C for 24 h under atmospheric pressure. The obtained SER-SUT conjugate was purified by dialysis (3.5 kDa MWCO) for 12 h against ethanol/water and for further 48 h

against water. The solution recovered was then frozen and lyophilized to a powder.

### **SDS-PAGE and silver staining**

All chemicals used in SDS-PAGE and gel staining were obtained from Bio-Rad Laboratories S.r.l. or Sigma-Aldrich (Milan, Italy) and the solutions were prepared in deionized water. The protein samples were solubilized in loading buffer and gels were run on a Protean III mini-electrophoresis unit (BioRad, Milan, Italy) according to Laemmli (Laemmli, 1970). After the run, gels were silver stained as reported elsewhere (Madeo, Carrisi et al., 2009, Zhao, Liu et al., 2012).

### ***In vitro* bioavailability studies**

The *in vitro* bioavailability study was carried out in a simulated gastric and intestinal environment through the previously reported method of the dialysis tubing procedure (Grande, Parisi et al., 2016). The experiment is based on two successive enzymatic phases: pepsin and pancreatin digestions, which occurs in the first 2 h and in the following 4 h, respectively. The two phases are described as follows.

*Pepsin digestion.* 30 mg of SER-SUT conjugate was put into a dialysis bag (MWCO 12-14 kDa) with 1.0 mL of a 0.85 N HCl solution, 3.0 mL of a sodium cholate solution (2% w/v in distilled water) and 24000 U of porcine pepsin per mL. The dialysis bag was carefully sealed on each end with clamps and immersed in 10 mL of a 0.85 N HCl solution (pH 1.0). The system was then left for 2 h into a water-bath at  $37 \pm 0.5^\circ\text{C}$ .

*Pancreatin digestion.* After 2 h, the dialysis bag was recovered and carefully opened in order to allow the addition of 1.3 mL of a 0.8 M  $\text{NaHCO}_3$  solution, 11 mg of amylase, 11 mg of esterase and 11 mg porcine pancreatin to the bag content. The dialysis bag was then sealed again and placed into 10 mL of a phosphate buffered saline (PBS) solution at pH 7.0. The incubation was repeated for further 4 h, into the shaking water bath at  $37 \pm 0.5^\circ\text{C}$ .

In order to evaluate the *in vitro* bioavailability of the sample, 3 mL of the medium used to mimic gastric and intestinal environment (0.85 N HCl solution pH 1.0 and PBS pH 7.0) were withdrawn at the time points of 2 and 6 h, respectively.

The concentrations of the samples were determined by UV/Vis spectroscopy (at  $\lambda_{\max} = 426$  nm) and calculated by using the equations obtained from the calibration curves of SUT standard solutions at pH 1.0 and 7.0, respectively. For this purpose, all the prepared standard solutions were analyzed by UV/Vis spectrophotometer and the correlation coefficient ( $R^2$ ) and slope of the regression equations obtained by the method of least squares were calculated at pH 1.0 and 7.0, respectively.

The same procedure was applied to evaluate the bioavailability of sunitinib pharmaceutical formulation, commercially available under the name of Sutent<sup>®</sup>, used as control for data comparison. Each experiment was repeated three times.

### ***In vitro* membrane permeability studies**

#### *Liposomes preparation*

Giant unilamellar vesicles (GUVs) were prepared according to the method reported by Moscho et al. (Moscho, Orwar et al., 1996, Walde, Cosentino et al., 2010). Briefly, 125 mg of PC was dissolved in 30 mL of a chloroform/methanol solution (1:2). 6.0 mL of the PC stock solution was put into a round bottom flask and 9.0 mL of PBS solution (pH 6.8) was gently poured along the flask walls. The organic solvents were removed using a rotary evaporator, under reduced pressure at 40°C and 40 rpm. The GUVs suspension was transferred in a 10 mL volumetric flask and brought to volume with PBS solution. In order to produce small unilamellar vesicles (SUVs), the suspension was sonicated in an ice-water bath. Sonication was performed for 2 min and repeated 4 times with 2 min of interval.

SUVs size and distribution were determined by dynamic light scattering (DLS) analysis using 90 Plus particle size analyzer (Brookhaven Instruments Corporation, New York, NY USA) at  $25.0 \pm 0.1^\circ\text{C}$  by measuring the autocorrelation function at  $90^\circ$ . The laser was operating at 658 nm. The distribution size and the polydispersity index were directly obtained from the instrument.

#### *Determination of partition coefficient*

SUVs obtained have been used as a cell membrane model to calculate membrane/buffer solution partition coefficient of SER-SUT conjugate, using

derivative spectrophotometry, as reported by Takegami et al. (Takegami, Kitamura et al., 2015).

Nine sample solutions containing SUT (20  $\mu\text{M}$ ) and various amounts of the SUV suspension with a concentration of PC in the range of 0-1200  $\mu\text{M}$  were prepared. The reference solutions were prepared without SUT. Each vial containing the sample was shaken and incubated for 2 h in order to reach the equilibrium state.

The absorption spectra were measured using 1 cm light-pass length cuvette, in the wavelength range between 400-550 nm with interval of 0.5 nm. The second-derivative spectra were calculated using “Spectra Manager” software v. 1.53.01, based on the Savitzky-Golay method in which the second-order polynomial convolution of 21 points was employed (Savitzky & Golay, 1964).

### **Cell viability assay**

Cell viability was determined using the 3-(4,5-dimethylthiazol-2-yl)-2,5-diphenyltetrazolium (MTT, Sigma-Aldrich, Milan, Italy) assay as reported by Saturnino et al. (Saturnino, Sinicropi et al., 2014) with some modifications. Briefly, MCF-7 cells were seeded on forty-eight well plates and grown in DMEM-F12 containing 10% fetal bovine serum (FBS), 1% L-Glutamine, 1 mg/ml penicillin-streptomycin. MCF-10A human mammary epithelial cells were cultured in DMEM-F12 supplemented with 10% horse serum (HS), 1% L-Glutamine, 1% penicillin/streptomycin, 0.5 mg/ml hydrocortisone, 20 ng/ml hEGF (human epidermal growth factor) and 0.1 mg/ml cholera enterotoxin (Sigma-Aldrich, Milan, Italy) and 10  $\mu\text{g/ml}$  insulin. SUT was dissolved in dimethyl sulfoxide (DMSO) (Sigma, St. Louis, Missouri, USA) at a concentration of 50 mM and diluted in DMEM/F12 medium supplemented with 1% FBS (MCF-7) or 1% HS (MCF-10A) to obtain the working concentration. SER-SUT conjugated and SER were directly dissolved in DMEM/F12 medium supplemented with 1% FBS (MCF-7) or 1% HS (MCF-10A). Before the treatment, cells were serum deprived for 24 h, then treated with six different concentrations of SUT, SER-SUT or SER for 72 hours in medium containing 1% FBS (MCF-7) or 1% HS (MCF-10A). At the end of the treatment, fresh MTT re-suspended in PBS was added to each well to a final concentration of 0.2 mg/mL. After 2 hours incubation at 37°C, cells were lysed with a solution containing 50% (v/v) N,N-dimethylformamide and 20% (w/v) SDS, pH of 4.5, and then optical density was measured at 570 nm with a reference wavelength of 620 nm, using a

microplate reader. MTT experiments have been performed in sextuplicate and repeated three times. Absorbance values were used to determine the IC<sub>50</sub> using GraphPad Prism 5 Software (GraphPad Inc., San Diego, CA). Data are representative of three independent experiments; standard deviations (SD) were shown.

### *Data analysis and statistical methods*

Statistical significance between control and treated cells was analyzed by the means of GraphPad Prism 5.0 (GraphPad Software, Inc.; La Jolla, CA) software, using the analysis of variance (ANOVA) with Kruskal-Wallace test and post hoc Dunn's Multiple Comparison Test. Significance was defined as \*  $p < 0.05$ , \*\*  $p < 0.01$ .

## RESULTS AND DISCUSSION

### **Sericin extraction yield**

Sericin, extracted and isolated from silk, can vary depending on extraction method and on source type. These two factors can highly influence the yield of extraction, as well as sericin molecular weight and its biological activity (Siritientong, Bonani et al., 2016). White cocoons of *Bombyx mori* strain were boiled in hot water, at atmospheric pressure. Sericin was then isolated and purified according to the procedure described in the experimental session. The yield of extraction was calculated comparing the dry weight of sericin purified to the dry extract of the cocoon boiling water. The yield obtained ranged between 19% and 22%. Molecular weight and biological activity on healthy tissue were evaluated and reported in the following sections.

### **Sericin-sunitinib conjugate synthesis**

Sericin-sunitinib (SER-SUT) conjugate was synthesized using a click chemistry approach. The reaction involved the direct free radical grafting of SUT onto a biopolymeric chain, such as the protein sericin. According to synthetic procedure used for the achievement of the SER-SUT conjugate, a covalent bond has been introduced between the protein and the drug.

SER is a hydrophilic polypeptide characterized by fine water solubility as well as by low cytotoxicity towards living tissues. SER, indeed, has been successfully applied in various fields, especially in pharmaceutical and biomedical ones.

In the present work, in order to obtain the SER-SUT grafted protein, the initiation of the reaction occurred through the employment of hydrogen peroxide/L-ascorbic acid redox pair (Lemma, Puoci et al., 2010). The high biocompatibility and water solubility of the initiating system allow the obtainment of the drug-conjugate in aqueous solutions, working at room temperature and avoiding the use of any organic solvent, which is not possible with conventional radical initiator systems (azo compounds and peroxides). Furthermore, non-toxic by-products are generated during the reaction.

The mechanism of the redox reaction is based on the oxidation of the L-ascorbic acid by  $H_2O_2$  generating hydroxyl radical and L-ascorbate radical intermediates, responsible for reaction initiation. In particular, hydroxyl radical is one of the most reactive radicals among the reactive oxygen species, and it is able to generate SER macroradicals centered on polar amino acids, on which labile hydrogens are abstracted (Song, Jin et al., 2006). The rate of hydrogen abstraction is dependent on the dissociation energy of the X-H bond to form the radical. The low molecular weight drug reacts with generated macroradicals and is grafted onto the SER biopolymeric chain.

The ratio 1:5 w/w between drug and protein was used for the grafting reaction.

FT-IR analyses were performed aiming at the identification and verification of the grafting of the drug on SER. Three different spectra were recorded (Figure 6.1): sunitinib malate (trace A); sericin-sunitinib conjugate (trace B) and sericin (trace C). The comparison of IR spectra showed the presence of a new signal at  $1031.73\text{ cm}^{-1}$  in the spectrum of SER-SUT conjugate, that is identified also in the spectrum of sunitinib malate and corresponding to the stretching vibration of carbon-fluorine bond (stretching vibration of carbon-halogen single bond shows a typical band at  $\nu < 1200\text{ cm}^{-1}$ ). On the contrary, the same peak is absent in the sericin spectrum.

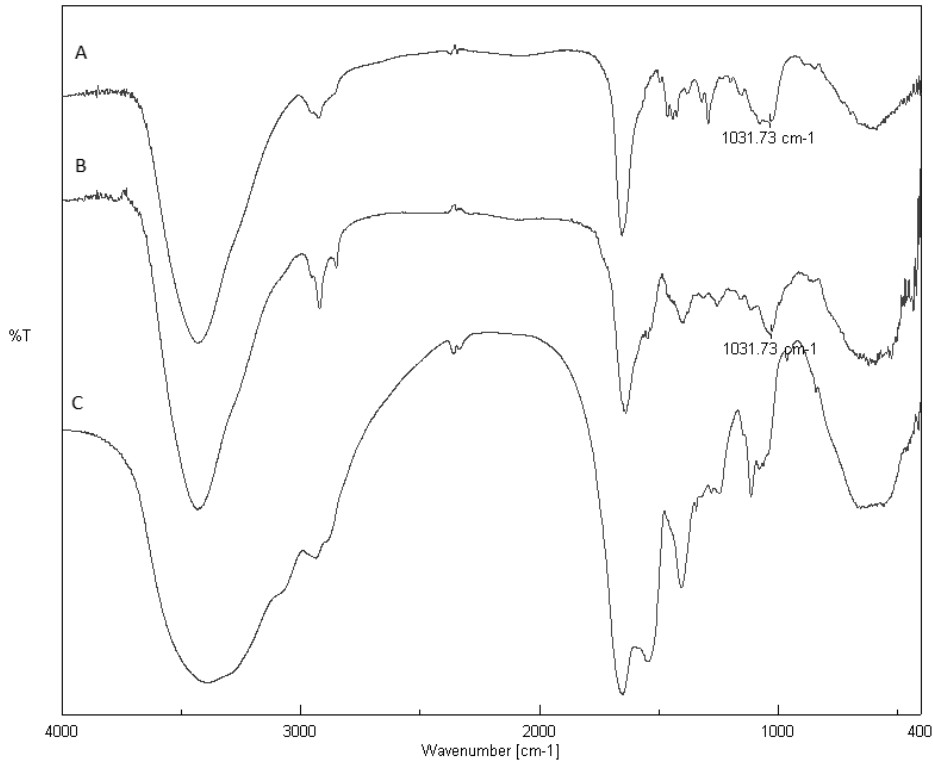


**Figure 6.1** FT-IR spectra of (A) sunitinib malate, (B) sericin-sunitinib conjugate and (C) sericin.

For further evidence, UV/Vis spectra of sericin, sunitinib malate and sericin-sunitinib conjugate were also recorded between 250 nm and 700 nm (data not shown). Sericin and sunitinib malate showed typical absorbance at  $\lambda_{\max} = 273$  nm and  $\lambda_{\max} = 426$  nm, respectively. As confirmation of the occurred grafting, both peaks can be observed in the SER-SUT conjugate spectrum.

With the help of UV/Vis spectroscopy the amount of grafted SUT was determined, through the equation of the calibration curve of sunitinib malate. The content of SUT calculated was 6.5 mg of SUT per g of SER-SUT conjugate.

Literature data reported that sericin from silk may exist in different molecular weight forms, depending on the extraction processes, processing time, temperature or pH (Aramwit, Siritientong et al., 2011). The sericin forms involved in grafting process were evaluated by means of Sodium Dodecyl Sulphate-PolyAcrylamide Gel Electrophoresis (SDS-PAGE). Stock solutions of



both SER and SER-SUT were prepared in loading buffer and 0.02  $\mu\text{g}$  were analyzed. First, the aliquots were heated to 100°C for 10 minutes, then loaded onto a 15% acrylamide gel (6% stacking gel and 15% resolving gel) and run under denaturing conditions. Electrophoresis was performed initially at 60 V until the samples migrated into the stacking gel, followed by 150 V until the last band of the marker reached the bottom of the gel. Immediately after the run, the gel was silver stained, in order to reveal protein bands. Only two faint protein bands with an apparent molecular weight ranging from 50 to 75 kDa were revealed by gel staining (Figure 6.2, black arrows), in both SER and SER-SUT conjugate, thus the grafting process did not produce any electrophoretic difference with respect to the original SER preformed biopolymeric chain.

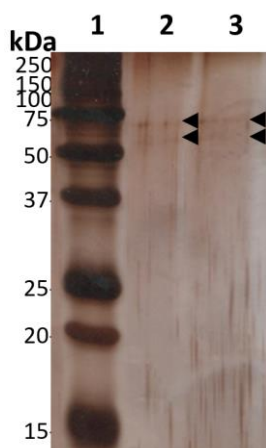


**Figure 6.2** SDS-PAGE of SER and SER-SUT conjugate. 0.02  $\mu\text{g}$  of proteins were separated by SDS-PAGE and stained with silver nitrate. Lane 1, marker; Lane 2, SER; Lane 3, SER-SUT conjugate. Black arrows indicate protein bands.

### ***In vitro* bioavailability studies**

Many anticancer drugs, like sunitinib, suffer from low *in vivo* bioavailability. This drawback usually depends on several factors, such as low intrinsic activity, poor absorption, rapid metabolization and/or elimination. Solubility also plays a key role in determining drug oral bioavailability, since only the soluble fraction is considered bioaccessible (Bouayed, Hoffmann et al., 2011). In order to evaluate the improvement of SER-SUT conjugate bioavailability, *in vitro* tests were performed. Resulting data were obtained using equation (6.1) and reported in Table 6.1 (see Experimental section for more details).

$$\text{Bioavailability (\%)} = \frac{\text{Sample content}}{\text{Total content}} \times 100 \quad (6.1)$$

In 2011, Di Gion et al. have presented a work regarding several TKIs pharmacokinetic parameters. In that article the reported absolute oral bioavailability percentage of sunitinib in humans, under fasted conditions, was around 50% (Di Gion, Kanefendt et al., 2011).

In our study, the bioavailability evaluation was performed comparing formulated sunitinib, also commercially known as Sutent<sup>®</sup> (Pfizer) and SER-SUT conjugate. Data reported shows a good bioavailability percentage after six hours for both samples, slightly improved in the case of the conjugate. However, a significative increase is yet observable after 2 hours, meaning a ready dissolution of the sericin protein-sunitinib conjugate in the gastric environment.

**Table 6.1** Bioavailability of sunitinib and SER-SUT conjugate.

<b>Time Points</b>	<b>Sutent<sup>®</sup> Bioavailability %</b>	<b>SER-SUT conjugate Bioavailability %</b>
<b>Phase I 2h</b>	20.3 ± 0.7	45.1 ± 0.9
<b>Phase II 4h</b>	47.5 ± 0.8	28.8 ± 0.7
<b>6h</b>	67.8 ± 1.0	73.9 ± 1.1

### ***In vitro* membrane permeability studies**

The ability of SER-SUT conjugate to cross biological membranes compared to free SUT has been investigated through permeability studies, using phosphatidylcholine liposomes.

It is well known that drug's therapeutic and cytotoxic activities, as well as absorption, distribution, metabolism and excretion, are governed by drug affinity with biological membranes. Interactions between drug and cell membrane is, indeed, responsible for its bioaccumulation. The entire drug life *in vivo* is influenced by its interaction with membranes and often the therapeutic target is within the membrane itself, as in the case of SUT.

Bioaccessibility and bioconcentration is strongly dependent on the ability of the drug to cross the phospholipidic bilayer *via* diffusion, thus on drug hydrophilic/hydrophobic ratio, which can be quantitatively expressed as partition

coefficient between two phases. A simple model widely used to determine drugs partition coefficient is based on a *n*-octanol/water system that is thermodynamically different from biological models and it is considered only an approximation of the physiological condition.

However, liposomal model is a more reliable system, able to mimic the cell environment. Liposomes are closed membranes made of amphiphilic lipids, characterized by a liquid crystal structure, that take into account of the surface charges involved in the drug/cell electrostatic interactions, particularly important for charged and polar drugs. In addition, the complexity of the bilayer structure and steric forces can contribute, either positively or negatively, in drugs bioaccessibility. For such reasons, the partition coefficient obtained by anisotropic membrane/buffer solution system better predicts drugs behaviour in biological environment than an isotropic 2-phase solvent system (i.e. *n*-octanol/water).

Analytical determination of membrane/buffer solution partition coefficient by spectrophotometry requires phase separation, which disturbs the established equilibrium state. The interruption of the equilibrium can cause inaccuracy of the measurement, as well as loss of the bilayer drug content. Furthermore, liposome suspensions cause interference in absorption spectra, especially in UV region, because of the intense background signal due to the light scattered by lipid vesicles. However, investigation by second derivative spectroscopic methodology can avoid vesicles interference, without disturbing partition equilibrium, improving at the same time the resolution of overlapped bands. Moreover, SUT absorbs in the visible region, where interference is completely eliminated in second derivative spectroscopy (Figure 6.3, black arrows).

Since the sunitinib peak is observable also in SER-SUT conjugate absorption spectrum, the same method could be applied for the determination of bioconjugate partition coefficient.

For the experimental procedure small unilamellar vesicles (SUVs) were produced *via* self-assembly of phosphatidylcholine (PC). SUVs size was measured by DLS analysis showing a homogeneous population of liposomes with a mean diameter in the range of 170-180 nm. The absorption spectra of 20  $\mu$ M SUT and SER-SUT conjugate with equal SUT concentration, recorded in suspensions containing various concentrations of PC liposomes, are shown in Figure 6.3.

The presence of isosbestic points in the overlaid spectra at different concentrations of PC confirmed the existence of an equilibrium between drug dissolved in the polar aqueous phase of the buffer solution and in the non-polar PC bilayer phase.

The membrane/buffer solution partition coefficient ( $K_p$ ) of both SUT and SER-SUT conjugate were calculated using the following equation (6.2) and applying the Scott-plot method:

$$\Delta D = \frac{K_p \Delta D_{max} [L]}{[W] + K_p [L]} \quad (6.2)$$

where  $\Delta D$  is the derivative intensity difference of drug before and after the addition of EPC SUV,  $[L]$  and  $[W]$  are the concentrations of EPC and water, respectively, and  $\Delta D_{max}$  is the maximum  $\Delta D$  value assuming all drug is partitioned in PC SUVs. Partition coefficient was expressed as  $\log(K_p)$  for a ready interpretation of the data. Results obtained are reported in Table 6.2 and expressed as mean value  $\pm$  standard deviation.

According to the Lipinski's "rule of five", one criterion for a good oral bioavailability is that the log of the partition coefficient,  $\log(K_p)$  or the log of the ratio of the solubility of the drug in *n*-octanol/water, should be less than 5. From the scientific literature, we know that  $\log(K_p)_{o/w}$  for sunitinib is 5.2 (Roskoski, 2007). However, in a more complex model, such as membrane/buffer solution system,  $\log(K_p)$  value take into account surface charges, electrostatic interactions and steric forces. Furthermore, the partitioning of the solutes within lipid membranes occur by a mechanism which is different from the one occurring in oil phase.

Using this model, SUT showed a good  $\log(K_p)$  value (see Table 6.2), while SER-SUT conjugate partition coefficient resulted augmented. In particular, this latter behaviour can be likely ascribed to the protein structure that confers plasticity and adaptability to the lipid bilayer.

**Table 6.2**  $\log(K_p)$  and  $IC_{50}$  values of sunitinib and SER-SUT conjugate.

Compound	$\log(K_p)$	$IC_{50}$ ( $\mu M$ )	
		MCF-7	MCF-10A
Sunitinib	$3.4 \pm 0.2$	$24.6 \pm 1.2$	> 76
Sericin-sunitinib conjugate	$4.1 \pm 0.3$	$7.8 \pm 0.9$	> 76

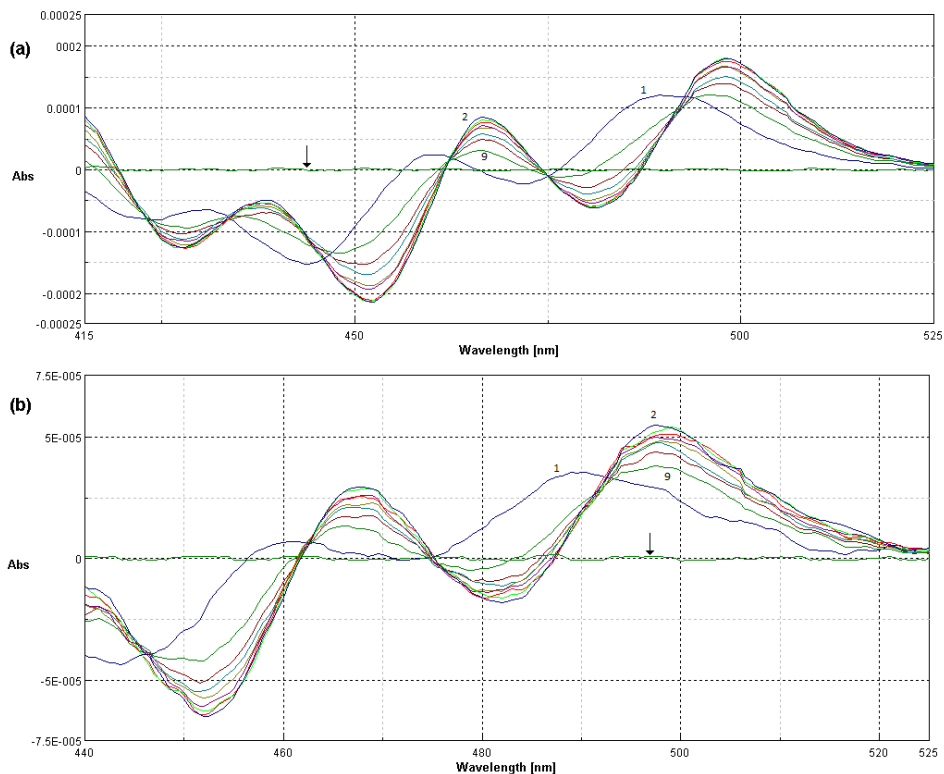


**Figure 6.3** Second derivative spectra of SUT (a) and SER-SUT conjugate (b) calculated from the absorption spectra, at different concentration of SUVs (1) 0  $\mu\text{M}$ , (2) 150  $\mu\text{M}$ , (3) 300  $\mu\text{M}$ , (4) 450  $\mu\text{M}$ , (5) 600  $\mu\text{M}$ , (6) 750  $\mu\text{M}$ , (7) 900  $\mu\text{M}$ , (8) 1050  $\mu\text{M}$ , (9) 1200  $\mu\text{M}$ . Black arrows indicate the second derivative absorption spectra of SUVs in absence of SUT or SER-SUT.

### Cell viability assay

In order to evaluate the antitumor activity of SER-SUT conjugate, estrogen receptor positive (ER<sup>+</sup>) MCF-7 cells were used. Concentrations of SER-SUT conjugate have been chosen taking into account the content of SUT conjugated to SER from UV/Vis experiments (see “Sericin-sunitinib conjugate synthesis” paragraph), so that same concentrations of SUT alone and SER-SUT conjugate were tested. Cells were grown up to 50-60% confluence and treated with increasing doses of both SUT and SER-SUT conjugate (see experimental procedures for details) and, after 72 hours, cell viability was determined by MTT assay (Iacopetta, Rosano et al., 2017). Both SUT and SER-SUT exhibited a dose-dependent reduction of MCF-7 cells viability at the end of the experiment (Figure 6.4, panel A) whereas no effect has been noticed on the normal MCF-10A cells

viability (Figure 6.4, panel B).  $IC_{50}$  values, reported in Table 6.2 and calculated for both SUT and SER-SUT in MCF-7 and MCF-10A cells, demonstrated an increase of SER-SUT conjugate cytotoxic effect, which is about three-times higher than that of SUT, in MCF-7 cells. On the contrary, neither SUT nor SER-SUT affect MCF-10A cells viability ( $IC_{50} > 76 \mu\text{M}$ , Table 6.2).

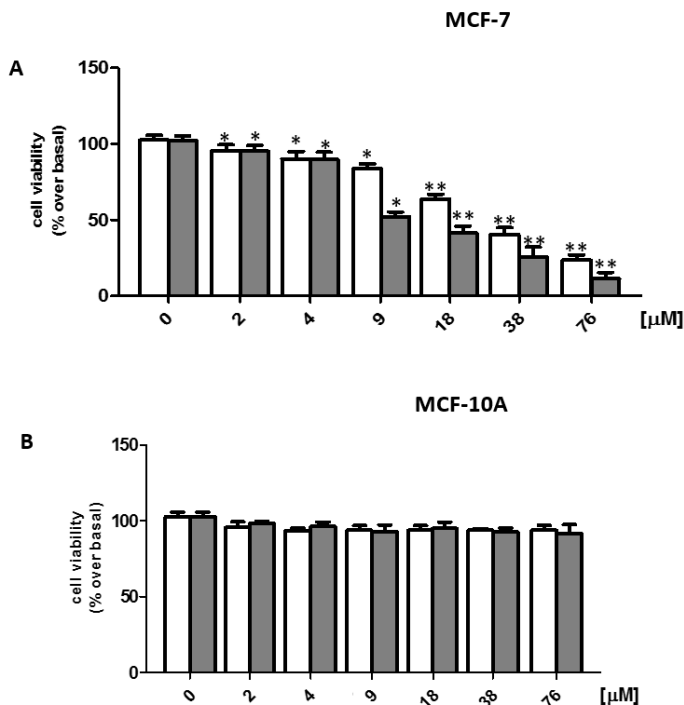


**Figure 6.4** Graphs of MCF-7 (A) and MCF-10A (B) cell viability, exposed to □Sunitinib; ■Sercin-sunitinib conjugate. \* $p < 0.05$  \*\* $p < 0.01$ .

The main concern for using SER for biomedical applications is its allergic property, hence its safety. This aspect has been recently discussed in a work of Ampawong et al., in which SER showed a tolerogenic activity (Ampawong & Aramwit, 2016). Moreover, at the same concentrations and conditions used in our experiments, SER alone did not exert any toxic effect on MCF-7 and MCF-10A cells (data not shown). These outcomes suggest that the increased antitumor activity might be due to the improved solubility and cell permeability of SER-SUT conjugate.

## CONCLUSIONS

In the present research paper, we have reported the free radical grafting of sunitinib onto sericin polypeptide chain, *via* single-step click reaction. The biocompatible and water soluble redox couple (L-ascorbic acid / hydrogen peroxide) has been employed in order to initiate the reaction. The covalent attachment of sunitinib has been obtained by hydroxyl radical action generated during the reaction. It was confirmed by FT-IR and UV/Vis spectroscopy, after protein purification.

*In vitro* gastrointestinal bioavailability experiments have highlighted an improved percentage of sunitinib that can cross the simulated GI lumen, compared to the commercially available drug (Sutent®). This effect is certainly due to augmented water solubility of the sericin-sunitinib conjugate and it is evident from the very first two hours, in which we observed the ready dissolution of the functionalized material.

Second derivative spectroscopy has given the opportunity to evaluate the interaction between sericin-sunitinib conjugates and cell membrane models, such as phosphatidylcholine small unilamellar vesicles. The study demonstrated an improvement of sericin-sunitinib membrane permeability, expressed as an increase of membrane/buffer solution partition coefficient.

In the end, the *in vitro* cytotoxicity tests showed that the newly synthesized sericin-sunitinib conjugate is three times more effective than free sunitinib, thanks to the characteristics acquired by conjugation with the protein.

Thanks to these results we can state that the production of a sericin-grafted biomaterial is a valuable method to improve bioavailability and permeability of drugs like sunitinib.

## REFERENCES

- Akash MSH, Rehman K, Parveen A, Ibrahim M (2016) Antibody-drug conjugates as drug carrier systems for bioactive agents. *International Journal of Polymeric Materials and Polymeric Biomaterials* 65: 1-10.
- Alley SC, Okeley NM, Senter PD (2010) Antibody–drug conjugates: targeted drug delivery for cancer. *Current opinion in chemical biology* 14: 529-537.
- Amidon GL, Lennernäs H, Shah VP, Crison JR (1995) A theoretical basis for a biopharmaceutical drug classification: the correlation of in vitro drug product dissolution and in vivo bioavailability. *Pharmaceutical research* 12: 413-420.
- Ampawong S, Aramwit P (2016) Tolerogenic responses of CD206+, CD83+, FOXP3+, and CTLA-4 to sericin/polyvinyl alcohol/glycerin scaffolds relevant to IL-33 and HSP60 activity. *Histology and histopathology*: 11733-11733.
- Aramwit P, Siritientong T, Srichana T (2011) Potential applications of silk sericin, a natural protein from textile industry by-products. *Waste Management & Research*: 0734242X11404733.
- Bouayed J, Hoffmann L, Bohn T (2011) Total phenolics, flavonoids, anthocyanins and antioxidant activity following simulated gastro-intestinal digestion and dialysis of apple varieties: Bioaccessibility and potential uptake. *Food Chemistry* 128: 14-21.
- Coburn JM, Kaplan DL (2015) Engineering Biomaterial–Drug Conjugates for Local and Sustained Chemotherapeutic Delivery. *Bioconjugate chemistry* 26: 1212-1223.
- Deng L, Zhang H, Yang M, Mandal N, Zhu L (2014) Improving properties of superabsorbent composite induced by using alkaline protease hydrolyzed-sericin (A<sub>Ph</sub>-sericin). *Polymer Composites* 35: 509-515.
- Di Gion P, Kanefendt F, Lindauer A, Scheffler M, Doroshenko O, Fuhr U, Wolf J, Jaehde U (2011) Clinical pharmacokinetics of tyrosine kinase inhibitors. *Clinical pharmacokinetics* 50: 551-603.
- Etrych T, Šubr V, Strohalm J, Šírová M, Říhová B, Ulbrich K (2012) H<sub>2</sub>PMA copolymer-doxorubicin conjugates: The effects of molecular weight and architecture on biodistribution and in vivo activity. *Journal of controlled release* 164: 346-354.



Fattahi A, Asgarshamsi M, Hasanzadeh F, Varshosaz J, Rostami M, Mirian M, Sadeghi-aliabadi H (2015) Methotrexate-grafted-oligochitosan micelles as drug carriers: synthesis and biological evaluations. *Journal of Materials Science: Materials in Medicine* 26: 1-10.

Grande F, Parisi OI, Mordocco RA, Rocca C, Puoci F, Scrivano L, Quintieri AM, Cantafio P, Ferla S, Brancale A (2016) Quercetin derivatives as novel antihypertensive agents: Synthesis and physiological characterization. *European Journal of Pharmaceutical Sciences* 82: 161-170.

Herbrink M, Nuijen B, Schellens JH, Beijnen JH (2015) Variability in bioavailability of small molecular tyrosine kinase inhibitors. *Cancer treatment reviews* 41: 412-422.

Iacopetta D, Rosano C, Puoci F, Parisi OI, Saturnino C, Caruso A, Longo P, Ceramella J, Malzert-Fréon A, Dallemagne P (2017) Multifaceted properties of 1, 4-dimethylcarbazoles: Focus on trimethoxybenzamide and trimethoxyphenylurea derivatives as novel human topoisomerase II inhibitors. *European Journal of Pharmaceutical Sciences* 96: 263-272.

Iemma F, Puoci F, Curcio M, Parisi OI, Cirillo G, Spizzirri UG, Picci N (2010) Ferulic acid as a comonomer in the synthesis of a novel polymeric chain with biological properties. *Journal of applied polymer science* 115: 784-789.

Izzedine H, Buhaescu I, Rixe O, Deray G (2007) Sunitinib malate. *Cancer Chemotherapy and Pharmacology* 60: 357-364.

Jabbour E, Kantarjian H, Cortes J (2015) Use of second-and third-generation tyrosine kinase inhibitors in the treatment of chronic myeloid leukemia: An evolving treatment paradigm. *Clinical Lymphoma Myeloma and Leukemia* 15: 323-334.

Kassem MG, Motiur Rahman AFM, Korashy HM (2012) Chapter 9 - Sunitinib Malate. In *Profiles of Drug Substances, Excipients and Related Methodology*, Harry GB (ed) pp 363-388. Academic Press.

Kok R, Grijpstra F, Nederhoed K, Moolenaar F, Zeeuw DD, Meijer D (1999) Renal drug delivery with low-molecular-weight proteins: The effect of charge modifications on the body distribution of drug-lysozyme conjugates. *Drug Delivery* 6: 1-8.

Laemmli UK (1970) Cleavage of structural proteins during the assembly of the head of bacteriophage T4. *nature* 227: 680-685.

Lamboni L, Gauthier M, Yang G, Wang Q (2015) Silk sericin: A versatile material for tissue engineering and drug delivery. *Biotechnology advances* 33: 1855-1867.

Liu B, Song Y-w, Jin L, Wang Z-j, Pu D-y, Lin S-q, Zhou C, You H-j, Ma Y, Li J-m (2015) Silk structure and degradation. *Colloids and Surfaces B: Biointerfaces* 131: 122-128.

Madeo M, Carrisi C, Iacopetta D, Capobianco L, Cappello AR, Bucci C, Palmieri F, Mazzeo G, Montalto A, Dolce V (2009) Abundant expression and purification of biologically active mitochondrial citrate carrier in baculovirus-infected insect cells. *Journal of bioenergetics and biomembranes* 41: 289-297.

Moscho A, Orwar O, Chiu DT, Modi BP, Zare RN (1996) Rapid preparation of giant unilamellar vesicles. *Proceedings of the National Academy of Sciences* 93: 11443-11447.

Napavichayanun S, Amornsudthiwat P, Pienpinijtham P, Aramwit P (2015) Interaction and effectiveness of antimicrobials along with healing-promoting agents in a novel biocellulose wound dressing. *Materials Science and Engineering: C* 55: 95-104.

Padamwar M, Pawar A (2004) Silk sericin and its applications: A review. *Journal of Scientific and Industrial Research* 63: 323-329.

Pang X, Du H-L, Zhang H-Q, Zhai Y-J, Zhai G-X (2013) Polymer–drug conjugates: present state of play and future perspectives. *Drug discovery today* 18: 1316-1322.

Papaetis GS, Syrigos KN (2009) Sunitinib: a multitargeted receptor tyrosine kinase inhibitor in the era of molecular cancer therapies. *BioDrugs : clinical immunotherapeutics, biopharmaceuticals and gene therapy* 23: 377-89.

Parisi OI, Fiorillo M, Scrivano L, Sinicropi MS, Dolce V, Iacopetta D, Puoci F, Cappello AR (2015) Sericin/poly (ethylcyanoacrylate) nanospheres by interfacial polymerization for enhanced bioefficacy of fenofibrate: in vitro and in vivo studies. *Biomacromolecules* 16: 3126-3133.

Parisi OI, Morelli C, Scrivano L, Sinicropi MS, Cesario MG, Candamano S, Puoci F, Sisci D (2015) Controlled release of sunitinib in targeted cancer therapy: smart magnetically responsive hydrogels as restricted access materials. *RSC Advances* 5: 65308-65315.

Puoci F, Morelli C, Cirillo G, Curcio M, Parisi OI, Maris P, Sisci D, Picci N (2012) Anticancer activity of a quercetin-based polymer towards HeLa cancer cells. *Anticancer research* 32: 2843-2847.

Roskoski R (2007) Sunitinib: a VEGF and PDGF receptor protein kinase and angiogenesis inhibitor. *Biochemical and biophysical research communications* 356: 323-328.

Saturnino C, Sinicropi MS, Parisi OI, Iacopetta D, Popolo A, Marzocco S, Caruso A, Cappello AR, Longo P, Puoci F (2014) Acetylated hyaluronic acid: enhanced bioavailability and biological studies. *BioMed research international* 2014.

Savitzky A, Golay MJ (1964) Smoothing and differentiation of data by simplified least squares procedures. *Analytical chemistry* 36: 1627-1639.

Siritientong T, Bonani W, Motta A, Migliaresi C, Aramwit P (2016) The effects of Bombyx mori silk strain and extraction time on the molecular and biological characteristics of sericin. *Bioscience, Biotechnology, and Biochemistry* 80: 241-249.

Song Y, Jin Y, Sun J, Wei D (2006) Graft copolymerization of methyl acrylate onto silk sericin initiated by tert-butyl hydroperoxide. *Polymer international* 55: 1350-1354.

Takegami S, Kitamura K, Ohsugi M, Ito A, Kitade T (2015) Partitioning of organophosphorus pesticides into phosphatidylcholine small unilamellar vesicles studied by second-derivative spectrophotometry. *Spectrochimica Acta Part A: Molecular and Biomolecular Spectroscopy* 145: 198-202.

Vicent MJ (2007) Polymer-drug conjugates as modulators of cellular apoptosis. *The AAPS journal* 9: E200-E207.

Vittorio O, Cirillo G, Iemma F, Di Turi G, Jacchetti E, Curcio M, Barbuti S, Funel N, Parisi OI, Puoci F (2012) Dextran-catechin conjugate: a potential treatment against the pancreatic ductal adenocarcinoma. *Pharmaceutical research* 29: 2601-2614.

Walde P, Cosentino K, Engel H, Stano P (2010) Giant vesicles: preparations and applications. *ChemBioChem* 11: 848-865.

Wu L, Zhang Z, Yao H, Liu K, Wen Y, Xiong L (2014) Clinical efficacy of second-generation tyrosine kinase inhibitors in imatinib-resistant gastrointestinal stromal tumors: a meta-analysis of recent clinical trials. *Drug design, development and therapy* 8: 2061.

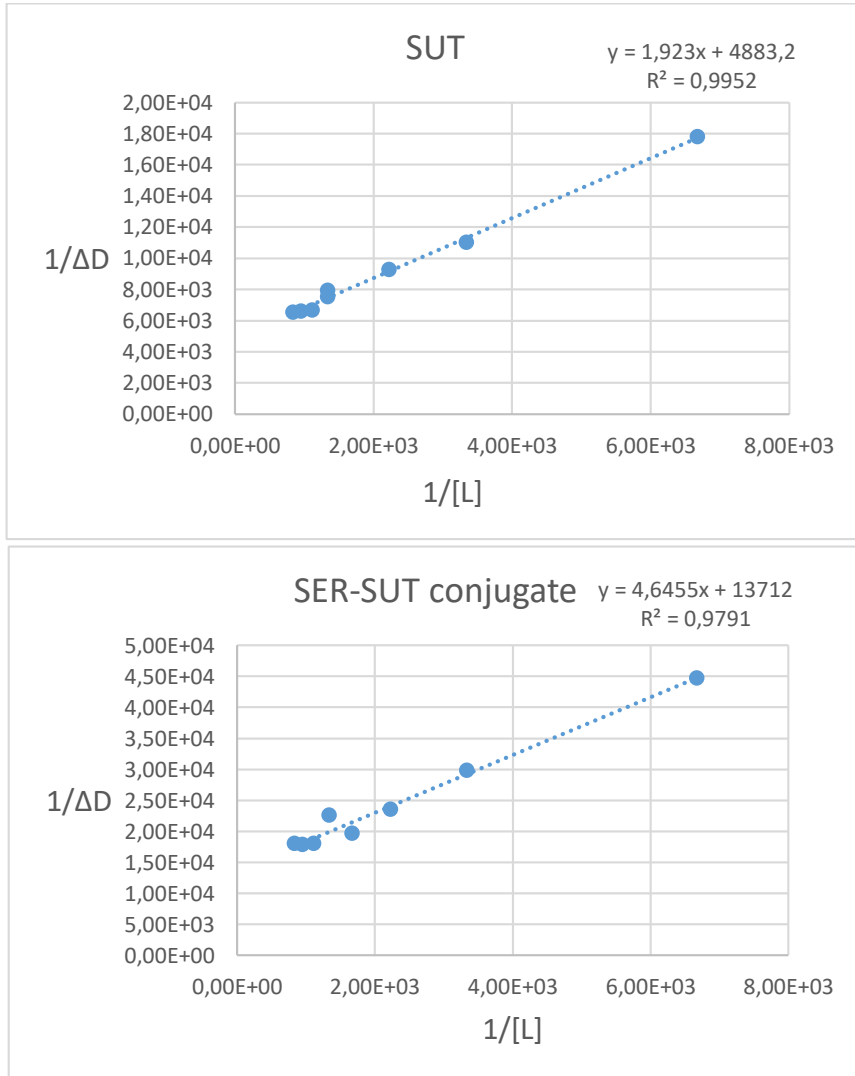
Zhang Y-Q, Ma Y, Xia Y-Y, Shen W-D, Mao J-P, Xue R-Y (2006a) Silk sericin–insulin bioconjugates: Synthesis, characterization and biological activity. *Journal of controlled release* 115: 307-315.

Zhang YQ, Tao ML, Shen WD, Mao JP, Chen Yh (2006b) Synthesis of silk sericin peptides–L-asparaginase bioconjugates and their characterization. *Journal of Chemical Technology and Biotechnology* 81: 136-145.

Zhao L, Liu C, Sun Y, Ban L (2012) A rapid and simplified method for protein silver staining in polyacrylamide gels. *Electrophoresis* 33: 2143-2144.

SUPPLEMENTARY MATERIALS

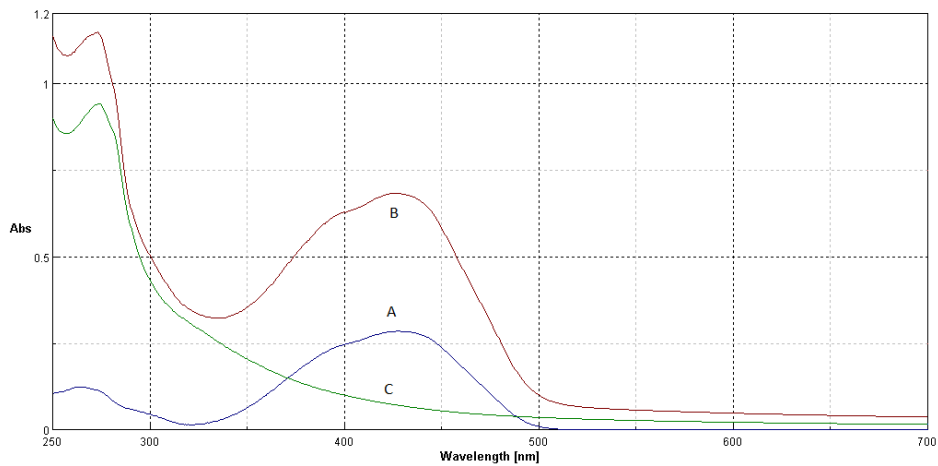
Sunitinib and Sericin-sunitinib conjugate membrane permeability



**Figure 6.1S** Scott-plot linearized data of (top) SUT and (bottom) SER-SUT conjugate membrane permeability.

Scott-plot linearized form of the equation (6.2)

$$\frac{1}{\Delta D} = \frac{[W]}{K_p \Delta D_{\max}} \frac{1}{[L]} + \frac{1}{\Delta D_{\max}}$$

**Sericin-sunitinib conjugate UV/Vis characterization**

**Figure 6.2S** UV/Vis spectra of (A) sunitinib malate, (B) sericin-sunitinib conjugate and (C) sericin..

## CHAPTER 7

# Biopolymeric self-assembled nanoparticles for enhanced antibacterial activity of Ag-based compounds

Dhanya Dhanyalayam<sup>a,1</sup>, Luca Scrivano<sup>a,1</sup>, Ortensia Ilaria Parisi<sup>a</sup>, Maria Stefania Sinicropi<sup>a</sup>, Antonietta Fazio<sup>a</sup>, Carmela Saturnino<sup>b,\*</sup>, Maria Rosaria Plutino<sup>c</sup>, Francesca Di Cristo<sup>d</sup>, Francesco Puoci<sup>a,\*</sup>, Anna Rita Cappello<sup>a</sup> and Pasquale Longo<sup>e</sup>

<sup>1</sup> These authors equally contributed to the manuscript

<sup>a</sup> Department of Pharmacy, Health and Nutritional Sciences, University of Calabria, Rende (CS), Italy.

<sup>b</sup> Department of Sciences, University of Basilicata, Potenza, Italy.

<sup>c</sup> Institute for the Study of Nanostructured Materials, ISMN-CNR, O.U. Palermo, c/o Dep. of ChiBioFarAm, University of Messina, Vill. S. Agata, Messina, Italy.

<sup>d</sup> Department of Pharmaceutical and Biomedical Sciences, University of Salerno, Fisciano (SA) Italy.

<sup>e</sup> Department of Chemistry and Biology, University of Salerno, Fisciano (SA), Italy.

*International Journal of Pharmaceutics* (2017), 517, 395-402.

DOI: 10.1016/j.ijpharm.2016.12.039

## ABSTRACT

Microbial infections still remain one of the main issue for human health. The rapid development of resistance towards the most common antimicrobial drugs in bacteria represents today a challenge in the infections management. In the present work we have investigated the antibacterial activity of a group of compounds, namely silver N-heterocyclic carbene complexes, against a broad spectrum of bacteria. For the most promising compound, a biopolymeric nanocarrier has been developed, in order to potentiate the metal complex activity against both Gram +ve and Gram -ve. The polymeric nanovehicle is based on dextran, modified with oleic acid residues, that confer amphiphilic properties to the polysaccharide. We have characterized the obtained biomaterial and studied its ability to self-assemble into nanoparticles in aqueous environment. Next, the transdermal diffusion analyses have been carried out to evaluate the ability of the polymeric particles to penetrate tissues. Thanks to the strategy adopted, we have fabricated an antibacterial system to which *K. pneumoniae* and *E. coli* are the most sensitive.



## INTRODUCTION

Microbial infections are still one of the major causes of death among world population. It is estimated that 26% of the total global deaths are caused by infectious diseases (IDs) and in sub-Saharan Africa, in particular, deaths for IDs reach 50-52% (Becker et al., 2006). Antibiotics are certainly an important weapon against IDs, however, their wide use to control microbial infections in humans, animals and in agriculture has caused the development of resistance in bacterial populations. Over time, this phenomenon has enabled the selection of drug-resistant bacteria, acquiring survival ability through three main mechanisms: the capture by bacteria of resistance genes from the surrounding environment; the freezing of polymorphism in antibiotic target genes that imparts drug-resistance (Andersson and Hughes, 2011); and the up-regulation of proteins involved in drug efflux (Cox and Wright, 2013; Fajardo et al., 2008) or enzymatic inactivation (Abraham and Chain, 1940). Besides this the infections, caused by Gram –ve bacteria, are difficult to treat because these organisms have a protective outer membrane consisting of lipopolysaccharides (Pagès et al., 2008).

For this reason, there is an urgent need of new antimicrobial agents that express antibacterial activity, particularly against Gram –ve pathogens and that could be used to fight drug resistance.

Metallic silver, silver salts and silver complexes have been used since antiquity in a variety of applications like water purification, wound management, eye-drops, anti-infective coatings in medical devices and in burn treatment because they have potent antimicrobial properties but low human toxicity (Clement and Jarrett, 1994; Klasen, 2000a; Tambe et al., 2001). Several silver compounds have been proven to be effective also in the treatment of open wounds, and suppurating wounds, chronic osteomyelitis, and urinary tract infections (De Gracia, 2001; Silver et al., 2006) and, among the various silver containing species, silver complexes are particularly interesting since the antimicrobial activity can be changed by varying type of ligands coordinated to silver (Özdemir et al., 2010). For example, the Ag(I) imidazolate complex has antibacterial and antifungal properties (Nomiya et al., 1997).

Nowadays among the silver derivatives, silver sulfadiazine remains one of the most common drug used in wound therapy and medicinal devices, although it

causes severe adverse effects, and it delays wound healing due to its cytotoxicity towards fibroblasts and keratinocytes (Kalinowska-Lis et al., 2016).

Although the cytotoxic effects of silver compounds against Gram +ve and Gram –ve bacteria have long been established, the exact mechanisms of action are not completely understood (Kyros et al., 2014). It has been reported that Ag<sup>+</sup>-treated bacterial cells show destabilization of the cellular envelope and increased membrane permeability (Morones-Ramirez et al., 2013); moreover, their cytoplasm displays molecules of condensed DNA that lose their ability to replicate. Another mechanism suggests that the silver binds to some components within the bacterial cell, inducing the subsequent inhibition of bacterial growth (Kyros et al., 2014; Modak and Fox, 1973). These changes can potentiate the activity of a broad range of antibiotics against Gram –ve bacteria as well as restore the antibiotic susceptibility of resistant bacterial strains (Morones-Ramirez et al., 2013).

In view of this, new and effective antimicrobial agents are required urgently. In recent years, there has been a considerable trend toward the development of metal complexes having biological properties (Chimento et al., 2015; Napoli et al., 2011; Saturnino et al., 2014; Sirignano et al., 2013a).

Metal N-heterocyclic carbene (M-NHC) complexes have appeared as an emerging field of research in medicinal chemistry where NHC complexes of coinage metals (Cu, Au, and Ag) proved to be better anticancer and antimicrobial agents (Iqbal et al., 2013; Melaiye et al., 2004; Tan et al., 2010).

For their excellent chemical properties and quite easy synthesis, different examples of NHC complexes of silver, gold platinum or other transition metals have been biologically evaluated, and they seem to have promising properties in biomedical sciences. (Bruno et al., 1995; Oehninger et al., 2013; Patil et al., 2015; Saturnino et al., 2010; Saturnino et al., 2014; Sirignano et al., 2013b). In particular, Ag-NHCs have long been used as antimicrobial agents for their high stability (Klasen, 2000b), as they can overcome the drawbacks associated with conventional silver antibiotics including resistance and fast loss of activity (Sinicropi et al., 2010a; Sinicropi et al., 2010b).

Silver-N-heterocyclic carbene complexes can, in fact, slowly release silver ions into the wound, enabling better prevention of infection and promoting healing (Hindi et al., 2008).

Herein we have investigated the *in vitro* efficacy against a broad spectrum of bacteria of a small library of silver N-heterocycles carbene complexes, Ag(1)-NHC, synthesized from some of us (Napoli et al., 2013).

The studied silver carbene complexes are of type  $[AgL_2]^+[AgI_2]^-$  (Mariconda et al., 2014). In particular, we have studied: Iodide[N-methyl-N-(2-hydroxycyclopentyl-imidazole-2-ylidene)silver(I), Iodide[N-methyl-N-(2-hydroxycyclohexyl)-imidazole-2-ylidene)silver(I) and Iodide[N-methyl-N-(2-hydroxy-2-phenyl)ethyl-imidazole-2-ylidene)silver(I), namely AgL6, AgL18 and AgL20 respectively (Figure 7.1). For AgL6, in particular, also a polymeric nanocarrier has been developed, in order to increase its efficacy.

Nanosystems have been proven to be successful antimicrobial carrier due to targeted drug delivery at infection sites, reduced drug-resistance by microbial organism and increased therapeutic index. These actions reduce side effects and improve patient compliance thanks to the decreased frequency of administrations.

Many materials can be used to prepare nanocarriers, such as lipids, polymers or inorganic particles. Among these, polymers are greatly interesting, due to the possibility of modification of their physical-chemical properties. Many polymeric particles can be produced, each characterized by peculiar properties. Hydrogels, dendrimers, drug-polymer conjugates and polymer vesicles represent few examples of nanosized particles based on polymeric materials and used as drug delivery systems.

Polymer nanovesicles are nanosized drug carriers, auto-assembled from amphiphilic block copolymers. They are organized in nanostructures in which the hydrophobic parts are inserted in the middle of the membrane, while the hydrophilic parts are exposed on both the inner and outer surfaces, delimiting a central aqueous core separated from the outside environment (Levine et al., 2008). This organization represents the major advantage of this kind of nanostructures, that can encapsulate hydrosoluble drugs in the aqueous core, and also hydrophobic or amphiphilic compounds in the thick membrane. Although they are generally identified as an individual type of drug nanocarriers, they should be considered as being a category of nanoparticles with a 'reservoir' architecture type (nanocapsules). The diversity of the building blocks can also be used to impart properties such as responsiveness to environmental stimuli, either endogenous (i.e. pH, enzymes, oxidative stress, etc.) or exogenous (i.e. temperature, magnetic field, light, ultrasound) (Ahmed et al., 2006a; Ahmed et

al., 2006b; Discher and Ahmed, 2006; Onaca et al., 2009). Polymeric nanovesicles can also be engineered for selective delivery through targeting molecules linkage to outer surface (Meng et al., 2005).

Despite a large number of scientific papers describing the development of polymer nanovesicles as drug delivery systems, only few have explored their application to antimicrobials (Geilich et al., 2015; Wayakanon et al., 2013).

Therefore, here we describe for the first time the production of polymer nanostructured in which dextran, a biopolymer widely used in the pharmaceutical field (Vittorio et al., 2012), and oleate residues represents the hydrophilic and the hydrophobic parts, respectively. The nanoparticles were loaded with one of the synthesized Ag-based drug, whose antimicrobial activity was not investigated yet.

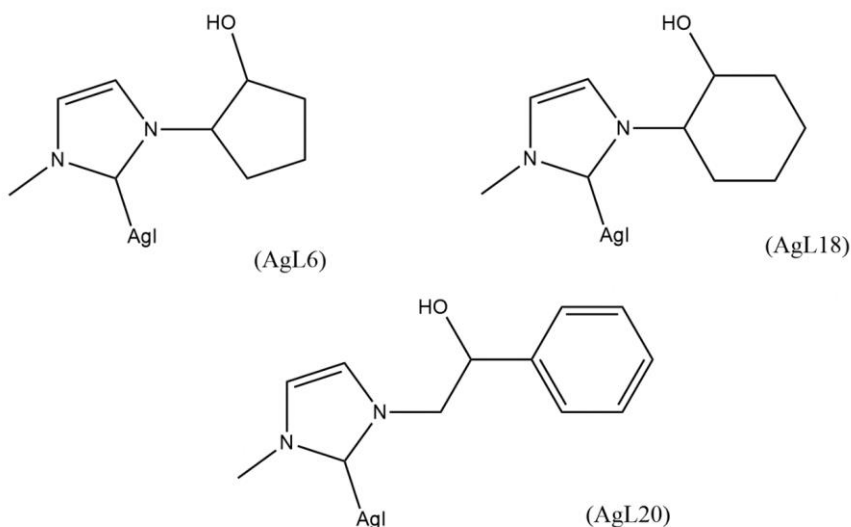


**Figure 7.1** Chemical structures of AgL6, AgL18 and AgL20.

## MATERIALS AND METHODS

### Materials

Dextran, sodium oleate, disodium hydrogen phosphate, sodium dihydrogen phosphate, potassium bromide (KBr), pyrene, dicyclohexyl carbodiimide (DCC), dimethylaminopyridine (DMAP), methanol, ethanol absolute, dimethyl sulfoxide

(DMSO) and tetrahydrofuran (THF) were purchased by Sigma-Aldrich (Sigma Chemical Co., St. Louis, MO, USA).

Dialysis tube (MWCO: 12000-14000 Da) were also provided by Sigma-Aldrich.

### **Instrumentations**

Absorption spectra were recorded with a UV/Vis JASCO V-530 spectrometer using 1 cm quartz cells.

Particles size and distribution were determined by dynamic light scattering (DLS) analyses using a 90 Plus particle size analyzer (Brookhaven Instruments Corporation, New York, NY USA), at  $25.0 \pm 0.1^\circ\text{C}$  by measuring the autocorrelation function at  $90^\circ$ . The laser was operating at 658 nm. The distribution size was directly obtained from the instrument fitting data by the inverse “Laplace transformation” method and by Contin methods (Provencher, 1982). The polydispersity index (P.I.) was used as a measure of the width of size distribution. P.I. less than 0.3 indicates a homogenous population of particles.

Each sample was measured three times and the results are expressed as mean  $\pm$  standard deviation.

IR spectra were recorded as KBr pellets on a Jasco FT-IR 4200.

### **Dextran-oleate synthesis**

The coupling of dextran and sodium oleate was achieved as follows: 500 mg of dextran was dissolved in 50 mL of DMSO. After complete dissolution, 100 mg of sodium oleate, 68 mg of DCC and 40 mg of DMAP, were added to the solution and left under magnetic stirring, for 4 h at  $60^\circ\text{C}$ , and at room temperature overnight. In order to recover the oleate-grafted dextran, the purification step was performed by precipitating the reaction mixture in cold ethanol. Then the product was collected in dialysis membrane and dialyzed against a mixture ethanol/water 50:50 for 24 h and against distilled water for further 48 h. Finally, dextran oleate was recovered and freeze-dried to a powder.

### **Determination of the critical aggregation concentration**

The critical aggregation concentration (CAC) of the dextran oleate aqueous solution was determined by fluorescence method using pyrene as a nonpolar fluorescent probe. 24.0  $\mu\text{L}$  of pyrene solution ( $2.5 \times 10^{-5}$  M) in acetone was added

in vials and evaporated under vacuum. Amounts of dextran oleate solution at various concentrations were added to the pyrene vials leading to a final pyrene concentration of  $6.0 \times 10^{-7}$  M. The mixture was kept under agitation for 4-5 h. Fluorescence measurements were conducted on each sample (excitation = 333 nm, emission = 350-500 nm) at a  $90^\circ$  angle in a 1 cm quartz cuvette. The average ratio of the intensity of the vibronic bands at 372 nm ( $I_1$ ) over 383 nm ( $I_3$ ), obtained from the fluorescence emission spectra of pyrene recorded at  $25^\circ\text{C}$ , was plotted versus log of the concentration for each sample. The CAC was determined as the polymer concentration at the intersection point of two regression lines.

### **Self-assembling of the polymer vesicle**

5 mg of dextran oleate was dissolved in 10 mL of THF in a 50 mL round bottom flask. Next, 10 mL of phosphate buffered saline (PBS) solution (0.01 M, pH 7.4) were gently poured along the flask walls. The organic solvent was removed using a rotary evaporator, under reduced pressure at  $40^\circ\text{C}$  and 40 rpm, yielding the dextran oleate vesicles suspension. AgL6 loaded vesicles were prepared as described above, by adding 1 mL of AgL6 solution to the phosphate buffer.

### **Drug encapsulation efficiency**

Drug encapsulation efficiency was determined using the dialysis method for separating the non-entrapped drug from dextran oleate vesicles (DOVs) (Maestrelli et al., 2005). According to this technique, 3 mL of AgL6-loaded DOVs dispersion was dropped into a dialysis bag immersed in 10 mL of distilled water and magnetically stirred. Free drug was dialyzed for 30 min each time and the dialysis was complete when no drug was detectable in the recipient solution. The encapsulation efficiency was expressed as the percentage of the drug entrapped into DOVs referred to the total amount of drug that is present in the non-dialyzed sample. It was determined by diluting 1 mL of dialyzed and 1 mL of non-dialyzed DOVs in 25 mL of methanol and obtaining two solutions whose concentrations are represented in equation (7.1) by [ND] and [D], respectively. The concentrations of AgL6 were calculated by measuring the absorbance of the two solutions between 200 nm and 400 nm. This procedure was necessary to breakdown DOVs.

$$\text{Encapsulation efficiency (\%)} = \frac{[ND] - [D]}{[ND]} \times 100 \quad (7.1)$$

### ***In vitro* diffusion study**

*In vitro* diffusion studies were performed at  $37 \pm 0.5^\circ\text{C}$  using Franz diffusion cells (Disa, Milan, Italy; permeation area  $0.4614\text{ cm}^2$ ).

For this purpose, Strat-M<sup>®</sup> membrane (Merck-Millipore) was placed between the donor and receptor compartments of the Franz cells and, then, the compartments were clamped together ensuring that the shiny side of the membrane was facing the donor compartment.

The receptor compartment was filled with 5.5 mL of phosphate buffer at pH 7.4 ( $1.0 \times 10^{-3}\text{ M}$ ) and, after 20-30 min when the receptor solution reached  $37^\circ\text{C}$ , 0.5 mL of the AgL6-loaded DOVs suspension was added to the donor compartment, which was covered with Parafilm<sup>™</sup> in order to prevent any loss. The content of the receptor compartment was removed at 1, 2, 4, 6, 8 and 24 hours for UV/Vis analysis and, at each time point, the amount withdrawn was replaced with fresh phosphate buffer. The *in vitro* diffusion experiments were performed in triplicate.

### **Bacterial strains**

The strains *Escherichia coli* (ATCC 25922), *Klebsiella pneumoniae* (ATCC 13883), *Pseudomonas aeruginosa* (ATCC 27853), *Staphylococcus aureus* (ATCC 25923) and *Streptococcus pyogenes* (ATCC 19615) were provided by REMEL. The cells were grown in Müller-Hinton broth II (MHB; Difco, Detroit, MI, USA) containing 2 g/L beef infusion solids, 17.5 g/L casein hydrolysate, 1.5 g/L starch. The final pH was adjusted to 7.4.

### **Antimicrobial tests**

#### *Disc-diffusion susceptibility testing*

The antimicrobial susceptibilities of the Ag-NHCs complexes were evaluated using the Kirby-Bauer disc-diffusion method (Bauer et al., 1966; Benson, 1998; Benson, 1967), performed according to CLSI guidelines and results were interpreted using CLSI breakpoints (Clinical and Laboratory Standards Institute, 2012a; Clinical and Laboratory Standards Institute, 2013). Cefotaxime discs (10  $\mu\text{g}$ ; from Oxoid<sup>™</sup>) and silver sulfadiazine (AgSD) discs (32  $\mu\text{g}$ ) were used as positive controls. The stock solutions of AgSD (from Sigma/Aldrich Company; St. Louis, MO, USA) and of all complexes were prepared by dissolving them in dimethyl sulfoxide (DMSO, from Sigma/Aldrich Company; St. Louis, MO,

USA) and were utilized to impregnate the Blank Antimicrobial Susceptibility Disks (Oxoid™).

Specifically, overnight cultures of bacteria tested were adjusted to a turbidity of 0.5 McFarland standards ( $10^6$  CFU/mL) before inoculation onto agar plates with sterile cotton swabs. A cotton swab dipped in the cell culture was streaked onto an agar plate surface in such a way as to obtain a uniform layer of bacteria across the whole surface. After 10-15 min, the cefotaxime or AgSD or novel complex discs were laid on the inoculated surface of the agar plates; then, all agar plates were incubated at 37°C, overnight. The diameters of inhibition were measured and susceptibility was expressed in terms of resistance (R), moderate susceptibility (I) and susceptibility (S).

Agar plates inoculated with bacteria tested with impregnated DMSO discs were used as controls. Analysis for each combination of bacteria tested and discs with positive controls and with several new compounds were repeated three times.

#### *Determination of MIC and MBC values*

The minimum inhibitory concentration (MIC) of the antibacterial compounds was determined using the broth dilution method, according to CLSI guidelines (Clinical and Laboratory Standards Institute, 2012b). Briefly, a solution of each Ag complex was diluted, serially, with MHB medium. Then, the suspensions of the microorganisms, prepared from overnight cultures of bacteria in the MHB medium, at a concentration of  $10^6$  cfu mL<sup>-1</sup>, were added to each dilution in a 1:1 ratio. Growth (or lack thereof) of the microorganisms was determined visually after incubation for 24 h at 37°C. AgSD and cefotaxime were also included as positive controls. The lowest concentration at which there was no visible growth (turbidity) was considered as the MIC value.

In order to determine the minimum bactericidal concentration (MBC), 10 µL aliquots of dilution representing the MIC value, and at least three of the more concentrated dilutions of the Ag-NHCs, cefotaxime and AgSD, were plated on Müller-Hinton agar. Then, the plates were incubated for 24 h, at 37°C. The MBC values were determined as the lowest concentration that causes at least a 99.9% decrease in cfu mL<sup>-1</sup> relative to the initial concentration (Kalinowska-Lis et al., 2014).



The negative control tubes did not contain bacterial inoculum while the positive control (or turbid) tubes were free of the compounds and contained only DMSO. The tests were repeated in triplicate.

## RESULTS AND DISCUSSION

### Polymer vesicles characterization

Evaluation by FT-IR spectra analyses has been performed in order to verify the coupling of oleate onto dextran backbone, comparing the FT-IR spectra of sodium oleate, dextran and dextran oleate conjugate. The sodium oleate spectrum (Figure 7.2 - Trace B) shows a strong peak at  $1560\text{ cm}^{-1}$ , which is the typical signal of the C=O stretching vibration of the carboxylic salt group. It can be also observed the presence of strong signals between  $2849$  and  $2950\text{ cm}^{-1}$  corresponding to stretching vibration of the C-H bond of the alkane portion of the molecule; while the double bond can be identified thanks to the band at  $3030\text{ cm}^{-1}$ , corresponding to the stretching vibration of =C-H bond. Dextran spectrum (Figure 7.2 - Trace A), on the contrary, does not show any signal that can be ascribed to C=O double bond, which is obviously absent in dextran structure. But information about the conformation of the polysaccharide can be acquired in the region  $600\text{-}950\text{ cm}^{-1}$ . A peak in the  $885\text{-}925\text{ cm}^{-1}$  region is the evidence of two CH in the axial position (AA), in the  $825\text{-}855\text{ cm}^{-1}$  region the equatorial-axial position (EA), in the  $790\text{-}825\text{ cm}^{-1}$  region in the equatorial-equatorial position (EE) and in  $860\text{-}885\text{ cm}^{-1}$  region in the axial-equatorial position (AE). The bands around  $915\text{ cm}^{-1}$  and  $850\text{ cm}^{-1}$ , indicating AA and EA fragments, confirm the glucopyranosyl conformation, which is not affected by oleate conjugation. In dextran oleate spectrum (Figure 7.2 - Trace C), in fact, these peaks are preserved, while a new strong band appeared. It can be found around  $1740\text{ cm}^{-1}$  indicating the presence of C=O bond stretching vibration of an ester group. This group came from the oleate moieties, but its spectroscopic signal has been shifted towards higher frequencies. This is certainly due to the new formation of the ester bond.

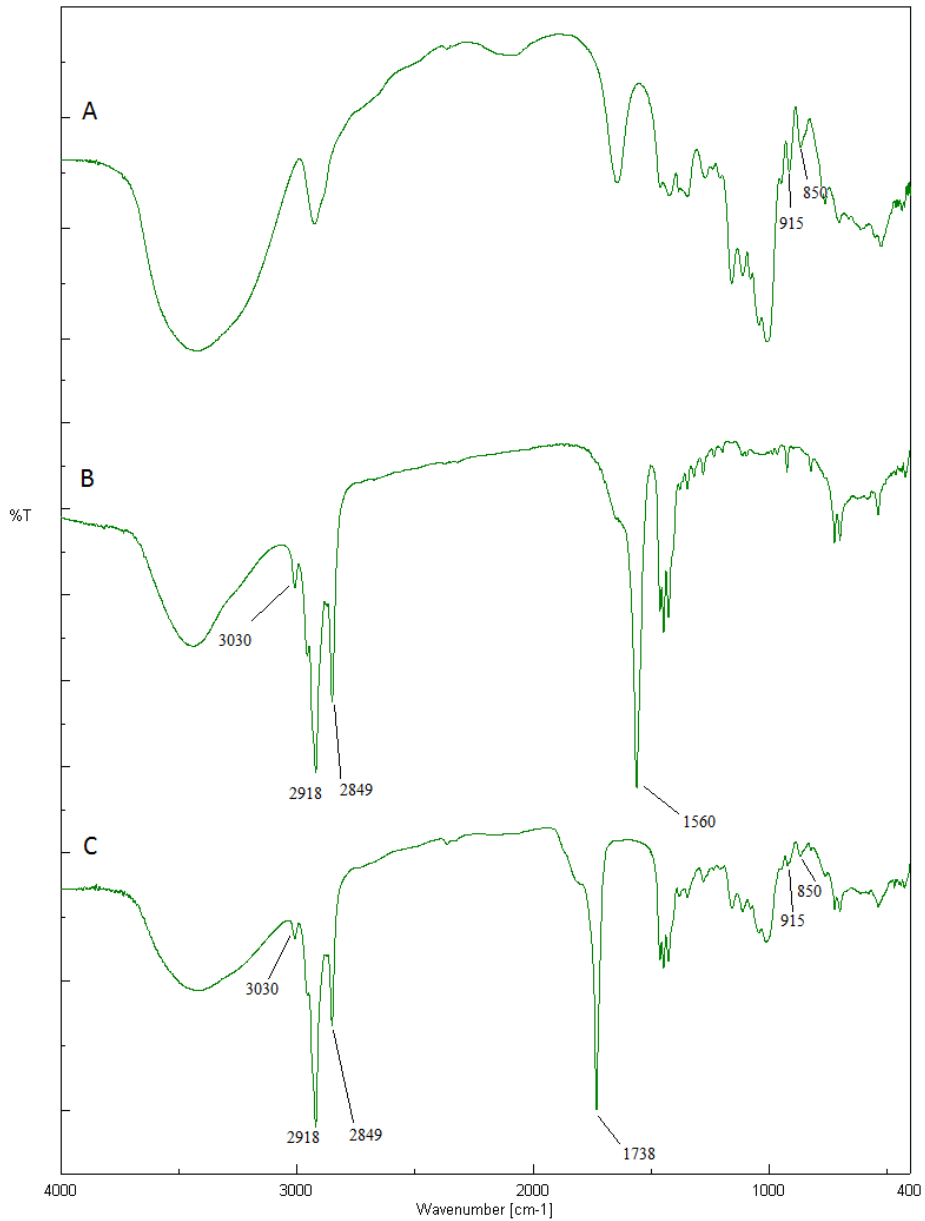


**Figure 7.2** FT-IR spectra of (A) dextran, (B) sodium oleate and (C) dextran oleate.

The polymer nanovesicles were prepared by self-assembling procedure and their dimensions were analyzed by dynamic light scattering.

The self-assembling technique involves the dissolution of the amphiphilic polymer in organic solvent, followed by the introduction of the aqueous phase, represented by phosphate buffered saline (PBS) solution at pH = 7.4. The non-polar organic phase is then removed under reduced pressure decreasing the dissolution of the hydrophobic block of dextran oleate. This led to the increase of hydrophilicity of the phase and, consequently, to the self-assembly of the nanosized DOVs.

The dimensional characterization of DOVs and DOVs-AgL6 was performed with DLS, putting a small amount of polymer vesicles in the PBS solution at pH 7.4. The mean hydrodynamic diameter found was different for the two polymer batches: 525 nm and 613 nm for DOVs and DOVs-AgL6, respectively (Figure 7.3). Data collected in Table 7.1, shows the presence of monodisperse homogeneous population of both empty and AgL6-loaded vesicles. Polydispersity index value is, in fact, below 0.3 and the mean diameter is below 700 nm.

There is a difference of almost 100 nm between the two systems and that can be ascribed to the presence of encapsulated drug. It seems that the presence of AgL6 in solution negatively affects the self-assembling of dextran oleate vesicles, resulting in larger nanoparticles. In particular, the Ag atoms can interfere with vesicles formation, due to its nature. However, the negative effect on DOVs dimension does not compromise their formation maintaining a mean diameter far below 1  $\mu\text{m}$ .

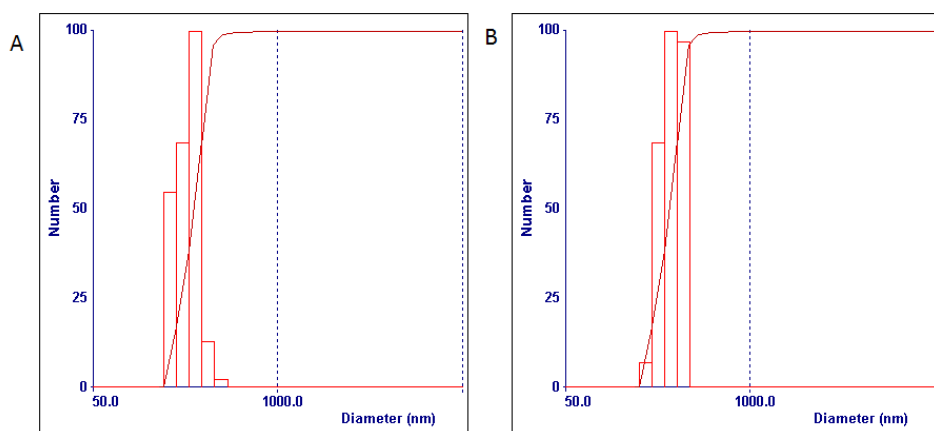


**Figure 7.3** Graph of size and size distribution obtained by DLS analysis of DOVs (Panel A) and DOVs-AgL6 (Panel B).

## PART II

**Table 7.1** Dimensional data. DOVs size and size distribution of both empty and AgL6-loaded DOVs are expressed as mean diameter  $\pm$  standard deviation and polydispersity index (P.I.).

	Mean diameter	Polydispersity index
DOVs	525 $\pm$ 14 nm	0.214
DOVs-AgL6	613 $\pm$ 17 nm	0.268

The amphiphilic character was conferred to dextran thanks to the conjugation with a hydrophobic group, i.e. the oleate residue. The so modified polysaccharide acquired the ability to self-assemble in an aqueous environment *via* hydrophobic interaction between lipid moieties.

The critical aggregation concentration (CAC) of dextran oleate in water was estimated from the dependence of pyrene fluorescence spectra ( $I_{372}/I_{383}$  ratio) as a function of the polysaccharide-lipid concentration (Figure 7.4). A sharp change was observed from 14  $\mu\text{g}/\text{mL}$ , which was considered to be the CAC.

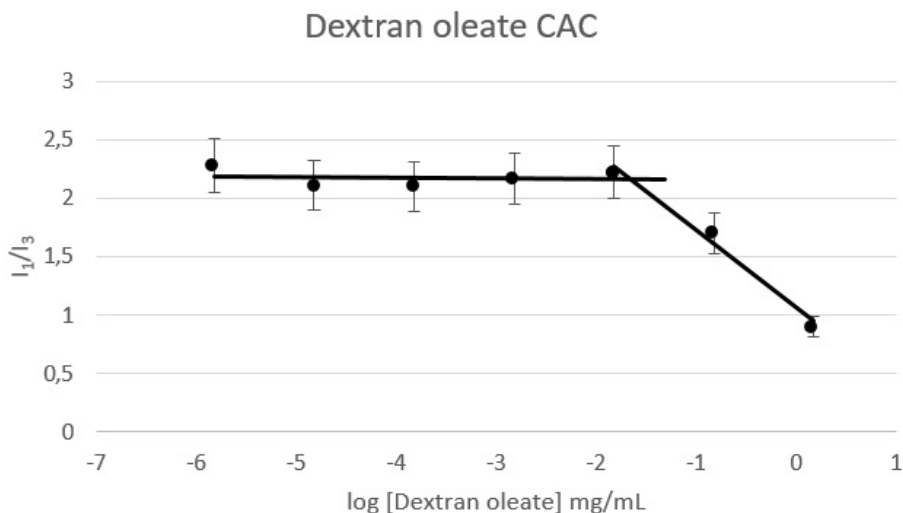


**Figure 7.4** Ratio of pyrene I1/I3 band fluorescence at various concentrations of dextran oleate in water. The critical aggregation concentration was calculated as the intersection point of the two linear regions of the plots.

### Drug encapsulation and release profile

Polymer nanovesicles possess the advantage of being optimal carrier for both hydrophobic and hydrophilic drugs, which can be loaded in the lipophilic membrane or in the aqueous core, respectively.

Dextran oleate vesicles (DOVs) were loaded with AgL6 during self-assembling and drug encapsulation was measured by UV/Vis spectrophotometry after dialysis against distilled water. The encapsulation efficiency has been calculated according to the equation (7.1) reported in the experimental method section. The obtained value for AgL6 was ca. 76%, supporting the vesicular structure of the carrier.

Strat-M<sup>®</sup> membranes, which are a synthetic model predictive of diffusion in human skin, were employed for transdermal diffusion testing. The diffusion of AgL6-loaded DOVs was compared to free AgL6 and the results are reported in Figure 7.5. From the release profile depicted in the figure, it is evident an increased amount of AgL6 recovered in the acceptor compartment of Franz diffusion cells from DOVs-AgL6, since the time point of 2 h, if compared to free AgL6. The trend is much more evident in the following hours, when DOVs-AgL6 released almost 95% of its payload after 24 h. On the other hand, free AgL6 diffusion is limited and it is not complete at the end point. The data confirmed that DOVs enhance drug penetration through limiting barriers, such as the skin. AgL6 incomplete penetration is certainly due to the chemical properties of the compound, which possesses a partial hydrophilicity that inhibits the absorption of the entire amount of drug (Saturnino et al., 2016).

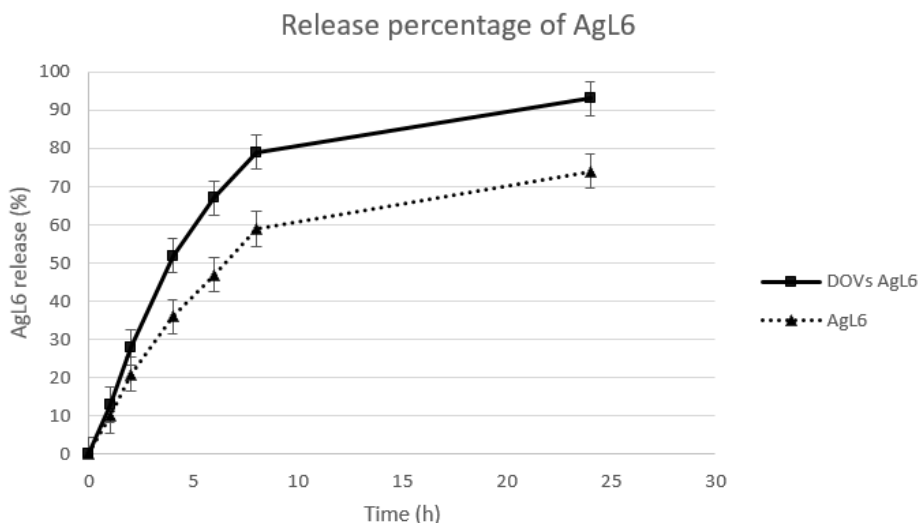


**Figure 7.5** Transdermal diffusion profile of AgL6 and DOVs-AgL6.

**Antimicrobial activity**

The antimicrobial activity of the Ag-NHCs was measured against two Gram +ve (*S. aureus* and *S. pyogenes*) and three Gram –ve bacterial strains (*E. coli*, *K. pneumoniae* and *P. aeruginosa*). The inhibition ratios of the silver carbene complexes against pathogenic strains were calculated from inhibition diameters values, measured at 32, 64 and 128 µg of each tested compound. The average of three inhibition zone diameter measurements was compared against commercial drugs (commercial cephalosporin cefotaxime and silver sulfadiazine (AgSD), commonly used in the treatment of skin infections), using the disc-diffusion susceptibility test (Kirby-Bauer test) (Bauer et al., 1966).

Final interpretation of the measurements enabled all of the bacteria strains tested to be grouped into three categories (Sensitive, Intermediate and Resistant) as summarized in Table 7.2. No inhibition zone was seen in the control (DMSO) (Data not shown).

The antibiotic sensitivity profile of the bacterial strains showed that, among the Ag-NHCs complexes tested, only AgL6 displayed antimicrobial activity against the microorganisms, but only when tested in large amounts, in comparison with cefotaxime. Indeed, a comparison of data obtained on the inhibition zones of the pathogenic bacteria proved that all five bacterial strains were Sensitive to 32 and 128 µg AgL6. Moreover, this compound was more effective than AgSD toward the Gram –ve pathogens tested. However, it may be said that AgL18 and AgL20 were much less effective than AgL6 and only against the Gram –ve strains; indeed *E. coli*, *K. pneumoniae* and *P. aeruginosa* were intermediate to 128 µg AgL18 and AgL20.

The Kirby-Bauer test could only test the bacterial susceptibility to various antimicrobial reagents at pre-designed dosage. Such information as minimal inhibitory concentration (MIC) of a specific compound could not be obtained from this test. Therefore, in order to determine MIC values for AgL6, the broth dilution method was performed. As expected, the MIC determination results were in good agreement with the disc-diffusion susceptibility test (Table 7.3). For example, in the disc-diffusion test, all five bacteria were found to be Sensitive to AgL6; in the dilution experiment, the MIC of this compound was found to be very high against all the strains, particularly against Gram +ve bacteria (MIC values were 32 µg/mL). The values obtained were greater than those reported for

the commercial drugs Cefotaxime (MIC ranging between 0.5 and 4  $\mu\text{g/mL}$ ) and AgSD (MIC ranging between 8 and 32  $\mu\text{g/mL}$ ). Both of these commercial drugs were found to be Sensitive according to the Kirby-Bauer test.

Similarly, minimal bactericidal concentration (MBC) values for AgL6 were also determined in bacterial cultures; the values were higher against Gram +ve bacteria than against Gram –ve bacteria.

Since limited cellular penetration could reduce the effectiveness of many antimicrobial treatments, we hypothesized that incorporating AgL6 into a “pharmaceutically-oriented device”, such as DOVs, could improve its cellular uptake and, consequently, its antimicrobial activity.

Literature data reported that the incorporation of novel synthetic compounds into suitable drug carriers can improve their antimicrobial effect and, consequently, may be a very promising strategy to enhance their cellular uptake (Parisi et al., 2014).

The MIC and MBC values for Ag-NHCs, after its incorporation into the carrier, confirmed our hypothesis, evidencing improved activity against all the bacteria strains (Table 7.3). Indeed, all MIC and MBC values decreased four times against all bacteria tested, while only the MBC value, against *P. aeruginosa*, was reduced two-fold.

These values were found to be closer to those for cefotaxime and, surprisingly, two-fold lower than for AgSD. In contrast, the vehicle alone did not exhibit antibacterial activity (Table 7.3).

Finally, our outcomes showed *K. pneumoniae* and *E. coli* to be the most sensitive microorganisms to AgL6, followed by *P. aeruginosa* while the Gram +ve bacteria were less sensitive to the prepared complex.

**PART II**

**Table 7.2** Antibiotic susceptibility profiles.

Compound	µg	Bacterial strains				
		<i>S.aureus</i>	<i>S.pyog.</i>	<i>E.coli</i>	<i>K.pneum.</i>	<i>P.aerug.</i>
<b>Cefotaxime</b>	10	S	S	S	S	S
<b>AgSD</b>	32	S	S	S	S	S
<b>AgL6</b>	32	S	S	S	S	S
	64	S	S	S	S	S
	128	S	S	S	S	S
<b>AgL18</b>	32	R	R	R	R	R
	64	R	R	R	R	R
	128	R	R	I	I	I
<b>AgL20</b>	32	R	R	R	R	R
	64	R	R	R	R	R
	128	R	R	I	I	I

**Table 7.3** MIC (top rows) and MBC (bottom rows) values of the investigated compounds.

Compound	MIC MBC (µg/mL)	Bacterial strains				
		<i>S. aureus</i>	<i>S. Pyog.</i>	<i>E. coli</i>	<i>K. pneum.</i>	<i>P. aerug.</i>
<b>Cefotaxime</b>	MIC	1	0.5	2	2	4
	MBC	1	1	4	2	8
<b>AgSD</b>	MIC	32	16	8	8	16
	MBC	32	32	16	16	16
<b>AgL6</b>	MIC	32	32	16	16	32
	MBC	64	64	32	32	32
<b>DOVs</b>	MIC	> 128	> 128	> 128	> 128	> 128
	MBC	> 128	> 128	> 128	> 128	> 128
<b>DOVs-AgL6</b>	MIC	8	8	4	4	8
	MBC	16	16	8	8	16

Bacteria: *S. aureus* = *Staphylococcus aureus* ATCC 25923; *S. pyog.* = *Streptococcus pyogenes* ATCC 19615; *E. coli* = *Escherichia coli* ATCC 25922; *K. Pneum.* = *Klebsiella pneumoniae* ATCC 13883; *P. aerug.* = *Pseudomonas aeruginosa* ATCC 27853.

S: Sensitive; R: Resistant; I: Intermediate



## CONCLUSIONS

The present study was aimed at investigating the antibacterial activity of silver N-heterocyclic carbene complexes. They were tested against both Gram +ve and Gram -ve bacteria. One of the compounds was found to be the most active (AgL6), while there is a natural bacterial resistance towards AgL18 and AgL20. The biopolymeric nanocarrier developed for AgL6 delivery, was successfully obtained by self-assembly of dextran oleate conjugate, in which dextran chain and oleic residues represent the hydrophilic and the hydrophobic parts of the amphiphilic material, respectively. The nanometric dimension of the particles have been confirmed by DLS analyses (mean diameter ranging between 500-600 nm). Finally, we have demonstrated that this nanosystem is an excellent tool that can greatly improve antibiotic activity of compounds, such as AgL6, reducing both MIC and MBC.

## REFERENCES

Abraham, EP, Chain, E (1940) An enzyme from bacteria able to destroy penicillin. *Nature* 146, 837.

Ahmed, F, Pakunlu, RI, Brannan, A, Bates, F, Minko, T, Discher, DE (2006)a Biodegradable polymersomes loaded with both paclitaxel and doxorubicin permeate and shrink tumors, inducing apoptosis in proportion to accumulated drug. *Journal of Controlled Release* 116, 150-158.

Ahmed, F, Pakunlu, RI, Srinivas, G, Brannan, A, Bates, F, Klein, ML, Minko, T, Discher, DE (2006)b Shrinkage of a rapidly growing tumor by drug-loaded polymersomes: pH-triggered release through copolymer degradation. *Molecular pharmaceutics* 3, 340-350.

Andersson, DI, Hughes, D (2011) Persistence of antibiotic resistance in bacterial populations. *FEMS microbiology reviews* 35, 901-911.

Bauer, A, Kirby, W, Sherris, JC, Turck, M (1966) Antibiotic susceptibility testing by a standardized single disk method. *American journal of clinical pathology* 45, 493.

Becker, K, Hu, Y, Biller-Andorno, N (2006) Infectious diseases—a global challenge. *International Journal of Medical Microbiology* 296, 179-185.

Benson, H (1998) Antimicrobial sensitivity testing: the Kirby-Bauer method. *Microbiological applications: laboratory manual in general microbiology*, 7th edn. McGraw Hill, Boston, Massachusetts, 139-141.

Benson, HJ (1967) *Microbiological applications; a laboratory manual in general microbiology*.

Bruno, G, Nicolo, F, Loschiavo, S, Sinicropi, MS, Tresoldi, G (1995) Synthesis and Spectroscopic Properties of Di-2-Pyridyl Sulfide (Dps) Compounds - Crystal-Structure of [Ru(Dps)<sub>2</sub>Cl<sub>2</sub>]. *J Chem Soc Dalton*, 17-24.

Chimento, A, Saturnino, C, Iacopetta, D, Mazzotta, R, Caruso, A, Plutino, MR, Mariconda, A, Ramunno, A, Sinicropi, MS, Pezzi, V (2015) Inhibition of human topoisomerase I and II and anti-proliferative effects on MCF-7 cells by new titanocene complexes. *Bioorganic & medicinal chemistry* 23, 7302-7312.

Clement, JL, Jarrett, PS (1994) Antibacterial silver. *Met Based Drugs* 1, 467-482.

Clinical and Laboratory Standards Institute (2012)a Performance Standard for Antimicrobial Disk Susceptibility Tests; Approved Standard. Document M02-A11 No. 1. Vol. 32. PA, USA: CLSI.

Clinical and Laboratory Standards Institute (2012)b Methods for dilution antimicrobial susceptibility test for bacteria that grow aerobically; approved standards. 9<sup>th</sup> ed. Document M07-A9. CLSI, Wayne, PA.

Clinical and Laboratory Standards Institute (2013) Performance Standards for Antimicrobial Susceptibility Testing. Twentieth Informational Supplement M100-S23. Wayne, PA: CLSI; 2013.

Cox, G, Wright, GD (2013) Intrinsic antibiotic resistance: mechanisms, origins, challenges and solutions. *International Journal of Medical Microbiology* 303, 287-292.

De Gracia, C (2001) An open study comparing topical silver sulfadiazine and topical silver sulfadiazine–cerium nitrate in the treatment of moderate and severe burns. *Burns* 27, 67-74.

Discher, DE, Ahmed, F (2006) Polymersomes. *Annu. Rev. Biomed. Eng.* 8, 323-341.

Fajardo, A, Martínez-Martín, N, Mercadillo, M, Galán, JC, Ghysels, B, Matthijs, S, Cornelis, P, Wiehlmann, L, Tümmler, B, Baquero, F (2008) The neglected intrinsic resistome of bacterial pathogens. *PLoS one* 3, e1619.

Geilich, BM, van de Ven, AL, Singleton, GL, Sepúlveda, LJ, Sridhar, S, Webster, TJ (2015) Silver nanoparticle-embedded polymersome nanocarriers for the treatment of antibiotic-resistant infections. *Nanoscale* 7, 3511-3519.

Hindi, KM, Siciliano, TJ, Durmus, S, Panzner, MJ, Medvetz, DA, Reddy, DV, Hogue, LA, Hovis, CE, Hilliard, JK, Mallet, RJ (2008) Synthesis, stability, and antimicrobial studies of electronically tuned silver acetate N-heterocyclic carbenes. *Journal of medicinal chemistry* 51, 1577-1583.

Iqbal, MA, Haque, RA, Ahamed, MBK, Majid, AA, Al-Rawi, SS (2013) Synthesis and anticancer activity of para-xylyl linked bis-benzimidazolium salts and respective Ag (I) N-heterocyclic carbene complexes. *Medicinal Chemistry Research* 22, 2455-2466.

Kalinowska-Lis, U, Felczak, A, Chęcińska, L, Szablowska-Gadomska, I, Patyna, E, Małecki, M, Lisowska, K, Ochocki, J (2016) Antibacterial Activity and Cytotoxicity of Silver (I) Complexes of Pyridine and (Benz) Imidazole Derivatives. X-ray Crystal Structure of [Ag (2, 6-di (CH<sub>2</sub>OH) py) 2] NO<sub>3</sub>. *Molecules* 21, 87.

Kalinowska-Lis, U, Szewczyk, EM, Chęcińska, L, Wojciechowski, JM, Wolf, WM, Ochocki, J (2014) Synthesis, characterization, and antimicrobial activity of silver (I) and copper (II) complexes of phosphate derivatives of pyridine and benzimidazole. *ChemMedChem* 9, 169-176.

Klasen, H (2000)a Historical review of the use of silver in the treatment of burns. I. Early uses. *Burns* 26, 117-130.

Klasen, HJ (2000)b A historical review of the use of silver in the treatment of burns. II. Renewed interest for silver. *Burns* 26, 131-138.

Kyros, L, Banti, C, Kourkoumelis, N, Kubicki, M, Sainis, I, Hadjikakou, S (2014) Synthesis, characterization, and binding properties towards CT-DNA and lipoxygenase of mixed-ligand silver (I) complexes with 2-mercaptothiazole and its derivatives and triphenylphosphine. *JBIC Journal of Biological Inorganic Chemistry* 19, 449-464.

Levine, DH, Ghoroghchian, PP, Freudenberg, J, Zhang, G, Therien, MJ, Greene, MI, Hammer, DA, Murali, R (2008) Polymersomes: a new multi-functional tool for cancer diagnosis and therapy. *Methods* 46, 25-32.

Maestrelli, F, González-Rodríguez, ML, Rabasco, AM, Mura, P (2005) Preparation and characterisation of liposomes encapsulating ketoprofen–cyclodextrin complexes for transdermal drug delivery. *International journal of pharmaceutics* 298, 55-67.

Mariconda, A, Grisi, F, Costabile, C, Falcone, S, Bertolasi, V, Longo, P (2014) Synthesis, characterization and catalytic behaviour of a palladium complex bearing a hydroxy-functionalized N-heterocyclic carbene ligand. *New Journal of Chemistry* 38, 762-769.

Melaiye, A, Simons, RS, Milsted, A, Pingitore, F, Wesdemiotis, C, Tessier, CA, Youngs, WJ (2004) Formation of water-soluble pincer silver (I)-carbene complexes: a novel antimicrobial agent. *Journal of medicinal chemistry* 47, 973-977.

Meng, F, Engbers, GH, Feijen, J (2005) Biodegradable polymersomes as a basis for artificial cells: encapsulation, release and targeting. *Journal of Controlled Release* 101, 187-198.

Modak, SM, Fox, CL (1973) Binding of silver sulfadiazine to the cellular components of *Pseudomonas aeruginosa*. *Biochemical pharmacology* 22, 2391-2404.

Morones-Ramirez, JR, Winkler, JA, Spina, CS, Collins, JJ (2013) Silver enhances antibiotic activity against gram-negative bacteria. *Science translational medicine* 5, 190ra181-190ra181.

Napoli, M, Saturnino, C, Cianciulli, EI, Varcamonti, M, Zanfardino, A, Tommonaro, G, Longo, P (2013) Silver (I) N-heterocyclic carbene complexes: Synthesis, characterization and antibacterial activity. *Journal of Organometallic Chemistry* 725, 46-53.

Napoli, M, Saturnino, C, Sirignano, E, Popolo, A, Pinto, A, Longo, P (2011) Synthesis, characterization and cytotoxicity studies of methoxy alkyl substituted metallocenes. *European journal of medicinal chemistry* 46, 122-128.

Nomiya, K, Tsuda, K, Sudoh, T, Oda, M (1997) Ag (I) N bond-containing compound showing wide spectra in effective antimicrobial activities: Polymeric silver (I) imidazolate. *Journal of inorganic biochemistry* 68, 39-44.

Oehninger, L, Rubbiani, R, Ott, I (2013) N-Heterocyclic carbene metal complexes in medicinal chemistry. *Dalton transactions* 42, 3269-3284.

Onaca, O, Enea, R, Hughes, DW, Meier, W (2009) Stimuli-Responsive Polymersomes as Nanocarriers for Drug and Gene Delivery. *Macromolecular bioscience* 9, 129-139.

Özdemir, İ, Özcan, EÖ, Günal, S, Gürbüz, N (2010) Synthesis and antimicrobial activity of novel Ag-N-hetero-cyclic carbene complexes. *Molecules* 15, 2499-2508.

Pagès, J-M, James, CE, Winterhalter, M (2008) The porin and the permeating antibiotic: a selective diffusion barrier in Gram-negative bacteria. *Nature Reviews Microbiology* 6, 893-903.

Parisi, OI, Fiorillo, M, Caruso, A, Cappello, AR, Saturnino, C, Puoci, F, Panno, A, Dolce, V, El-Kashef, H, Sinicropi, MS (2014) Enhanced cellular uptake by

“pharmaceutically oriented devices” of new simplified analogs of Linezolid with antimicrobial activity. *International journal of pharmaceutics* 461, 163-170.

Patil, SA, Patil, SA, Patil, R, Keri, RS, Budagumpi, S, Balakrishna, GR, Tacke, M (2015) N-heterocyclic carbene metal complexes as bio-organometallic antimicrobial and anticancer drugs. *Future medicinal chemistry* 7, 1305-1333.

Provencher, SW (1982) A constrained regularization method for inverting data represented by linear algebraic or integral equations. *Computer Physics Communications* 27, 213-227.

Saturnino, C, Barone, I, Iacopetta, I, Mariconda, A, Sinicropi, MS, Rosano, C, Campana, A, Catalano, S, Longo, P, Andò, S (2016) N-heterocyclic carbene complexes of silver and gold as novel tools against breast cancer progression. *Future Medicinal Chemistry* 8, 2213-2229.

Saturnino, C, Napoli, M, Paolucci, G, Bortoluzzi, M, Popolo, A, Pinto, A, Longo, P (2010) Synthesis and cytotoxic activities of group 3 metal complexes having monoanionic tridentate ligands. *European journal of medicinal chemistry* 45, 4169-4174.

Saturnino, C, Sirignano, E, Botta, A, Sinicropi, MS, Caruso, A, Pisano, A, Lappano, R, Maggiolini, M, Longo, P (2014) New titanocene derivatives with high antiproliferative activity against breast cancer cells. *Bioorganic & medicinal chemistry letters* 24, 136-140.

Silver, S, Phung, LT, Silver, G (2006) Silver as biocides in burn and wound dressings and bacterial resistance to silver compounds. *Journal of Industrial Microbiology and Biotechnology* 33, 627-634.

Sinicropi, MS, Amantea, D, Caruso, A, Saturnino, C (2010)a Chemical and biological properties of toxic metals and use of chelating agents for the pharmacological treatment of metal poisoning. *Archives of toxicology* 84, 501-520.

Sinicropi, MS, Caruso, A, Capasso, A, Palladino, C, Panno, A, Saturnino, C (2010)b Heavy metals: toxicity and carcinogenicity. *Pharmacology* 2, 329-333.

Sirignano, E, Saturnino, C, Botta, A, Sinicropi, MS, Caruso, A, Pisano, A, Lappano, R, Maggiolini, M, Longo, P (2013)a Synthesis, characterization and cytotoxic activity on breast cancer cells of new half-titanocene derivatives. *Bioorganic & medicinal chemistry letters* 23, 3458-3462.

Sirignano, E, Saturnino, C, Botta, A, Sinicropi, MS, Caruso, A, Pisano, A, Lappano, R, Maggiolini, M, Longo, P (2013)b Synthesis, characterization and cytotoxic activity on breast cancer cells of new half-titanocene derivatives. *Bioorganic & medicinal chemistry letters* 23, 3458-3462.

Tambe, S, Sampath, L, Modak, S (2001) In vitro evaluation of the risk of developing bacterial resistance to antiseptics and antibiotics used in medical devices. *Journal of Antimicrobial Chemotherapy* 47, 589-598.

Tan, SJ, Yan, YK, Lee, PPF, Lim, KH (2010) Copper, gold and silver compounds as potential new anti-tumor metallodrugs. *Future medicinal chemistry* 2, 1591-1608.

Vittorio, O, Cirillo, G, Iemma, F, Di Turi, G, Jacchetti, E, Curcio, M, Barbuti, S, Funel, N, Parisi, OI, Puoci, F, Picci, N (2012) Dextran-catechin conjugate: A potential treatment against the pancreatic ductal adenocarcinoma. *Pharmaceutical Research* 29, 2601-2614.

Wayakanon, K, Thornhill, MH, Douglas, CI, Lewis, AL, Warren, NJ, Pinnock, A, Armes, SP, Battaglia, G, Murdoch, C (2013) Polymersome-mediated intracellular delivery of antibiotics to treat *Porphyromonas gingivalis*-infected oral epithelial cells. *The FASEB Journal* 27, 4455-4465.





## **CHAPTER 8**

# **Nanobody-conjugated polymeric micelles for targeted delivery of a hydrophobic photosensitizer in photodynamic therapy**

Work in collaboration with Yanna Liu<sup>a</sup>, Irati Beltran-Hernandez<sup>a,b</sup>, Javier Sastre-Toraño<sup>c</sup>, Sabrina Oliveira<sup>a,b</sup>, Cornelus F. van Nostrum<sup>a</sup> and Wim Hennink<sup>a</sup>.

<sup>a</sup> Department of Pharmaceutics, Utrecht Institute for Pharmaceutical Sciences, Utrecht University, Utrecht, The Netherlands.

<sup>b</sup> Division of Cell Biology, Department of Biology, Utrecht University, Utrecht, The Netherlands.

<sup>c</sup> Department of Chemical Biology & Drug Discovery, Utrecht Institute for Pharmaceutical Sciences, Utrecht University, Utrecht, The Netherlands.

## ABSTRACT

Over the last three decades, photodynamic therapy (PDT) has attracted much attention as new treatment for head and neck squamous cells carcinoma (HNSCC). *m*-tetra(hydroxyphenyl)chlorin (mTHPC) is one of the EMA approved drugs for the treatment of this type of tumor in clinic but, being highly hydrophobic, it is poorly soluble in aqueous media, such as biological fluids. Moreover, mTHPC liposomal formulations are instable in serum and for this reason a more stable and suitable carrier is necessary. In this project, benzyl-poly( $\epsilon$ -caprolactone)-*b*-poly(ethylene glycol)-based polymeric micelles have been proposed as a delivery system for mTHPC. In addition, a nanobody targeting the epidermal growth factor receptor (EGFR), namely EGa1, was used as targeting moiety to promote specific cell uptake by EGFR-overexpressing cells, such as in HNSCC. In this work, micelles of three different diameters, ranging between 17 and 42 nm were prepared, loaded with mTHPC and conjugated with EGa1. Best conditions for EGa1 modification and conjugation were investigated and uptake and binding of these micelles were analyzed by confocal fluorescent microscopy. Active uptake of EGa1-conjugated micelles seems to be size-dependant in EGFR over-expressing A431 cells. Indeed, for the smallest micelle formulation, mTHPC was detected in cells regardless of EGFR availability, whereas for larger micelles mTHPC was solely detected in EGFR-overexpressing cells, suggesting that micelles are actively taken up through EGa1-EGFR interaction.

## INTRODUCTION

Head and neck cancer represents the sixth most common cancer disease among the world population. Six percent of all types of cancer belongs to this category, with 650000 new cases and 350000 deaths per year (Vigneswaran & Williams, 2014). The term “head and neck cancer” includes many squamous cell carcinomas (HNSCC) located in the mouth, throat, larynx, pharynx, sinuses and/or neck lymph nodes. Tobacco and alcohol abuse are considered high risk factors for this kind of cancer, since they are implicated in 75% of all cases, whereas another related risk factor seems to be Human Papilloma Virus (HPV) infection. In particular, the HPV genomic DNA of the oncogenic subtypes 16 and 18 can be detected in 25% of all head and neck cancers (Argiris, Karamouzis et al., 2008).

Although, surgical resection and radiotherapy have been for long time the most employed treatment, since the late 70s a new approach based on photodynamic therapy (PDT) has been considered. PDT is a light-based therapy, in which typically a photosensitizer (PS) is administered and subsequently activated by light of appropriate wavelength and intensity. The application of near infrared (NIR) and visible light can excite the PS from the ground state to its excited state (PS\*). PS\* can, in turn, either generate radical intermediates that produce reactive oxygen species (ROS), responsible for the intracellular irreversible damage and cellular toxicity (type I reaction), or directly generate ROS through the excitation of the tissue triplet oxygen ( $^3\text{O}_2$ ) from its ground state to the excited state, namely singlet oxygen ( $^1\text{O}_2$ ) (type II reaction). The latter mechanism is the most relevant for PDT applications (Figure 8.1) (Dolmans, Fukumura et al., 2003, Mehraban & Freeman, 2015)

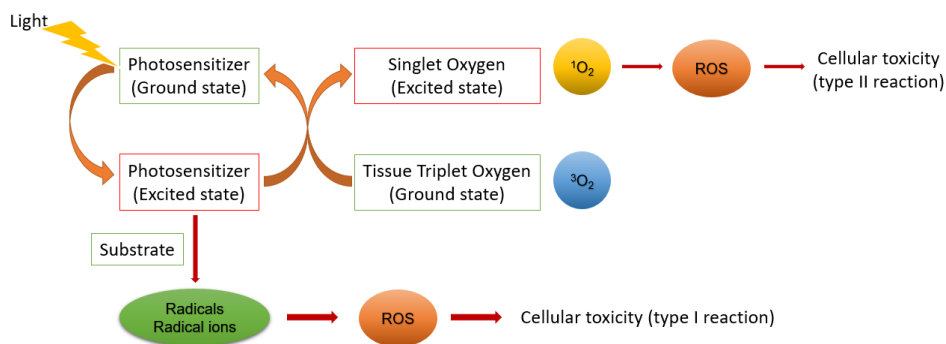


**Figure 8.1** Schematic representation of the mechanism of action of photodynamic therapy (PDT) in which the three basic elements are involved: light, photosensitizer and oxygen.

Currently, PDT has been approved in clinic in the United States, European Union, Canada, Russia, and Japan.

One of the EMA approved PS is meta-tetra(hydroxyphenyl)chlorin (mTHPC). This PS is used for PDT of early head and neck cancers and palliative treatment of patients with advanced HNSCC failing prior therapies and unsuitable for radiotherapy, surgery or systemic chemotherapy. mTHPC is known by the generic name of Temoporfin and the commercial name of Foscan<sup>®</sup> (i.e. an ethanol/propylene glycol 40:60 v/v solution) (Biel, 2016). mTHPC is a hydrophobic compound, poorly soluble in aqueous media and characterized by a very high log  $P_{o/w}$  (=9.24) (Figure 8.2) (Chen, Liu et al., 2011). In order to overcome this drawback, liposomal mTHPC was tested and approved by EMA. Nowadays, there are two commercially available liposomal formulations, Foslip<sup>®</sup> and Fospeg<sup>®</sup>, non-PEGylated and PEGylated mTHPC-loaded liposomes, respectively. Unfortunately, liposomal mTHPC has shown some limitations due to the high instability of the drug-loaded lipid vesicles in serum. In particular, 20% of non-PEGylated liposomes is readily destroyed during the first 5 min of incubation in mouse serum, and almost 60% after 6 h. On the other hand, PEGylated liposomes are more stable: they remain intact for the first 6 h and only 20% is destroyed after 24 h. However, both formulations are characterized by a very fast release of the drug, showing a burst effect within the first 3 h after injection (Reshetov, Lassalle et al., 2013). This behaviour does not guarantee the reaching of the target before drug release, making these carriers unsuitable candidates for targeting purposes, and thus a more stable mTHPC carrier is needed.

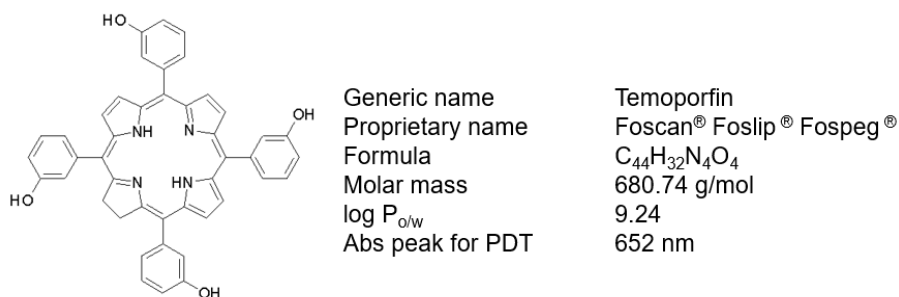


**Figure 8.2** (left) Chemical structure of meta-tetra(hydroxyphenyl)chlorin (mTHPC); (right) Compound data.

In the present work, polymeric micelles based on benzyl-poly( $\epsilon$ -caprolactone)-*b*-methoxy-poly(ethylene glycol) (BPCL-mPEG) block copolymer have been investigated as carriers for the actively targeted delivery of mTHPC to epidermal growth factor receptor (EGFR) over-expressing cells. It is well known that elevated levels of EGFR can be detected in primary tumors of HNSCC patients (Grandis, Melhem et al., 1998). Previous researches demonstrated that biodegradable BPCL-mPEG micelles can be easily prepared by thin film hydration method and are small in size. They also showed high mTHPC loading efficiency, thanks to the presence of the aromatic terminal group that improves the stability of the compound within the micelle core (Hofman, Carstens et al., 2008, Wennink, Liu et al., 2017). On the other hand, regarding the tumor site-specific delivery, anti-EGFR nanobody (EGa1) has been chosen as a targeting ligand for mTHPC-loaded BPCL-mPEG micelles.

A nanobody (NB) consists of heavy chain antibodies found in camelids. Compared to human immunoglobulins, heavy chain antibodies are smaller and composed only of heavy chains in which the target recognition module is represented by a single variable domain (VHH or NB), whereas the minimal target recognition module of a conventional human antibody is made by two non-covalently associated variable domains (VH and VL), one of the heavy chain and one of the light chain (Figure 8.3). The advantages of using NBs instead of antibodies are their higher stability and solubility in plasma and their excellent tissue penetration properties *in vivo*. Furthermore, they can be easily conjugated to Fc-domains, other nanobodies, peptide tags, toxins, drugs, radionuclides, photosensitizers or nanoparticles (Bannas, Hambach et al., 2017).

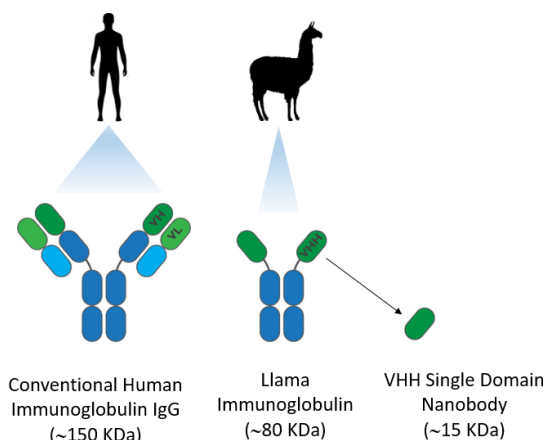


**Figure 8.3** Schematic representation of human and llama's antibody and nanobody.

For this project, three different BPCL-mPEG polymeric micelles characterized by three different hydrophobic block lengths and different particle dimensions were prepared *via* thin film hydration method. The nanometric size of the micelles, in the range of 17-45 nm, can be advantageously exploited in cancer therapy thanks to enhanced permeability and retention (EPR) effect. EPR effect can be described as the ability of nanoparticles to extravasate and accumulate in solid tumors due to the excessive angiogenesis and abnormal vascular structure caused by the presence of various permeability factors, such as nitric oxide, prostaglandins, bradykinin, cytokines, etc., and the poor lymphatic drainage (Fang, Nakamura et al., 2011, Torchilin, 2011). Furthermore, modification and conjugation of EGal nanobody have been investigated in order to increase micelles uptake in tumor site and *in vitro* uptake was evaluated by confocal fluorescence microscopy.

## EXPERIMENTAL SECTION

### Materials

Benzyl alcohol,  $\epsilon$ -caprolactone, Tin(II) 2-ethylhexanoate (Stannous octoate), p-nitrophenyl chloroformate (pNC), methoxy-poly(ethylene glycol) 2000 g/mol (mPEG), Disodium ethylenediaminetetraacetate dihydrate (EDTA), 5,5'-dithiobis(2-nitrobenzoic acid) (Ellman's reagent), Tris(2-carboxyethyl) phosphine (TCEP) hydrochloride, hydroxylamine hydrochloride were purchased by Sigma-Aldrich (Zwijndrecht, the Netherlands).

*N*-succinimidyl *S*-acetylthioacetate (Pierce™ SATA) was purchased by Thermo Fisher Scientific (Massachusetts, United States).

Maleimide-poly(ethylene glycol)-amine trifluoroacetic acid (malPEG-NH<sub>2</sub> TFA) was acquired by JenKem Technology USA.

mTHPC was obtained by Molekula (Germany).

All solvents were HPLC-grade or peptide synthesis-grade and purchased by VWR Chemicals (Amsterdam, the Netherlands) or Biosolve Chimie SARL (Dieuze, France).

## Instrumentation

All  $^1\text{H}$  NMR spectra were recorded using a Gemini NMR spectrometer (600 MHz, Varian Associates Inc. NMR instruments). Samples were prepared dissolving  $\sim 10$  mg of polymer in 1 mL of  $\text{CDCl}_3$ . Peak multiplicity was denoted as s (singlet), d (doublet), dd (double doublet), t (triplet), q (quartet), m (multiplet), and b (broad signal).

Number average molecular weight  $M_n$ , weight average molecular weight  $M_w$  and polydispersity index ( $M_w/M_n$ ) were obtained by gel permeation chromatography (GPC, Waters Alliance System) using a Mesopore Column  $300 \times 7.5$  mm equipped with a guard column  $50 \times 7.5$  mm. Refractive index method was employed for peak detection. Samples were prepared in a dimethylformamide (DMF) solution of lithium chloride (LiCl) 10 mM at a concentration of  $\sim 3$  mg/mL. 100  $\mu\text{L}$  of each samples were injected in the system at  $30^\circ\text{C}$  at flow rate of 1 mL/min using DMF with 10 nM LiCl as eluent. Molecular weights were obtained from the calibration curve of broad poly(ethylene glycol) standards ranging from 430 to 26100 g/mol.

Thermogravimetric analysis (TGA) was carried out using a Q50 TA Instruments heating samples up to  $350^\circ\text{C}$ , in order to obtain the degradation point of the polymers.

Differential scanning calorimetry (DSC) was carried out using Discovery DSC TA Instruments. Polymer samples of  $\sim 5$  mg were accurately loaded and sealed into aluminum pans. After equilibration at room temperature, samples were heated up to  $160^\circ\text{C}$  (modulated) at a ramping rate of  $3^\circ\text{C}/\text{min}$  under nitrogen flow. Next, samples were cooled down to  $-80^\circ\text{C}$  (modulated  $3^\circ\text{C}/\text{min}$ ). Afterwards, samples were heated up again to  $160^\circ\text{C}$  (modulated ramp  $3^\circ\text{C}/\text{min}$ ). The second heating cycle was used to determine glass transition temperatures ( $T_g$ ) and melting point ( $T_m$ ).  $T_g$  is defined as the point of inflection of the step change observed in the heat flow curve.

Liquid chromatography coupled to electrospray time-of-flight mass spectrometry (LC-ESI-TOF-MS) analysis of EGa1 protein was performed using a 6560 ion mobility QTOF LC/MS with an A 1290 Infinity UHPLC system (Agilent Technologies) for UHPLC measurements. System consisted of a binary pump, an autosampler, and a thermostated column compartment at  $60^\circ\text{C}$ . Column was an Acquity UPLC C18 1.7 micrometer  $2.1 \times 50$  mm. For analysis of EGa1 samples,

a gradient method was used with the mobile phase A water–formic acid (99.9:0.1 v/v) and mobile phase B acetonitrile. Elution started using A-B mixture 95:5 for 5 min, the eluent B linearly changed from 5% to 100% in 25 min with a flow rate of 0.5 mL/min. Electrospray ionization (ESI) was performed in the positive ion mode using an Agilent Technologies ion source and interface. The mass spectroscopy (MS) settings were capillary voltage of 2 kV, nebulizer pressure of 60 psi, dry gas flow of 11 L/min, dry gas temperature of 350°C, and scan range of  $m/z$  50–1500. Spectra were deconvoluted using maximum entropy algorithm.

UV/Vis spectra were recorded using a UV-2450 Shimadzu spectrophotometer. Fixed wavelength UV/Vis absorptions were measured using Spectrostar Nano Spectrophotometer (BMG Labtech).

Dynamic light scattering (DLS) and electrophoretic light scattering (ELS) analyses were carried out using DLS Zetasizer 4000 Malvern Instrument at 25°C and measuring the correlation function at 90° and laser set at 632.8 nm. Polydispersity index (PDI) lower than 0.3 indicates the presence of a homogeneous population of particles.

### **Synthesis of benzyl-poly( $\epsilon$ -caprolactone)**

Benzyl-poly( $\epsilon$ -caprolactone)<sub>n</sub> (BPCL<sub>n</sub>-OH) was synthesized in bulk *via* ring-opening polymerization (ROP). Three different polymers with three different degrees of polymerization were synthesized (theoretical degree of polymerization DP  $n=5.5$  or  $n=14.2$  or  $n=23$ ). Briefly, benzyl alcohol (BenzOH) (10 mmol, 1.03 mL) and  $\epsilon$ -caprolactone ( $\epsilon$ -CL) (55 mmol, 6.09 mL or 142 mmol, 15.74 mL or 230 mmol, 25.49 mL) were put in a round bottom flask, prior drying through a 4Å molecular sieve. Mixture was put under magnetic stirring in an oil bath at 130°C and vacuum was applied for 5 h, in order to remove traces of water. Afterwards stannous octoate (0.5 mmol, 0.02 mL) was added and reaction was allowed to occur for 4 h, 5 h or 6 h, depending on DP, in nitrogen atmosphere. For the exact amounts of reagents used see Table 8.1. Final product was cooled down to room temperature, dissolved in 10 mL of dry dichloromethane (DCM) and purified by precipitation in a 20-fold excess of diethyl ether at -20°C. Product was recovered by filtration and remaining organic solvent was removed from the residue through evaporation under nitrogen stream and the whitish powder was finally dried under vacuum overnight (yield:  $n=9$  61.9%;  $n=15$  80.9%;  $n=23$  82.2%).



$^1\text{H}$  NMR ( $\text{CDCl}_3$ ):  $\delta = 7.35$  (b, aromatic protons, benzyl alcohol), 5.11 (s,  $\text{CCH}_2\text{O}$ ), 4.05 (m,  $\text{CH}_2\text{CH}_2\text{O}$ ), 3.65 (t,  $\text{CH}_2\text{CH}_2\text{OH}$ ), 2.30 (m,  $\text{OC(O)CH}_2$ ), 1.65 (m,  $\text{CH}_2\text{CH}_2\text{CH}_2\text{CH}_2\text{CH}_2$ ), 1.38 (m,  $\text{CH}_2\text{CH}_2\text{CH}_2\text{CH}_2\text{CH}_2$ ).

**Table 8.1** Reagents for BPCL<sub>n</sub>-OH polymerization.

	DP (n=)	moles (mol)	ratio	m.w. (g/mol)	density (g/mL)	volume (mL)
<b>BenzOH</b>		0.01	1	108.14	1.045	1.03
<b>St.Oct.</b>		0.0005	0.005	405.12	1.251	0.02
<b><math>\epsilon</math>-CL</b>	9	0.055	5.5	114.14	1.03	6.09
<b><math>\epsilon</math>-CL</b>	15	0.142	14.2	114.14	1.03	15.74
<b><math>\epsilon</math>-CL</b>	23	0.230	23	114.14	1.03	25.49

### Synthesis of benzyl-poly( $\epsilon$ -caprolactone)-p-nitrophenyl formate

Hydrophobic benzyl-poly( $\epsilon$ -caprolactone)<sub>n</sub>-p-nitrophenyl formate (BPCL<sub>n</sub>-pNF) was synthesized in order to obtain a good leaving group, namely p-nitrophenol, for the later conjugation with the hydrophilic block. Briefly, 4 g of dry BPCL<sub>n</sub>-OH was dissolved in 20 mL of toluene, previously dried through a 4Å molecular sieve, under nitrogen atmosphere inside a round bottom flask. Triethylamine (TEA) was added to the solution under magnetic stirring and later an equimolar amount of p-nitrophenyl chloroformate (pNC) was added until complete dissolution. The used BPCL<sub>n</sub>-OH/pNC/TEA molar ratio was 1:3.5:3.5 (see Table 8.2). Reaction was left overnight under magnetic stirring, at room temperature in nitrogen atmosphere. Then solution was centrifuged at 5100 rpm at room temperature to remove TEA·HCl pellet. Supernatant was precipitated in cold diethyl ether (-20°C), and powder was collected by filtration, dissolved in dry toluene and precipitated again in cold diethyl ether. Purified product was recovered by filtration, remaining organic solvent was evaporated from the residue under nitrogen stream and the white powder was dried overnight under vacuum (yield: n=9 58.2%; n=15 72.8%; n=23 75.8%).

$^1\text{H}$  NMR ( $\text{CDCl}_3$ ):  $\delta = 8.27$  (d, aromatic protons, pNF), 7.38 (m, aromatic protons, benzyl alcohol and pNF), 5.11 (s,  $\text{CCH}_2\text{O}$ ), 4.29 (m,  $\text{CH}_2\text{CH}_2\text{OC(O)O}$ ), 4.05 (m,  $\text{CH}_2\text{CH}_2\text{O}$ ), 2.30 (m,  $\text{OC(O)CH}_2$ ), 1.65 (m,  $\text{CH}_2\text{CH}_2\text{CH}_2\text{CH}_2\text{CH}_2$ ), 1.38 (m,  $\text{CH}_2\text{CH}_2\text{CH}_2\text{CH}_2\text{CH}_2$ ).

**Table 8.2** Reagents for BPCL<sub>n</sub>-pNF synthesis.

	volume (mL)	mass (g)	m.w. (g/mol)	d (g/mL)	moles (mol)	ratio
<b>BPCL<sub>9</sub>-OH</b>	–	4	1135	–	0.0035	1
<b>pNC</b>	–	2.64	201.56	–	0.0130	3.5
<b>TEA</b>	1.83	1.33	101.19	0.7255	0.0130	3.5
<b>BPCL<sub>15</sub>-OH</b>	–	4	1820	–	0.0022	1
<b>pNC</b>	–	1.55	201.56	–	0.0077	3.5
<b>TEA</b>	1.07	0.78	101.19	0.7255	0.0077	3.5
<b>BPCL<sub>23</sub>-OH</b>	–	4	2733	–	0.00146	1
<b>pNC</b>	–	1.03	201.56	–	0.00511	3.5
<b>TEA</b>	0.71	0.52	101.19	0.7255	0.00511	3.5

### Synthesis of methoxy-poly(ethylene glycol)-amine

Methoxy-poly(ethylene glycol)-amine (mPEG-NH<sub>2</sub>) 2000 g/mol was kindly provided by Yanna Liu, who synthesized it following the already published procedure (Wennink, Liu et al., 2017). In summary, 50 g of mPEG-OH 2000 g/mol (24 mmol) was dissolved in 700 mL of dry toluene. Dry TEA solution in DCM was added to the mPEG-OH solution in an ice-bath. Subsequently, an excess of mesyl chloride was added dropwise under magnetic stirring and reaction was left overnight. Solution was filtered and precipitated in cold diethyl ether. mPEG-mesylate product was reacted with aqueous ammonia solution for 4 days at room temperature. mPEG-NH<sub>2</sub> product was extracted 3 times with DCM and precipitated in cold diethyl ether. For more details, see the cited reference.

### Synthesis of benzyl-poly( $\epsilon$ -caprolactone)-*b*-methoxy-poly(ethylene glycol)

Benzyl-poly( $\epsilon$ -caprolactone)<sub>n</sub>-*b*-methoxy-poly(ethylene glycol) (BPCL<sub>n</sub>-mPEG) was synthesized starting from BPCL<sub>n</sub>-pNF and mPEG-NH<sub>2</sub>. In brief, dry mPEG-NH<sub>2</sub> (0.6 g 0.3 mmol) was added to 10 mL of dry toluene in a round bottom flask and sonicated until complete dissolution. Afterwards, 0.2 mmol of BPCL<sub>n</sub>-pNF was added to the mixture (n=9 260 mg; n=15 397 mg; n=23 580 mg) and reaction was left overnight under magnetic stirring in nitrogen atmosphere. The yellowish

solution was precipitated in diethyl ether at room temperature, the yellowish powder was collected by filtration and organic solvent was removed by evaporation under nitrogen stream. The product was then suspended in deionized water and dialyzed against water at pH ~5 using dialysis tube MWCO: 10 kDa. The dialysis step was applied in order to remove traces of the yellowish p-nitrophenyl and unreacted mPEG-NH<sub>2</sub>. Suspension within the tube was freeze-dried and the white powder was collected and stored for micelles preparation (yield: n=9 81.8%; n=15 56.3%; n=23 57.0%).

<sup>1</sup>H NMR (CDCl<sub>3</sub>): δ = 7.35 (b, aromatic protons, benzyl alcohol), 5.11 (s, CCH<sub>2</sub>O), 4.05 (m, CH<sub>2</sub>CH<sub>2</sub>O), 3.64 (m, PEG protons), 3.38 (s, OCH<sub>3</sub>), 2.30 (m, OC(O)CH<sub>2</sub>), 1.65 (m, CH<sub>2</sub>CH<sub>2</sub>CH<sub>2</sub>CH<sub>2</sub>CH<sub>2</sub>), 1.38 (m, CH<sub>2</sub>CH<sub>2</sub>CH<sub>2</sub>CH<sub>2</sub>CH<sub>2</sub>).

### Synthesis of benzyl-poly(ε-caprolactone)-*b*-poly(ethylene glycol)-maleimide

Benzyl-poly(ε-caprolactone)<sub>n</sub>-*b*-poly(ethylene glycol)-maleimide (BPCL<sub>n</sub>-malPEG) was synthesized starting from BPCL<sub>n</sub>-pNF and maleimide-PEG-NH<sub>2</sub>·TFA (Table 8.3). Briefly, dry BPCL<sub>n</sub>-pNF and dry TEA were dissolved in 10 mL of dry toluene in a round bottom flask, under magnetic stirring at room temperature. After complete dissolution, maleimide-PEG-NH<sub>2</sub>·TFA was added to the mixture, prior drying overnight under vacuum at room temperature. Reaction was proceeded overnight under nitrogen atmosphere at room temperature. Product was centrifuged to separate the TFA·TEA salt from the supernatant, which was later precipitated in diethyl ether at room temperature. Product collected by filtration, was dissolved in 10 mL of dry toluene and precipitated again in diethyl ether. Finally, the purified product was collected and stored for micelles preparation (yield: n=9 77.8%; n=15 24%; n=23 73.7%).

<sup>1</sup>H NMR (CDCl<sub>3</sub>): δ = 7.35 (m, aromatic protons, benzyl alcohol), 6.70 (s, maleimide protons), 5.11 (s, CCH<sub>2</sub>O), 4.05 (m, CH<sub>2</sub>CH<sub>2</sub>O), 3.64 (m, PEG protons), 2.30 (m, OC(O)CH<sub>2</sub>), 1.65 (m, CH<sub>2</sub>CH<sub>2</sub>CH<sub>2</sub>CH<sub>2</sub>CH<sub>2</sub>), 1.38 (m, CH<sub>2</sub>CH<sub>2</sub>CH<sub>2</sub>CH<sub>2</sub>CH<sub>2</sub>).

The presence of the maleimide as the terminal functional group of the polymer chain was confirmed also by UV/Vis spectroscopy. Spectra of BPCL<sub>n</sub>-malPEG in DCM 5 mg/mL were recorded in the range 240-350 nm using quartz cuvette (1 cm).

**Table 8.3** Reagents for BPCL<sub>n</sub>-malPEG synthesis.

	volume (mL)	mass (g)	m.w. (g/mol)	d (g/mL)	ratio	moles (mol)
malPEG-NH <sub>2</sub> ·TFA		0.413	2000		1	0.000206
BPCL <sub>9</sub> -pNF		0.268	1301		1	0.000206
TEA	0.035	0.025	101.19	0.7255	1.2	0.000248
malPEG-NH <sub>2</sub> ·TFA		0.304	2000		1	0.000152
BPCL <sub>15</sub> -pNF		0.302	1985		1	0.000152
TEA	0.025	0.018	101.19	0.7255	1.2	0.000182
malPEG-NH <sub>2</sub> ·TFA		0.205	2000		1	0.000103
BPCL <sub>23</sub> -pNF		0.297	2898		1	0.000103
TEA	0.017	0.012	101.19	0.7255	1.2	0.000123

### Polymeric micelles preparation

Polymeric micelles were prepared according to the thin film hydration method. Briefly, 1 mL of a solution BPCL<sub>n</sub>-mPEG/BPCL<sub>n</sub>-malPEG 10 mg/mL (ratio 9:1 w/w) in DCM was put into a glass vial under nitrogen stream overnight, in order to let the organic solvent evaporate and obtain a solid thin polymeric film. 1 mL of phosphate buffered saline (PBS) solution was used to hydrate the film and the vial was vortexed for 30 sec, until complete polymer resuspension. The mixture was slowly heated up to 70°C in a water bath for 15 min and then sonicated for 2 min at 40°C. Polymer suspension was equilibrated at room temperature for further 15 min and then extruded through 0.2 μm regenerated cellulose (RC) syringe filter. Size and Z-potential were obtained by DLS and ELS.

mTHPC loaded micelles were prepared using 5%, 5% and 10% as feeding percentage (w/w) of drug for BPCL<sub>9</sub>-mPEG/BPCL<sub>9</sub>-malPEG, BPCL<sub>15</sub>-mPEG/BPCL<sub>15</sub>-malPEG and BPCL<sub>23</sub>-mPEG/BPCL<sub>23</sub>-malPEG, respectively. 100 or 200 μL of a solution of mTHPC 5 mg/mL in THF was added to the polymer DCM solution and the previously described procedure was followed. Drug loading capacity (DLC) and drug loading efficiency (DLE) were calculated from the UV/Vis spectra of diluted samples of micelles in DMF at 651.5 nm, through the calibration curve of mTHPC in DMF and using the following equations:

$$DLC (\%) = \frac{W_{ld}}{W_{ld} + W_p} \quad (8.1)$$

$$DLE (\%) = \frac{W_{ld}}{W_{fd}} \quad (8.2)$$

in which  $W_{ld}$ ,  $W_{fd}$  and  $W_p$  represent the mass of loaded drug inside the micelles, the feeding amount of drug and the polymer mass, respectively. Absorption spectra were recorded using a UV-2450 Shimadzu spectrophotometer.

### EGa1 nanobody production

60 mL of Lysogeny Broth (LB) medium, 6 mL of 20% glucose solution and 60  $\mu$ L of antibiotics (Kanamycin and Chloramphenicol to a final concentration of 50  $\mu$ g/mL) were put into a sterile flask. Afterwards, a small frozen granule of *E. coli* BL21, containing pET28-EGa1-myc-his plasmid for the production of EGa1 nanobody, was added to the mixture. Flask was incubated at 37°C for 16 h under shaking at 180 rpm and then it was cooled down at room temperature for 3 h. 8 mL of the bacteria suspension was transferred in a bigger flask together with 800 mL of yeast extract tryptone (YT) medium, 4 mL of 20% glucose solution and 800  $\mu$ L of Kanamycin solution to a final concentration of 50  $\mu$ g/mL. Latter step was repeated six times in order to obtain six flasks, subsequently incubated at 37°C under shaking at 200 rpm. Optical Density (OD) at 600 nm was measured using a spectrophotometer and YT medium was used for blank correction. After 3 h OD value was  $\sim$ 0.9 and EGa1 production was induced by addition of 800  $\mu$ L isopropyl  $\beta$ -D-1-thiogalactopyranoside (IPTG). Flasks were incubated at 25°C overnight under shaking at 180 rpm. Afterwards, bacteria suspension was centrifuged at 4600 rpm for 20 min at 4°C, supernatant was discarded and bacteria pellet was resuspended in 120 mL of PBS. Suspension was evenly distributed in four 50 mL Falcon tubes and stored overnight at -20°C to allow the formation of ice crystals responsible for the cell wall lysis. Bacteria suspension was thawed on ice, frozen and thawed again. Suspension was centrifuged at 4700 rpm for 20 min at 4°C to remove the cellular debris and supernatant, containing the periplasmic proteins, was stored at 4°C.

### EGa1 nanobody purification

3 mL of Nickel-nitrilotriacetic acid (Ni-NTA) resin suspended in ethanol (QIAGEN GmbH) was transferred to a 50 mL Falcon tube and 40 mL of PBS was added. Resin beads were gently shaken and centrifugation at 900 G with 4 G of deceleration was applied for 3 min at 4°C. Supernatant was discarded and

washing step with PBS was repeated. After the second centrifugation, supernatant was discarded, 40 mL of PBS was added and the suspension was distributed in four 50 mL Falcon tubes, each containing 10 mL of Ni-NTA beads suspended in PBS. Centrifugation was repeated again, supernatant was removed and the four previously stored supernatant containing the periplasmic proteins was transferred in the tubes containing the Ni-NTA beads. Tubes were left under rotation at 15 rpm for 1.5 h at 4°C. Afterwards, centrifugation was applied and the supernatant collected as resin flowthrough and stored at 4°C. Beads were resuspended in 30 mL of PBS, centrifuged at 900 G (9 G acceleration; 4 G deceleration) for 3 min at 4°C and supernatant was discarded. Wash with PBS alternated with centrifugation was repeated 3 times. Supernatant was discarded and beads were resuspended using 10 mL of PBS. A 20 mL column (BioRad) was washed with 5-10 mL of PBS and then beads suspension was transferred to it. PBS was allowed to flow from the column and discarded. The column was capped on the tip and incubated for 5 min with 1 mL of imidazole solution 300 mM pH 7.2 with the packed beads. Cap was removed and sample was collected in an Eppendorf. Elution with 1 mL of imidazole solution was repeated more times and samples were collected in Eppendorfs. Protein concentrations and 260/280 ratios were measured using Nanodrop spectrophotometer 1000 (ISOGEN Life sciences) and calculated using 2.018 as absorption coefficient. Finally, protein solution was purified by dialysis overnight against PBS at 4°C, using Snakeskin Dialysis Tubing MWCO: 3.5 kDa, 16 mm dry, Thermo Fisher Scientific. PBS medium was refreshed and dialysis was continued for further 2 h at room temperature. Purified EGa1 concentration and 260/280 ratio was measured again using Nanodrop. EGa1 stock was stored in Eppendorfs at -20°C. Purification procedure was repeated one more time starting from the collected resin flowthrough.

In order to confirm EGa1 production, Sodium Dodecyl Sulphate - PolyAcrylamide Gel Electrophoresis (SDS-PAGE) was run at 80 V, using Bolt 4-12% Bis-Tris Plus Invitrogen and 2-(N-morpholino)ethanesulfonic acid (MES) buffer as prefilled cassette gel and electrophoretic running solution, respectively. Gel was stained using PageBlue Protein Staining Solution (Thermo Fisher Scientific). Samples were diluted and heated at 80°C for 10 min prior loading into the gel with lithium dodecyl sulfate (LDS) running buffer in reducing condition.

### **Addition of protected sulfhydryl groups on EGa1 nanobody**

In order to insert thio-modifications on EGa1, SATA reagent was employed. Three different SATA-modified EGa1 batches were prepared using different EGa1/SATA molar ratios (1:2, 1:5 and 1:10). In brief, EGa1 stock solution 1.4 mg/mL in PBS pH 7.4 was left to thaw on ice and then 3 aliquots of 150  $\mu$ L were put in three suitable Eppendorfs. A SATA solution was prepared dissolving 3.5 mg in 1 mL of dimethyl sulfoxide (DMSO) and a two-fold diluted SATA solution was prepared adding 100  $\mu$ L of SATA solution to 100  $\mu$ L of DMSO. 7.47  $\mu$ L and 3.73  $\mu$ L of SATA solution were added to two Eppendorfs and 3  $\mu$ L of diluted SATA solution was added to the last Eppendorf, to obtain the EGa1-SATA 1:10, EGa1-SATA 1:5 and EGa1-SATA 1:2 ratios, respectively. Eppendorfs were left on a rolling bench for 1 h at 25°C. Samples were collected and put in Vivaspin 6 tubes (MWCO: 3 kDa) and washed four times with 2 mL of PBS by centrifugation at 5100 rpm for 45 min at 4°C (acceleration 9 G; deceleration 4 G). Afterwards PBS was added to reach the final volume of 500  $\mu$ L and samples were stored at -20°C.

### **Ellman's assay**

Ellman's assay was performed to quantify the sulfhydryl groups inserted on EGa1 after modification with SATA group. Briefly, Ellman's reagent was prepared dissolving 8.9 mg of 5,5'-dithiobis-(2-nitrobenzoic acid) (DTNB) in 20 mL of reaction buffer (EDTA 1 mM in PBS pH 8), whereas SATA deprotection solution was prepared dissolving 695 mg of hydroxylamine hydrochloride (1 M) in 50 mM EDTA solution in PBS, pH adjusted to 7.2. Assay was conducted mixing 50  $\mu$ L of EGa1-SATA solution, 10  $\mu$ L deprotection solution, 50  $\mu$ L Ellman's reagent and 170  $\mu$ L reaction buffer; native EGa1 sample was prepared mixing 50  $\mu$ L of EGa1 solution, 50  $\mu$ L Ellman's reagent and 180  $\mu$ L reaction buffer; reduced native EGa1 sample was prepared adding TCEP 1:1 molar ratio compared to nanobody amount. Solutions were loaded on polystyrene 96 multi-well plate and incubated at room temperature for 15 min. Afterwards, absorption at 412 nm was measured and average -SH groups per protein was calculated using the calibration curve of cysteine (Cys).

**EGa1-SATA LC-ESI-TOF-MS analysis**

LC-MS experiments were performed using an Agilent Technologies 6300 series LC/MSD ion-trap mass spectrometer (Santa Clara, CA, USA). A C18 column was used at room temperature. For analysis of native EGa1 and SATA-modified EGa1, a gradient elution was used with the mobile phase A water-acetonitrile-formic acid (95:5:0.1, v/v/v) and mobile phase B acetonitrile-formic acid (100:0.1, v/v). The eluent A after 5 min linearly changed from 100% to 50% in 25 min with a flow rate of 0.5 mL/min. The sample injection volume was 1  $\mu$ L. Electrospray ionization (ESI) was performed in the positive ion mode using an Agilent Technologies ion source and interface. The MS settings were capillary voltage of 2 kV, nebulizer pressure of 60 psi, dry gas flow of 11 L/min, dry gas temperature of 350°C, and scan range of m/z 300-3000.

**EGa1-SATA reactivity towards maleimide**

Nanobody solutions containing 20  $\mu$ g of native EGa1, EGa1-SATA 1:2, EGa1-SATA 1:5 or EGa1-SATA 1:10 were put in Eppendorfs and incubated with 5  $\mu$ L of hydroxylamine deprotection solution for 15 min at room temperature (see Ellman's assay section). Afterwards, 0.28  $\mu$ L of IRDye 800CW solution of 20 mg/mL in DMSO (1:4 EGa1/800CW molar ratio) was added to each Eppendorf and left for 2 h on a rolling bench at room temperature. In order to separate free dye from dye-conjugated EGa1, SDS-PAGE was run at 100 V for 15 min and 120 V for further 40 min, using 15% Gel and TGS as running buffer. Samples were prepared by diluting 0.5  $\mu$ L of reaction mixture, 18.25  $\mu$ L of PBS and 6.25  $\mu$ L of Laemmli reducing sample buffer with no bromophenol blue to reduce interference. Gel was scanned in fluorescence at 800 nm, intensity L2, using Odyssey Imaging Systems (LI-COR Biosciences).

Remaining nanobodies were washed to remove unconjugated dye using Zeba Spin Desalting Columns, MWCO: 7 kDa, 0.5 mL (Thermo Fisher Scientific). Columns were washed 3 times with 300  $\mu$ L of PBS through centrifugation at 1500 G for 1 min at 4°C. Nanobody solutions were added to the columns together with 15  $\mu$ L of PBS and centrifuged inside Eppendorfs. Samples were read using Nanodrop at 280 nm and 774 nm wavelengths, protein and dye absorption peaks, respectively. To calculate protein concentration and dye/protein ratio, the following equations (8.3) and (8.4) were applied:



$$[Protein] (mg/mL) = \frac{A_{280} - 0.03 \times A_{774}}{\epsilon_{protein}} \times MW_{protein} \times DF \quad (8.3)$$

$$Dye/Protein \text{ ratio} = \frac{A_{774}}{\epsilon_{dye}} \div \frac{A_{280} - 0.03 \times A_{774}}{\epsilon_{protein}} \quad (8.4)$$

in which  $A_{280}$  is the absorption value at 280 nm,  $A_{774}$  is the absorption value at 774 nm,  $MW_{protein}$  is EGa1 molecular weight (=17097.87 Da),  $\epsilon_{protein}$  is extinction coefficient of EGa1 at 280 nm (=34505  $M^{-1} \text{ cm}^{-1}$ ),  $\epsilon_{dye}$  is the extinction coefficient of IRDye 800CW at 774 nm (=240000  $M^{-1} \text{ cm}^{-1}$ ) and DF is the dilution factor.

### EGa1 conjugation to mTHPC-loaded micelles

mTHPC-loaded BPCL<sub>9</sub>-mPEG/BPCL<sub>9</sub>-malPEG, BPCL<sub>15</sub>-mPEG/BPCL<sub>15</sub>-malPEG and BPCL<sub>23</sub>-mPEG/BPCL<sub>23</sub>-malPEG micelles were conjugated to EGa1-SATA 1:5 according to the following procedure: 1 mL of freshly prepared EGa1-SATA 1:5 1.22 mg/mL was deprotected by adding 150  $\mu\text{L}$  of hydroxylamine solution 1 M in PBS containing EDTA 50 mM pH 7.2 for 15 min at room temperature. Different amount of deprotected EGa1-SATA 1:5 were added to 2 mL of BPCL<sub>9</sub>-mPEG/BPCL<sub>9</sub>-malPEG, BPCL<sub>15</sub>-mPEG/BPCL<sub>15</sub>-malPEG or BPCL<sub>23</sub>-mPEG/BPCL<sub>23</sub>-malPEG micelles using maleimide/EGa1 molar ratio 100:4.5. Reaction occurred in glass vials on a rolling bench for 1 h at room temperature and at 4°C for further 16 h. Afterwards, 100  $\mu\text{L}$  of Cys solution 0.33 M in PBS pH 7.4 was added to reaction mixtures for 1 h at room temperature, in order to saturate the unreacted maleimide groups. Control micelles were prepared by adding 100  $\mu\text{L}$  of Cys solution 0.33 M in PBS pH 7.4 to 2 mL of mTHPC-loaded BPCL<sub>n</sub>-mPEG/BPCL<sub>n</sub>-malPEG for 1 h at room temperature. Micelles were washed 10 times with fresh PBS using Vivaspin 6 tubes (MWCO: 50 kDa for n=9 and n=15; 100 kDa for n=23) centrifuged at 5100 rpm at 4°C for 15 min. To confirm the conjugation, SDS-PAGE of diluted micelles was run at 80 V, using Bolt 4-12% Bis-Tris Plus Invitrogen and MES Buffer as prefilled cassette gel and electrophoretic running solution, respectively. Gel was stained using Pierce Silver Stain Kit (Thermo Fisher Scientific). Samples were diluted and heated at 80°C for 10 min prior loading into the gel with LDS running buffer in reducing condition.

**Cell culture**

The human epithelial carcinoma cell line A431 (CRL-1555) and the human cervical carcinoma cell line HeLa (CCL-2) were both obtained from ATCC (LGC Standards, Wesel, Germany).

Vial of A431 cells (passage 10) was thawed on dry ice and cell suspension was put inside a T-flask 75 cm<sup>2</sup> with 15 mL of low glucose Dulbecco's Modified Eagle Medium (DMEM) containing 10% fetal bovine serum (FBS). Flask was incubated at 37°C, relative humidity 95% and CO<sub>2</sub> 5%. When confluence reached 70-80%, medium was removed and cells were washed with 7 mL of PBS and passed using 1 mL of 0.025% (w/v) trypsin / 0.53 mM EDTA solution and with 2 min incubation. Trypsin was inactivated by addition of 9 mL of fresh low glucose DMEM containing 10% FBS. 1 mL was added to a new T-flask 75 cm<sup>2</sup> containing 14 mL of fresh low glucose DMEM containing 10% FBS and incubated at 37°C, relative humidity 95% and CO<sub>2</sub> 5%.

Vial of HeLa cells (passage 9) was thawed on dry ice and cell suspension was put inside a T-flask 75 cm<sup>2</sup> with 15 mL of high glucose DMEM containing 10% FBS. Cell passaging was similar to A431 cells.

**EGFR expression in A431 and HeLa cells**

In brief, 100000 A431 or HeLa cells/well were distributed in a 96 multi-well plate (U-bottom). Cells were centrifuged and medium was removed and replaced twice with PBS containing 1% bovine serum albumin (BSA). Afterwards 50 µl/well of primary antibody (mouse anti-EGFR Ab-10, stock solution 0.2 mg/mL) was added to the cells. After 45 min incubation at 4°C, plate was washed two times with PBS containing 1% BSA and 50 µl/well of secondary antibody (goat anti-mouse IgG-A488, stock 1 mg/mL) was added. Plate was incubated for 30 min at 4°C and then washed two times with PBS containing 1% BSA. Measurement was carried out using FACS Canto II, counting at least 10000 events per sample. EGFR expression in A431 cells was considered 100%

**EGa1-SATA binding affinity assay**

10000 A431 cells/well were seeded in a 96 multi-well plate (flat bottom) with 100 µL of DMEM low glucose containing FBS 10% and incubated overnight at 37°C, relative humidity 95% and CO<sub>2</sub> 5%. Cells were washed two times at 4°C

with 100  $\mu\text{L}$  of binding buffer, consisting in DMEM with no phenol red, containing HEPES buffer 25 mM and 1% BSA. 100  $\mu\text{L}$  of native EGa1 solution in binding buffer with different concentration, ranging between 100 and 0.19 nM were added to the wells. Plate was incubated at 4°C for 2 h and then washed two times with 100  $\mu\text{L}$  of binding buffer and 1 time with 100  $\mu\text{L}$  of PBS. 60  $\mu\text{L}$  of 4% paraformaldehyde (pFA) in PBS was added to each well and plate was incubated for 10 min at room temperature. Cells were washed one time with 100  $\mu\text{L}$  of PBS and one time with 100  $\mu\text{L}$  of PBS containing BSA 1%. 50  $\mu\text{L}$  of anti-VHH antibody (rabbit anticamelid antibody - primary antibody) 0.6 mg/mL was added to the cells and incubated for 1 h at room temperature. Cells were washed two times with 100  $\mu\text{L}$  of PBS containing BSA 1% and 50  $\mu\text{L}$  of goat antirabbit-800CW antibody (secondary antibody) 0.5 mg/mL was added to each well and incubated for 1 h at room temperature. Cells were washed two times with 100  $\mu\text{L}$  of PBS containing BSA 1% and finally left with no medium inside the wells. Plate was scanned using Odyssey Imaging Systems at 800 nm, intensity 7. Experiments were carried out in triplicates. Fluorescence values were plotted against concentration using GraphPad Prism 7 software (non-linear regression fit; binding saturation; specific binding - one site method). The same procedure was followed for EGa1-SATA 1:2, EGa1-SATA 1:5 and EGa1-SATA 1:10.

### **mTHPC-loaded EGa1-conjugated micelles uptake and binding studies**

For micelles binding test 10000 A431or HeLa cells/well were seeded in a 96 multi-well plates (flat bottom, black walls) with 100  $\mu\text{L}$  of culture medium and incubated overnight at 37°C, relative humidity 95% and CO<sub>2</sub> 5%. Medium was removed and 180  $\mu\text{L}$  of fresh DMEM was added together with 20  $\mu\text{L}$  of BPCL<sub>n</sub>-mPEG/BPCL<sub>n</sub>-malPEG-EGa1 micelles 10 mg/mL in PBS. For competition test, 172  $\mu\text{L}$  of fresh medium was added together with 20  $\mu\text{L}$  of BPCL<sub>n</sub>-mPEG/BPCL<sub>n</sub>-malPEG-EGa1 micelles 10 mg/mL and 8  $\mu\text{L}$  of native EGa1 1.4 mg/mL in PBS. Plates were incubated at 4°C for 1 h. Afterwards, cells were washed three times with 100  $\mu\text{L}$  PBS. 60  $\mu\text{L}$  of 4% paraformaldehyde (pFA) in PBS was added to each well and plates were incubated for 10 min at room temperature. pFA was removed and replaced with 100  $\mu\text{L}$  PBS.

For micelles uptake test 10000 A431or HeLa cells/well were seeded in 96 multi-well plates (flat bottom, black walls) with 100  $\mu\text{L}$  of culture medium and

incubated overnight at 37°C, relative humidity 95% and CO<sub>2</sub> 5%. Medium was removed and 180 µL of fresh DMEM containing 10% FBS was added with 20 µL of BPCL<sub>n</sub>-mPEG/BPCL<sub>n</sub>-malPEG-EGa1 micelles 10 mg/mL in PBS. For competition test 172 µL of fresh medium was added with 20 µL of BPCL<sub>n</sub>-mPEG/BPCL<sub>n</sub>-malPEG-EGa1 micelles 10 mg/mL and 8 µL of native EGa1 1.4 mg/mL in PBS. After different time points (0.5 h, 1 h, 2 h, 3.5 h and 7 h) incubation at 37°C, cells were washed three times with 100 µL OptiMEM with no phenol red.

For both experiments, plates were read using Yokogawa CV 7000s confocal fluorescence microscope, laser set at 405 nm ( $\lambda_{\text{excitation}}$ ) and acquisition at 676/29 nm ( $\lambda_{\text{emission}}$ ), exposure time 50/100 msec. Images were elaborated with Columbus software ( $X_{\text{min}}=105$ ;  $X_{\text{max}}=130$ ,  $X_{\text{mid}}=0.52$ ) and ImageJ software. Uptake rate was plotted as normalized mean integrated intensity versus time. Statistical significance between control and samples was analyzed using GraphPad Prism 7 software (two-way ANOVA; significance was defined as \* $p < 0.0001$ ).

## **RESULTS AND DISCUSSION**

### **Polymers synthesis and characterization**

A library of BPCL<sub>n</sub>-mPEG and BPCL<sub>n</sub>-malPEG was synthesized through three subsequent steps. In the first step the synthesis of BPCL<sub>n</sub>-OH was achieved by ROP procedure in which benzyl alcohol,  $\epsilon$ -caprolactone and stannous octoate were employed as initiator, cyclic monomer and catalyst, respectively (Figure 8.4) (Labet & Thielemans, 2009). Compared to conventional condensation polymerization, ROP has several advantages: mild experimental conditions, no additional by-products due to water molecule production, controllable molecular weight with narrow distribution and polydispersity index (PDI)  $\leq 1.2$ .

Prior addition of the catalyst, vacuum at 130°C was applied in order to reduce water traces that could act as co-initiator and lead to polymer chains without benzyl groups. Water content in the reaction mixture was measured by Karl Fischer coulometric titration. After 5 h, the water content remained stable and polymerization was initiated by addition of the catalyst (Figure 8.5).

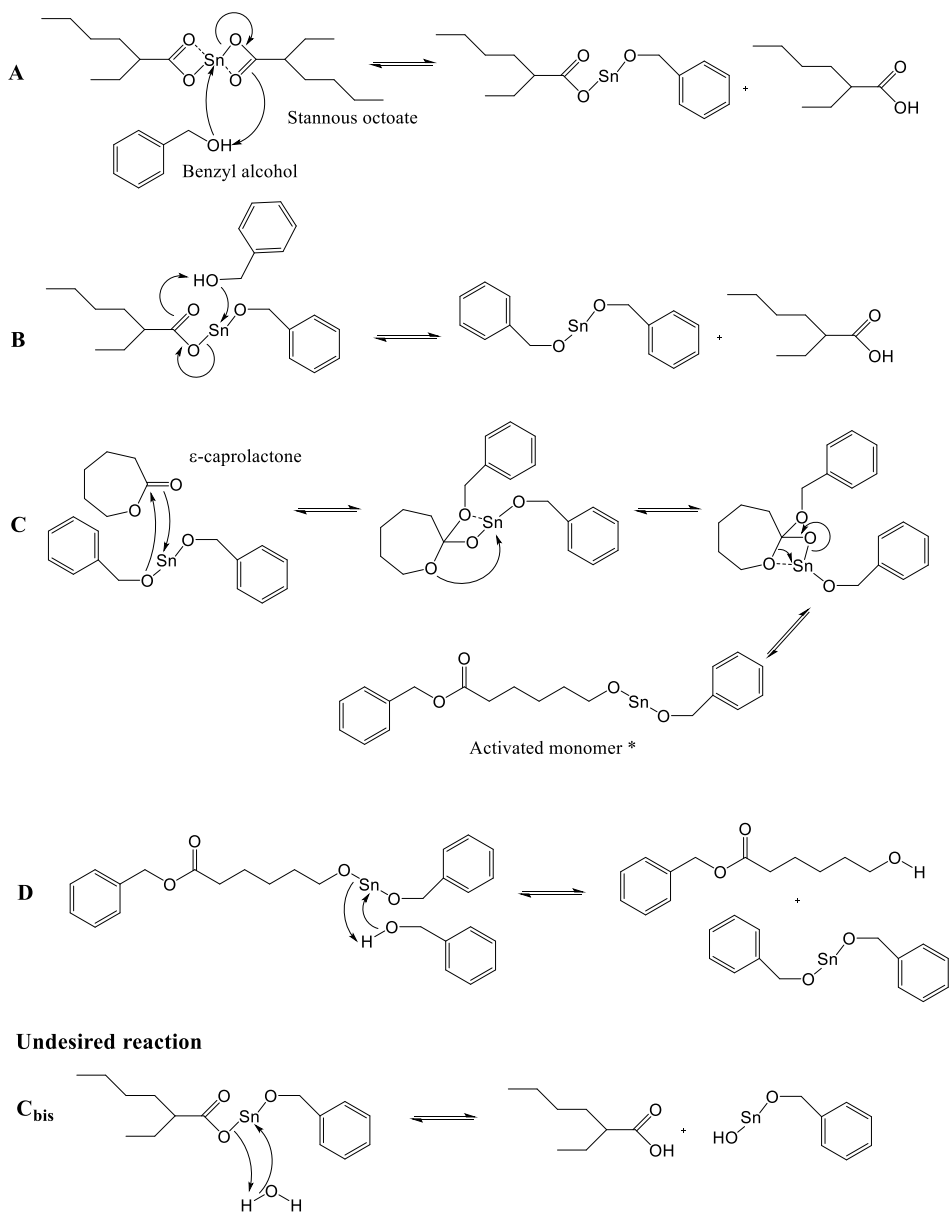


**Figure 8.4** Mechanism of reaction of ring-opening polymerization of the  $\epsilon$ -caprolactone.

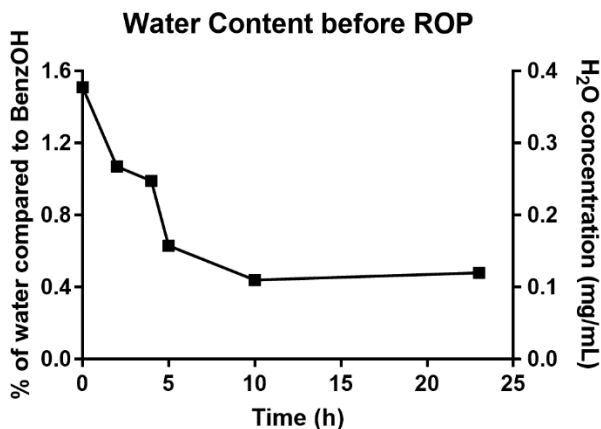


**Figure 8.5** Water content in the reaction mixture after 2 h, 4 h, 5 h, 10 h, 23 h of vacuum at 130°C.

The average degree of polymerization, reported in Table 8.4, was calculated from  $^1\text{H}$  NMR spectra, by comparing the integration of the peak corresponding to the methylene protons of the benzyl group with the methylene protons of the  $\epsilon$ -caprolactone of the pure product. In the same way, conversion percentage was calculated from the ratio between shifted and not-shifted peak corresponding to methylene protons of  $\epsilon$ -caprolactone units of the reaction mixture. For all the three polymers, conversion percentage was found to be 100% (Spectra in Supplementary Data).

In the second step, the modification of the hydroxyl end group of the polycaprolactone product into a good leaving group was achieved using *p*-nitrophenyl chloroformate (pNC). Reaction must be carried out in absence of water in order to not destroy the reagent and lose the leaving group, namely *p*-nitrophenol (Figure 8.6).

From  $^1\text{H}$  NMR spectra it is possible to notice the appearance of new peaks at 7.4 and 8.3 ppm corresponding to the aromatic protons of the nitrophenyl group; moreover, the signal corresponding to the protons of the methylene group connected to the carbonate group shifted from 3.6 to 4.3 ppm. The integration of this signal obtained from the  $^1\text{H}$  NMR spectrum of the reaction mixture was also used for the calculation of the conversion percentage, comparing it with the integrated peak corresponding to the methylene protons of the benzyl group. For all the three polymers, conversion percentage was found to be 100% (Table 8.4, Spectra in Supplementary Data).

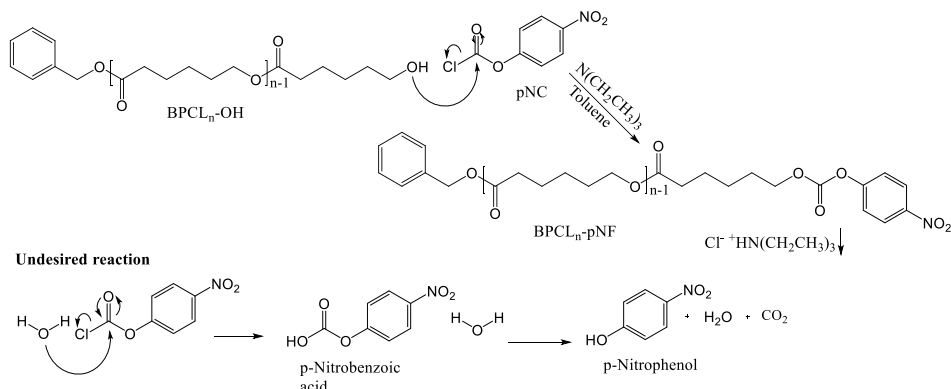


**Figure 8.6** Mechanism of reaction of BPCL<sub>n</sub>-OH with pNC.

In the third step, a certain amount of BPCL<sub>n</sub>-pNF was reacted with mPEG-NH<sub>2</sub> and another amount was reacted with malPEG-NH<sub>2</sub> (Figure 8.7). The maleimide group present at the end of the hydrophilic chain was later used for further functionalization of the assembled polymeric micelles (see below). Also in this case, reaction must be conducted in absence of water to prevent early loss of the leaving group. After the reaction, a stable carbamate bond was obtained as covalent bridge between the hydrophobic block and the hydrophilic block.

From the recorded <sup>1</sup>H NMR spectra (see Supplementary Data) of the final products, the integration of the residual peak at 4.3 ppm of the CH<sub>2</sub> connected to the p-nitrophenyl formate group, which after the reaction shifted to 4.05 ppm, was used for the calculation of the conversion percentage. As second evidence of the successful coupling of PEG to BPCL chain, the appearance of a new peak at 3.6 ppm is due to the methylene protons of PEG chain. Moreover, in BPCL<sub>n</sub>-malPEG spectra a peak ascribed to maleimide protons can be observed at 6.70 ppm. Conversion percentages of BPCL<sub>n</sub>-mPEG were 75%, 73% and 47% for n=9, n=15 and n=23, respectively, whereas conversion percentages of BPCL<sub>n</sub>-malPEG were 46%, 41% and 58% for n=9, n=15 and n=23, respectively.

A good correlation has been found between molecular weights calculated from <sup>1</sup>H NMR spectra and molecular weights obtained by GPC (Table 8.4 and Table 8.5). Moreover, the polydispersity indexes calculated from GPC data were all around 1 and never higher than 1.18, except for BPCL<sub>23</sub>-malPEG that was 1.40, which was still acceptable for micelles assembly purpose. Taking into account the experimental error, it is possible to state that the molecular weight of the three polymers with three different degrees of polymerization (n=9, n=15 and n=23)

increases by almost 800 Da as the DP increases by  $\sim 7$  units ( $\epsilon$ -CL unit m.w.  $114.14 \text{ g/mol} \times 7 \text{ units} = 798.98 \text{ Da}$ ).

Furthermore, the presence of maleimide group on BPCL<sub>n</sub>-malPEG was confirmed by UV/Vis spectra of the polymers that shows a peak at 293 nm, corresponding to the absorption of the maleimide group, which is also present in the spectrum of malPEG-NH<sub>2</sub> but absent in the spectra of mPEG-NH<sub>2</sub> and BPCL<sub>n</sub>-mPEG (Figure 8.30S in Supplementary Data).

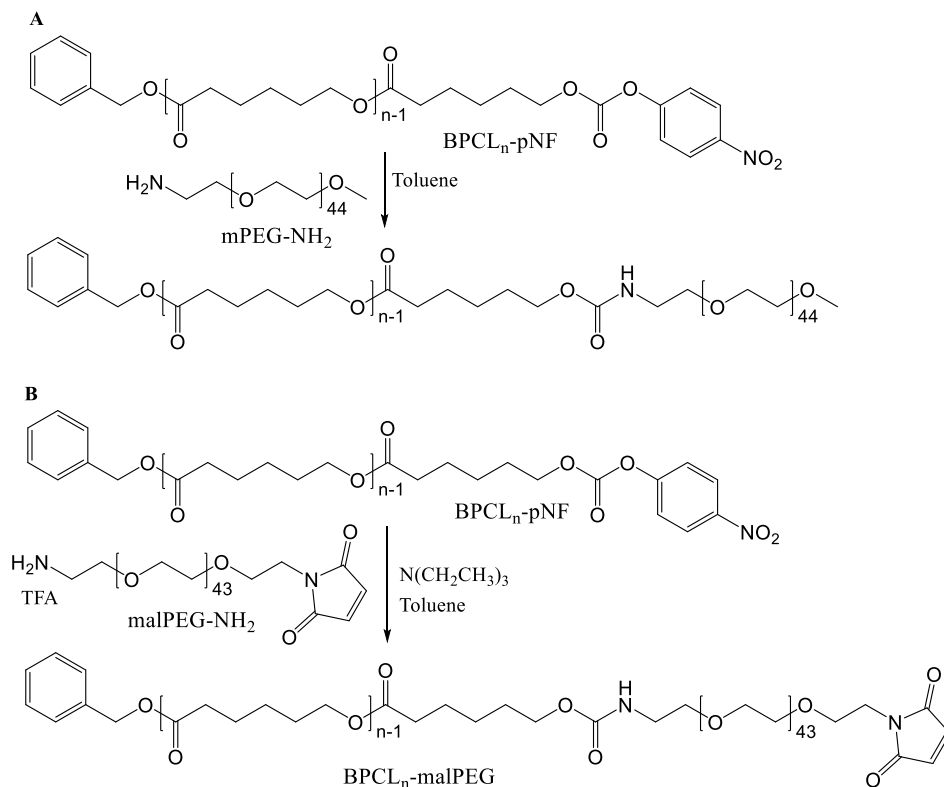


**Figure 8.7** Mechanism of reaction of BPCL<sub>n</sub>-pNF with mPEG-NH<sub>2</sub> or with malPEG-NH<sub>2</sub>.

TGA data shows that the degradation point of all the polymers is never lower than  $180^\circ\text{C}$  and never higher than  $240^\circ\text{C}$ . Moreover, it is possible to notice that with the increase of the molecular weight also the degradation point is increased (Table 8.5; Graphs in Supplementary Data).



On the other hand, from DSC analysis the melting point ( $T_m$ ) was obtained. This value represents an important parameter because it is fundamental to melt the polymer during self-assembling step of the polymeric micelles. In particular, it is important to underline that the melting points of BPCL<sub>n</sub>-mPEG and BPCL<sub>n</sub>-malPEG were found to range between 40°C and 50°C. Finally, glass transition temperature  $T_g$  was obtained from DSC, although is evident from all the graphs that the amorphous component of the material is higher than the crystalline component (Graphs in Supplementary Data).

**Table 8.4** Reaction yields and polymers data obtained by <sup>1</sup>H NMR spectra.

Polymer	Yield (%)	<sup>1</sup> H-NMR		
		Conversion (%)	Degree of Polymerization	Molecular Weight (kDa)
BPCL <sub>9</sub> -OH	58	100	9	1.1
BPCL <sub>9</sub> -pNF	58	99	9	1.3
BPCL <sub>9</sub> -mPEG	82	75	9+44	3.1
BPCL <sub>9</sub> -malPEG	78	46	9+50	3.5
BPCL <sub>15</sub> -OH	81	100	15	1.8
BPCL <sub>15</sub> -pNF	73	100	15	2.0
BPCL <sub>15</sub> -mPEG	56	73	15+44	3.8
BPCL <sub>15</sub> -malPEG	24	41	15+50	4.1
BPCL <sub>23</sub> -OH	82	100	23	2.7
BPCL <sub>23</sub> -pNF	76	100	23	2.9
BPCL <sub>23</sub> -mPEG	57	47	23+44	4.7
BPCL <sub>23</sub> -malPEG	74	58	23+50	5.1
mPEG-NH <sub>2</sub>	n.a.	n.a.	44	2.0
malPEG-NH <sub>2</sub>	n.a.	n.a.	50	2.6

**Table 8.5** Polymers GPC data and thermal analysis data.

Polymer	GPC			TGA	DSC	
	Mw (kDa)	Mn (kDa)	PDI	Degradation point (°C)	T <sub>m</sub> (°C)	T <sub>g</sub> (°C)
<b>BPCL<sub>9</sub>-OH</b>	0.7	0.6	1.1	179	31	-63
<b>BPCL<sub>9</sub>-pNF</b>	0.7	0.6	1.1	189	31	-57
<b>BPCL<sub>9</sub>-mPEG</b>	2.7	2.5	1.1	222	49	-64
<b>BPCL<sub>9</sub>-malPEG</b>	3.0	2.9	1.0	228	38	-60
<b>BPCL<sub>15</sub>-OH</b>	1.4	1.2	1.2	196	46	-64
<b>BPCL<sub>15</sub>-pNF</b>	1.3	1.2	1.2	198	43	-54
<b>BPCL<sub>15</sub>-mPEG</b>	3.3	3.0	1.1	222	49	-46
<b>BPCL<sub>15</sub>-malPEG</b>	5.4	4.6	1.2	232	38	-61
<b>BPCL<sub>23</sub>-OH</b>	2.1	1.8	1.1	214	48	-64
<b>BPCL<sub>23</sub>-pNF</b>	2.0	1.9	1.1	212	47	-55
<b>BPCL<sub>23</sub>-mPEG</b>	3.7	3.2	1.2	240	47	-52
<b>BPCL<sub>23</sub>-malPEG</b>	5.8	4.1	1.4	236	48	-53
<b>mPEG-NH<sub>2</sub></b>	1.7	1.6	1.0	195	51	-58
<b>malPEG-NH<sub>2</sub></b>	2.0	2.0	1.0	226	39	-35

### Polymeric micelles preparation and characterization

Polymeric micelles are nanosized particles characterized by a hydrophobic core/hydrophilic shell structure. They can be self-assembled in aqueous solution, starting from amphiphilic block copolymers, when polymer concentration is above the critical micelle concentration (CMC). At polymer concentrations above the CMC, a dynamic equilibrium between the amphiphilic unimers and the micellar form is established. The hydrophobic particle core may act as a reservoir for hydrophobic drugs, whereas the hydrophilic shell contributes to aqueous solubility and colloidal stability. The outer surface plays also an important role in preventing opsonisation and protein adsorption and it can be conjugated with fluorescent dyes, radioligands, antibodies or other targeting ligands. Micelles *in vivo* distribution is mainly dictated by size and surface properties and not by hydrophobic core characteristics. A major issue of polymeric micelles application *in vivo* is recognition by reticuloendothelial systems (RES) that removes and destroys particles in the blood (Torchilin, 2007).

In the present work, three different polymeric micelles (BPCL<sub>9</sub>-mPEG/BPCL<sub>9</sub>-malPEG; BPCL<sub>15</sub>-mPEG/BPCL<sub>15</sub>-malPEG and BPCL<sub>23</sub>-mPEG/BPCL<sub>23</sub>-malPEG) were prepared according to the thin layer hydration method. For the shell poly(ethylene glycol) (PEG) was chosen as hydrophilic block because it is non-toxic, soluble in water media and increases blood circulation time avoiding opsonization and RES recognition (Owens Iii & Peppas, 2006). For the core, hydrophobic poly( $\epsilon$ -caprolactone) was chosen as biodegradable polymer. The benzyl group attached at the end of the hydrophobic block aims at the reduction of the CMC, improving the hydrophobic interactions within the core of the micelle and increasing the stability of the nanoparticles, as reported in literature (Carstens, Bevernage et al., 2007). CMC was calculated using the pendant drop method and the Wilhelmy plate method (data not shown). In the first experiment, no significant difference is existing between polymers (CMC in the range 0.04-0.05 mg/mL) (Wennink et al., 2017), whereas, using the second method, calculated CMC was approximately 0.01 mg/mL for BPCL<sub>23</sub>-mPEG and 0.05 mg/mL for BPCL<sub>15</sub>-mPEG, BPCL<sub>9</sub>-mPEG's CMC was expected to be slightly higher.

Z-average hydrodynamic diameter of the particles (Z-ave), size distribution (PDI) and surface Z-potential were measured by DLS and ELS in PBS at 25°C. DLC and DLE were calculated from UV/Vis spectra of diluted micelles in DMF. Data shown in Table 8.6 demonstrate the nanometric size of the particles in the range of 17-43 nm, with a low polydispersity. Moreover, mTHPC was efficiently encapsulated (up to DLC ~7%) inside particles core, in agreement with the well-known capability of polymeric micelles to load high amount of drug.

**Table 8.6** Polymeric micelles Z-ave, PDI, Z-potential, DLC and DLE data.

Polymer	Z-ave (nm)	PDI	Z-potential (mV)	DLE (%)	DLC (%)
<b>BPCL9-mPEG/ BPCL9-malPEG</b>	17	0.081	-2	64	3
<b>BPCL15-mPEG/ BPCL15-malPEG</b>	25	0.175	-2	53	3
<b>BPCL23-mPEG/ BPCL23-malPEG</b>	42	0.154	-2	76	7

## EGa1 production and modification

EGa1 is an anti-EGFR nanobody derived from llama's heavy chain antibodies, characterized by a molecular weight of 17097.87 Da and a pI ~6.6. Its sequence consists of only 153 amino acids and only one intramolecular disulphide bond is present between two cysteines, in form of cystine. For EGa1 production, an engineered *E. coli* bacteria containing pET28-EGa1-myc-his plasmid was employed. EGa1 was successfully produced and purified (see Figure 8.8) yielding up to ~77 mg of pure nanobody after the second purification step. From the Nanodrop absorption spectrum of EGa1 the 260/280 nm intensity ratio was 0.45. For proteins, a value of 260/280 ratio lower than 0.7 indicates a good quality and purity of the sample.

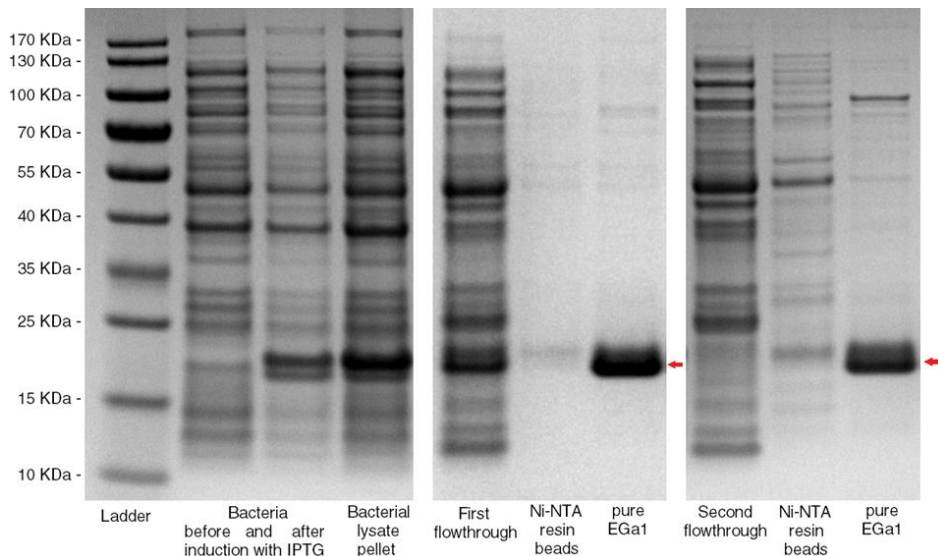


**Figure 8.8** SDS-PAGE of pure EGa1 and samples collected during EGa1 production and purification.

After production and purification, EGa1 nanobody was modified using *N*-succinimidyl *S*-acetylthioacetate (SATA) reagent in order to insert protected thiol groups on the protein for later conjugation with maleimide groups present on polymeric micelles surface. Reaction occurs between SATA and amino groups of the protein (five lysine groups and one N-terminus) (Figure 8.9). Three different EGa1/SATA ratios were prepared (1:2, 1:5 and 1:10). Reaction yield was high and the protein quality was preserved (Table 8.7).

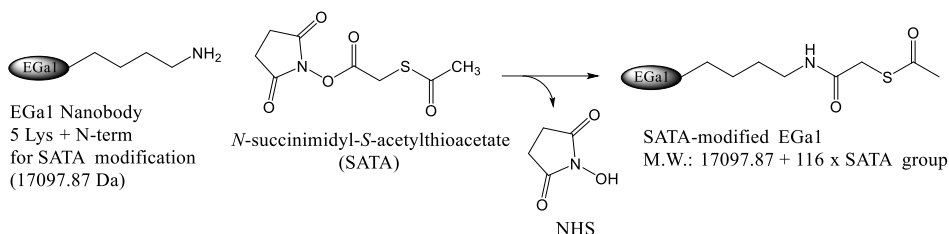


**Figure 8.9** Mechanism of reaction between EGA1 nanobody and SATA reagent.

**Table 8.7** Data collected after EGA1 nanobody modification and purification.

Nanobody	260/280 ratio	Yield (%)
<b>EGa1-SATA 1:2</b>	0.46	91
<b>EGa1-SATA 1:5</b>	0.48	89
<b>EGa1-SATA 1:10</b>	0.51	99

In order to quantify the average number of thio groups inserted on EGA1 nanobody two analyses were carried out: Ellman's assay and LC-ESI-TOF-MS analysis. Through Ellmann's assay it is possible to quantify the average number of sulfhydryl groups in the deprotected SATA-modified nanobody. As controls native EGA1 and reduced native EGA1 were employed. In Table 8.8, reporting the results from both quantification methods, for increasing EGA1/SATA ratio used, increasing numbers of sulfhydryl groups (protected or deprotected, according to the used method) can be observed, up to 2.2 per protein molecule.

Through LC-ESI-TOF-MS deconvoluted spectra it is possible to observe the change in molecular weight of the modified protein (Table 8.8). Each newly introduced SATA group can indeed increase the molecular weight by 116 Da. Data reported in Table 8.8 shows that certain amounts of unmodified EGA1 are still present in the samples, in particular in EGA1-SATA 1:2 the amount of unmodified protein is higher than 80%. On the other hand, in EGA1-SATA 1:10 almost 25% of the protein has 2 or 3 SATA groups that might cause inter-micellar cross-linking during conjugation.

**PART II**

**Table 8.8** Quantification of SATA modification inserted on EGa1 nanobody.

Nanobody	Ellman's assay	LC-ESI-TOF-MS analysis		
	Average no of sulfhydryls	Average no of modifications	No of modifications	Modifications (%)
<b>Native EGa1</b>	0.2	0	0	100
<b>Reduced EGa1</b>	1.8	n.a.	n.a.	n.a.
<b>EGa1-SATA 1:2</b>	1.3	0.2	0	83
			1	14
			2	3
<b>EGa1-SATA 1:5</b>	1.8	0.4	0	64
			1	28
			2	8
<b>EGa1-SATA 1:10</b>	2.2	1.0	0	34
			1	41
			2	19
			3	6

In order to verify the reactivity of the SATA-modified nanobody, a dye bearing a maleimide group, namely IRDye 800CW maleimide, was conjugated to deprotected EGa1-SATAs (Figure 8.10).

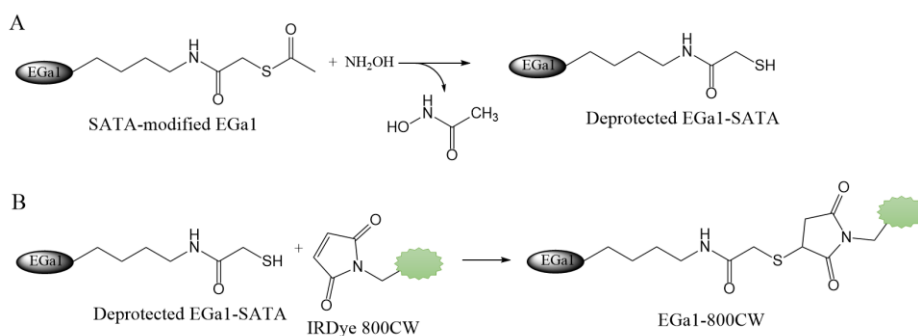


**Figure 8.10** (A) Mechanism of deprotection of SATA-modified EGa1; (B) Mechanism of reaction between deprotected EGa1-SATA and IRDye 800CW, i.e. mechanism of reaction between thio and maleimide groups.

After conjugation, a SDS-PAGE was performed and the protein was detected without staining but only *via* fluorescence emission of the conjugated dye at 800 nm. In this manner only the protein attached to the dye was observed. From the run of the gel, it is indeed possible to separate free unconjugated dye from EGa1-800CW (Figure 8.11). The low EGa1-SATA 1:2 reactivity can be explained by the few number of SATA modification present on the nanobody (Table 8.9). On the other hand, EGa1-SATA 1:5 and EGa1 1:10 showed a good reactivity towards maleimide groups, with a conjugation efficiency higher than 20%. Moreover, not a significant difference in dye/protein ratio can be obtained using EGa1-SATA 1:5 or EGa1-SATA 1:10.

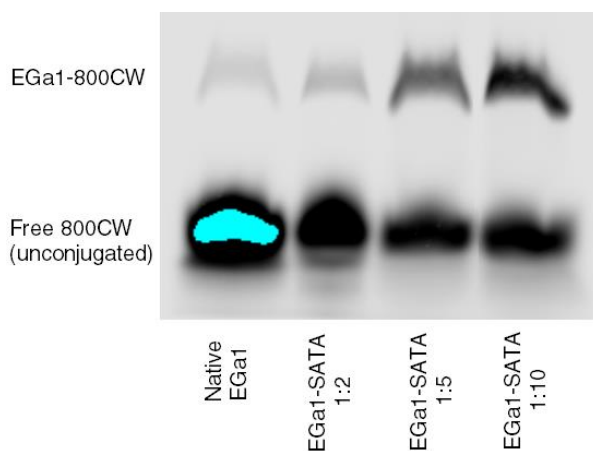


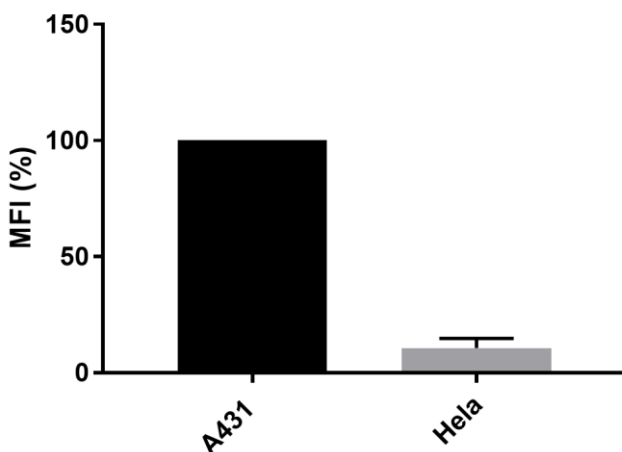
Figure 8.11 SDS-PAGE of EGa1-800CW samples.

Table 8.9 EGa1-800CW conjugation data.

Nanobody	Nanodrop	SDS-PAGE	
	Dye/Protein Ratio	Dye/Protein Ratio	Conjugation efficiency (%)
EGa1-SATA 1:2	0.09	0.05	1
EGa1-SATA 1:5	0.45	0.91	22
EGa1-SATA 1:10	0.59	1.24	31

## EGFR expression and binding affinity of EGa1-SATA to EGFR on cells

As mentioned before, EGa1 is an anti-EGFR nanobody, which can be used as targeting agent for EGFR over-expressing cells. Two different cell lines were selected for *in vitro* experiments: A431 vulvar squamous cancer cells and HeLa cervical cancer cells, EGFR over-expressing and low EGFR expressing cells, respectively. As shown in Figure 8.12, A431 express 90% more EGFR compared to HeLa cells and, for this reason A431 cells were chose for *in vitro* experiments, whilst HeLa were used as control cell line.



**Figure 8.12** EGFR expression in A431 cells and HeLa cells.

EGa1-EGFR binding affinity assay was evaluated in A431 cells. Different concentrations of SATA-modified EGa1 nanobodies were incubated with cells at 4°C and binding was detected using a primary antibody and a secondary antibody labelled with a dye. From the graph depicted in Figure 8.13,  $K_d$  and  $B_{max}$  were calculated (Table 8.10): EGa1-SATA 1:2 showed a  $K_d$  relatively equal to the native one, confirming that the nature of the modified nanobody is similar to unmodified EGa1. On the other hand, EGa1-SATA 1:10 has a  $K_d$  10-fold higher than native EGa1 that can be ascribed to the relatively high number of modifications that reduce nanobody affinity for its target. Despite the number of modifications present in EGa1-SATA 1:5, this modified nanobody showed a still acceptable  $K_d$ , only 3.3-fold higher than the native one and for this reason, it has been chosen as candidate for micelles conjugation.



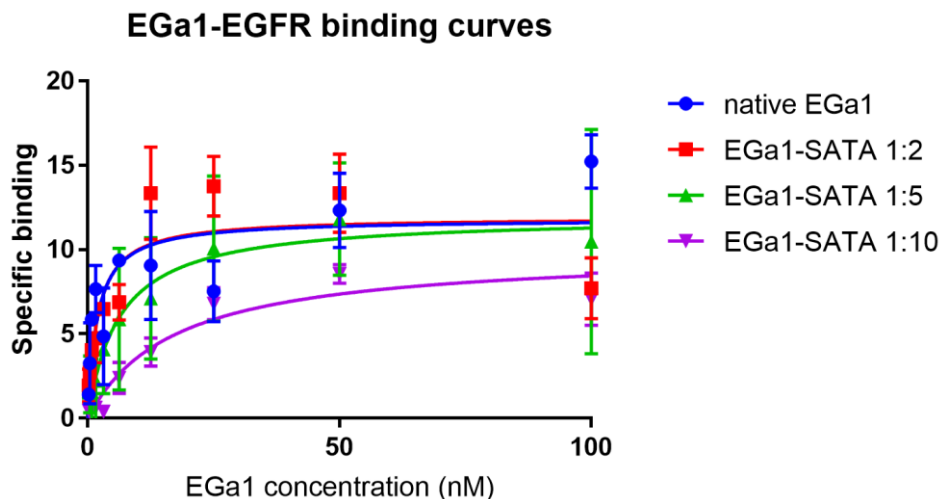


**Figure 8.13** EGFR binding curve of SATA-modified EGa1 nanobodies.

**Table 8.10** EGa1-SATA binding data (One site – Specific binding).

Specific binding	Native EGa1	EGa1 SATA 1:2	EGa1 SATA 1:5	EGa1 SATA 1:10
$B_{\max}$	$11.8 \pm 1.1$	$11.9 \pm 0.9$	$12.0 \pm 1.6$	$9.9 \pm 1.0$
$K_d$ (nM)	$1.9 \pm 0.8$	$1.9 \pm 0.6$	$6.3 \pm 3.0$	$17.2 \pm 4.5$

### Conjugation of EGa1-SATA 1:5 to mTHPC-loaded polymeric micelles

BPCL<sub>9</sub>-mPEG/BPCL<sub>9</sub>-malPEG, BPCL<sub>15</sub>-mPEG/BPCL<sub>15</sub>-malPEG and BPCL<sub>23</sub>-mPEG/BPCL<sub>23</sub>-malPEG micelles were prepared using BPCL<sub>n</sub>-mPEG/BPCL<sub>n</sub>-malPEG molar ratio of 9:1. Subsequently, micelles were conjugated with deprotected EGa1-SATA 1:5 using maleimide/nanobody molar ratio 100:4.5. Unreacted maleimide groups were saturated with Cys solution. After washing, conjugation was confirmed by SDS-PAGE (Figure 8.14). For all the three conjugated micelles it is possible to observe a band at higher molecular weight than EGa1 band as a result of the connection with a polymer chain. Bands from BPCL<sub>23</sub>-mPEG/BPCL<sub>23</sub>-malPEG-EGa1 and BPCL<sub>15</sub>-mPEG/BPCL<sub>15</sub>-malPEG-EGa1 are slightly over BPCL<sub>9</sub>-mPEG/BPCL<sub>9</sub>-malPEG-EGa1 due to the higher molecular weight of the polymers that differ of ~2 kDa (see GPC data). No unconjugated EGa1 was present in the samples, confirming its removal through Vivaspin washes.

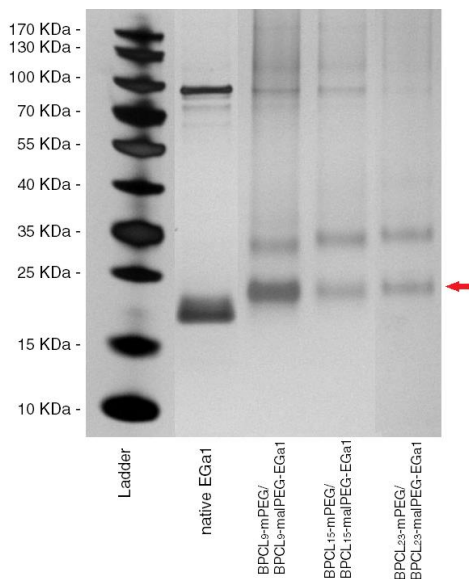


**Figure 8.14** SDS-PAGE of diluted EGa1-conjugated micelles.

### EGa1-micelles binding and uptake studies

The ability of EGa1-conjugated micelles to target EGFR over-expressing cells, A431, was demonstrated with cell uptake and binding studies. For this purpose, mTHPC-loaded EGa1-conjugated micelles, as well as mTHPC-loaded control micelles were prepared. All the prepared micelles showed the uptake of the fluorescent mTHPC by A431 cells (Figure 8.16, left panels). In particular, mTHPC was clearly taken up by the cells using BPCL<sub>9</sub>-mPEG/BPCL<sub>9</sub>-malPEG micelles (See Supplementary Data, Figure 8.59S). However, there are no statistically significant differences in uptake between control micelles and EGa1-conjugated micelles in both targeted and competition tests, suggesting that there is another non EGFR-mediated pathway for the uptake of this kind of particles, like passive diffusion or other endocytic processes, or most likely the uptake of the released mTHPC occurs. On the other hand, selective binding of targeted micelles to the cell surface is slightly visible in *in vitro* association test at 4°C, in which transports across cell membrane are inhibited (Figure 8.15, panel A), but at 37°C most likely the EGFR-mediated uptake is relatively less dominant than others non-identified mechanisms.

For BPCL<sub>15</sub>-mPEG/BPCL<sub>15</sub>-malPEG and BPCL<sub>23</sub>-mPEG/BPCL<sub>23</sub>-malPEG micelles there is a statistically significant difference between EGa1-targeted and

control micelles, especially after 5 and 7 h of incubation with the formulations (Figure 8.16, left panels, red versus blue curves). Moreover, uptake can be blocked and reduced to not significant levels by the addition of free unconjugated and unmodified EGa1, confirming that in these cases uptake mechanism of mTHPC is EGFR mediated of the loaded and EGa1-targeted micelles (Figure 8.16, green curves). Indeed, binding studies at 4°C showed a clear association of targeted micelles to the cell membrane surface for BPCL<sub>15</sub>-mPEG/BPCL<sub>15</sub>-malPEG-EGa1 and BPCL<sub>23</sub>-mPEG/BPCL<sub>23</sub>-malPEG-EGa1 micelles (Figure 8.15, panels B and C respectively), while much less for BPCL<sub>9</sub>-mPEG/BPCL<sub>9</sub>-malPEG-EGa1 micelles. Several hypotheses can be drawn to explain this difference: one may be that EGFR-mediated internalization is micelle size-dependant, probably due to the curvature of particle surface that makes less accessible the conjugated nanobody to its target, and probably the smallest micelles can penetrate cell membrane more easily than bigger ones through passive pathways; a more likely reason for mTHPC non selective internalization for BPCL<sub>9</sub>-mPEG/BPCL<sub>9</sub>-malPEG formulation may be that small micelles are less stable leading to premature release of mTHPC (less visible in the binding assay at 4°C), which can easily diffuse within the cells because of its hydrophobicity. In HeLa cells there is no difference in uptake for all the three micelles in both targeted and competition test (Figure 8.16, right panels). Furthermore, micelles binding and association is relatively lower than in A431 (Figure 8.15, panels D-F).

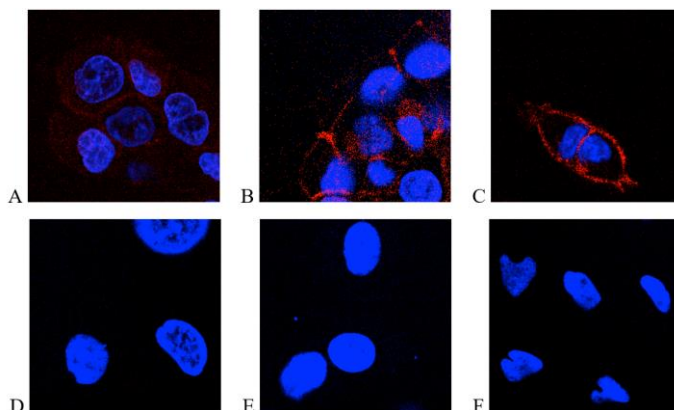


**Figure 8.15** Binding of (A) BPCL<sub>9</sub>-mPEG/BPCL<sub>9</sub>-malPEG-EGa1 micelles; (B) BPCL<sub>15</sub>-mPEG/BPCL<sub>15</sub>-malPEG-EGa1 micelles and (C) BPCL<sub>23</sub>-mPEG/BPCL<sub>23</sub>-malPEG-EGa1 micelles in A431 cells at 4°C. Binding of (D) BPCL<sub>9</sub>-mPEG/BPCL<sub>9</sub>-malPEG-EGa1 micelles; (E) BPCL<sub>15</sub>-mPEG/BPCL<sub>15</sub>-malPEG-EGa1 micelles and (F) BPCL<sub>23</sub>-mPEG/BPCL<sub>23</sub>-malPEG-EGa1 micelles in HeLa cells at 4°C.

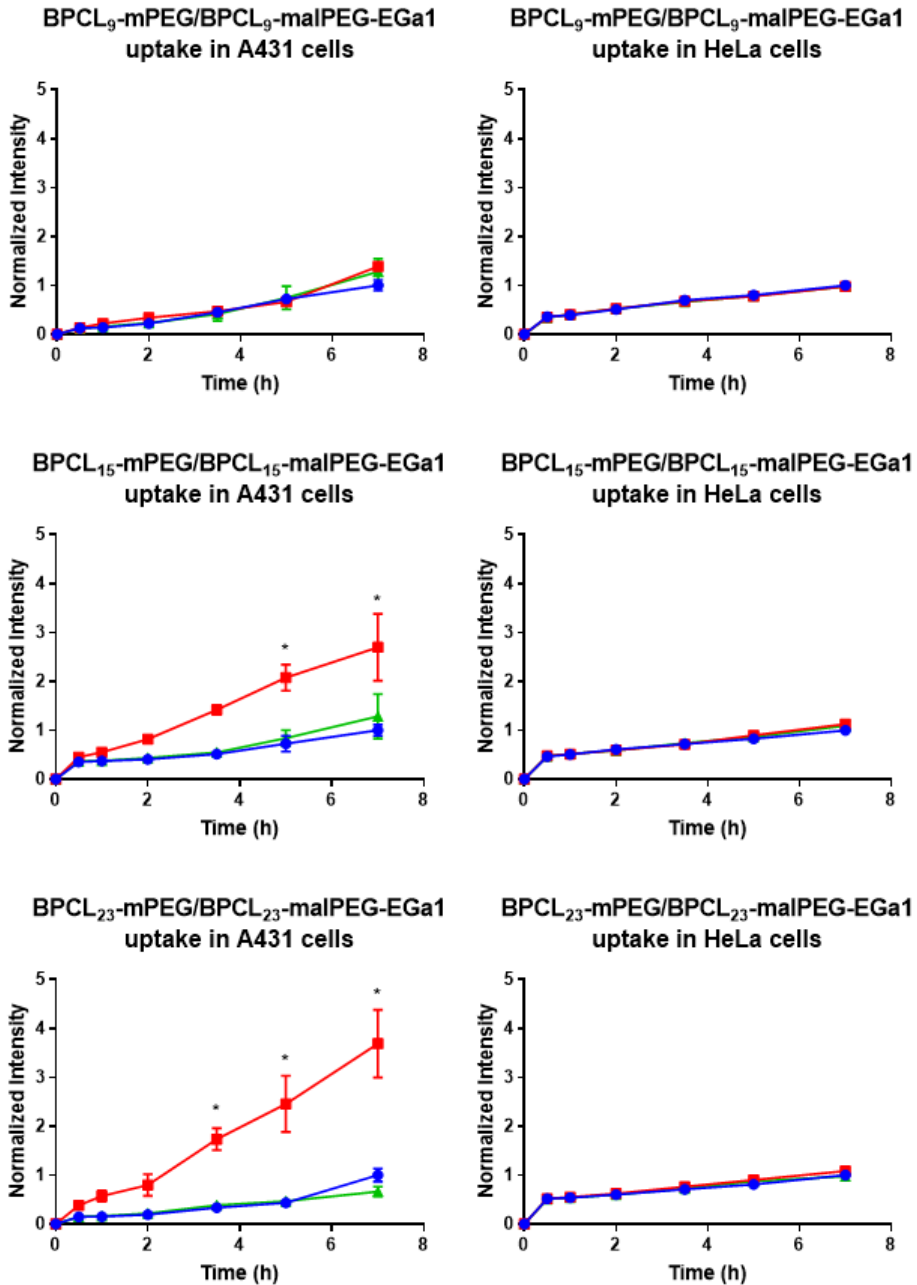


**Figure 8.16** Uptake profiles of mTHPC by BPCL<sub>n</sub>-mPEG/BPCL<sub>n</sub>-malPEG micelles in (*left*) A431 and (*right*) HeLa cells. —●— Control —■— Targeted micelles —▲— Competition Control micelles uptake values after 7 h was used for data normalization. \**p* < 0.0001.

## CONCLUSIONS

Three BPCL<sub>n</sub>-mPEG di-block copolymers with different lengths of the hydrophobic blocks were successfully synthesized *via* ring-opening polymerization procedure. Polymers were characterized and molecular weights ranged between 3000 and 5000 Da. No clear glass transition temperature could be detected suggesting that the amorphous component is higher than the crystalline one. Self-assembled micelles were prepared using the thin film hydration method and particles sizes ranged between 17 and 42 nm with almost neutral surface charge. mTHPC photosensitizer was loaded with high efficiency and capacity inside the micelles without any aggregation of the drug. In order to functionalize the micelles with an active targeting agent, EGa1 anti-EGFR nanobody was chosen as ligand and it was produced with a high yield. EGa1 modification, for subsequent conjugation, was investigated and best conditions were selected. Finally, uptake was evaluated in EGFR over-expressing A431 cell line: from these preliminary data it seems that mTHPC was taken up through EGFR by EGa1-conjugated micelles in a size-dependant manner, although non EGFR-mediated mechanism was more relevant for mTHPC uptake *via* the smallest micelles, while mTHPC uptake *via* larger targeted particles was mediated by EGa1-EGFR interaction. However, further studies need to be carried out in order to better understand the mechanism behind EGa1-conjugated micelles.

## REFERENCES

Argiris A, Karamouzis MV, Raben D, Ferris RL (2008) Head and neck cancer. *The Lancet* 371: 1695-1709.

Bannas P, Hambach J, Koch-Nolte F (2017) Nanobodies and nanobody-based human heavy chain antibodies as antitumor therapeutics. *Frontiers in immunology* 8: 1603.

Biel MA (2016) Photodynamic Therapy of Head and Neck Cancer—What's Old and What's New. In *HANDBOOK OF PHOTODYNAMIC THERAPY: Updates on Recent Applications of Porphyrin-Based Compounds*, pp 439-458. World Scientific.

Carstens MG, Bevernage JJL, van Nostrum CF, van Steenbergen MJ, Flesch FM, Verrijck R, de Leede LGJ, Crommelin DJA, Hennink WE (2007) Small Oligomeric Micelles Based on End Group Modified mPEG–Oligocaprolactone with Monodisperse Hydrophobic Blocks. *Macromolecules* 40: 116-122.

Chen M, Liu X, Fahr A (2011) Skin penetration and deposition of carboxyfluorescein and temoporfin from different lipid vesicular systems: in vitro study with finite and infinite dosage application. *International journal of pharmaceutics* 408: 223-234.

Dolmans DE, Fukumura D, Jain RK (2003) Photodynamic therapy for cancer. *Nature reviews cancer* 3: 380.

Fang J, Nakamura H, Maeda H (2011) The EPR effect: unique features of tumor blood vessels for drug delivery, factors involved, and limitations and augmentation of the effect. *Advanced drug delivery reviews* 63: 136-151.

Grandis JR, Melhem MF, Gooding WE, Day R, Holst VA, Wagener MM, Drenning SD, Tweardy DJ (1998) Levels of TGF- $\alpha$  and EGFR protein in head and neck squamous cell carcinoma and patient survival. *JNCI: Journal of the National Cancer Institute* 90: 824-832.

Hofman, JW, Carstens MG, van Zeeland F, Helwir C, Flesch FM, Hennink WE & Van Nostrum, CF (2008). Photocytotoxicity of mTHPC (temoporfin) loaded polymeric micelles mediated by lipase catalyzed degradation. *Pharmaceutical research* 25(9), 2065-2073.

Labet M, Thielemans W (2009) Synthesis of polycaprolactone: a review. *Chemical Society Reviews* 38: 3484-3504.

Mehraban N, Freeman H (2015) Developments in PDT sensitizers for increased selectivity and singlet oxygen production. *Materials* 8: 4421-4456.

Owens Iii DE, Peppas NA (2006) Opsonization, biodistribution, and pharmacokinetics of polymeric nanoparticles. *International journal of pharmaceutics* 307: 93-102.

Reshetov V, Lassalle H-P, François A, Dumas D, Hupont S, Gräfe S, Filipe V, Jiskoot W, Guillemin F, Zorin V (2013) Photodynamic therapy with conventional and PEGylated liposomal formulations of mTHPC (temoporfin): comparison of treatment efficacy and distribution characteristics in vivo. *International journal of nanomedicine* 8: 3817.

Torchilin V (2011) Tumor delivery of macromolecular drugs based on the EPR effect. *Advanced drug delivery reviews* 63: 131-135.

Torchilin VP (2007) Micellar nanocarriers: pharmaceutical perspectives. *Pharmaceutical research* 24: 1.

Vigneswaran N & Williams MD. (2014). Epidemiologic trends in head and neck cancer and aids in diagnosis. *Oral and Maxillofacial Surgery Clinics* 26(2), 123-141.

Wennink JWH, Liu Y, Mäkinen PI, Setaro F, de la Escosura A, Bourajjaj M, Lappalainen JP, Holappa LP, van den Dikkenberg JB, al Fartousi M (2017) Macrophage selective photodynamic therapy by meta-tetra (hydroxyphenyl) chlorin loaded polymeric micelles: A possible treatment for cardiovascular diseases. *European Journal of Pharmaceutical Sciences* 107: 112-125.

## SUPPLEMENTARY DATA

## Polymers characterization

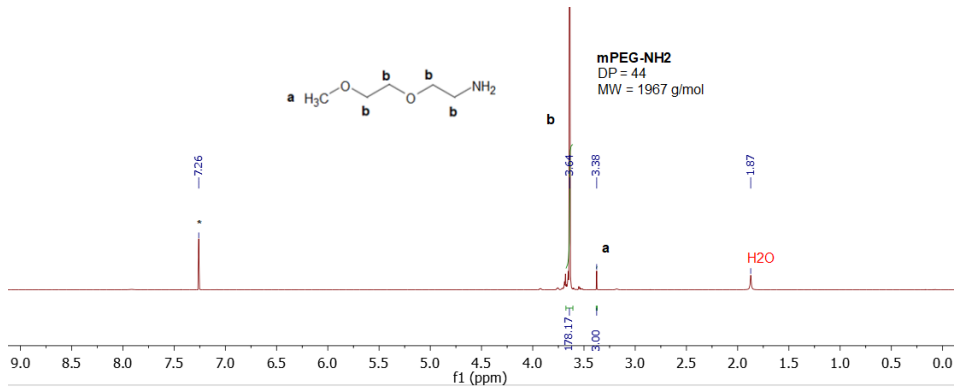


**Figure 8.1S** <sup>1</sup>H NMR spectrum of mPEG-NH<sub>2</sub> in CDCl<sub>3</sub>.

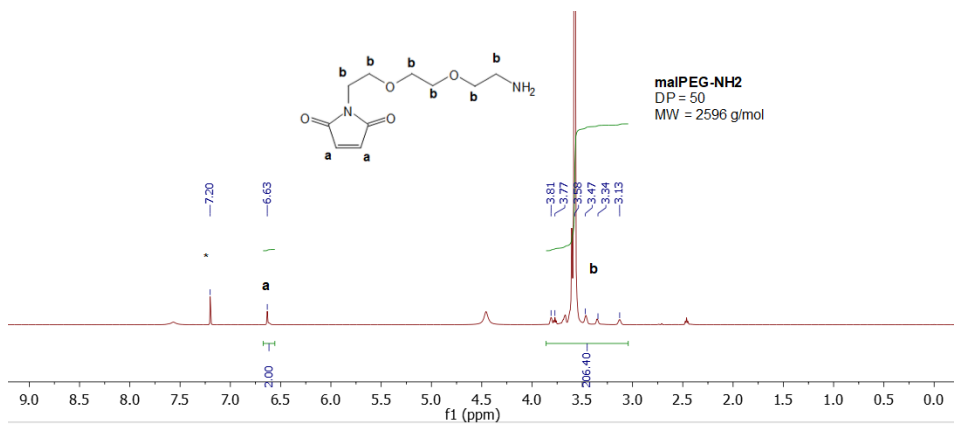


**Figure 8.2S** <sup>1</sup>H NMR spectrum of malPEG-NH<sub>2</sub> in CDCl<sub>3</sub>.



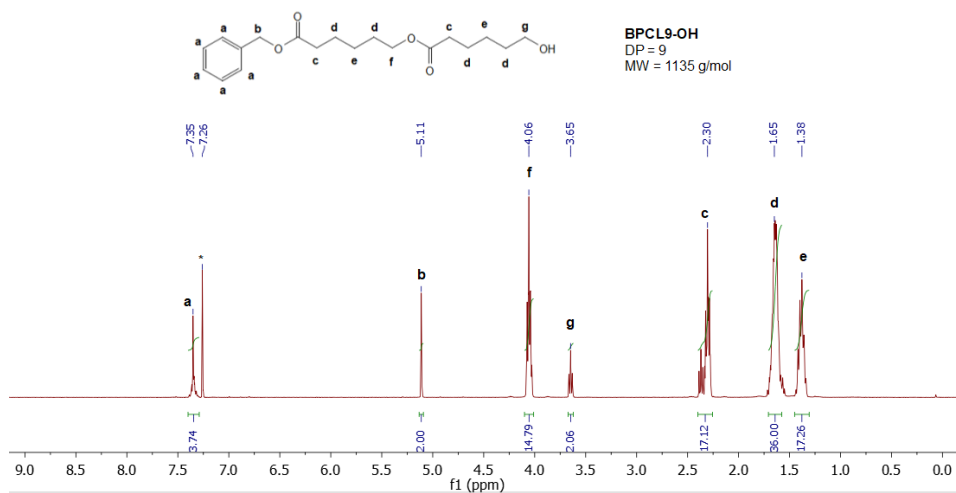


**Figure 8.3S** <sup>1</sup>H NMR spectrum of BPCL<sub>9</sub>-OH in CDCl<sub>3</sub>.

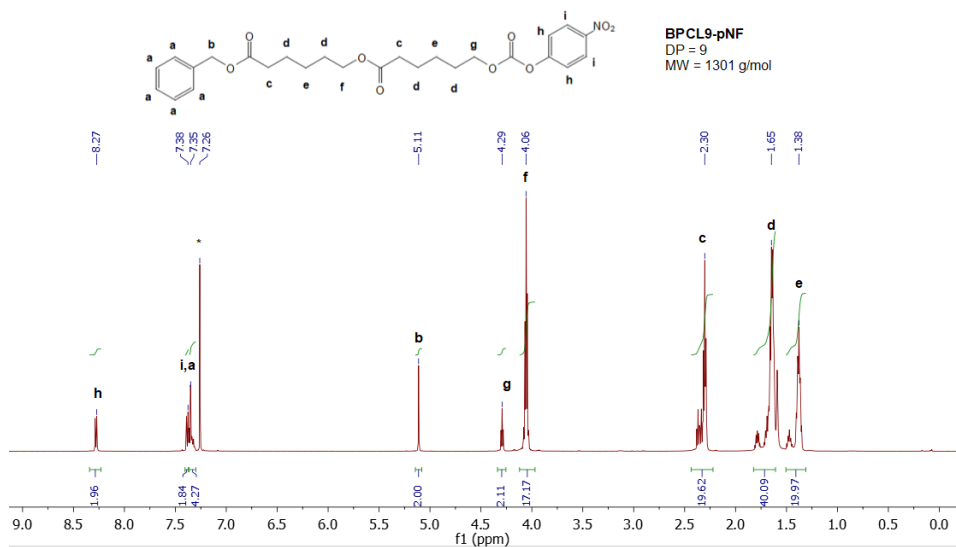


**Figure 8.4S** <sup>1</sup>H NMR spectrum of BPCL<sub>9</sub>-pNF in CDCl<sub>3</sub>.

PART II

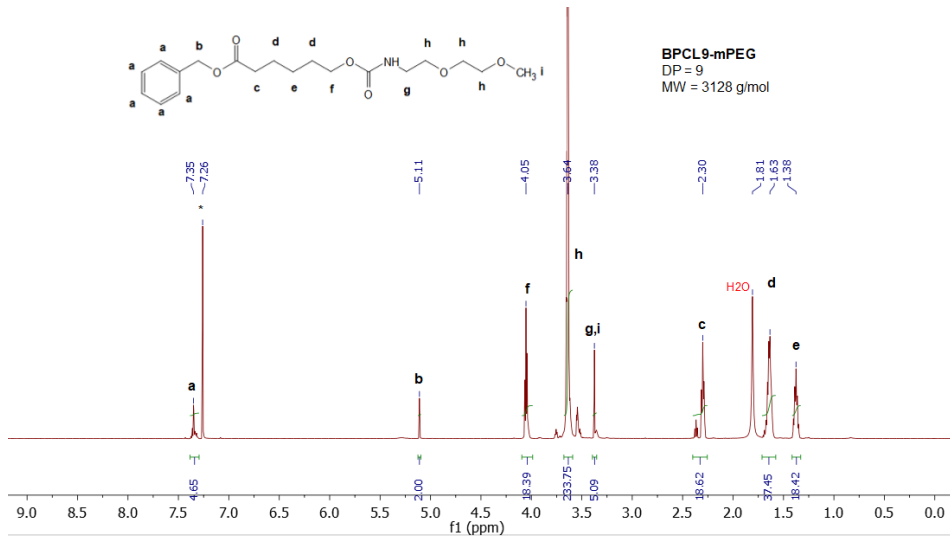


Figure 8.5S <sup>1</sup>H NMR spectrum of BPCL<sub>9</sub>-mPEG in CDCl<sub>3</sub>.

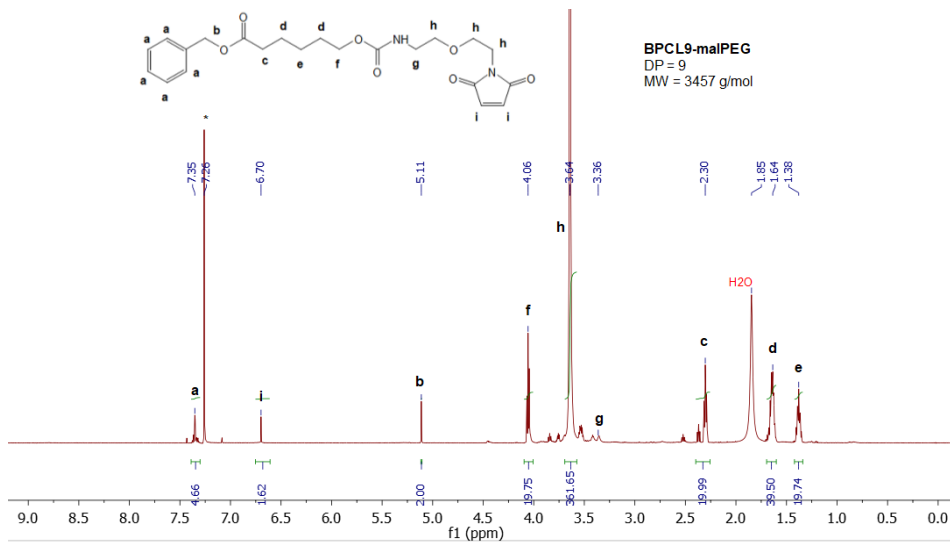


Figure 8.6S <sup>1</sup>H NMR spectrum of BPCL<sub>9</sub>-malPEG in CDCl<sub>3</sub>.

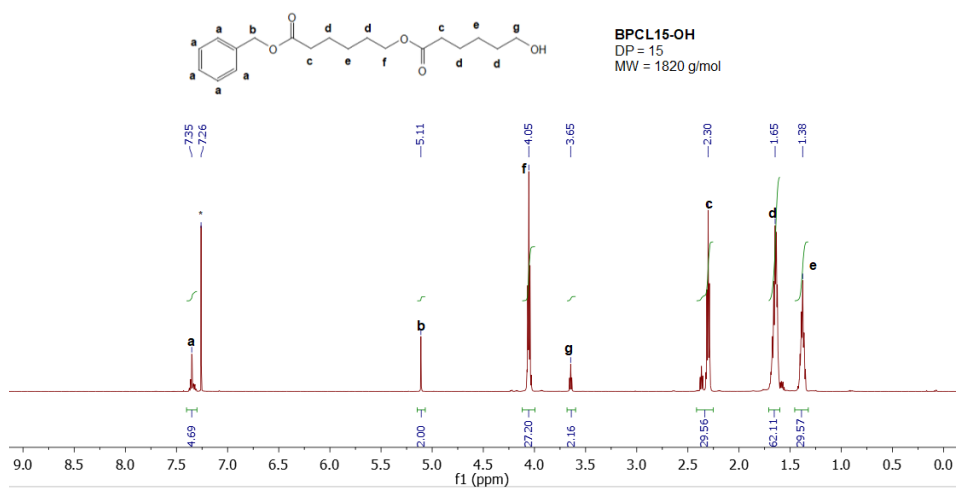


Figure 8.7S <sup>1</sup>H NMR spectrum of BPCL<sub>15</sub>-OH in CDCl<sub>3</sub>.

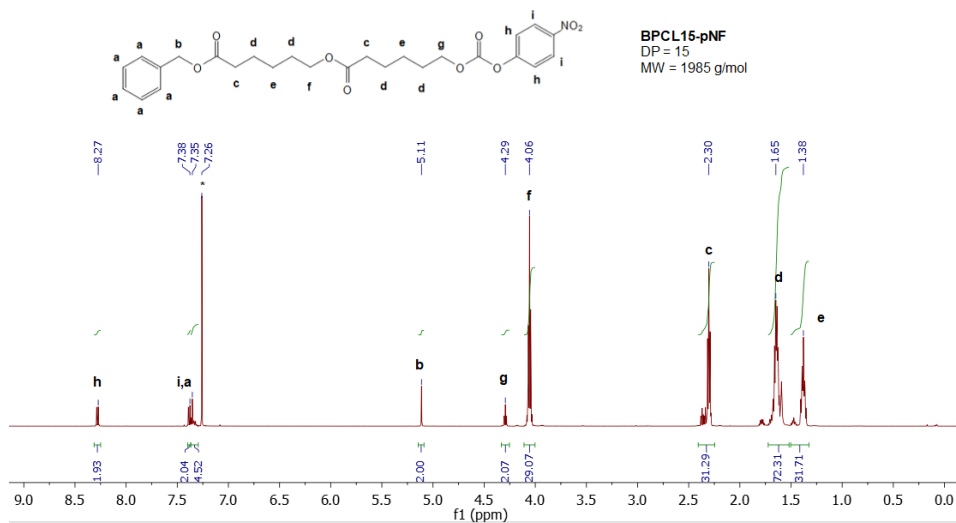


Figure 8.8S <sup>1</sup>H NMR spectrum of BPCL<sub>15</sub>-pNF in CDCl<sub>3</sub>.

PART II

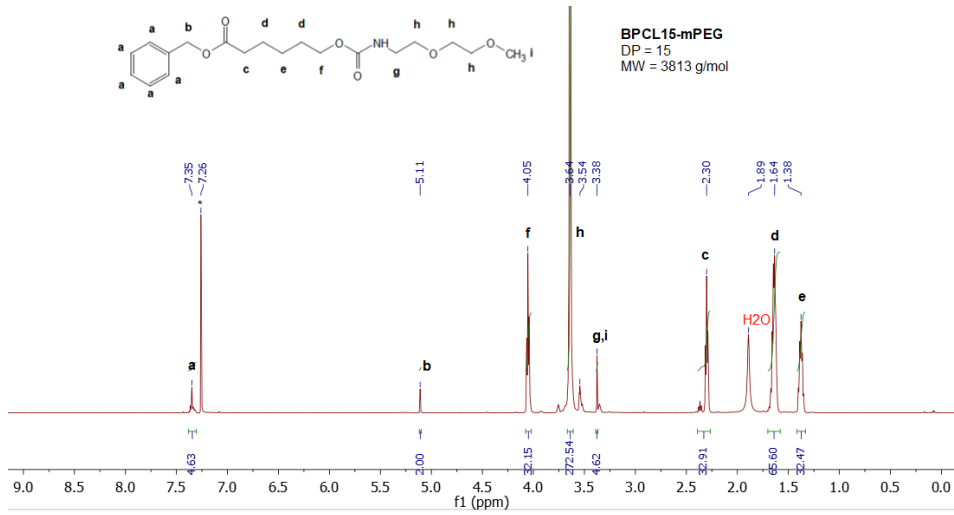


Figure 8.9S <sup>1</sup>H NMR spectrum of BPCL<sub>9</sub>-mPEG in CDCl<sub>3</sub>.

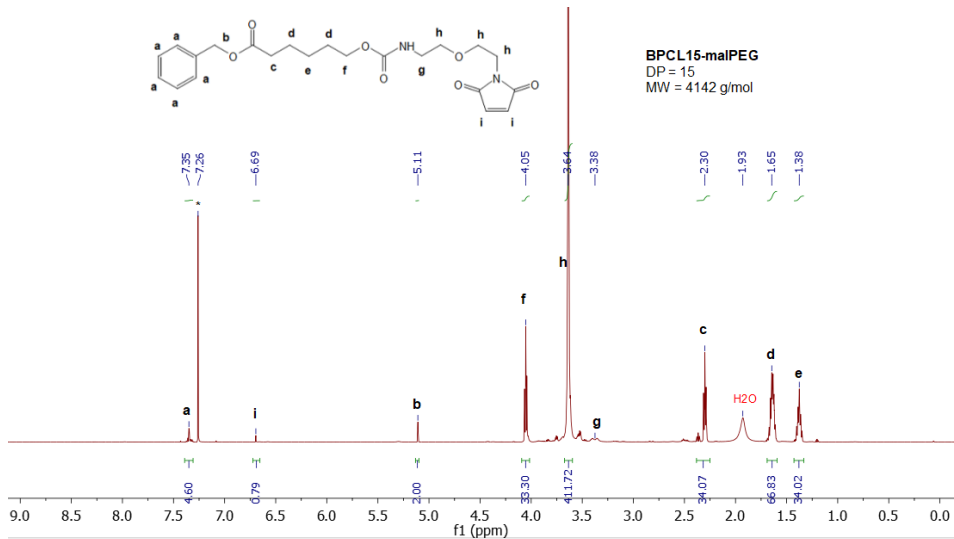


Figure 8.10S <sup>1</sup>H NMR spectrum of BPCL<sub>15</sub>-malPEG in CDCl<sub>3</sub>.

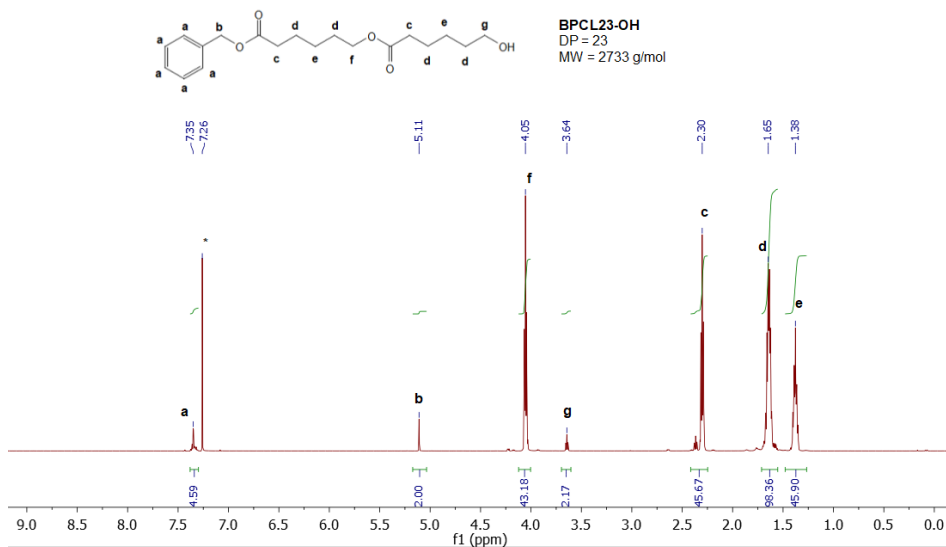


Figure 8.11S  $^1\text{H}$  NMR spectrum of BPCL<sub>23</sub>-OH in CDCl<sub>3</sub>.

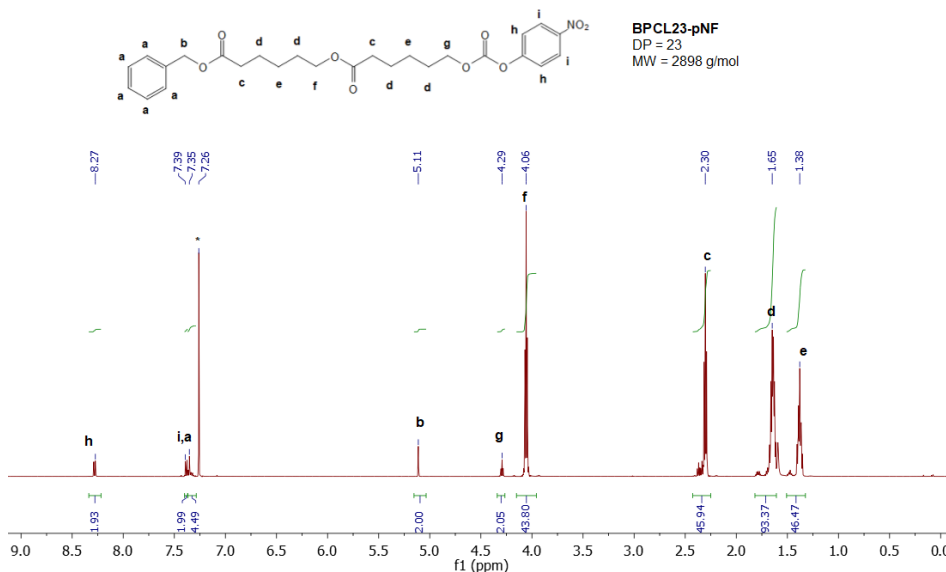


Figure 8.12S  $^1\text{H}$  NMR spectrum of BPCL<sub>23</sub>-pNF in CDCl<sub>3</sub>.

PART II

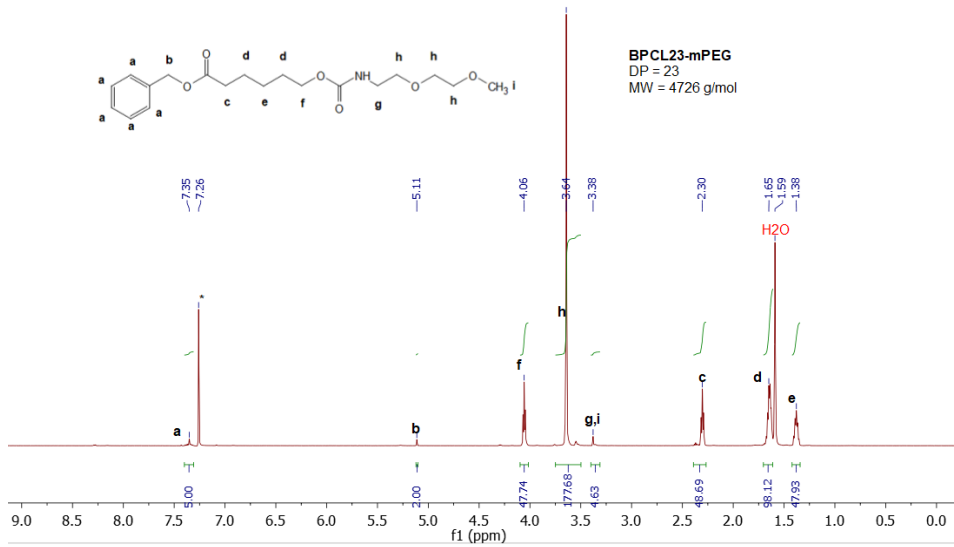


Figure 8.13S <sup>1</sup>H NMR spectrum of BPCL<sub>23</sub>-mPEG in CDCl<sub>3</sub>.

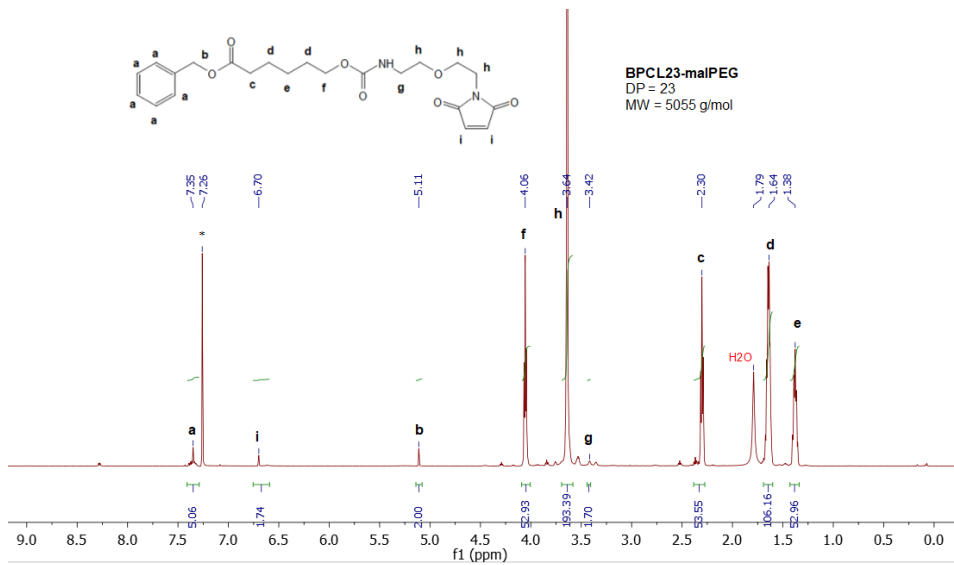
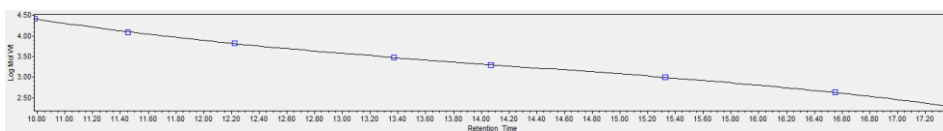
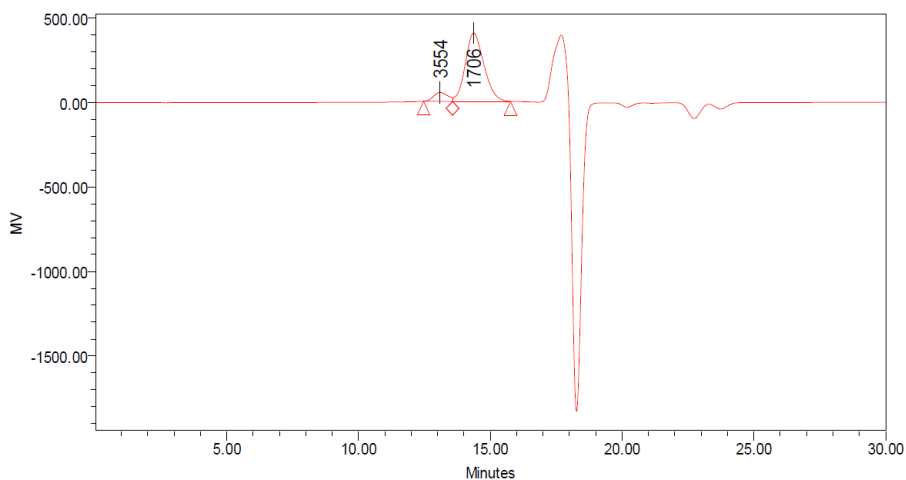


Figure 8.14S <sup>1</sup>H NMR spectrum of BPCL<sub>23</sub>-malPEG in CDCl<sub>3</sub>.



**Figure 8.15S** GPC calibration curve of PEG (Log Mol.Wt. =  $28.3 - 4.78 t + 31.7 t^2 - 0.0074 t^3$   $R^2=0.999845$ ).

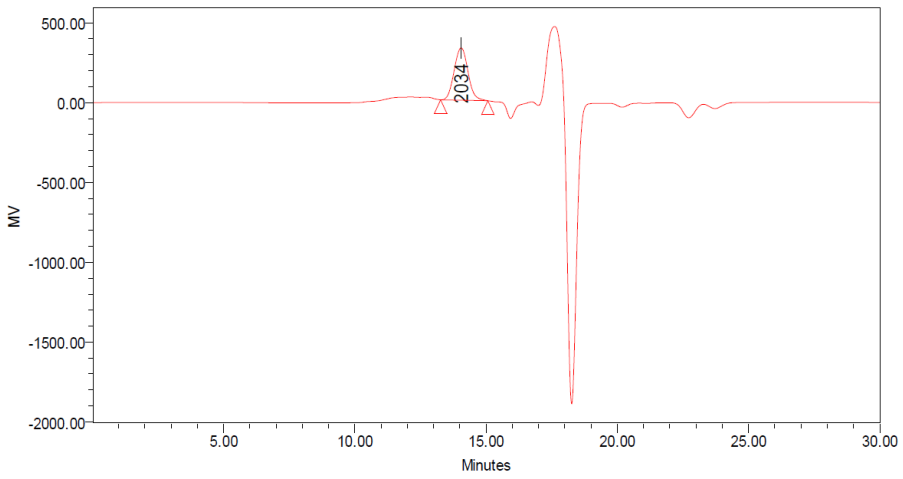


**GPC Results**

	Retention Time (min)	Mw	MP	Mn	Polydispersity	Area ( $\mu V \cdot sec$ )
1	13.091	3517	3554	3448	1.019996	1935328
2	14.366	1673	1706	1614	1.036878	19888507

**Figure 8.16S** GPC chromatogram of mPEG-NH<sub>2</sub>.

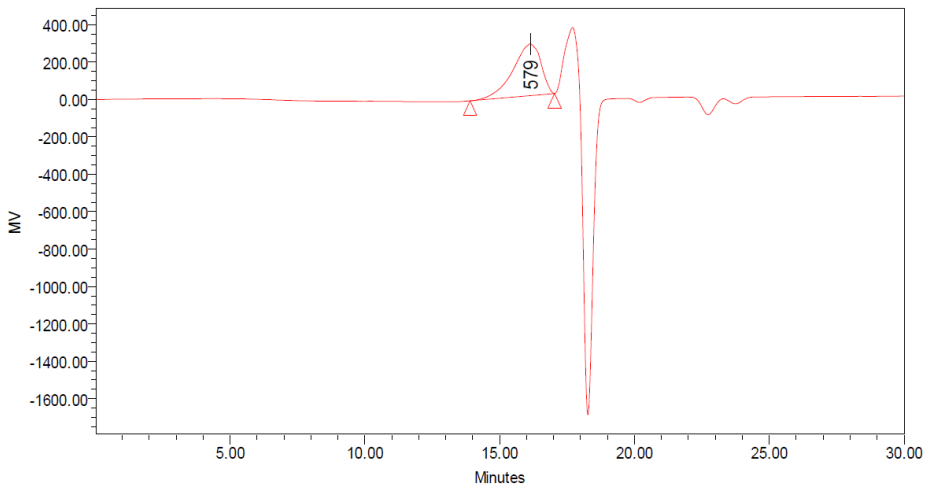
**PART II**



**GPC Results**

	Retention Time (min)	Mw	MP	Mn	Polydispersity	Area (μV*sec)
1	14.048	2040	2034	2002	1.019155	11995420

**Figure 8.17S** GPC chromatogram of mPEG-NH<sub>2</sub>.

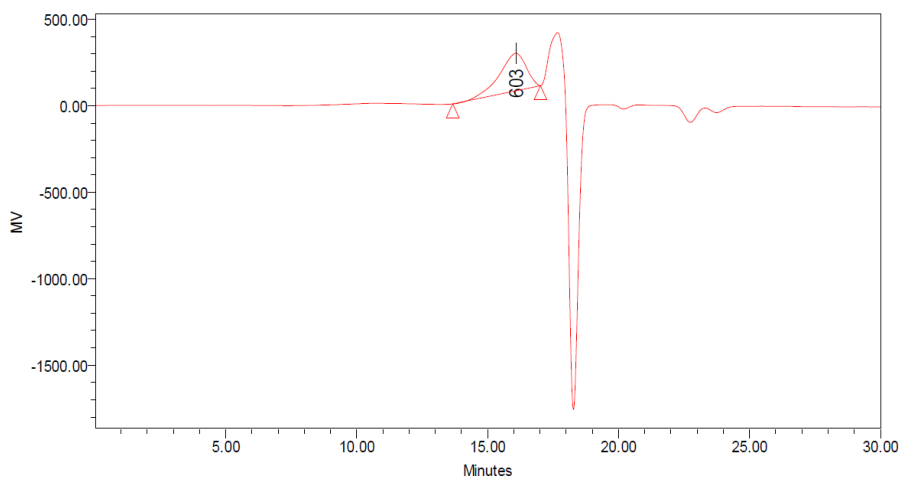


**GPC Results**

	Retention Time (min)	Mw	MP	Mn	Polydispersity	Area (μV*sec)
1	16.135	697	579	622	1.120750	19993606

**Figure 8.18S** GPC chromatogram of BPCL<sub>9</sub>-OH.

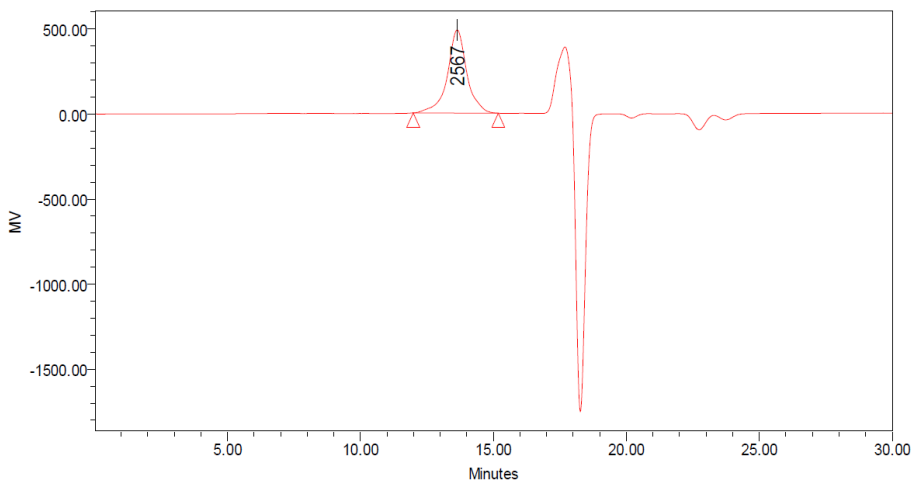




GPC Results

Retention Time (min)	M <sub>w</sub>	MP	M <sub>n</sub>	Poly dispersity	Area (μV <sup>2</sup> sec)
16.077	723	603	645	1.120698	15624919

Figure 8.19S GPC chromatogram of BPCL<sub>9</sub>-pNF.

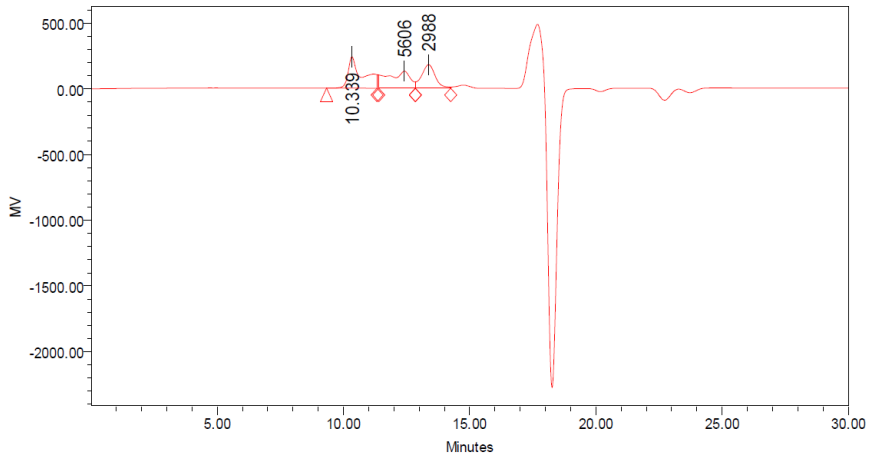


GPC Results

Retention Time (min)	M <sub>w</sub>	MP	M <sub>n</sub>	Poly dispersity	Area (μV <sup>2</sup> sec)
13.635	2675	2567	2518	1.062330	24743747

Figure 8.20S GPC chromatogram of BPCL<sub>9</sub>-mPEG.

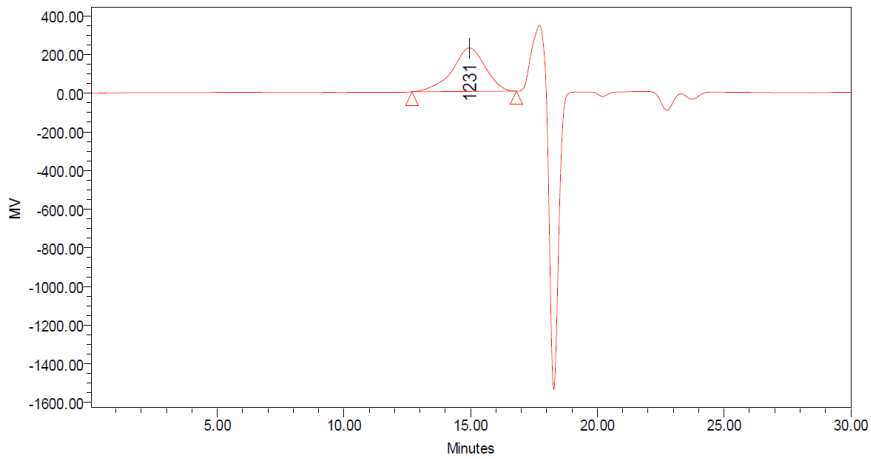
**PART II**



**GPC Results**

	Retention Time (min)	M <sub>w</sub>	MP	M <sub>n</sub>	Poly dispersity	Area (μV*sec)
1	10.339					9253834
2	12.417		5606			7969806
3	13.376	3020	2988	2945	1.025488	6739107

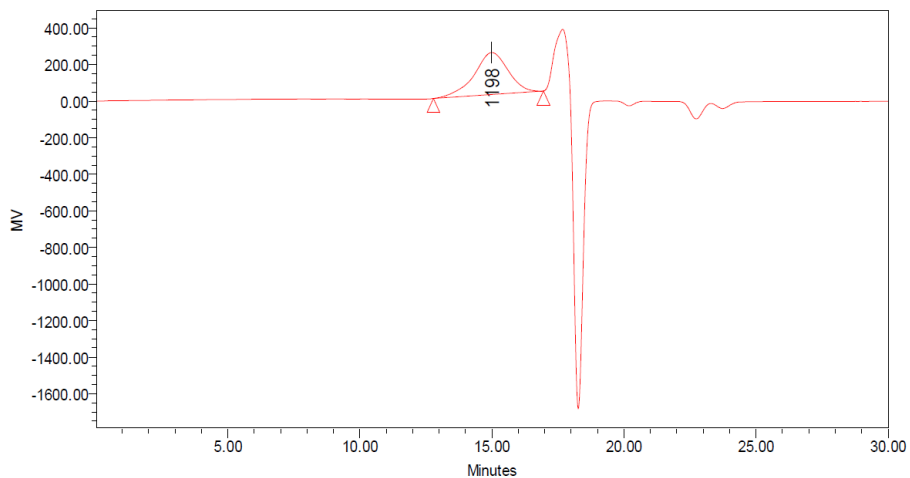
**Figure 8.21S** GPC chromatogram of BPCL<sub>9</sub>-malPEG.



**GPC Results**

	Retention Time (min)	M <sub>w</sub>	MP	M <sub>n</sub>	Poly dispersity	Area (μV*sec)
1	14.950	1351	1231	1172	1.152516	20391972

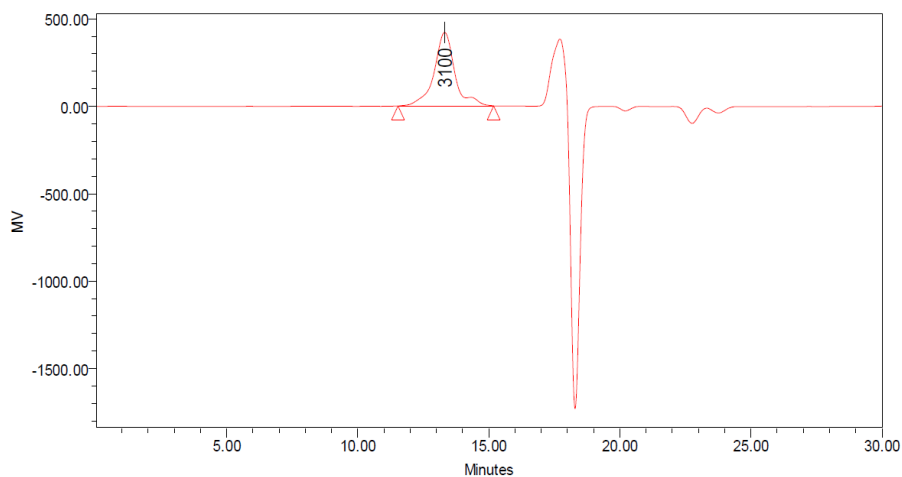
**Figure 8.22S** GPC chromatogram of BPCL<sub>15</sub>-OH.



GPC Results

	Retention Time (min)	Mw	MP	Mn	Poly dispersity	Area ( $\mu\text{V}\cdot\text{sec}$ )
1	14.996	1308	1198	1141	1.147194	20492708

Figure 8.23S GPC chromatogram of BPCL<sub>15</sub>-pNF.

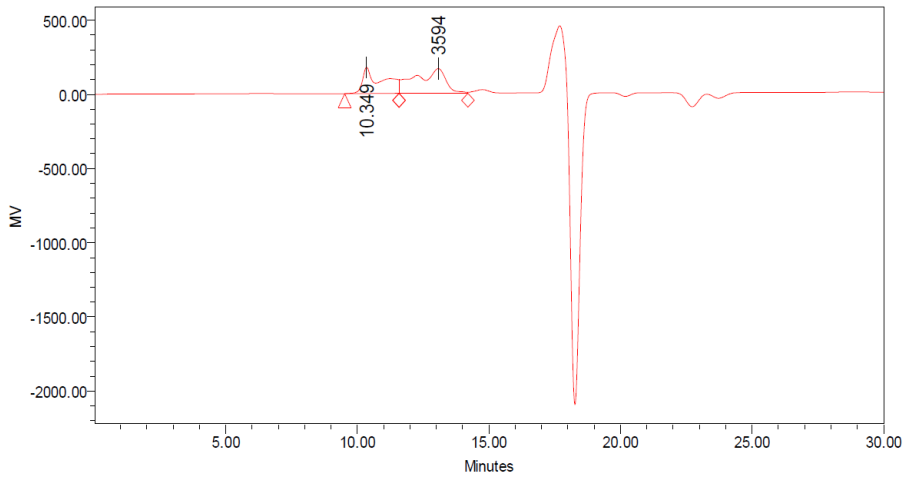


GPC Results

	Retention Time (min)	Mw	MP	Mn	Poly dispersity	Area ( $\mu\text{V}\cdot\text{sec}$ )
1	13.314	3251	3100	2983	1.089801	22983787

Figure 8.24S GPC chromatogram of BPCL<sub>15</sub>-mPEG.

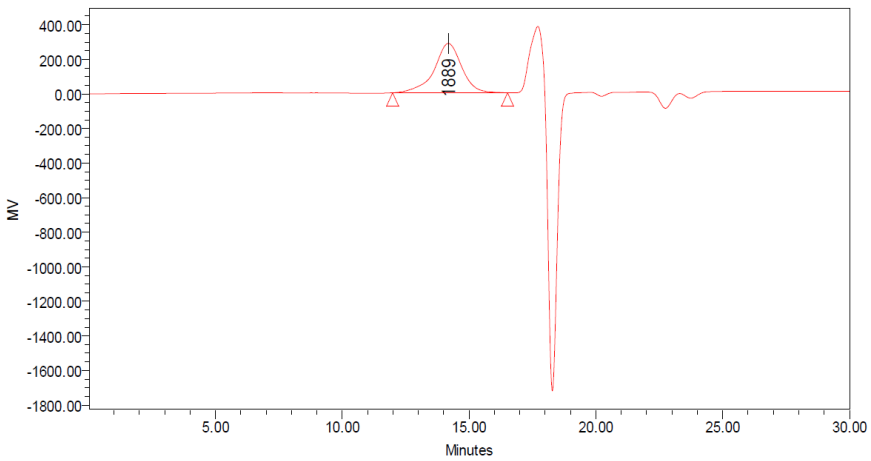
**PART II**



**GPC Results**

	Retention Time (min)	Mw	MP	Mn	Poly dispersity	Area ( $\mu V \cdot sec$ )
1	10.349					9026331
2	13.074	5387	3594	4559	1.181708	13298543

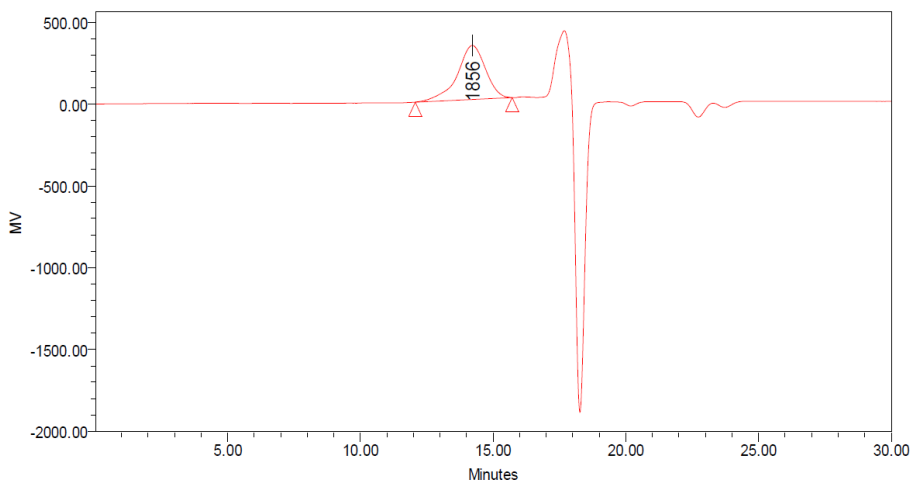
**Figure 8.25S** GPC chromatogram of BPCL<sub>15</sub>-malPEG.



**GPC Results**

	Retention Time (min)	Mw	MP	Mn	Poly dispersity	Area ( $\mu V \cdot sec$ )
1	14.182	2051	1889	1832	1.119875	21569262

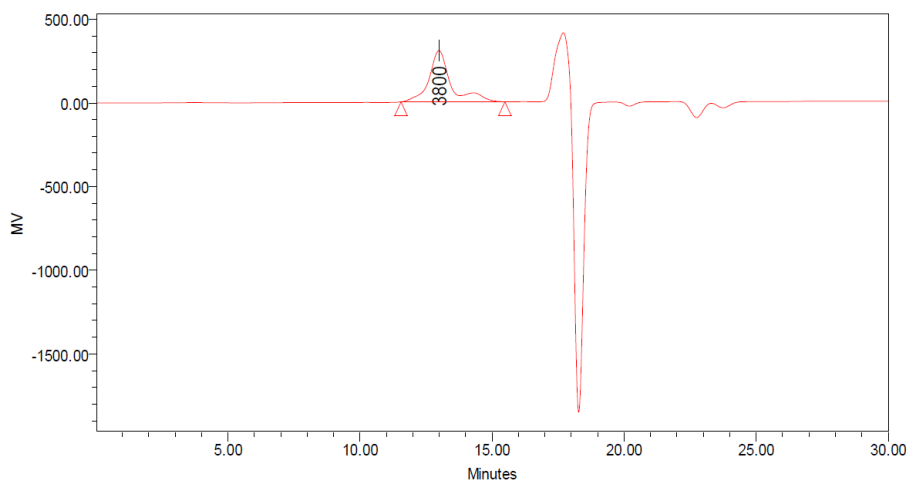
**Figure 8.26S** GPC chromatogram of BPCL<sub>23</sub>-OH.



GPC Results

	Retention Time (min)	Mw	MP	Mn	Poly dispersity	Area ( $\mu\text{V} \cdot \text{sec}$ )
1	14.213	2043	1856	1855	1.100974	24231192

Figure 8.27S GPC chromatogram of BPCL<sub>23</sub>-pNF.

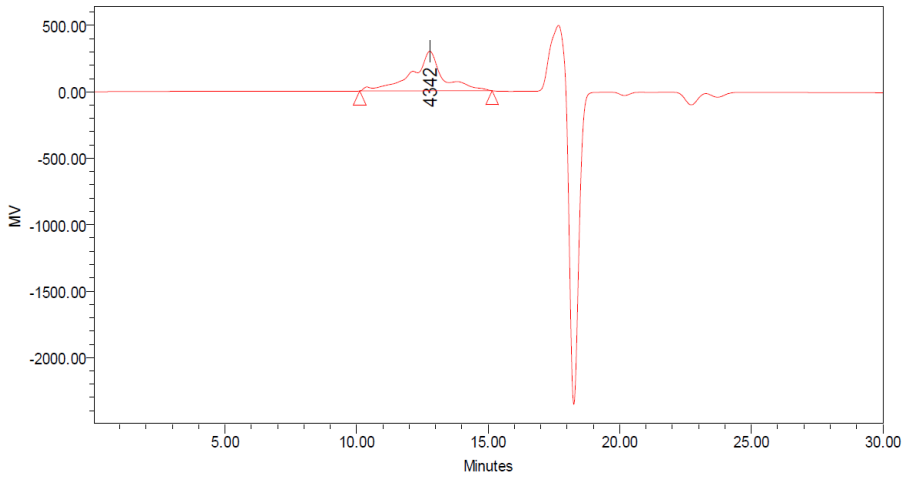


GPC Results

	Retention Time (min)	Mw	MP	Mn	Poly dispersity	Area ( $\mu\text{V} \cdot \text{sec}$ )
1	12.986	3726	3800	3218	1.158054	17607257

Figure 8.28S GPC chromatogram of BPCL<sub>23</sub>-mPEG.

**PART II**



**GPC Results**

	Retention Time (min)	Mw	MP	Mn	Polydispersity	Area ( $\mu\text{V} \cdot \text{sec}$ )
1	12.782	5816	4342	4141	1.404317	24208752

**Figure 8.29S** GPC chromatogram of BPCL<sub>23</sub>-malPEG.

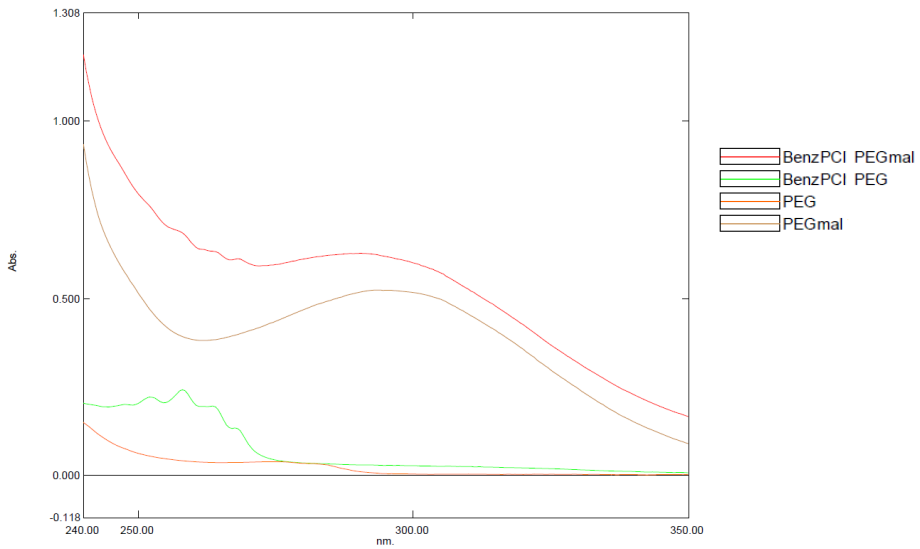


**Figure 8.30S** UV/Vis Spectra of (top) BPCL<sub>n</sub>-malPEG; malPEG-NH<sub>2</sub>; BPCL<sub>n</sub>-mPEG; mPEG-NH<sub>2</sub> (bottom).

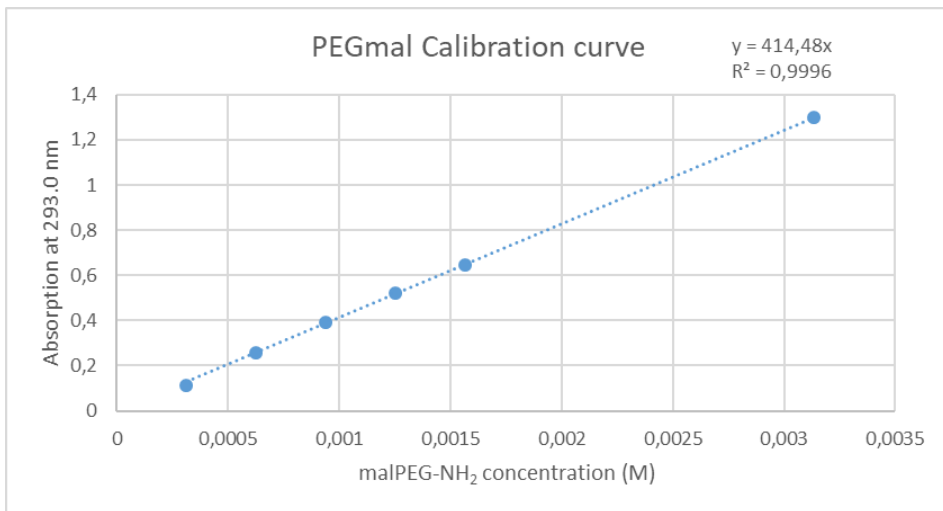


**Figure 8.31S** Calibration curve of malPEG-NH<sub>2</sub> in DCM.

Here are reported as representative only TGA graphs of mPEG-NH<sub>2</sub> and of polymers with  $n=23$ .

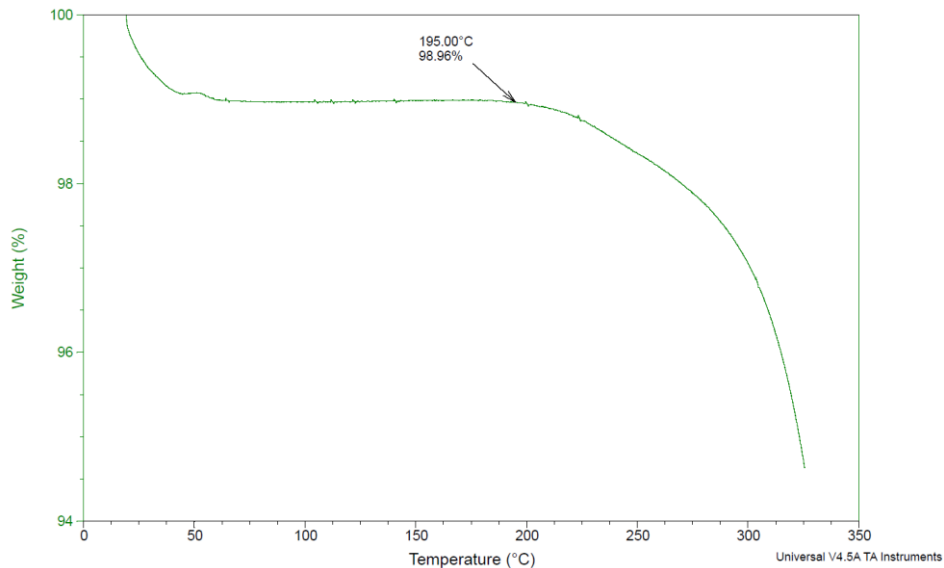


**Figure 8.32S** TGA graph of mPEG-NH<sub>2</sub>.

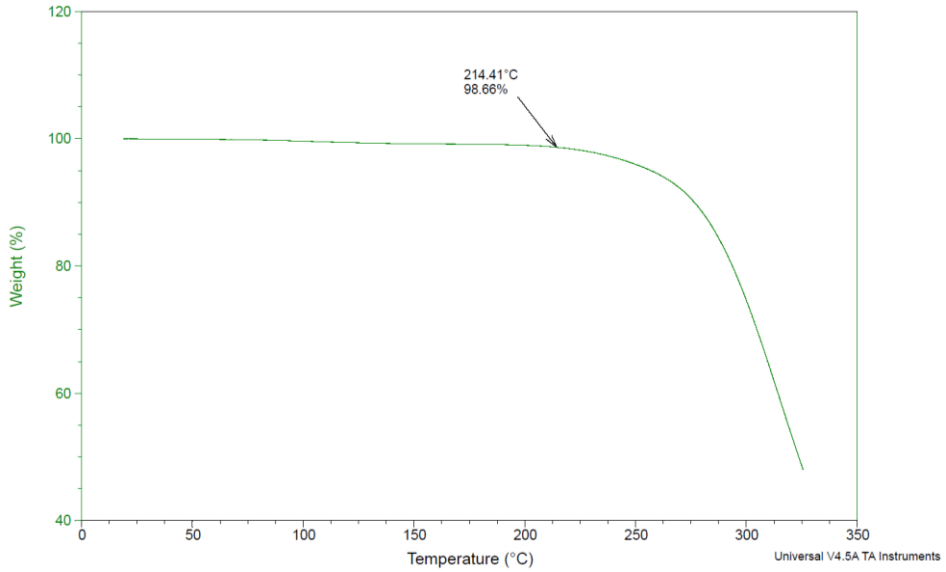


Figure 8.33S TGA graph of BPCL<sub>23</sub>-OH.

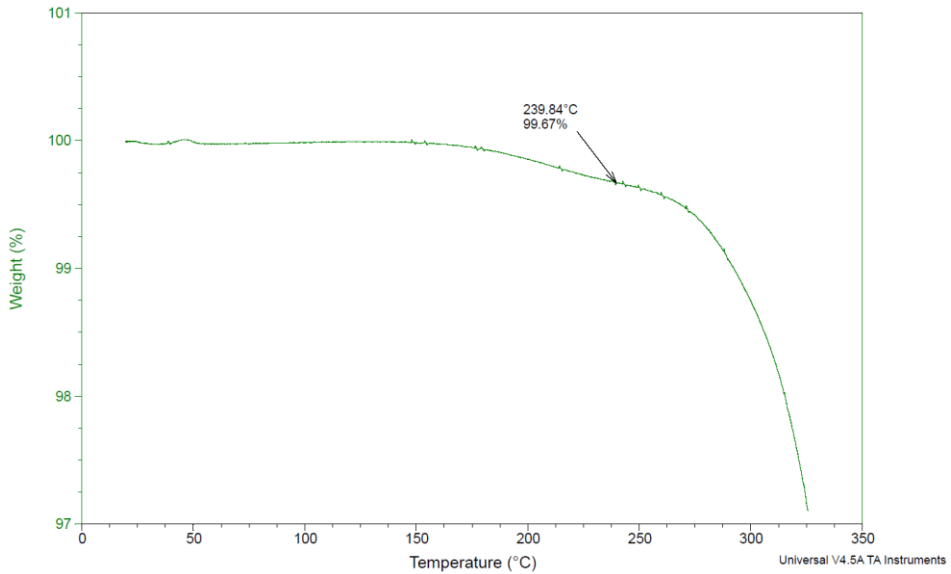


Figure 8.34S TGA graph of BPCL<sub>23</sub>-mPEG.



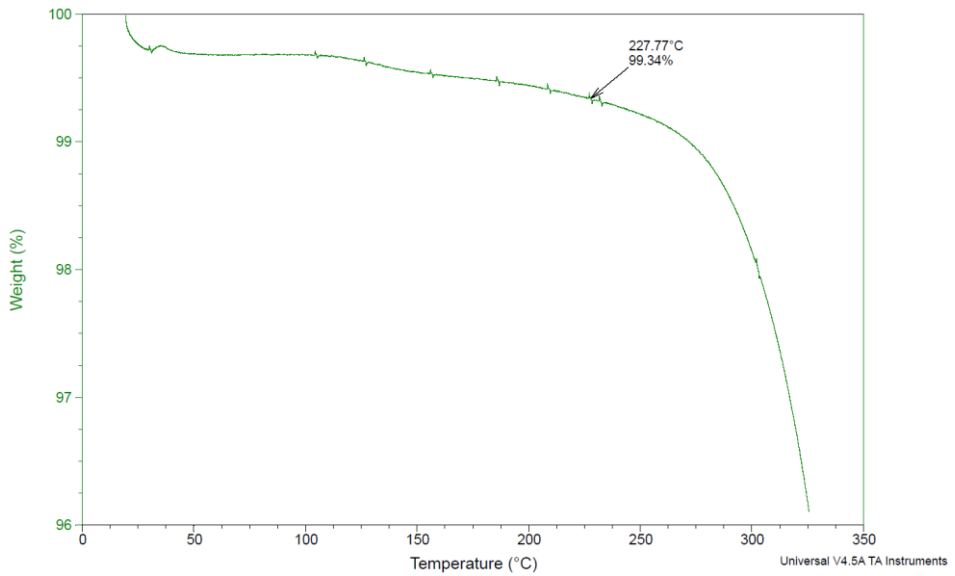


Figure 8.35S TGA graph of BPCL<sub>23</sub>-malPEG.

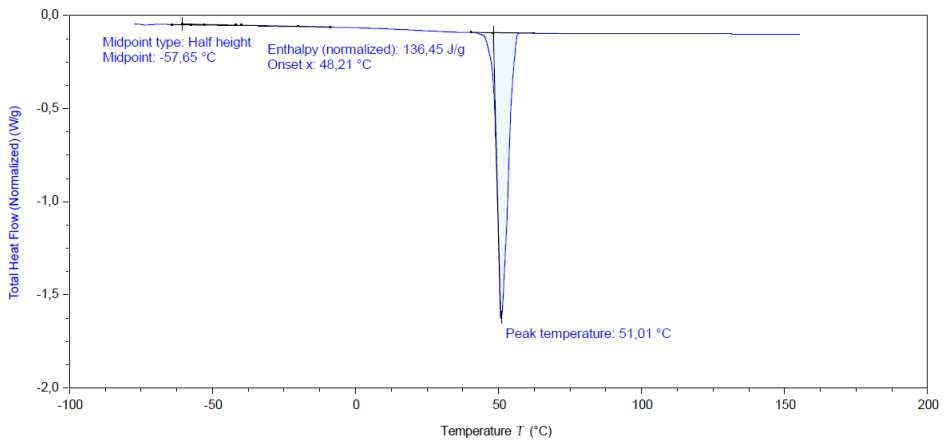


Figure 8.36S DSC graph of mPEG-NH<sub>2</sub>.

## PART II

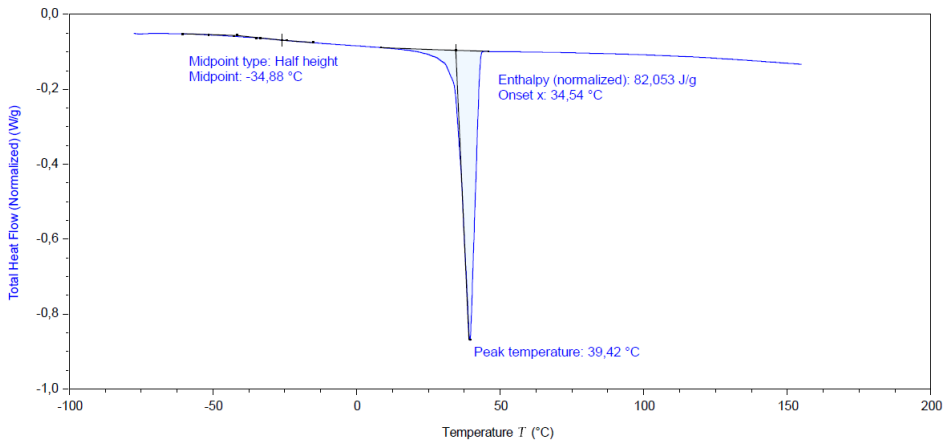


Figure 8.37S DSC graph of malPEG-NH<sub>2</sub>.

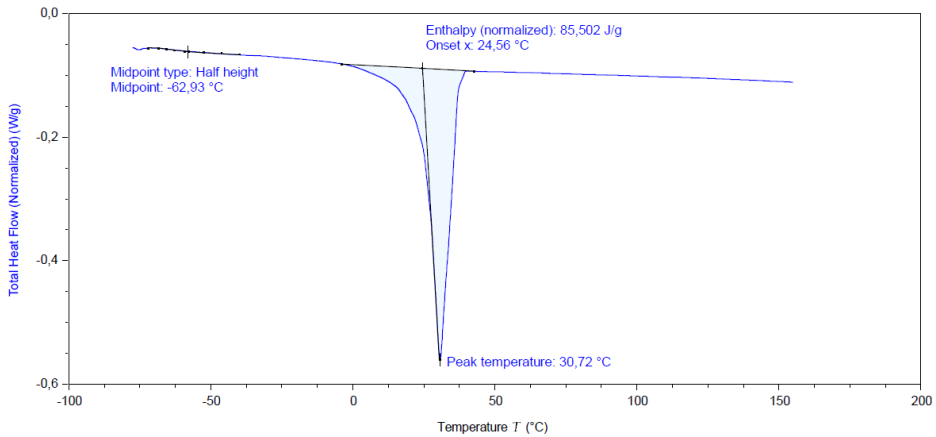


Figure 8.38S DSC graph of BPCL<sub>9</sub>-OH.

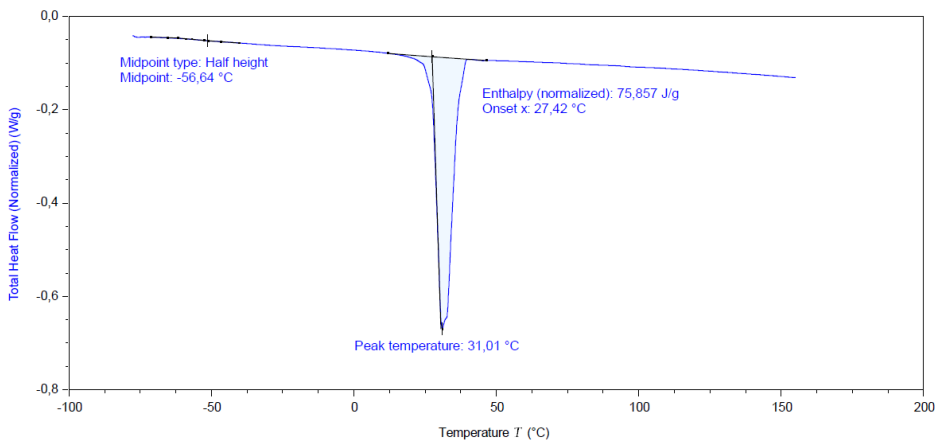


Figure 8.39S DSC graph of BPCL<sub>9</sub>-pNF.

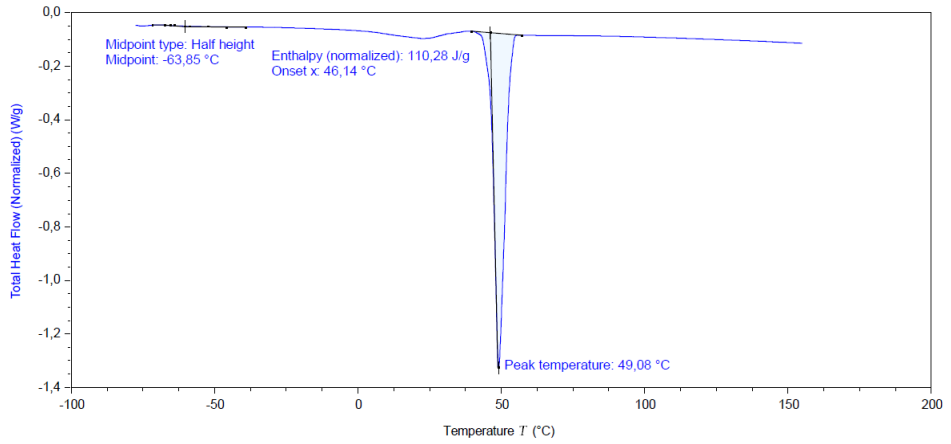


Figure 8.40S DSC graph of BPCL<sub>9</sub>-mPEG.

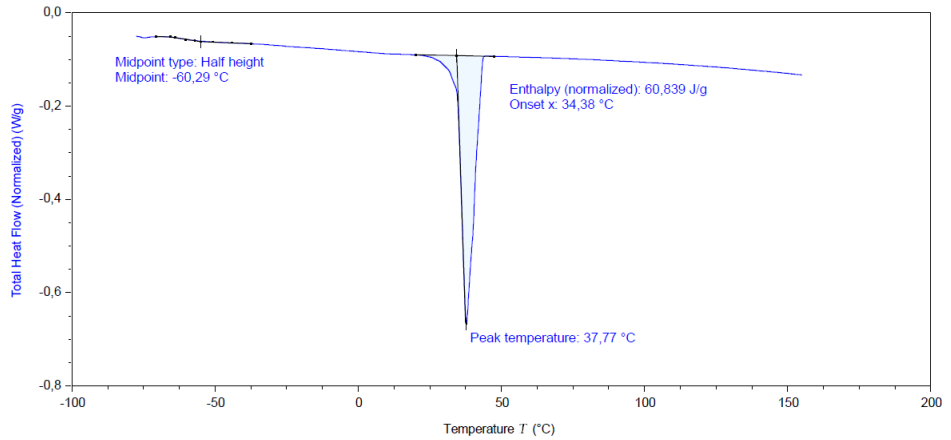


Figure 8.41S DSC graph of BPCL<sub>9</sub>-malPEG.

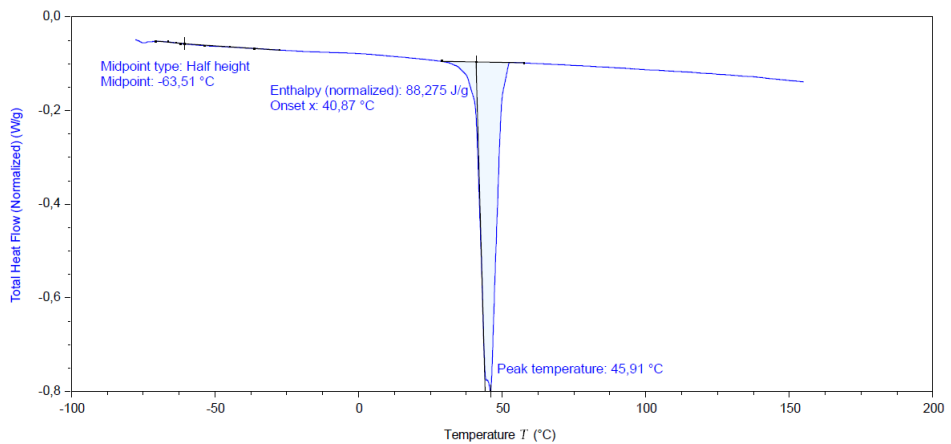


Figure 8.42S DSC graph of BPCL<sub>15</sub>-OH.

## PART II

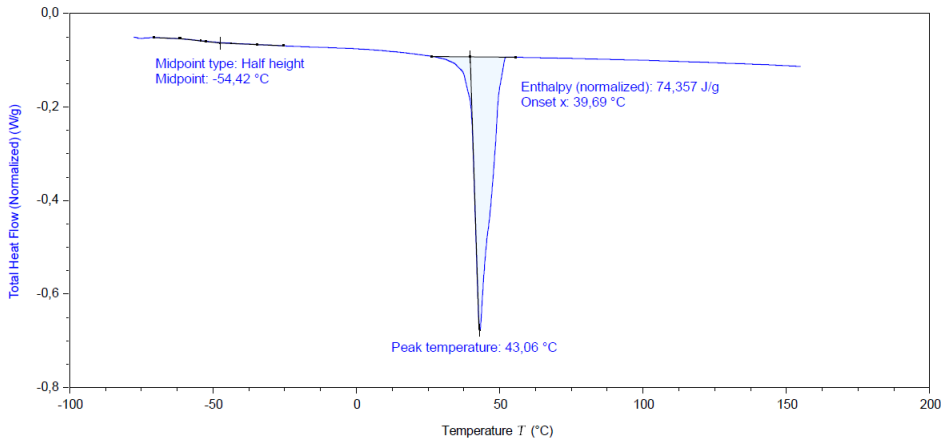


Figure 8.43S DSC graph of BPCL<sub>15</sub>-pNF.

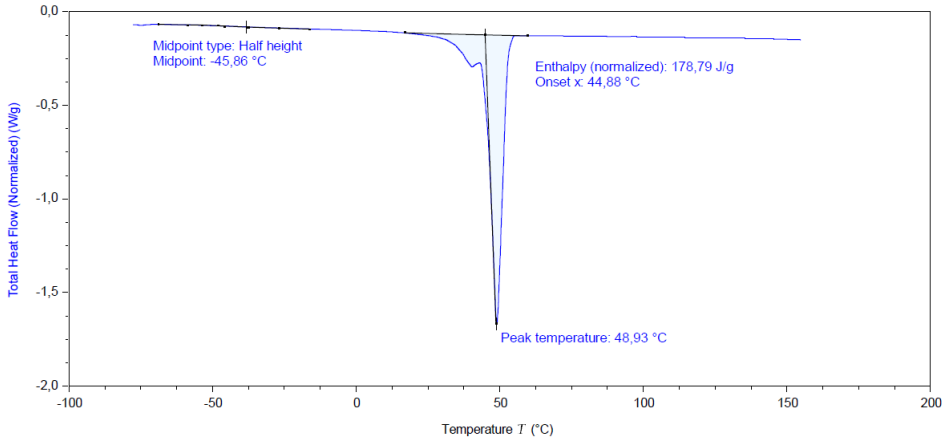


Figure 8.44S DSC graph of BPCL<sub>15</sub>-mPEG.

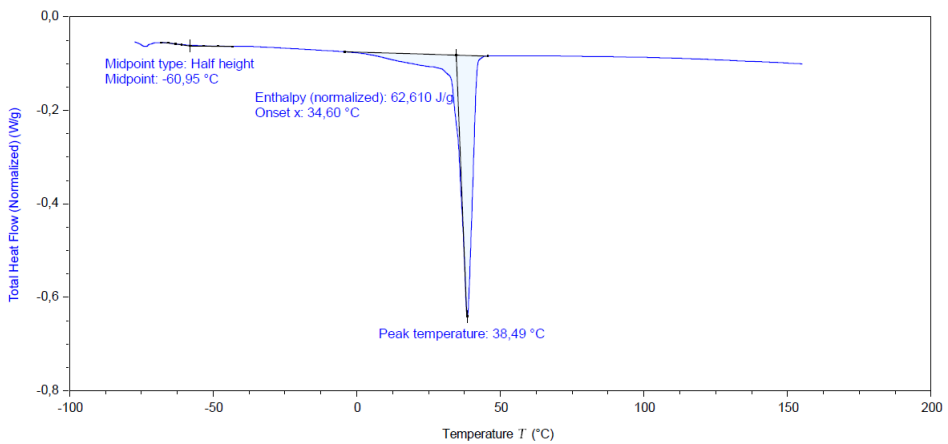


Figure 8.45S DSC graph of BPCL<sub>15</sub>-malPEG.

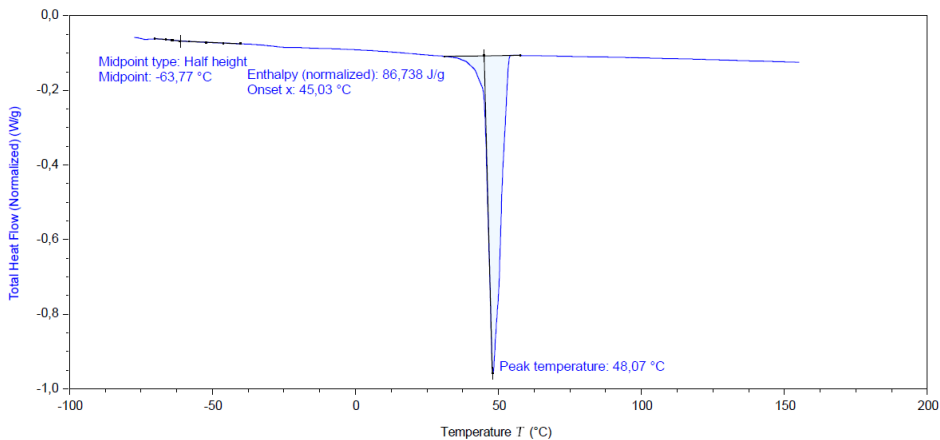


Figure 8.46S DSC graph of BPCL<sub>23</sub>-OH.

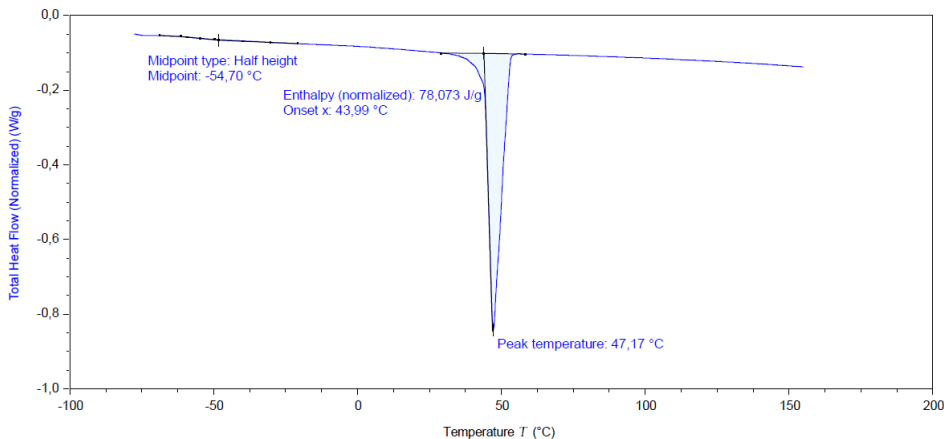


Figure 8.47S DSC graph of BPCL<sub>23</sub>-pNF.

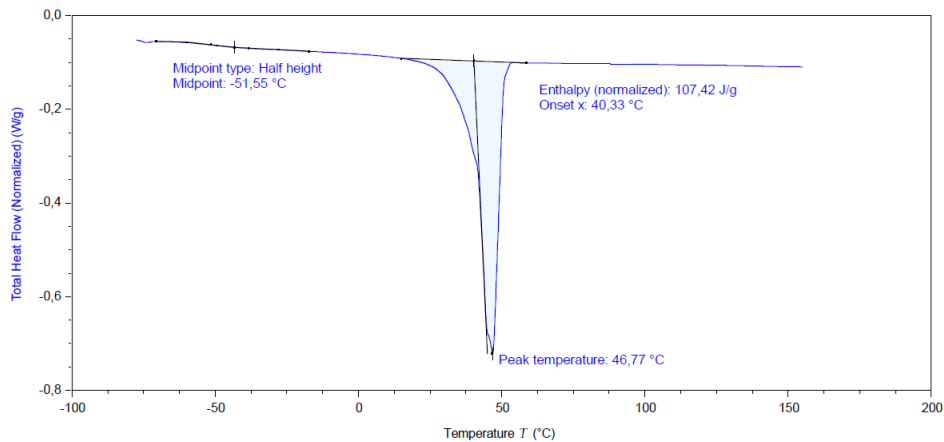


Figure 8.48S DSC graph of BPCL<sub>23</sub>-mPEG.

## PART II

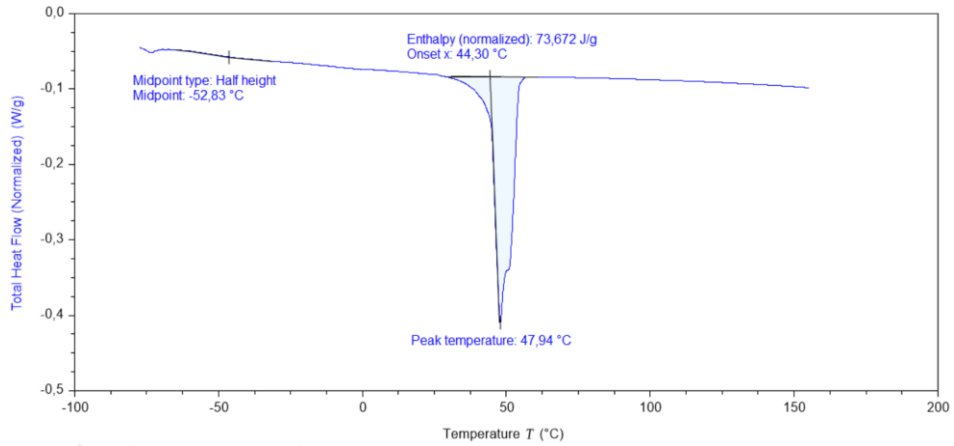


Figure 8.49S DSC graph of BPCL<sub>23</sub>-malPEG.

## Micelles characterization

	Size (d.nm):	% Intensity:	St Dev (d.nm):
Z-Average (d.nm): 17.40	Peak 1: 18.92	100.0	5.290
Pdl: 0.081	Peak 2: 0.000	0.0	0.000
Intercept: 0.965	Peak 3: 0.000	0.0	0.000
Result quality : Good			

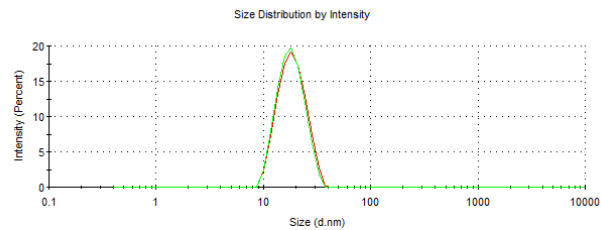


Figure 8.50S DLS graph of BPCL<sub>9</sub>-mPEG/BPCL<sub>9</sub>-malPEG micelles.

	Size (d.nm):	% Intensity:	St Dev (d.nm):
Z-Average (d.nm): 25.14	Peak 1: 27.94	97.9	10.80
Pdl: 0.175	Peak 2: 4434	2.1	906.8
Intercept: 0.975	Peak 3: 0.000	0.0	0.000
Result quality : Good			

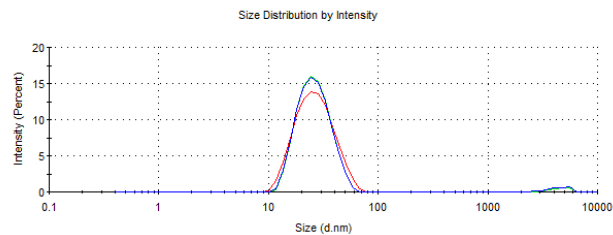


Figure 8.51S DLS graph of BPCL<sub>15</sub>-mPEG/BPCL<sub>15</sub>-malPEG micelles.

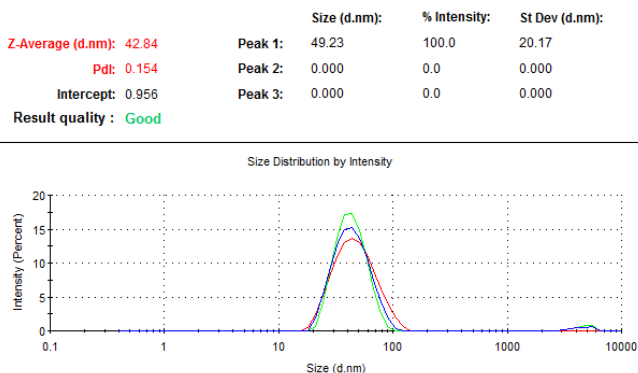


Figure 8.52S DLS graph of BPCL<sub>23</sub>-mPEG/BPCL<sub>23</sub>-malPEG micelles.

### Calibration curves

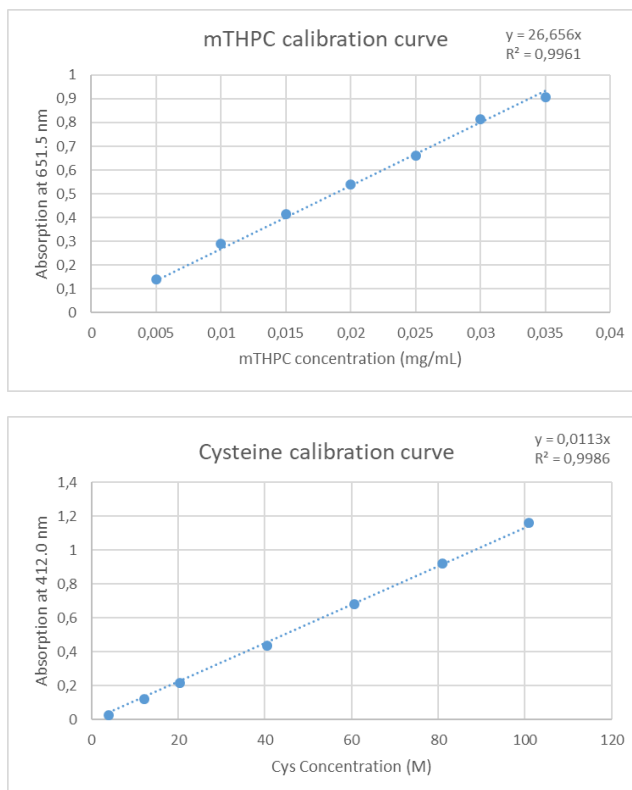
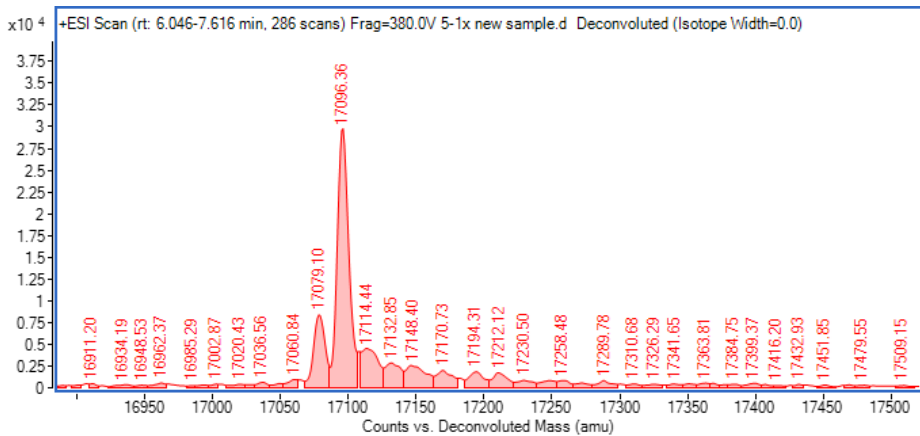


Figure 8.53S (top) Calibration curve of mTHPC in DMF; (bottom) Calibration curve of Cys through Ellman's assay.

## EGa1 characterization

**Table 8.1S** Theoretical molecular weights of SATA-modified EGa1.

NANOBODY	Theoretical MW (Da)
Native EGa1	17097
EGa1 + 1 SATA	17213
EGa1 + 2 SATA	17329
EGa1 + 3 SATA	17445
EGa1 + 4 SATA	17561
EGa1 + 5 SATA	17677
EGa1 + 6 SATA	17793



**Figure 8.54S** LC-ESI-TOF-MS deconvoluted spectrum of native EGa1.

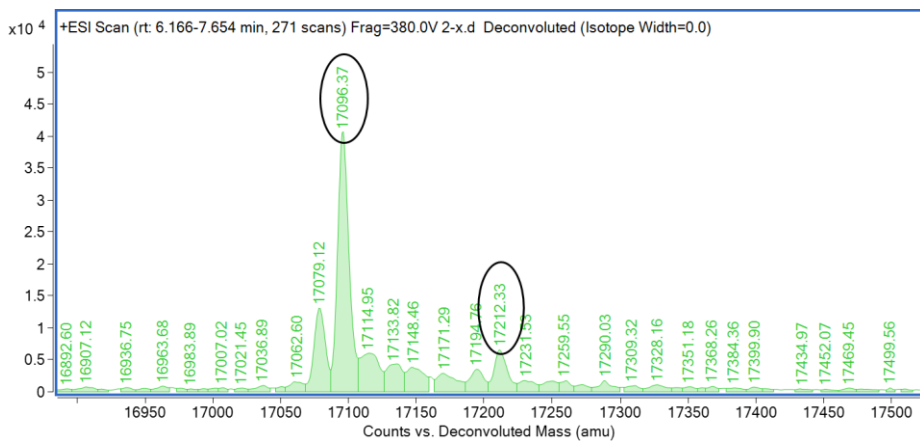


**Figure 8.55S** LC-ESI-TOF-MS deconvoluted spectrum of EGa1-SATA 1:2.



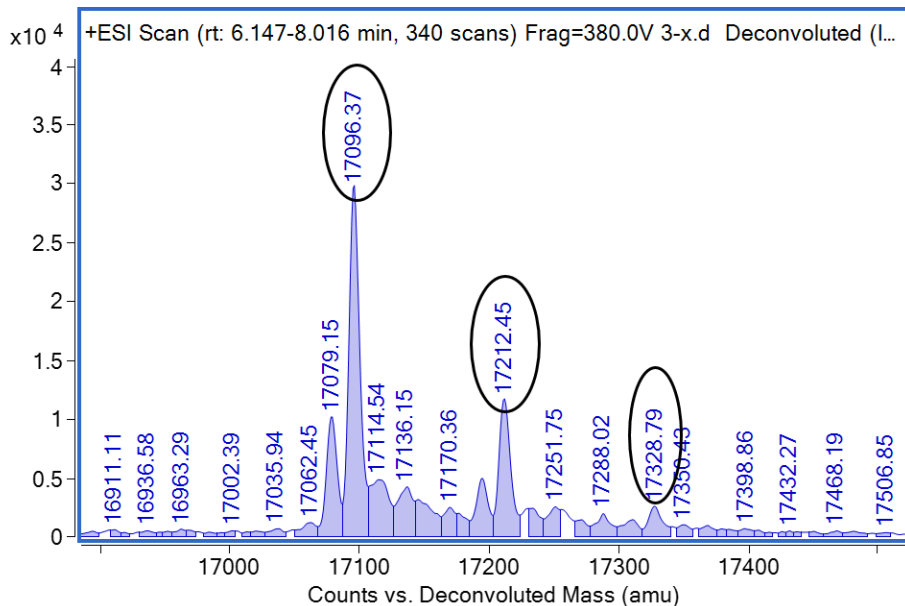


Figure 8.56S LC-ESI-TOF-MS deconvoluted spectrum of EGal-SATA 1:5.

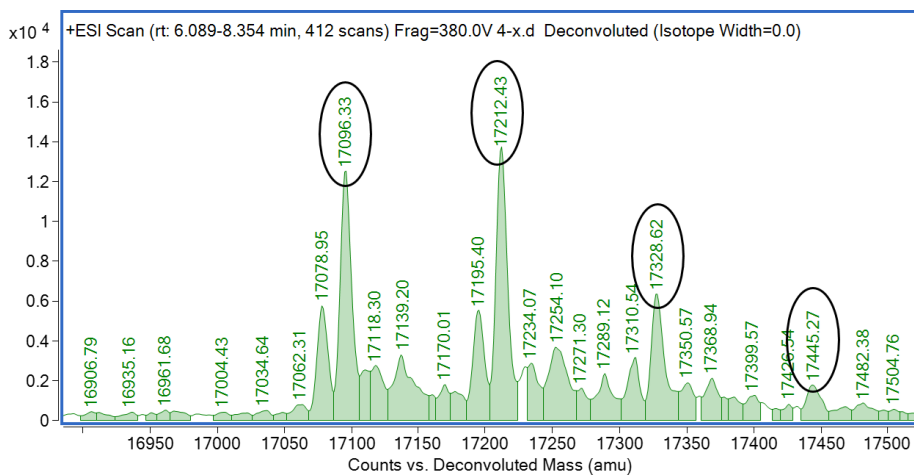
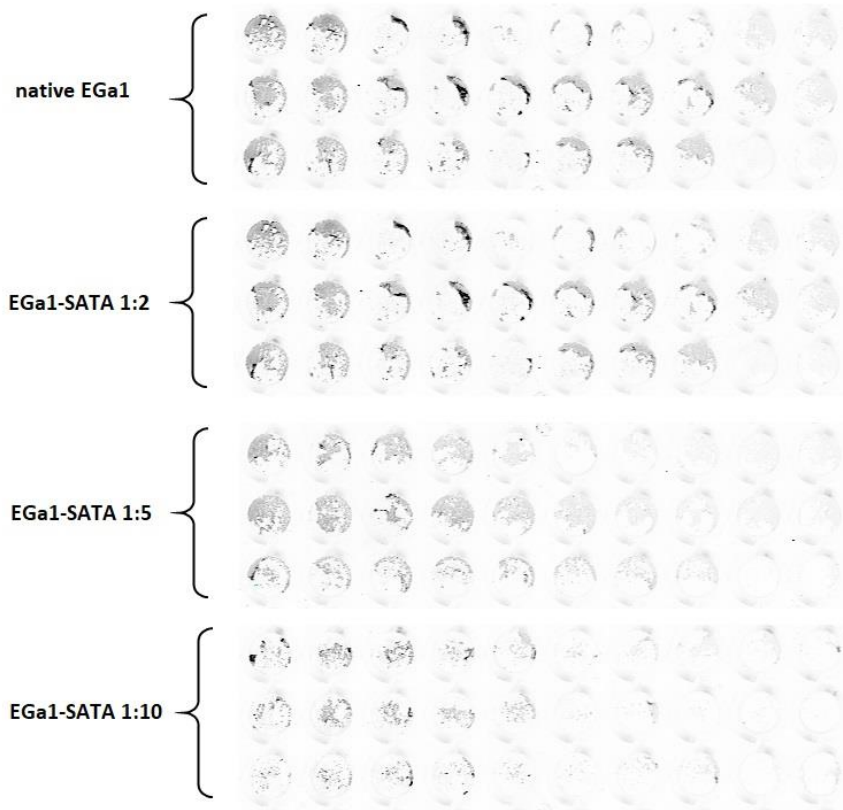
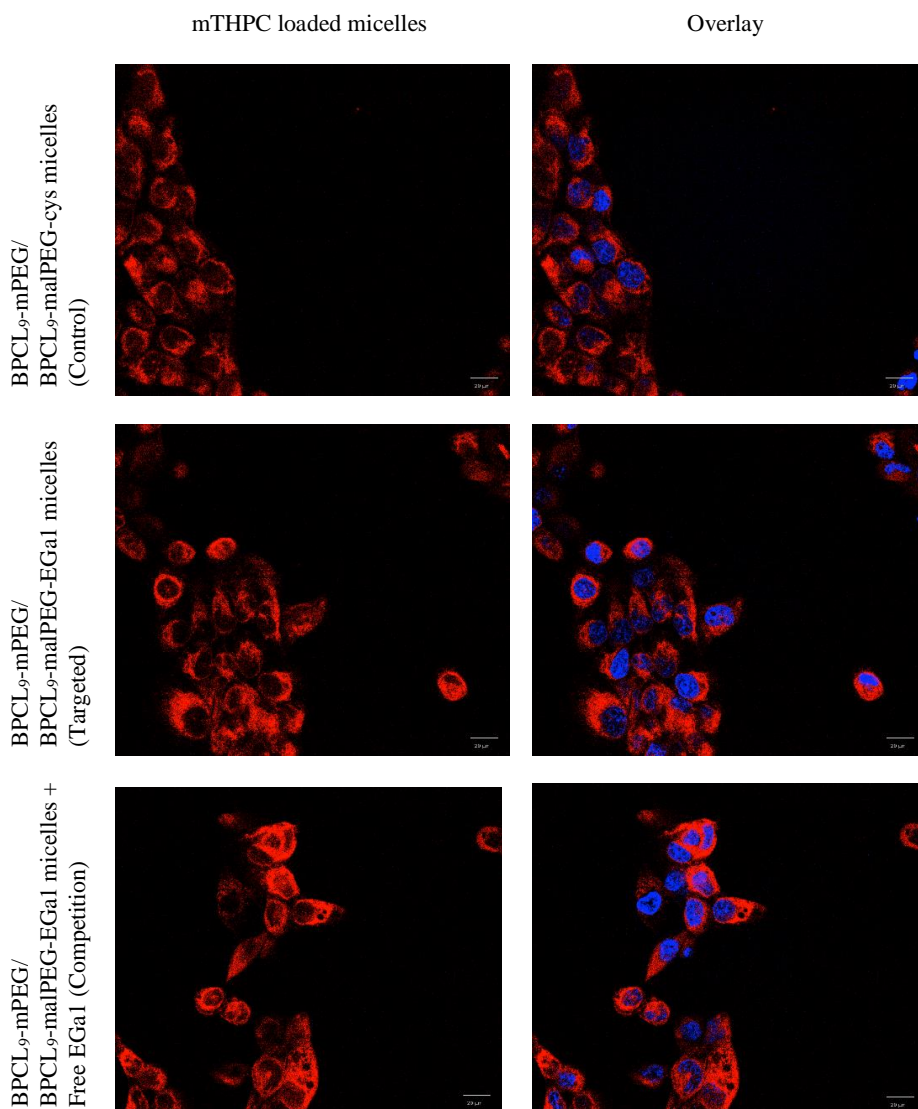


Figure 8.57S LC-ESI-TOF-MS deconvoluted spectrum of EGal-SATA 1:10.



**Figure 8.58S** EGFR binding affinity assay of modified EGa1.

## Uptake studies of mTHPC-loaded micelles



**Figure 8.59S** BPCL<sub>9</sub>-mPEG/BPCL<sub>9</sub>-malPEG-EGal micelles uptake in A431 cells at 37°C after 7 h of incubation (50 msec exposure time).

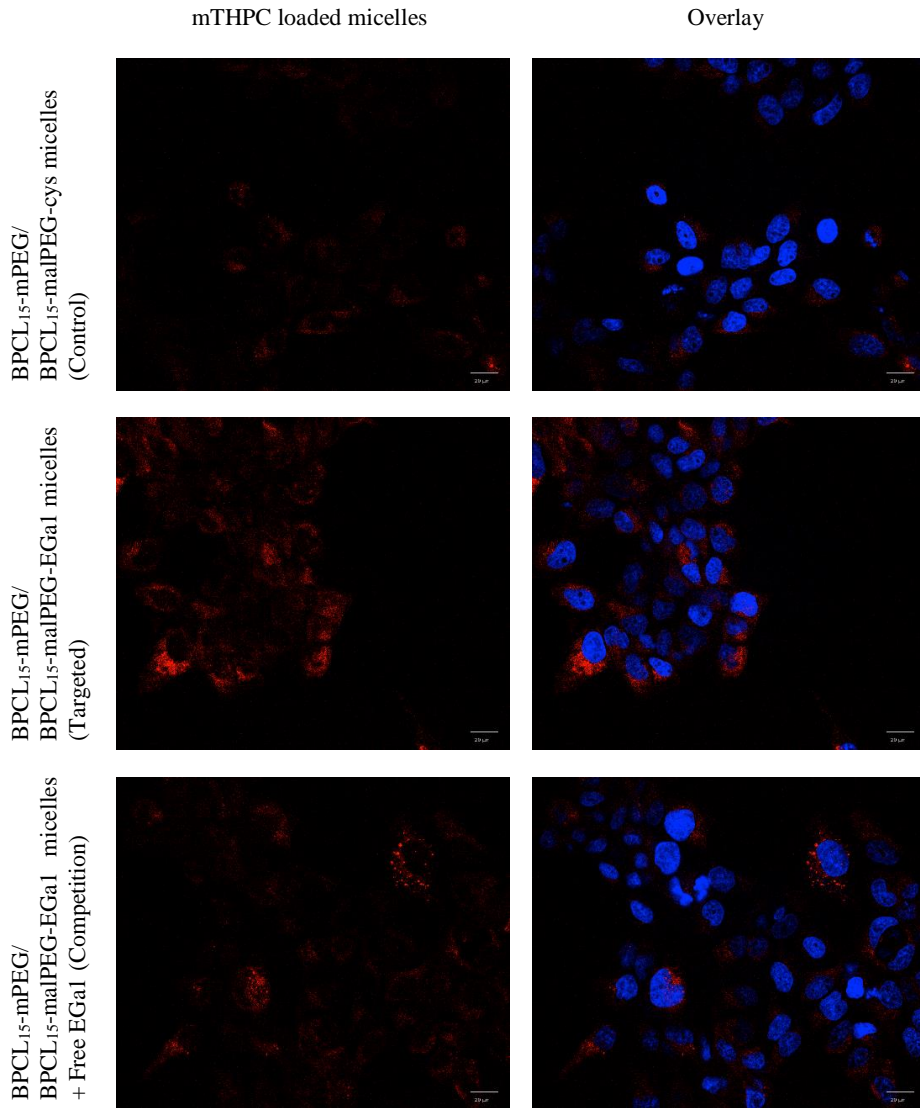


**Figure 8.60S** BPCL<sub>15</sub>-mPEG/BPCL<sub>15</sub>-malPEG-EGal micelles uptake in A431 cells at 37°C after 7 h of incubation (50 msec exposure time).

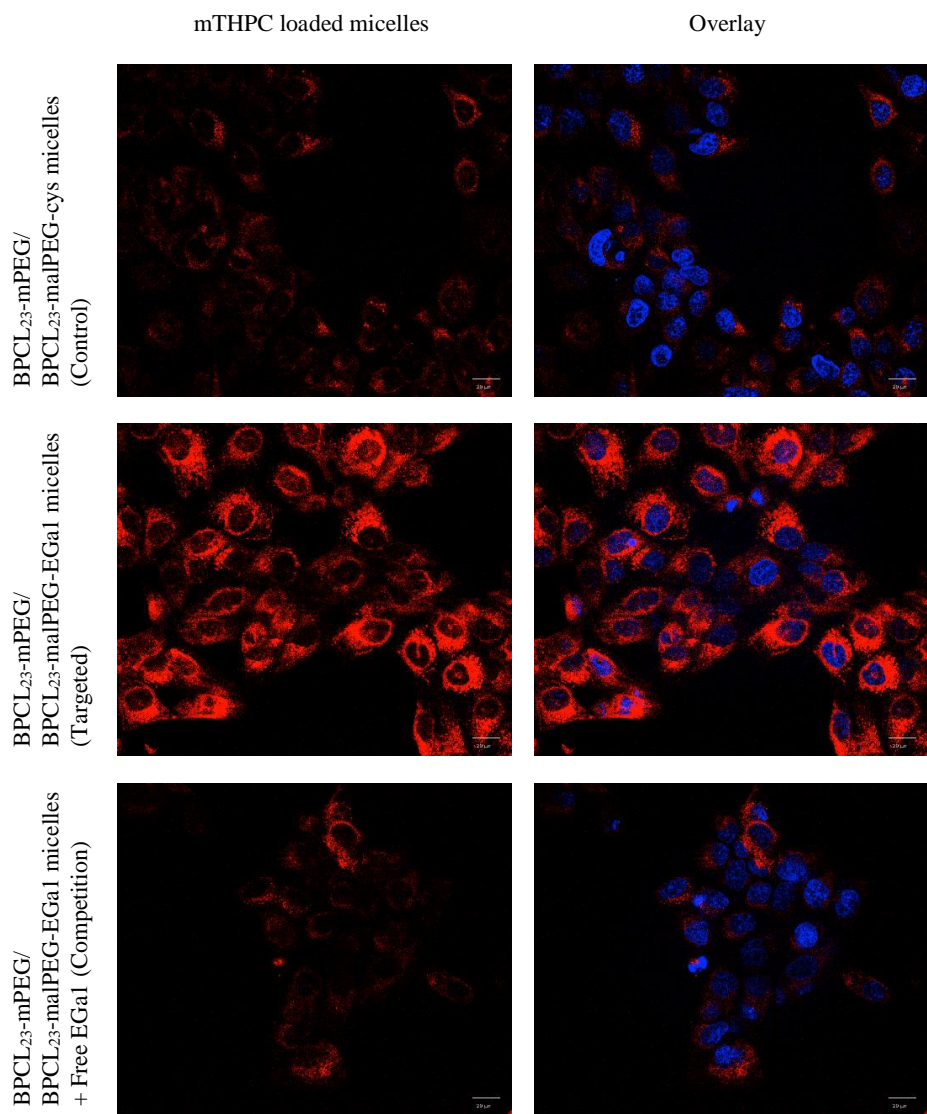


**Figure 8.61S** BPCL<sub>23</sub>-mPEG/BPCL<sub>23</sub>-malPEG-EGal micelles uptake in A431 cells at 37°C after 7 h of incubation (50 msec exposure time).

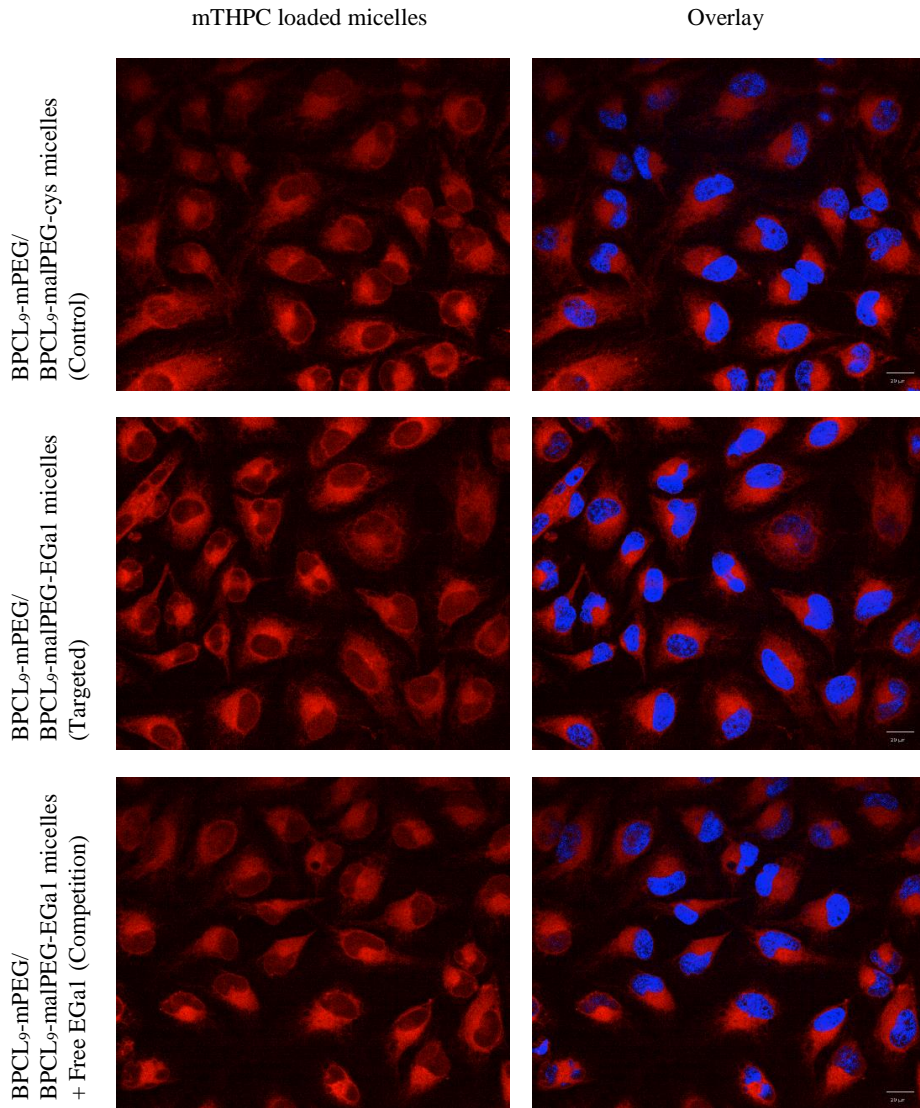


**Figure 8.62S** BPCL<sub>9</sub>-mPEG/BPCL<sub>9</sub>-malPEG-EGal micelles uptake in HeLa cells at 37°C after 7 h of incubation (100 msec exposure time).



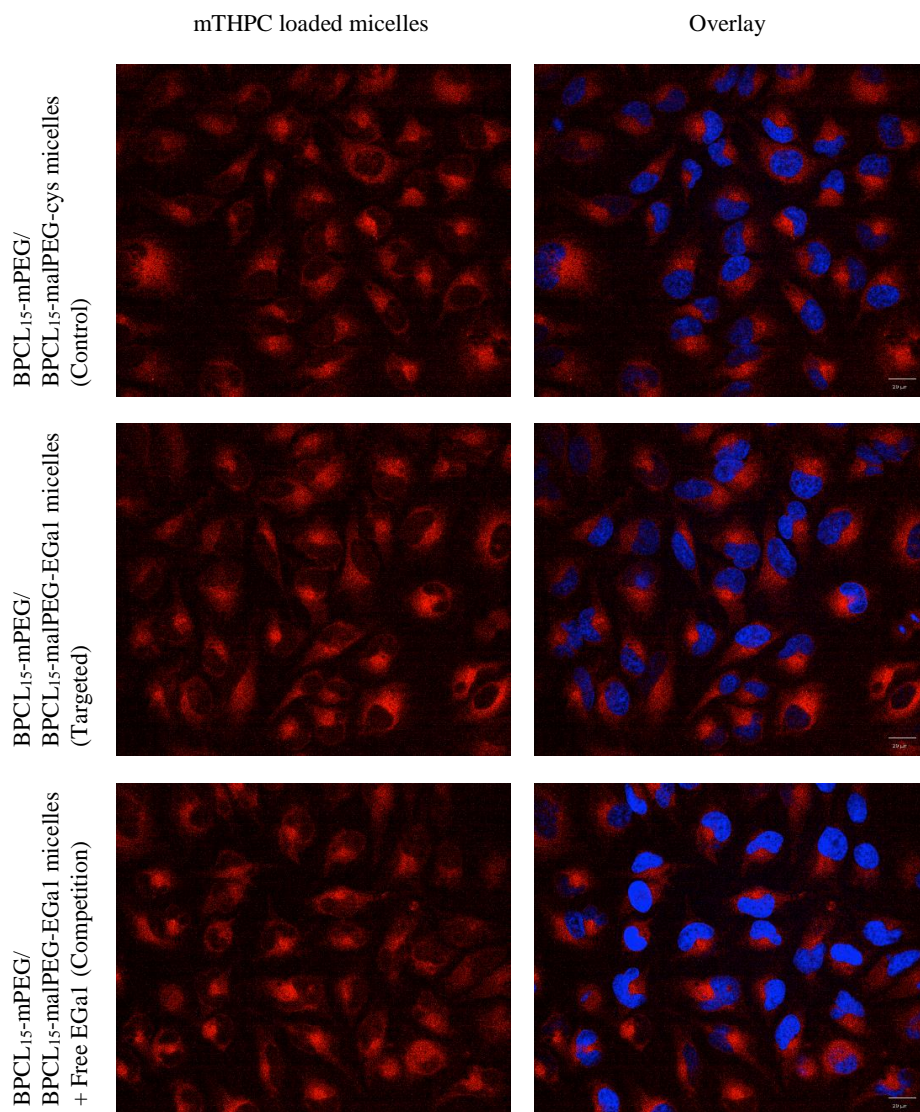


**Figure 8.63S** BPCL<sub>15</sub>-mPEG/BPCL<sub>15</sub>-malPEG-EGal micelles uptake in HeLa cells at 37°C after 7 h of incubation (100 msec exposure time).

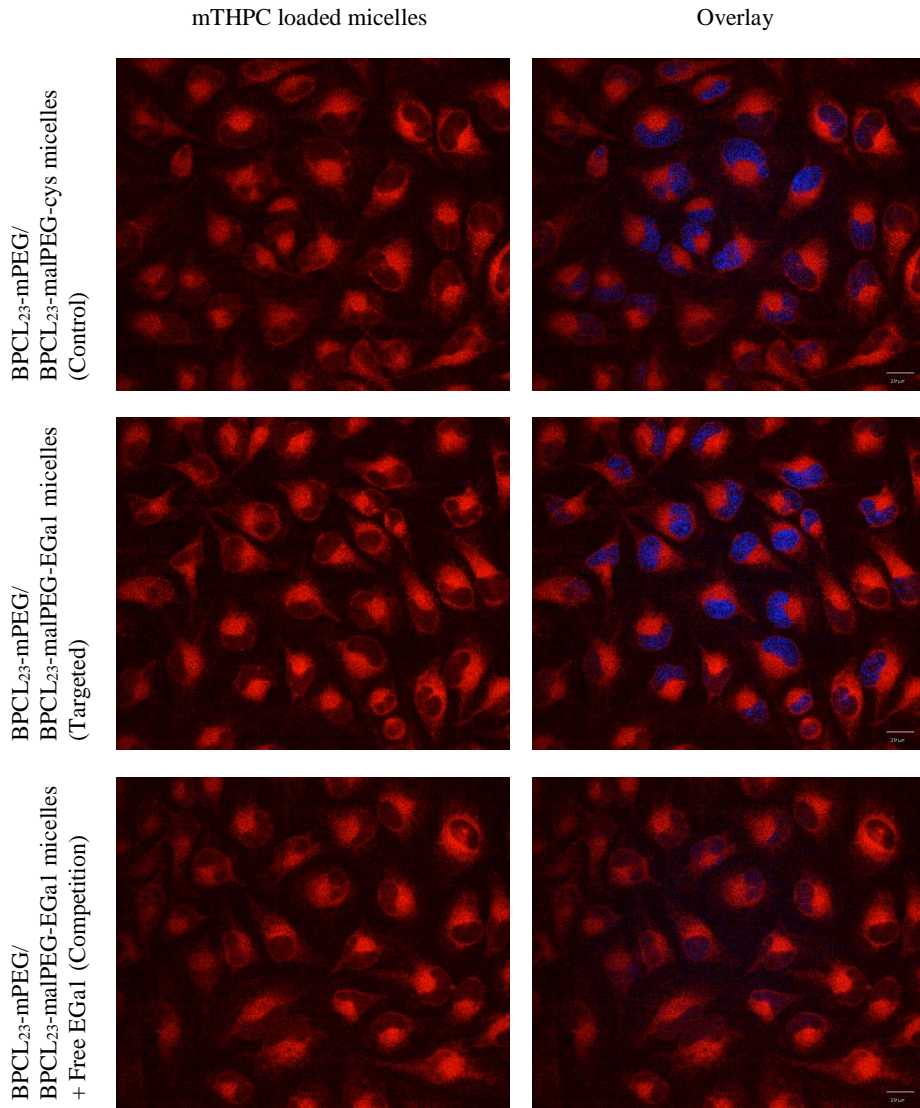


**Figure 8.64S** BPCL<sub>23</sub>-mPEG/BPCL<sub>23</sub>-malPEG-EGal micelles uptake in HeLa cells at 37°C after 7 h of incubation (100 msec exposure time).







# CONCLUSIONS



## FINAL REMARKS

This thesis offers a wide view of the world of the polymer-based drug delivery systems. In particular, four different kinds of polymeric carriers were chosen in order to investigate their versatility and specific properties: molecularly imprinted polymers (MIPs), polymer-drug conjugates, polymeric vesicles and polymeric micelles.

To methacrylic acid-*co*-ethylene glycol dimethacrylate MIPs, an entire part of this work was dedicated and this is due to their great versatility as biomaterials. Drug imprinted MIPs, indeed, can be easily prepared *via* bulk or precipitation polymerization. They showed great stability as materials, preserving biocompatibility thanks to their ability to absorb large amounts of water that makes them hydrogel systems. Despite this interaction with water, prepared MIPs were insoluble, due to their high degree of cross-linking and, for this reason, they kept a certain stiffness which makes them non suitable for intravenous injection. MIPs, in agreement with the literature, had high drug loading capacity, which was always released by the polymeric particles in a controlled manner. However, because of the specific binding of the drug within the polymer matrix, an incomplete release of the drug was often observed. Furthermore, MIPs can be synthesized with different shapes (sphere, rod-like or irregular) and dimensions and employed for the preparation of hybrid formulations.

Polymer-drug conjugates represent the smallest polymeric carrier. They can greatly improve water solubility of hydrophobic drugs and they are soluble themselves that is a necessary characteristic for injectable formulations. If compared to MIPs, they showed lower stability, especially in biological fluids, in which both drug and polymer can be metabolized by enzymes, reducing the efficacy of the drug and limiting the amount of drug that can reach the target. Nevertheless, probably the major disadvantage of this kind of system is the very low drug loading capacity, because only a few molecules are usually linked to the polymer chain, as in the case reported in this thesis.

Vesicles and micelles are colloidal systems capable of very high hydrophobic drug loading. They are very small (< 800 nm) and they can easily penetrate cells as the polymer-drug conjugates. Like MIPs but not like the conjugates, they can protect the encapsulated drug from the action of metabolic enzymes, prolonging

## CONCLUSIONS

---

its circulation time. Although these properties make vesicles and micelles perfect candidates for intravenous formulations, they have a great limit: the dilution that occurs during administration, usually decrease the polymer concentration to values very close to the critical aggregation concentration which may cause instability of the colloidal system and particles may fall apart, causing the premature loss of the drug in the bloodstream.

At this point, if we would like to answer to question “which is the best polymer-based drug delivery systems?” we can say none and all of them. It is not an easy task to try to find the ultimate drug delivery system. Each of them may offer great advantages, such as stability, controlled release, high loading capacity and improved solubility of hydrophobic drugs. But not all of them come together in the same polymeric carrier, so a selection must be done carefully, by taking into account the physical-chemical properties of the drug and the physio-pathological characteristics of the diseased tissue.







# APPENDICES



# ABSTRACT IN ITALIANO

## SISTEMI POLIMERICI DI RILASCIO DI FARMACI: UNO STUDIO SU MICRO E NANOPARTICELLE COME CARRIER DI MOLECOLE BIOATTIVE

I lavori presentati in questo testo rappresentano i risultati ottenuti nei tre anni di ricerca effettuata dal Dottorando, Luca Scrivano, presso il Dipartimento di Farmacia e Scienze della Salute e della Nutrizione dell'Università della Calabria (IT). Il suo lavoro di ricerca si è focalizzato sullo sviluppo di materiali polimerici per la preparazione di sistemi di rilascio di farmaci di dimensioni nano- o micrometriche. Sono state valutate diverse strategie e sono state studiate in particolare quattro categorie di particelle polimeriche: polimeri a memoria molecolare, coniugati farmaco-polimerici, vescicole polimeriche e micelle polimeriche. Per lo sviluppo di tali sistemi sono stati impiegati sia polimeri naturali che di sintesi. La tesi è suddivisa in due parti:

La Parte I è incentrata sui polimeri a memoria molecolare impiegati come sistemi di rilascio di farmaci. Dopo una breve introduzione fatta nel Capitolo 1 sull'imprinting molecolare, nel Capitolo 2 è riportato il classico approccio per la sintesi di polimeri a memoria molecolare per il rilascio controllato di un farmaco antitumorale, il sunitinib. Nel Capitolo 3 è invece presentata una strategia innovativa per la sintesi di microtubuli polimerici a memoria molecolare attraverso la tecnica della polimerizzazione in mesofase. Infine, nel Capitolo 4 è riportato l'utilizzo di polimeri a memoria molecolare per la realizzazione di garze per il rilascio transdermico di diclofenac.

La Parte II è incentrata sullo sviluppo di nanoparticelle per la veicolazione di farmaci poco idrosolubili. Nel Capitolo 5, introduttivo alla sezione, sono descritti in generale i tre differenti sistemi utilizzati nei capitoli successivi: coniugati farmaco-polimerici, vescicole polimeriche e micelle polimeriche. In particolare, nel Capitolo 6 vengono approfondite sintesi e applicazioni di un coniugato sericina-sunitinib: per l'ottenimento del prodotto finale è stata utilizzata una tecnica di grafting radicalico in ambiente acquoso. Nel Capitolo 7 il destrano è

stato modificato con acido oleico per la preparazione di vescicole polimeriche, utilizzate per la veicolazione di un nuovo composto antibatterico sintetizzato dal gruppo di Chimica Farmaceutica del Dipartimento di Farmacia e Scienze della Salute e della Nutrizione dell'Università della Calabria. Infine, nel Capitolo 8 è riportato il lavoro di ricerca su micelle polimeriche per la veicolazione sito-specifica di un composto porfirinico per applicazioni nella terapia fotodinamica, effettuato presso il Department of Pharmaceutical Sciences, Utrecht University (NL), sotto la supervisione del Prof. Wim Hennink, del Dr. Cornelus F. van Nostrum e della Dr. Sabrina Oliveira.

Nell'intento di esplorare il vasto mondo dei sistemi di veicolazione di farmaci, ai fini della ricerca scientifica svolta dal dottorando, sono stati scelti esclusivamente carrier polimerici. Tra questi sono stati selezionati quelli che avrebbero potuto offrire grandi vantaggi, in termini di stabilità, rilascio controllato, capacità di caricamento e di solubilizzazione di farmaci idrofobici. Ma, accanto ai vantaggi, risiedono gli svantaggi: è infatti riportato nelle conclusioni che non tutte le qualità ideali sono racchiuse in un unico sistema e che la selezione del carrier polimerico deve essere condotta con attenzione, tenendo in considerazione le proprietà chimico-fisiche del farmaco di interesse e le caratteristiche fisiopatologiche del tessuto malato – sito di azione dei composti biologicamente attivi.

## CURRICULUM VITAE

Luca Scrivano was born on October 31<sup>st</sup> 1983 in Cosenza, Italy. After graduating from secondary school at Liceo Scientifico “Pitagora” in Rende (CS), he started the 5-years Master program in Chemistry and Pharmaceutical Technology at University of Calabria. During this period, he performed a 12 months research on pH-sensitive poly(vinyl pyrrolidone)-*graft*-(methacrylic acid) for the stabilization and delivery of antioxidant molecules, at the Laboratory of Pharmaceutical Technology and Macromolecular Chemistry at University of Calabria under the supervision of Prof. Francesco Puoci. In 2013, Luca obtained his Master’s Degree *cum laude* and started working as private tutor for Master’s students at Centro Studi CEPU in Cosenza. In 2014, he started a collaboration with Prof. Francesco Puoci on the project “Controlled release of sunitinib in targeted cancer therapy: smart magnetically responsive hydrogels as restricted access materials” and in 2015, he started a Ph.D. project at the Department of Pharmacy, Health and Nutritional Sciences under his supervision.

During this period, he was also teaching tutor for the Master Course of “Cosmesi funzionale in dermatologia e tricologia” coordinated by Prof. Francesco Puoci and for the teaching course of “Laboratorio di Dispositivi Medici e Controllo di Qualità di Forme Farmaceutiche e Cosmetiche” held by Dr. Roberta Cassano.

In 2018, he carried out a 7 months research project on nanobody-conjugated polymeric micelles for the targeted delivery of a hydrophobic photosensitizer, at the Department of Pharmaceutical Sciences, Utrecht University, under the supervision of Dr. Cornelus F. van Nostrum, Dr. Sabrina Oliveira and Prof. Wim Hennink.

His research is mainly focused on molecularly imprinted polymers and polymeric nanoparticles for the delivery of hydrophobic drugs. The results of his work is presented in this book.

# LIST OF PUBLICATIONS

## ARTICLES INCLUDED IN THIS THESIS

Scrivano L., Parisi O.I., Iacopetta D., Ruffo M., Ceramella J, Sinicropi M.S., Puoci F., Molecularly imprinted hydrogels for sustained release of sunitinib in breast cancer therapy. *Polymers for Advanced Technology* (2018).

DOI: 10.1002/pat.4512

Parisi O.I., Scrivano L., Candamano S., Ruffo M., Vattimo A.F., Spanedda M.V. and Puoci F., Molecularly imprinted microrods *via* mesophase polymerization. *Molecules* (2018) 23, 63.

DOI:10.3390/molecules23010063

Parisi O.I., Ruffo M., Scrivano L., Malivindi R., Vassallo A. and Puoci F., Smart bandage based on molecularly imprinted polymers (MIPs) for diclofenac controlled release. *Pharmaceuticals* (2018) 11(4), 92.

DOI: 10.3390/ph11040092

Scrivano L., Parisi O.I. and Puoci F. Polymer-based nanodevices for effective antimicrobial therapy: synthetic strategies and applications. *Current Applied Polymer Science* (2017) 1, 3-18.

DOI: 10.2174/2452271601666170221123833

Scrivano L., Iacopetta D., Sinicropi M. S., Saturnino C., Longo P., Parisi O. I. and Puoci F. Synthesis of sericin-based conjugates by click chemistry: enhancement of sunitinib bioavailability and cell membrane permeation. *Drug Delivery* (2017) 24(1), 482-490.

DOI: 10.1080/10717544.2016.1267822

Dhanyalayam D.<sup>1</sup>, Scrivano L.<sup>1</sup>, Parisi O. I., Sinicropi M. S., Fazio A., Saturnino C., Plutino M.R., Di Cristo F., Puoci F., Cappello A.R. and Longo P. Biopolymeric self-assembled nanoparticles for enhanced antibacterial activity of Ag-based compounds. *International Journal of Pharmaceutics* (2017) 517(1), 395-402.

DOI: 10.1016/j.ijpharm.2016.12.039

**OTHER ARTICLES**

Lupi, F.R., Mancina, V., Baldino, N., Parisi, O.I., Scrivano, L., Gabriele, D., Effect of the monostearate/monopalmitate ratio on the oral release of active agents from monoacylglycerol organogels. *Food and Function* (2018) 9(6), 3278-3290.

DOI: 10.1039/C8FO00594J

Parisi, O.I., Scrivano, L., Amone, A., Malivindi, R., Ruffo, M., Vattimo, A.F., Pezzi, V. Puoci, F., Interconnected PolymerS TeChnology (IPSTiC): an effective approach for the modulation of 5 $\alpha$ -reductase activity in hair loss conditions. *Journal of Functional Biomaterials* (2018) 9(3), 44.

DOI: 10.3390/jfb9030044

Parisi O.I., Scrivano L., Sinicropi M.S., Puoci F. Polymeric nanoparticle constructs as devices for antibacterial therapy. *Current Opinion in Pharmacology* (2017) 36, 72-77.

DOI: 10.1016/j.coph.2017.08.004

Iacopetta D., Grande F., Caruso A., Mordocco R.A., Plutino M.R., Scrivano L., Ceramella J., Muià N., Saturnino C., Puoci F., Rosano C. and Sinicropi M.S. New insights for the use of quercetin analogs in cancer treatment. *Future Medicinal Chemistry* (2017).

DOI: 10.4155/fmc-2017-0118

Parisi O.I., Malivindi R., Amone F., Malanchin R., Carlomagno F., Piangiolino C., Pezzi V., Scrivano L. and Puoci F. Safety and efficacy of dextran-rosmarinic acid conjugates as innovative polymeric antioxidants in skin whitening: what is the evidence? *Cosmetics* (2017) 4(3), 28.

DOI: 10.3390/cosmetics4030028

Ruffo M., Parisi O.I., Scrivano L., Restuccia D., Amone F., Sinicropi M.S., Malivindi R., Aiello G. and Puoci F. Role of calabrian black rice in metabolic syndrome: *in vitro* evaluation of *Oryza sativa* L. Indica biological properties. *Current Nutrition & Food Science* (2017) 13, 1-17.

DOI: 10.2174/1573401313666170405153603

Ruffo M., Parisi O.I., Amone F., Malivindi R., Gorgoglione D., De Biasio F., Scrivano L., Pezzi V. and Puoci F. Calabrian goji vs. chinese goji: a comparative study on biological properties. *Foods* (2017) 6(4), 30.

DOI: 10.3390/foods6040030

Parisi O.I., Aiello D., Casula M.F., Puoci F., Malivindi R., Scrivano L. and Testa F. Mesoporous nanocrystalline TiO<sub>2</sub> loaded with ferulic acid for sunscreen and photoprotection: safety and efficacy assessment. *RSC Advances* (2016) 6, 83767-83775.

DOI: 10.1039/C6RA07653J

Parisi O.I., Scrivano L., Sinicropi M.S., Picci N. and Puoci F. Engineered Polymer-based nanomaterials for diagnostic, therapeutic and theranostic applications. *Mini-Reviews in Medicinal Chemistry* (2016) 16 (9), 754-761.

DOI: 10.2174/1389557515666150709112122

Grande F., Parisi O.I., Mordocco R., Rocca C., Puoci F., Scrivano L., Quintieri A.M., Cantafio P., Ferla S., Brancale A., Saturnino C., Cerra M.C., Sinicropi M.C. and Angelone T. Quercetin derivatives as novel antihypertensive agents: synthesis and physiological characterization. *European Journal of Pharmaceutical Science* (2016) 82, 161-170.

DOI: 10.1016/j.ejps.2015.11.021

Parisi O.I., Fiorillo M., Scrivano L., Sinicropi M.S., Dolce V., Iacopetta D., Puoci F. and Cappello A.R. Sericin/poly(ethylcyanoacrylate) nanospheres by interfacial polymerization for enhanced bioefficacy of fenofibrate: *in Vitro* and *in Vivo* studies. *Biomacromolecules* (2015) 16 (10), 3126-3133.

DOI: 10.1021/acs.biomac.5b00746

Parisi O.I., Morelli C., Scrivano L., Sinicropi M.S., Cesario M.G., Candamano S., Puoci F. and Sisci D. Controlled release of sunitinib in targeted cancer therapy: smart magnetically responsive hydrogels as restricted access materials. *RSC Advances* (2015) 5, 65308-65315.

DOI: 10.1039/C5RA12229E



---

## CONTRIBUTIONS

Scrivano L.\*, Parisi O.I., Malivindi R., Pezzi V., Puoci F. Functionalized sericin nanoparticles for theranostic application. Advanced school in nanomedicine Pula (Cagliari), Italy. 25-28 September 2017.

Scrivano L.\*, Parisi O.I., Malivindi R., Pezzi V., Puoci F. Synthesis and *in vitro* anti-cancer evaluation of cross-linked poly(ethyl cyanoacrylate) nanoparticles loaded with quercetin. Functional Materials for Healthcare (Fun4Health). Arcavacata di Rende, Italy. 6 April 2017.

Scrivano L.\*, University of Calabria (Oral presentation) Molecularly imprinted polymers for the controlled release of sunitinib. Società Chimica Italiana (SCI) - Workshop delle Sezioni Sicilia e Calabria 2016-17. Messina, Italy. 9-10 February 2017.

Parisi O.I., Scrivano L.\*, Iacopetta D., Sinicropi M.S., Saturnino C., Plutino M.R., Longo P. and Puoci F. Coniugati polimerici a base di sericina per il rilascio del sunitinib. Società Chimica Italiana (SCI) - Workshop delle Sezioni Sicilia e Calabria 2016-17. Messina, Italy. 9-10 February 2017.

Scrivano L.\*, Parisi O.I., Iacopetta D., Sinicropi M.S., Amone F., Ruffo M., Vattimo A.F. and Puoci F. Molecularly imprinted polymers for sunitinib sustained release in breast cancer therapy. II Corso permanente di aggiornamento per i dottorandi del settore tecnologico-farmaceutico (ADRITELF). Arcavacata di Rende (CS), Italy. 5-8 September 2016.

Scrivano L.\*, Iacopetta D., Parisi O.I., Mordocco R., Sinicropi M.S. and Puoci F. Sericin conjugation *via* free radical grafting for sunitinib delivery and enhanced cell accessibility in cancer therapy. Controlled Release Society (CRS) Italy Local Chapter: Micro and Nanotechnologies to Overcome Biological Barriers. Naples, Italy. 12-14 November 2015.

Scrivano L.\*, Parisi O.I., Sisci D., Morelli C., Cesario M.G. and Puoci F. Phosphatidylcholine giant unilamellar vesicles as membranes models for permeability evaluation of sericin-sunitinib conjugates. 585. WE Heraeus Seminar: Advanced Microscopy in Membrane Biophysics. Bad Honnef, Germany. 7-10 April 2015.





